High Frequency Asymptotics of Antenna/Structure Interactions



John Coats

Wolfson College

University of Oxford

A thesis submitted for the degree of

Doctor of Philosophy

Hilary 2002

I have not had a moment's peace or happiness in respect to electromagnetic theory since November 28, 1846. Since then I have been liable to fits of dipsomania, kept away at intervals only by rigorous abstention from thought on the subject.

Lord Kelvin

Acknowledgements

I cannot submit this thesis without thanking the people who have made it possible. I am indebted to my supervisors Professor Jon Chapman and Dr. John Ockendon for the intellectual stimulation, mathematical enthusiasm and enormous patience that they have provided during the last three years. They have directed my research and mathematical development whilst at the same time allowing me the freedom to pursue my own ideas. Through their contacts I have also had the opportunity to have numerous discussions with other leading researchers in the field. I am extremely grateful to both.

I would not have had the opportunity to carry out my research had it not been for the generous funding provided by BAe Systems ATC Sowerby. I would like to extend my sincere thanks to my industrial contact Dr. Colin Sillence who has provided support and maintained an active role in proceedings at all stages of the project. He also provided the wide range of interesting industrial problems which have motivated this thesis.

At a more personal level, I must thank DH9 and DH10 for a continual supply of people in the same boat as me, especially Jim (for starting and finishing at the same time), Andrew (for having a much harder problem than me), 'Boson' (for never being there), Dave (for being from Buckingham), Breward, Chris, Xblast and Backgammon.

Outside of OCIAM I should also like to thank everyone at Wolfson College and especially those in the boat club for making sure I kept a perspective on things. Too many to mention—in the unlikely event that you are reading this, you know who you are! Lastly, it goes without saying that I must thank my family for their support and encouragement throughout.

Abstract

This thesis is motivated by the need to calculate the electromagnetic fields produced by sources radiating in the presence of conductors.

We begin by reviewing existing theory concerning sources in the presence of flat structures. Various extensions to the canonical Sommerfeld problem are considered. In particular we investigate the asymptotic solution for a finite source that focusses its energy at a point.

In §5 we review and extend the asymptotic results concerning illumination of a convex perfect conductor by an incident plane wave and outline the procedure for decoupling the electromagnetic surface field into two scalar modes. In §6 we place a source on a perfect conductor and obtain a complete asymptotic solution for the fields. Special attention is paid to the asymptotic structure that smoothly matches between the leading order lit and shadow regions. We also investigate the degenerate case where one of the curvatures of the perfect conductor is zero. The case where the source is just off the surface is also investigated. In §8 we use the Euler-Maclaurin summation formula to cheaply calculate the fields due to complicated arrays of point dipoles.

The final chapter combines many earlier results to consider more general sources on the surface of a perfect conductor. In particular we must introduce new asymptotic regions for open sources. This then enables us to consider the focussing of the surface field due to a finite source. The nature of the surface and geometrical optics fields depends on the size of the source in comparison to the curvatures of the surface on which they lie. We discuss this in detail and conclude with the practical example of a spiral antenna.

Contents

I Introduction **1**

1 Introduction **2**

1.1 Industrial Motivation 3

1.2 Thesis Outline 5

1.3 Statement of Originality 6

2 Electromagnetism **7**

2.1 Maxwell's Equations 7

2.1.1 Boundary Conditions 8

2.1.2 Time-Harmonic Solutions 10

2.2 Nondimensionalisation 11

2.3 Solutions of Maxwell's Equations 12

2.3.1 Exact Solutions 12

2.3.2 Three-Dimensional Problems 12

2.3.3 Field due to a dipole 13

2.3.4 Two-Dimensional Problems 16

2.4 The Helmholtz Equation 17

2.4.1 Acoustics 17

2.4.2 Elasticity 17

2.4.3 Sommerfeld Radiation Condition 18

3 Ray Theory **20**

3.1 Illustrative Example—Geometrical Optics 22

3.2 Geometrical Theory of Diffraction 26

3.2.1 Edge Diffraction of a Plane Wave 27

3.2.2 Conical Tips 28

3.2.3 Grazing Rays 29

3.2.4 Changes in the Material Properties 29

3.2.5 Caustics 30

II Sources Remote from Structures 31

4 Flat Structures 32

4.1 Sommerfeld Problem 32
4.1.1 Solution Away from the Origin 34
4.1.2 The Reflected Shadow Boundary Region 34
4.2 Field Due to an Excited Flat Plate 37
4.2.1 Terminology 39
4.2.2 The Fraunhofer Region 39
4.3 Ray Picture for a General Radiating Source 40
4.4 Field Due to an Antenna in Three Dimensions 41
4.4.1 Axi-symmetric E-M Field 41
4.4.2 Semi-infinite Line Source 42
4.4.3 Axi-symmetric Shadow Boundary Region 47
4.5 Field Due to a Finite Antenna 48
4.6 Sommerfeld Problem with Line Source Illumination 49
4.6.1 Geometrical Optics Field 50
4.6.2 Reflected Shadow Boundary 51
4.7 Converging Shadow Boundary Regions 52

5 Curved Structures 58

5.1 Geodesic Normal Coordinates 59
5.2 Surface Field Propagation along Geodesics 61
5.3 Plane Wave-Field Incident Upon a Convex Scatterer 62
5.3.1 The Airy Layer 63
5.3.2 Fock-Leontovič Region 67
5.3.3 Shed Creeping Ray Field 72
5.3.4 Shadow Boundary Structure 73
5.3.5 Finite Bodies 81
5.3.6 Ray Solutions 81
5.4 Oblique Plane Wave Incidence 83
5.4.1 Fock-Leontovič Region 84
5.4.2 Airy Layer Field 87
5.4.3 Shadow Boundary Structure 88

5.5 A Dipole at an $\mathcal{O}(1)$ Distance from a Perfectly Conducting Convex Surface . . . 90
5.6 Illumination by a Field from a Line Source . . . 92
5.6.1 Geometrical Optics Field . . . 93
5.6.2 Fock-Leontovic, Airy Layer and Creeping Ray Fields . . . 94
5.6.3 Shadow Boundary Region . . . 95
5.6.4 Transition Region . . . 96
5.7 Concave Surfaces . . . 98
5.7.1 Whispering Gallery Modes . . . 98
5.7.2 Open Problem . . . 99
5.8 Discussion . . . 102

III Sources Close to Structures 103

6 Point Sources on a Convex Surface 104
6.1 Geodesic Polar Coordinates . . . 104
6.2 Airy Layer . . . 106
6.3 Fock-Leontovič Region . . . 107
6.4 Inner-Fock-Leontovič Region . . . 109
6.5 Fock-Leontovič Region Solution . . . 110
6.6 Geometrical Optics Field . . . 112
6.7 Creeping Ray Field . . . 113
6.8 Shadow Boundary Structure . . . 115
6.9 Surface Fields Due to a Point Source on a Circular Cylinder . . . 121
6.10 Sources at Inflexion Points . . . 125
6.11 Sources on Saddle Points . . . 127

7 Sources Close to a Convex Surface 130
7.1 Magnetically Polarised Solutions . . . 132
7.2 Electrically Polarised Solutions . . . 136
7.3 Limiting Cases . . . 138

8 Arrays of Localised Sources 141
8.1 Exact Solutions for Arrays of Point Sources . . . 141
8.1.1 One-dimensional Arrays . . . 141
8.1.2 Two-dimensional Arrays . . . 142
8.2 Asymptotic Solutions for Arrays of Point Sources . . . 144

8.2.1 One-dimensional Arrays . . . 144
8.2.2 Two-dimensional Arrays . . . 146
8.3 Arrays of Continuously Distributed Sources . . . 148
8.4 Comparison of Arrays with Unperforated Continuously Distributed Sources . . . 150
8.4.1 One-dimensional Arrays . . . 151
8.4.2 Two-dimensional Arrays . . . 151
8.5 Larger Arrays . . . 152

9 Conformal Antennas on Curved Surfaces 153
9.1 Closed Line Sources . . . 154
9.1.1 Sources of $\mathcal{O}(1)$ Size . . . 154
9.1.2 Sources of Size $k^{-2/3}$. . . . 158
9.1.3 Sources of Size $k^{-1/3}$ . . . 160
9.1.4 Smaller Sources . . . 160
9.2 Semi-infinite Sources . . . 161
9.2.1 Inner-Fock-Leontovič Region . . . 162
9.2.2 Surface Fresnel Region . . . 164
9.2.3 Matching the Surface Fresnel Solution to the Airy Layer Solutions 166
9.3 Focussing Effects . . . 168
9.4 Application: A Spiral Antenna . . . 173
9.4.1 Out of Phase excitation . . . 177
9.4.2 Discontinuous Sources . . . 177

10 Conclusions and Further Work 180
10.1 Summary of Results . . . 180
10.2 Further Work . . . 184

A Fourier Transform of the Heaviside Function 186

B Canonical Problem for Small α 188

C Maxwell's Equations in Geodesic Coordinates 192

D Reciprocity 196

E Maxwell's Equations for Surface Fresnel Regions 198

Bibliography 201

Part I

Introduction

Chapter 1

Introduction

Thomas Young refuted Newton's corpuscular theory of light in the early 19th century. Since then much energy has been devoted to explaining and quantifying the phenomena arising due to the wave-like nature of the electromagnetic (E-M) spectrum. Making the assumption that the radiation is of a high frequency—or more precisely, that the wavelength of the radiation is small compared to the length scales of any scatterers that may be present—the lowest order approximation reveals that the waves travel along straight lines or rays. We are able to integrate initial data along these rays to obtain the solution. This is the basis of geometrical optics (GO). Using this model we can successfully explain reflection at surfaces and the bending of light (refraction) as it passes through optically different media. However, this leading order approximation does not give the complete picture.

Shine a light horizontally on a half full coffee cup. A caustic is clearly visible due to the limiting GO reflected rays. A sensitive light meter placed on the dark side of the caustic would detect a field that was slightly stronger than the incident field. This does not conform to the claims of GO which would predict that the only field present on the dark side of the caustic was the incident field.

Go to the famous Whispering Gallery in St Paul's Cathedral. Here, a whisper close to the wall on one side can be clearly heard at the other side of the dome. While there is a straight line connecting speaker and listener, the GO model says that the distances involved should mean that the whisper is inaudible.

Place a large obstacle between a sound source and a microphone. The microphone will pick up a non-zero amplitude despite the fact that there are clearly no straight lines connecting source and microphone.

Another example where GO fails spectacularly is best illustrated using water waves.

Consider parallel wave-fronts on the ocean. Upon entering a harbour through a narrow gap in the harbour walls they will become circular. Drawing straight lines does not explain what is going on here.

The four examples cited above should all be covered by GO as in the respective cases the wavelength of the radiation is small compared to the coffee cup, St Paul's Cathedral, etc. There are many cases where it is vital to properly understand the higher order effects. Seismology and oceanography are just two examples. Consideration of just the GO fields would not enable us to calculate the location of a tectonic movement or the nature of the ocean floor. Keller's Geometrical Theory of Diffraction (GTD) [21] explains each of the above phenomena via the solutions to a set of canonical problems. The idea is that any complex wave/structure interaction may be reduced to a ray tracing procedure specific to the geometry of the individual problem along with a catalogue of canonical problems, each of which only needs to be solved once. For example, every time an incident ray (along which we know the wave field via GO) interacts with a scatterer, we decide which canonical problem is most appropriate to the interaction. We then feed the relevant data into the black box for this canonical problem—in many cases this will be an explicit mathematical expression, but in others a numerical evaluation will be required. In general this generates a new family of rays which can then be tracked. The nature of the field along these rays is obtained via the black box and GO. If these rays interact further with obstacles, the process must be repeated. As the higher order fields are much smaller than the incident field, to achieve a given accuracy a finite number of ray/structure interactions will be required.

Despite the work of Keller and many others, the catalogue of canonical problems that is needed to successfully implement a ray tracing scheme is far from complete. This thesis investigates a variety of those involving sources in the neighbourhood of scatterers.

1.1 Industrial Motivation

The motivation for this work comes from an industrial link between OCIAM and BAE SYSTEMS, Filton. This work builds on previous collaboration, with a view to ultimately providing qualitative and quantitative results concerning electromagnetic radiation that can be compared to observation and experiments on an aeroplane.

On a modern military aircraft there will be several hundred antennas, either mounted

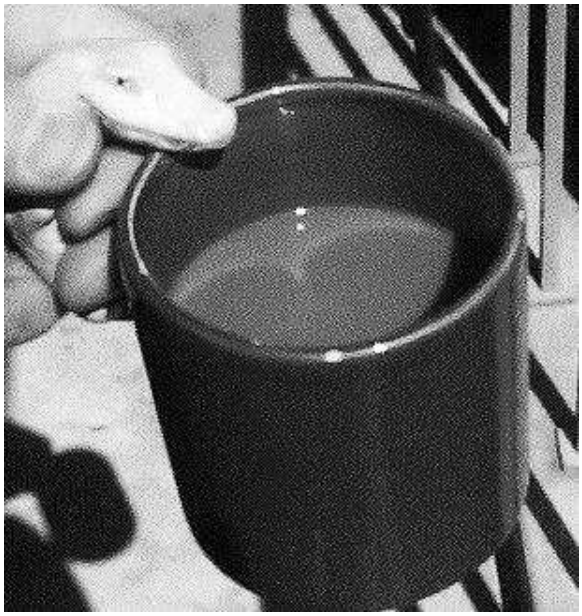


Figure 1.1: Coffee cup illuminated from the front. The caustic is clearly visible on the surface of the liquid.

individually or in arrays, protruding from or lying on the surface and they may be receiving or transmitting. The receiving antennas will be extremely sensitive, being required to detect weak signals over large distances and the transmitting antennas will be very powerful. Thus, even a small amount of interference between the receiving and transmitting antennas will prove significant. Diffraction effects (not to mention constraints placed on the aircraft geometry by conflicting design requirements) make it impossible to produce an aircraft with no electromagnetic interference between the different systems. Our task is to quantify these effects for a given aircraft geometry and antenna design. In particular, a better understanding of the so-called *creeping rays* and *whispering gallery* (WG) modes is required. These allow electromagnetic energy from a transmitting antenna to diffract around the aircraft geometry and to corrupt other antenna sites on the aeroplane. Creeping rays diffract energy around convex geometries and WG modes propagate energy along concave surfaces.

The aerospace industry uses large-scale ray-tracing computer codes to analyse the installed performance and interoperability of antennas on aircraft and other structures. Real antennas can be characterized in their immediate environments either by near-field probing (measurements) or by using Computational Electromagnetics (CEM). At high frequencies (above say 1GHz) the whole structure is however out of reach of CEM, even with the largest computers—hence the need for an asymptotic approach

implemented numerically through ray-tracing. For many antenna types, and particularly distributed antennas, the current schemes for launching (and receiving) rays at antennas are inaccurate, cannot cope with subsequent interaction with the structure unless this occurs a long way from the antenna, and suffer from 'dead zones' in the launching patterm. There is a pressing need therefore for a hybrid approach to the problem, with 'exact' measured or CEM antenna data translated into a sophisticated and efficient scheme for ray-launching and receiving. This context has motivated many of the problems studied and solved in this thesis.

The canonical diffraction problems that we will consider will be of inherent mathematical interest in addition to being of practical relevance to the aerospace industry.

1.2 Thesis Outline

In chapter 2 we set up our model and comment on its relationship to other physical phenomena. We nondimensionalise the model and describe how to retrieve the dimensional solutions from the nondimensional results that we will obtain later. We also calculate the fields radiated by an electric dipole which will be needed later.

Chapter 3 introduces the ray theory technique. Here a WKB ansatz is used to deduce that, in the high frequency limit, information propagates along straight lines, or rays. We use ray theory to solve the problem of an incident wave-field on a curved structure. This is seen to break down at the point where the incident field is tangent to the surface. This is one of the canonical problems considered by Keller and we review his theory here.

In Chapter 4 we spend some time examining extensions to the canonical Sommerfeld problem of a plane wave-field impinging on a semi-infinite plate. We introduce *shadow boundary* regions to provide a smooth field everywhere. For finite plates, the shadow boundary regions from either end of the plate will be seen to merge, providing us with several interesting scenarios.

Chapter 5 investigates in detail the breakdown of the geometrical optics ray solution obtained in §3. We describe how to reduce the vector Maxwell's equations to two scalar equations. A rich asymptotic structure is developed based on the acoustic results of [33]. Various extensions to this problem are carried out.

Chapter 6 considers the field due to the irradiation of a surface by a source on the surface. Now the vector Maxwell's equations can be reduced to a single scalar equation. Again we build on previous acoustic results. The main development in this chapter

is the establishment of the structure of the asymptotic solution in the transition region between the geometrical optics *illuminated* and *shadow* regions. We also look in some detail at the surface fields that arise when a source is placed on a cylinder. Here the standard expressions for the surface field are not valid everywhere and new asymptotic regions need to be introduced.

In Chapter 7 we remove the source slightly from the surface and obtain the solutions in the corresponding asymptotic regions. This will help us understand the change in the asymptotic structures that exists between chapters 5 and 6.

Chapter 8 is devoted to obtaining asymptotic solutions to the field when we have an array of a large number of elements on the surface.

Chapter 9 is an amalgamation of the results of earlier chapters. We consider arbitrary line sources on a smooth, convex, perfectly conducting surface and describe how to obtain the asymptotic solutions. We conclude with a discussion of the fields due to a specific source geometry which is of particular industrial interest—that of a spiral.

We finish with a discussion of our results and an outline of directions for future work.

1.3 Statement of Originality

Originality is claimed for the results of §4.2, §4.4.2 - 4.4.3, §4.5, §4.6.2 and §4.7. Although the method used to deal with the E-M fields in §5 is based on [36], the full asymptotic solution for the E-M problem does not appear in the literature. The results of §5.3.4, §5.4, §5.5 and §5.6 are original. The results of §6 - 6.7 are original as regards the calculation of the E-M field, but may be found elsewhere in the acoustics literature. The remainder of chapter 6 is original. Chapter 7 onwards, with the exception of §9.1.1, is original work.

Chapter 2

Electromagnetism

2.1 Maxwell's Equations

Maxwell's equations in linear isotropic media relate electric and magnetic fields $\mathcal{E}, \mathcal{H}$, electric current density $\mathcal{J}$ and electric charge density ρ_e as follows

$$\nabla \wedge \mathcal{E} + \mu \frac{\partial \mathcal{H}}{\partial t} = \mathbf{0}, \tag{2.1}$$

$$\nabla \wedge \mathcal{H} - \epsilon \frac{\partial \mathcal{E}}{\partial t} = \mathcal{J}, \tag{2.2}$$

$$\nabla \cdot \epsilon \mathcal{E} = \rho_e, \tag{2.3}$$

$$\nabla \cdot \mu \mathcal{H} = 0, \tag{2.4}$$

where ϵ and μ are the permittivity and permeability of the medium. Equation (2.1) is Faraday's law of electromagnetic induction which states that a current is induced in a conductor that moves through a magnetic field, (2.2) is Maxwell's version of the Biot-Savart Law which asserts that a current flowing along a straight wire induces an azimuthal magnetic field around the wire, and equations (2.3) and (2.4) are conservation of electric and magnetic charges, respectively. Further discussion of this system of equations can for example be found in [5]. For closure of the system we must also include Ohm's Law which is a constitutive relation between the electric current and the electric field

$$\mathcal{J} = \sigma \mathcal{E}, \tag{2.5}$$

where σ is the conductivity.

2.1.1 Boundary Conditions

We will consider the boundary conditions on the surface Γ of a smooth, perfectly conducting scatterer for a configuration typical of the problems to follow. We assume that any current sources lie on the surface of the perfect conductor—*i.e.* the electric current and charge densities are zero exterior to the scatterer. A perfect conductor has infinite conductivity and so (2.5) implies that $\mathcal{E}$, and hence $\mathcal{H}$ via Maxwell's equations, is zero inside the conductor. We introduce a locally cartesian coordinate system on the surface of the scatterer, with the x and y-axes tangential to the surface, and the z-axis normal to it. Integrating (2.4) over the 'pill-box' S in Figure 2.1 gives us

$$\oint_S \mathcal{H} \cdot \mathbf{n} \, \mathrm{d}S \;=\; 0. \tag{2.6}$$

For a small cross-section, $\mathcal{H} \sim$ constant. Letting the length of the cylinder, δl, go to zero we get

$$[\mathcal{H} \cdot \mathbf{n}] \;=\; 0, \tag{2.7}$$

across the boundary. As $\mathcal{H} \equiv \mathbf{0}$ inside the perfect conductor we have

$$\mathcal{H}_3 \;=\; 0, \tag{2.8}$$

on the boundary. To obtain the boundary conditions involving the tangential components of $\mathcal{E}$ we observe that we may write (2.1) in conservation form which lets us derive 'Rankine-Hugoniot' jump conditions across the boundary. We thus write the 1st component of (2.1) as

$$\mu \frac{\partial \mathcal{H}_1}{\partial t} + \nabla \cdot (0, \mathcal{E}_3, -\mathcal{E}_2) \;=\; 0. \tag{2.9}$$

If we now introduce an arbitrarily differentiable test function ψ such that ψ vanishes on the surface γ in Figure 2.2, then for all solutions to (2.9) we have

$$\mu \frac{\partial}{\partial t}(\psi \mathcal{H}_1) + \frac{\partial}{\partial y}(\psi \mathcal{E}_3) - \frac{\partial}{\partial z}(\psi \mathcal{E}_2) \;\equiv\; \mu \mathcal{H}_1 \frac{\partial \psi}{\partial t} + \mathcal{E}_3 \frac{\partial \psi}{\partial x} - \mathcal{E}_2 \frac{\partial \psi}{\partial y}. \tag{2.10}$$

Applying Green's theorem to (2.10) in the regions D_+ and D_- in Figure 2.2 and adding the results gives us

$$\int_{\Gamma_+} \psi(\mu \mathcal{H}_1, 0, \mathcal{E}_3, -\mathcal{E}_2) \cdot \mathrm{d}\mathbf{S} - \int_{\Gamma_-} \psi(\mu \mathcal{H}_1, 0, \mathcal{E}_3, -\mathcal{E}_2) \cdot \mathrm{d}\mathbf{S} \;=\; 0, \tag{2.11}$$

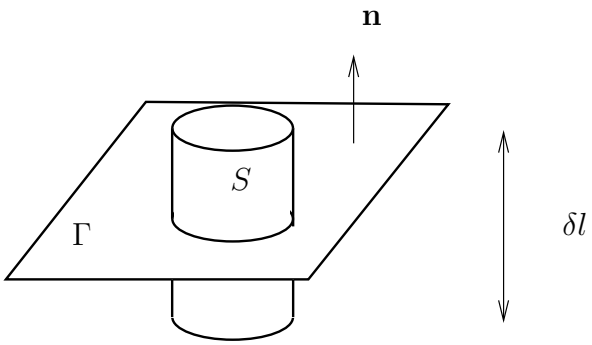


Figure 2.1:

We note that the surface element d$\mathbf{S}$ in (2.11) has non-zero components in the t and z directions only. As (2.11) holds for all test functions ψ we can deduce that

$$[\mu\mathcal{H}_1]^+_- v_n \;\; = -[\mathcal{E}_2]^+_-, \tag{2.12}$$

across the boundary, where v_n is the normal velocity of the boundary. Working in a frame where our scatterer is at rest and reminding ourselves that $\mathcal{E} = 0$ inside the conductor, we can deduce that

$$\mathcal{E}_2 = 0, \tag{2.13}$$

on the surface of the perfect conductor. The second component of (2.1) similarly implies

$$\mathcal{E}_1 \;\; = \;\; 0, \tag{2.14}$$

on the boundary.

Surface current and charge $\mathcal{J}_s, \rho_s$ may exist on the surface of the perfect conductor. Treating (2.3) and (2.2) in the same way as (2.4) and (2.1) it can be shown that these are related to the exterior fields by the relationships

$$\epsilon\mathcal{E}_3 \;\; = \;\; \rho_s, \tag{2.15}$$

$$\mathcal{H} \wedge \mathbf{n} \;\; = \; -\mathcal{J}_s. \tag{2.16}$$

In what follows we will take μ, ϵ exterior to the scatterer to be equal to their free space values μ_0, ϵ_0 respectively.

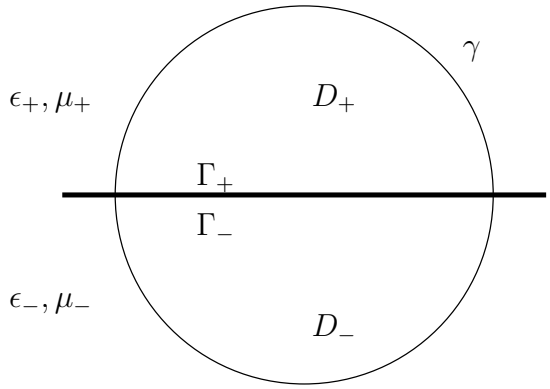


Figure 2.2:

2.1.2 Time-Harmonic Solutions

At this point we will restrict our attention to time-harmonic E-M fields, *i.e.* those where the sources, and hence the fields, have a time-dependence proportional to $\exp(-i\omega t)$. We introduce the variables

$$\begin{aligned} \mathrm{Re}(\mathbf{E}e^{-i\omega t}) &= \epsilon_0^{1/2}\mathcal{E}, & (2.17)\\ \mathrm{Re}(\mathbf{H}e^{-i\omega t}) &= \mu_0^{1/2}\mathcal{H}, & (2.18)\\ \mathrm{Re}(\mathbf{J}e^{-i\omega t}) &= \mu_0^{1/2}\mathcal{J}, & (2.19)\\ \mathrm{Re}(\rho e^{-i\omega t}) &= \epsilon_0^{-1/2}\rho_e, & (2.20) \end{aligned}$$

whereupon (2.1) - (2.4) become[1]

$$\begin{aligned} \nabla \wedge \mathbf{E} - ik'\mathbf{H} &= \mathbf{0}, & (2.21)\\ \nabla \wedge \mathbf{H} + ik'\mathbf{E} &= \mathbf{J}, & (2.22)\\ \nabla \,.\, \mathbf{E} &= \rho, & (2.23)\\ \nabla \,.\, \mathbf{H} &= 0, & (2.24) \end{aligned}$$

where $k' = \omega\sqrt{\epsilon_0\mu_0} = \omega/c$ is the dimensional wave-number, and c is the velocity of light.

Our perfectly conducting boundary conditions may now be written as

$$\begin{aligned} \mathbf{H} \,.\, \mathbf{n} &= 0, & (2.25)\\ \mathbf{E} \wedge \mathbf{n} &= \mathbf{0}, & (2.26) \end{aligned}$$

where $\mathbf{n}$ is the normal vector to the surface.

[1] Although we will never actually use (2.21) - (2.24) as they stand, we caution the practically minded reader that the units of these equations will be different from those of (2.1) - (2.4).

2.2 Nondimensionalisation

In a complicated physical system we may often simplify the mathematical model by neglecting certain terms on the premise that their magnitude is much less than that of the other terms in an equation. Nondimensionalisation is the process by which we evaluate the relative importance of each term. For our model, (2.21) - (2.24), we nondimensionalise with respect to the length scale L of the problem. For problems where there is a source in the presence of a scattering surface we will take $L = 1/\kappa$, where κ is a *typical* curvature of the scatterer and E to be a *typical* value of $|\mathbf{E}|$. We set $\mathbf{x} = L\mathbf{x}^*$, $\nabla = \nabla^*/L$, $\mathbf{E} = E\mathbf{E}^*$, $\mathbf{H} = E\mathbf{H}^*$, $\mathbf{J} = E/L\mathbf{J}^*$, $\rho = E/L\rho^*$. We thus obtain the nondimensional versions of (2.21) - (2.24)

$$\begin{aligned} (\nabla\wedge)^* \mathbf{E}^* - ik^*\mathbf{H}^* &= \mathbf{0}, && (2.27)\\ (\nabla\wedge)^* \mathbf{H}^* + ik^*\mathbf{E}^* &= \mathbf{J}^*, && (2.28)\\ \nabla\,.\,\mathbf{E}^* &= \rho^*, && (2.29)\\ \nabla\,.\,\mathbf{H}^* &= 0, && (2.30) \end{aligned}$$

where $k^* = k'L = \omega L/c$ is the *nondimensional wave-number*. In what follows we assume that we are dealing with high frequency E-M fields. That is to say that $k^* \gg 1$. This is a reasonable assumption to make as, for the scattering problems we will be considering, we typically have $c = 3\times10^8 \mathrm{ms}^{-1}$, $\omega = 2\pi(10^8 - 10^{10})\mathrm{s}^{-1}$, $L = 1\mathrm{m}$. Thus $k^* \sim 2 - 200$.

In this thesis we will often obtain results that are specific to say sources of size $\mathcal{O}(k^{*m})$. To apply our results to physical situations in future chapters we need to know how this non-dimensional length scale translates to a dimensional one. Suppose x and $k = \omega/c$ are the dimensional variables representing distance and wave-number respectively. Our starred non-dimensional variables are $x^* = x/L, k^* = kL$. If our non-dimensional length scale is k^{*m} this implies that

$$\frac{x}{L} \sim L^m k^m. \qquad (2.31)$$

This means that the dimensional length scale is

$$x \sim L^{m+1} k^m. \qquad (2.32)$$

As k is inversely proportional to the wavelength λ, this can be rewritten as

$$x \sim L^{m+1} \lambda^{-m}. \qquad (2.33)$$

In the rest of this thesis the stars on the nondimensional variables will be dropped. As we will mostly be working with non-dimensional equations this should not cause any confusion.

2.3 Solutions of Maxwell's Equations

2.3.1 Exact Solutions

Although we will be deriving asymptotic representations of the E-M field for various configurations, exact solutions for certain problems do exist. Jones, [19], calculates the scattered field arising from an incident field impinging on a sphere, and Fock, [16], calculates the corresponding scattered field for a paraboloid of revolution. In addition, solutions in the time domain can be found in the literature—there are several solutions to problems involving impulsive sources in [11]. The ability of these cases to be solved relies on being able to introduce a coordinate system in which the boundary conditions for the different components of the $\mathbf{E}$ and $\mathbf{H}$ fields separate. For general geometries of the scattering body this is not possible and we will address this difficulty in what follows.

2.3.2 Three-Dimensional Problems

Manipulation of (2.1) - (2.4) reveals that each component f of $\mathbf{E}$ and $\mathbf{H}$ satisfies the Helmholtz equation

$$\nabla^2 f + k^2 f = g, \tag{2.34}$$

where g is some source term, possibly equal to zero. If we write

$$\mathbf{E} = \mathbf{E_0} e^{iku(\mathbf{x})}, \tag{2.35}$$

$$\mathbf{H} = \mathbf{H_0} e^{iku(\mathbf{x})}, \tag{2.36}$$

in (2.21) - (2.24), taking $k \gg 1$, we obtain leading order equations

$$\mathbf{H_0} \wedge \nabla u - \mathbf{E_0} = \mathbf{0}, \tag{2.37}$$

$$\mathbf{E_0} \wedge \nabla u + \mathbf{H_0} = \mathbf{0}. \tag{2.38}$$

These imply that in the high frequency limit $\mathbf{E_0}, \mathbf{H_0}$ and ∇u form a right-handed set[2]. Level sets of u define wavefronts, and so ∇u is the direction of propagation of

[2]By considering Poynting vector—see [19]—it can be shown that this is actually true at all frequencies.

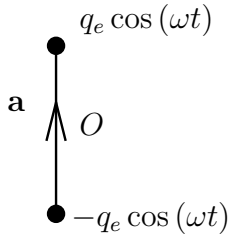


Figure 2.3: A dipole at the origin.

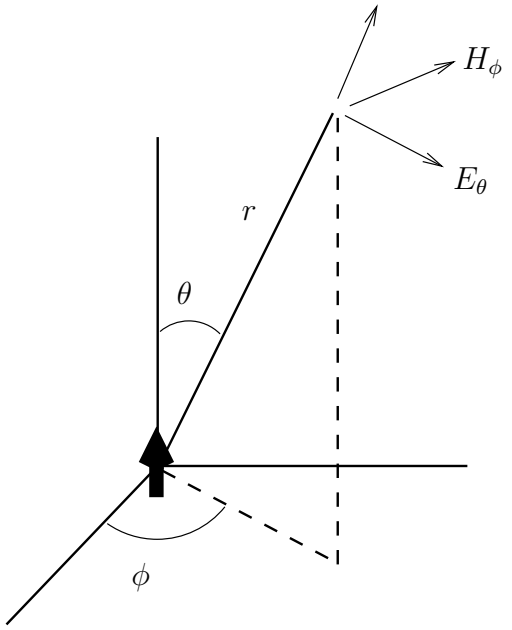


Figure 2.4: Fields due to a dipole at the origin.

the E-M fields. This tells us that **E** and **H** are not only perpendicular to each other but are also at right angles to the direction of propagation of the field—*i.e.* the E-M fields are transverse. This fact will be useful later when we are dealing with fields close to general scattering surfaces.

2.3.3 Field due to a dipole

Later we will wish to calculate the fields due to a point source of current either on or near a perfectly conducting surface. Since conservation of charge must be satisfied, a time-harmonic point source is not a realizable source of E-M radiation. Instead we consider a dipole at the origin (see Figure 2.3). Here we take two point charges $-q_e \cos(\omega t), q_e \cos(\omega t)$ whose midpoint is the origin. The vector from the negative to positive charge is given by $\mathbf{a}$. We then let $q_e \to \infty$ and $\mathbf{a} \to \mathbf{0}$ in such a way that

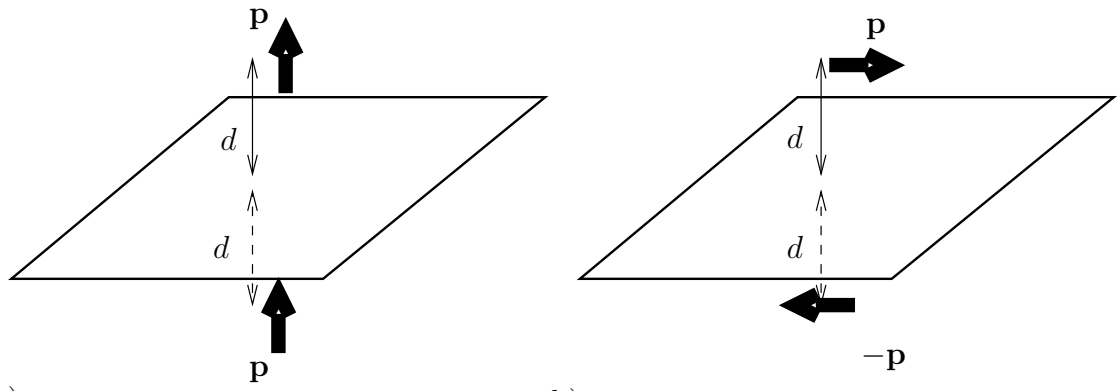


Figure 2.5: Dipole and image oriented a) perpendicular to the surface, b) parallel to the surface. Image dipoles must be introduced

the *dipole moment*

$$\mathbf{p}_e = q_e \mathbf{a}, \tag{2.39}$$

is finite. There is an effective current flowing between the two charges given by

$$\mathcal{J} = -\omega \mathbf{p}_e \sin(\omega t)\, \delta(\mathbf{x}). \tag{2.40}$$

We define

$$\mathrm{Re}\left(\mathbf{p} e^{-i\omega t}\right) = \epsilon_0^{-1/2} \mathbf{p}_e, \tag{2.41}$$

whereupon (2.40) becomes

$$\mathbf{J} = -ik' \mathbf{p} \delta(\mathbf{x}). \tag{2.42}$$

Non-dimensionalizing as usual (we define $\mathbf{p} = EL^3 \mathbf{p}^*$, where E is a typical value of $|\mathbf{E}|$ and L is an arbitrary length scale) and dropping the starred variables we obtain

$$\mathbf{J} = -ik \mathbf{p} \delta(\mathbf{x}). \tag{2.43}$$

To solve Maxwell's equations for this configuration we first introduce a vector potential[3] $\mathbf{A}$ which ensures that (2.30) is satisfied,

$$\mathbf{H} = \nabla \wedge \mathbf{A}. \tag{2.44}$$

Then (2.27) implies

$$\mathbf{E} = ik\mathbf{A} - \nabla V, \tag{2.45}$$

[3]This is not the same as the vector potential that usually appears in the literature which is dimensional and defined by $\mu \mathcal{H} = \nabla \wedge \mathbf{A}$.

for some scalar V. However the decomposition of the fields into vector and scalar potentials is not unique—if $\mathbf{A}_0$ and V_0 are solutions then so are

$$\mathbf{A} = \mathbf{A}_0 - \nabla\psi, \tag{2.46}$$

$$V = V_0 - ik\psi, \tag{2.47}$$

for any gauge ψ. Hence we make the gauge choice

$$\nabla \cdot \mathbf{A} - ikV = 0. \tag{2.48}$$

Introducing the *Hertz vector* $\mathbf{\Pi}$ such that

$$\mathbf{A} = ik\mathbf{\Pi}, \tag{2.49}$$

$$V = \nabla \cdot \Pi, \tag{2.50}$$

we find that (2.28) implies

$$\nabla^2\mathbf{\Pi} + k^2\mathbf{\Pi} = \frac{i}{k}\mathbf{J}. \tag{2.51}$$

We have thus reduced Maxwell's equations to a single vector equation, the solution to which is[4]

$$\mathbf{\Pi} = -\frac{i}{4\pi k}\int \mathbf{J}(\mathbf{r}')\frac{e^{ik|\mathbf{r}-\mathbf{r}'|}}{|\mathbf{r}-\mathbf{r}'|}\,\mathrm{d}V, \tag{2.52}$$

where $\mathbf{r}'$ is the variable of integration. For the dipole that we have described (2.52) reduces to

$$\mathbf{\Pi} = -\frac{e^{ikr}}{4\pi r}\mathbf{p}. \tag{2.53}$$

We can now calculate $\mathbf{E}, \mathbf{H}$. To leading order in powers of k we find that these are

$$\begin{array}{lllllll} H_r = 0, & H_\phi = -\dfrac{pk^2\sin\theta}{4\pi r}e^{ikr}, & H_\theta = 0, \\ E_r = 0, & E_\phi = 0, & E_\theta = -\dfrac{pk^2\sin\theta}{4\pi r}e^{ikr}, \end{array} \tag{2.54}$$

where r, ϕ, θ are the spherical polar coordinates based at the dipole as in Figure 2.4 and $p = |\mathbf{p}|$. The component of $\mathbf{H}$ in the r direction is denoted by H_r, etc.

We now place the same dipole near a flat perfectly conducting surface. Without loss of generality there are two possible orientations. In Figure 2.5a) we have $\mathbf{a}$ perpendicular

[4]We caution the reader that we have required the our solution to be outgoing at infinity—see §2.4.3 for a further discussion.

to the surface and in Figure 2.5b) **a** is parallel to the surface. Consideration of the perfectly conducting boundary condition (2.26) implies that for the first case we must include an image source with dipole moment **p** at the image point of the original dipole and that for the second we must introduce an image source with dipole moment $-\mathbf{p}$ at the image point. Letting the distance from the dipole to the surface decrease, we find that for a dipole *on* the surface with an orientation as in Figure 2.4a), the field exterior to the perfect conductor is twice that for the equivalent dipole in free space. For a dipole on the surface with the orientation of Figure 2.5b) the field will be zero.

2.3.4 Two-Dimensional Problems

In a two-dimensional electromagnetic scattering problem, assuming no dependence on z, we find that the E-M problem reduces to two scalar problems as described below.

We consider (2.27) and (2.28) in the absence of current sources. These imply that the components of the **E** and **H** fields can be written in terms of E_z and H_z.

$$E_x = \frac{i}{k}\frac{\partial H_z}{\partial y}, \tag{2.55}$$

$$E_y = -\frac{i}{k}\frac{\partial H_z}{\partial x}, \tag{2.56}$$

$$H_x = -\frac{i}{k}\frac{\partial E_z}{\partial y}, \tag{2.57}$$

$$H_y = \frac{i}{k}\frac{\partial E_z}{\partial x}, \tag{2.58}$$

with E_z, H_z both satisfying the homogenous Helmholtz equation (2.34). The perfectly conducting boundary conditions (2.25) - (2.26) tell us that we must have

$$E_z = 0, \quad \frac{\partial H_z}{\partial n} = 0, \quad \text{on } n = 0.$$

The two-dimensional vector problem has thus been reduced to two uncoupled scalar problems for E_z and H_z, with a Dirichlet or a Neumann boundary condition respectively. The linearity of the governing equations means that the two problems can be solved independently to give the final solution.

Thus, all two-dimensional problems may be formulated as scalar problems and solved for both Dirichlet and Neumann boundary data.

2.4 The Helmholtz Equation

Sections 2.3.2 and 2.3.4 justify our emphasising the Helmholtz equation,

$$\nabla^2\phi + k^2\phi \;\; = \;\; 0, \tag{2.59}$$

for ϕ in the domain exterior to the scatterer, with either a Dirichlet or a Neumann boundary condition on the scatterer. Before doing this it is interesting to note the relevance of this model to other physical situations.

2.4.1 Acoustics

When solving for small pressure variations $p(\mathbf{x}, t)$ in a compressible fluid that is at rest, we find that p satisfies the wave equation

$$\nabla^2 p = \frac{1}{c^2}\frac{\partial^2 p}{\partial t^2}, \tag{2.60}$$

where c is the velocity of sound in the fluid. Looking for time-harmonic solutions $p = P\exp(-i\omega t)$ turns (2.60) into the Helmholtz equation for P. The boundary condition $P = 0$ is termed a *sound-soft* boundary condition and would be applied for example on an untensioned membrane. The Neumann boundary condition is termed *sound-hard* and would be applied to a rigid surface.

It is for this reason that the scalar Helmholtz equation is often referred to as the acoustic version of the E-M problem.

2.4.2 Elasticity

If $\mathbf{u}$ is the displacement vector of the deformation of an elastic solid due to elastic waves, it can be shown that we can write $\mathbf{u} = \nabla\psi + \nabla\wedge\mathbf{A}$ where both ψ and $\mathbf{A}$ satisfy the Helmholtz equation. $\nabla\psi$, $\nabla\wedge\mathbf{A}$ are the displacements in a pressure (P) wave and a shear (S) wave respectively. As the pressure and shear wave speeds are different in an elastic solid, we will get *two* nondimensional wave speeds for this problem. In addition we no longer have homogenous Dirichlet or Neumann boundary conditions which means there is mode conversion between P and S waves at the boundaries. For a ray theory approach to the elasticity problem a systematic investigation of several problems is carried out in [39].

2.4.3 Sommerfeld Radiation Condition

If we try to solve the Helmholtz equation in an unbounded domain then, unless we impose a constraint on the field at infinity, we cannot guarantee a unique solution to the problem. Consider the non-homogenous Helmholtz equation

$$\nabla^2\phi + k^2\phi = f(\mathbf{x}), \tag{2.61}$$

where f represents a source term which has compact support. To show uniqueness we are interested in showing that the only solution to the homogenous version with zero Dirichlet or Neumann boundary conditions on any scatterers is $\phi \equiv 0$.

In three dimensions, as we let r, the distance from the source, increase, the region containing the sources will appear to shrink toward a point source and so it is reasonable to expect that the solution will be outward going of the form e^{ikr} with decay algebraic in r. The condition

$$\phi = \mathcal{O}(r^{-1}), \qquad \frac{\partial\phi}{\partial r} - ik\phi = o(r^{-1}), \qquad r \to \infty, \tag{2.62}$$

is known as *Sommerfeld's radiation condition* and ensures that at infinity we have an outward going wave with the correct algebraic decay. Bleistein, [6] proves rigourously that this does indeed give a unique solution to the original problem *provided* that the boundary data is given on a finite domain.

For the two-dimensional problem, we can adapt Bleistein's proof to show that the conditions

$$\phi = \mathcal{O}(r^{-1/2}), \qquad \frac{\partial\phi}{\partial r} - ik\phi = o(r^{-1/2}), \qquad r \to \infty, \tag{2.63}$$

imply a unique solution.

However, problems arise when our source data is given on a semi-infinite or infinite domain. For example, if we are solving the two-dimensional problem

$$\nabla^2\phi + k^2\phi = 0, \quad y > 0, \tag{2.64}$$

$$\phi = e^{ikx\cos\alpha}, \quad y = 0, \tag{2.65}$$

we see that $\phi = \exp(ikx\cos\alpha + iky\sin\alpha)$ and $\phi = \exp(ikx\cos\alpha - iky\sin\alpha)$ both satisfy (2.64) and (2.65). These solutions represent a plane wave travelling towards infinity at an angle α to the x-axis and a plane wave travelling from infinity at an angle $\pi - \alpha$ to the x-axis, respectively. However, neither of these solutions satisfies either of Sommerfeld's conditions (2.63). Since we must have a non-zero solution to be able

to satisfy the non-zero boundary condition we cannot discard both of these solutions, and so insist instead that any legitimate solution must be outgoing at infinity. Hence in this example we would have to discount the second of the two wave fields.

Chapter 3

Ray Theory

We give a brief description of ray theory for the Helmholtz equation. Its strengths and weaknesses will be illustrated by considering a specific example.

We wish to solve

$$\nabla^2\phi + k^2\phi = 0, \tag{3.1}$$

with some boundary data and an outgoing wave condition at infinity. The nondimensional wave number $k = L\omega/c$ is taken to be large compared to 1. This is known as *high-frequency asymptotics*. Although c can be taken as a function of position—see [23]—we will consider homogenous media only.

We look for a solution using a WKB-type ansatz (see e.g. [18])

$$\phi \sim \sum_{n=0}^{\infty} A_n(\mathbf{x})(ik)^{-n} e^{iku(\mathbf{x})}. \tag{3.2}$$

The A_n are amplitude functions and u is the phase function.[1]. Putting (3.2) into (3.1) and comparing powers of k we obtain the *eikonal equation* for the phase and one *transport equation* for each of the amplitudes

$$(\nabla u)^2 = 1, \tag{3.3}$$

$$2\nabla A_0 \cdot \nabla u + A_0\nabla^2 u = 0, \tag{3.4}$$

$$2\nabla A_j \cdot \nabla u + A_j\nabla^2 u = -\nabla^2 A_{j-1}. \tag{3.5}$$

As k is a large parameter, it will be sufficient to look at just the first amplitude function as it will give a good approximation to the full solution, provided that (3.2)

[1]Strictly speaking the phase is ku. In the remainder of the thesis 'phase' is to be interpreted as meaning u.

is an asymptotic expansion.

The eikonal equation (3.3) can be solved using Charpit's method (see *e.g.* [28]). In vector notation this gives us

$$\dot{\mathbf{x}} = \mathbf{p}, \tag{3.6}$$

$$\dot{\mathbf{p}} = \mathbf{0}, \tag{3.7}$$

$$\dot{u} = 1, \tag{3.8}$$

where $\mathbf{p} = \nabla u = (p, q)$, and the dot is differentiation with respect to τ, the distance along a characteristic. From (3.6) and (3.7) the characteristic curves (or rays) are straight lines. The eikonal equation, along with data $u_0(s)$ given on $\mathbf{x}_0(s)$, provides two possible values for $\mathbf{p}$, namely the solutions of

$$p_0(s)^2 + q_0(s)^2 = 1, \tag{3.9}$$

$$u_0'(s) = p_0(s)x_0'(s) + q_0(s)y_0'(s). \tag{3.10}$$

The solution families are written

$$\mathbf{x} = \mathbf{p}\tau + \mathbf{x_0}(s), \tag{3.11}$$

$$u = \tau + u_0(s), \tag{3.12}$$

one for each value of $\mathbf{p}$. If either of these solutions fails to satisfy the outgoing wave condition it must be discarded.

To solve (3.4) for A_0 we observe that, along a ray,

$$\nabla A_0 \cdot \nabla u = \nabla A_0 \cdot \frac{\mathrm{d}\mathbf{x}}{\mathrm{d}\tau} = \frac{\mathrm{d}A_0}{\mathrm{d}\tau}.$$

Considering the two-dimensional case, calculating the Jacobian $J = \partial(x, y)/\partial(s, \tau)$ from (3.11) and using the following identities

$$\nabla^2 u = \nabla \cdot \mathbf{p} = p_0'(s)\frac{\partial s}{\partial x} + q_0'(s)\frac{\partial s}{\partial y}, \tag{3.13}$$

$$\begin{pmatrix} \dfrac{\partial s}{\partial x} & \dfrac{\partial s}{\partial y} \\ \dfrac{\partial \tau}{\partial x} & \dfrac{\partial \tau}{\partial y} \end{pmatrix} = J^{-1} \begin{pmatrix} \dfrac{\partial y}{\partial \tau} & -\dfrac{\partial x}{\partial \tau} \\ -\dfrac{\partial y}{\partial s} & \dfrac{\partial x}{\partial s} \end{pmatrix}, \tag{3.14}$$

we can deduce that

$$\nabla^2 u = \frac{J_\tau}{J}. \tag{3.15}$$

Putting all this into (3.4) and integrating gives us the solution as

$$A_0(s,\tau) \;=\; A_0(s,0)\left(\frac{J(s,0)}{J(s,\tau)}\right)^{1/2}. \tag{3.16}$$

We note that in higher dimensions, (3.16) will not change its form. If we are solving the problem in an $n+1$-dimensional space with data given on a manifold of dimension n then we would replace s in (3.16) with an n-dimensional vector $\mathbf{s}$.

As the energy transmitted by an acoustic or electromagnetic field is proportional to the square of the amplitude, equation (3.16) has a very nice physical interpretation as conservation of energy in a ray-tube. This implies that as the ray-tube converges to a point (as for example at a caustic of rays where $J = 0$) the amplitude of the field must become infinite. As this is unphysical, it must be the case that the ray theory appoximation breaks down at singular points or regions such as these and we need to investigate 'inner solutions' near these points.

We can see that the introduction of the ansatz solution has reduced a second-order linear elliptic PDE to 1st-order hyperbolic equations for both the phase and the leading order amplitude, which can easily be solved. Whereas the elliptic equation cannot harbour any discontinuities, the solutions to the hyperbolic equation may do so. Thus any discontinuities that occur in our solutions will have to be removed.

3.1 Illustrative Example—Geometrical Optics

Let us consider an incident plane wave $\phi_i = \exp(ikx)$ impinging on a convex cylinder in a plane perpendicular to the axis of the cylinder, with a Dirichlet boundary condition on the cylinder—the problem is thus two-dimensional. We use the normal and tangential coordinates n, s as in Figure 3.1. The angle ψ denotes the angle between the tangent and the horizontal. For a convex cylinder there will be two points where the incident field is tangential to the cylinder. For simplicity we restrict our attention to the upper of these and so are implicitly assuming that the cylinder is unbounded. Writing $\phi = \phi_i + \phi_r$, we are thus solving

$$\nabla^2\phi_r + k^2\phi_r \;=\; 0, \qquad n > 0, \tag{3.17}$$

$$\phi_r \;=\; -e^{ikx}, \quad n = 0, \tag{3.18}$$

along with an outgoing wave condition in $n > 0$.

Equation (3.11) gives us the equations for the rays once we have calculated $\mathbf{p}$. This

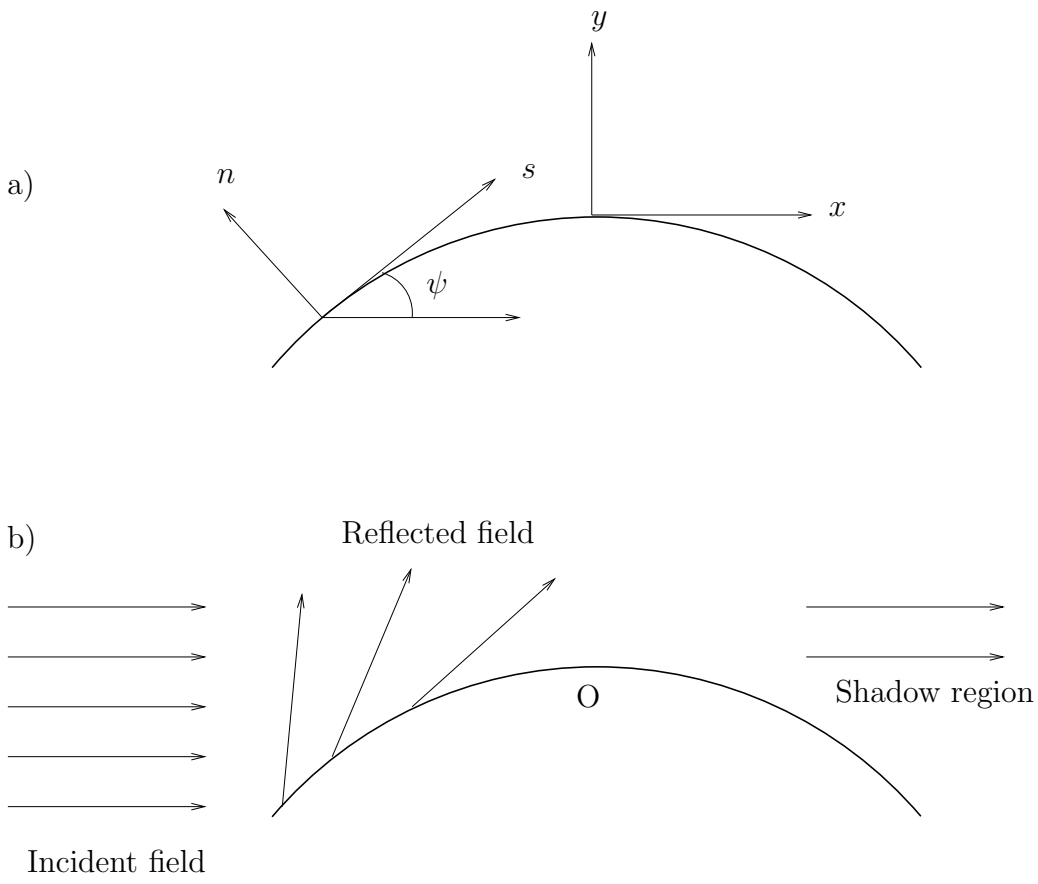


Figure 3.1: a) Normal and tangential coordinate system. b) Ray picture for geometrical optics field due to planar incident radiation on a smooth surface.

we do by solving (3.9) - (3.10). We obtain two possible values for $\mathbf{p}$ which correspond to two families of rays, namely

$$p_0 = 1, \qquad q_0 = 0, \tag{3.19}$$

and

$$p_0 = \cos 2\psi(s), \qquad q_0 = \sin 2\psi(s), \tag{3.20}$$

with initial data given on the curve

$$x = x_0(s), \quad y = y_0(s), \quad \tan\psi(s) = \frac{\mathrm{d}y_0(s)}{\mathrm{d}x_0(s)}. \tag{3.21}$$

The first set of rays has solutions

$$\mathbf{x} = (x_0(s) + \tau, y_0(s)), \tag{3.22}$$

$$u = x_0(s) + \tau, \tag{3.23}$$

and is associated with the incident radiation since $u = x$. To the left of the tangency point these rays are not outgoing and so must be discounted to satisfy the outgoing wave condition.

The second set of rays have solutions

$$\mathbf{x} = (x_0(s) + \tau\cos 2\psi(s), y_0(s) + \tau\sin 2\psi(s)), \tag{3.24}$$

$$u = x_0(s) + \tau, \tag{3.25}$$

and are reflected rays whose angle of reflection can be seen to be equal to the angle of incidence (see Figure 3.1).

We next consider the leading order amplitude functions, looking at the second set of rays first. Using (3.16) and (3.24) we find

$$\phi_{r_0}(s,\tau) = \phi_{r_0}(s,0)\left(\frac{\sin\psi}{\sin\psi - 2\tau\psi'}\right)^{\frac{1}{2}}, \tag{3.26}$$

and as we know that $\phi_{r_0}(s,0) = -1$, this forces,

$$\phi_{r_0}(s,\tau) = -\left(\frac{\sin\psi}{\sin\psi - 2\tau\psi'}\right)^{\frac{1}{2}}. \tag{3.27}$$

This solution is seen to be singular at the tangency point, *i.e.* when $\sin\psi - 2\tau\psi' = 0$. Therefore the second set of rays can only be launched from the cylinder from points

to the left of the tangency point. For the cylinder drawn in Figure 3.1, ψ' is always negative. For a general non-convex cylinder (*e.g.* the illumination of the interior of the coffee cup in Figure 1.1) we may have ψ' positive at some point to the left of the tangency point. Equation (3.27) would then imply that the amplitude along each of the rays leaving points where $\psi' > 0$ will become infinite at some point. This corresponds to a caustic of rays. Ray theory would obviously break down here as an infinite amplitude is unphysical. An inner expansion needs to be carried out in the vicinity of the caustic—see §3.2.5 for further discussion.

Solving for the amplitude of the first family of rays gives

$$\phi_{r_0}(s,\tau) \;=\; \phi_{r_0}(s,0). \tag{3.28}$$

As this family of rays only satisfies the outgoing wave condition in $x > 0$ these rays are only launched from the cylinder for $s > 0$.

If we now add in the previously subtracted incident field we find the total field is

$$\phi \;=\; \begin{cases} 0, & x > 0, y < 0, \\ e^{ikx} - \left(\dfrac{\sin\psi}{\sin\psi - 2\tau\psi'}\right)^{1/2} e^{ikx_0 + ik\left((x-x_0)^2+(y-y_0)^2\right)^{1/2}}, & \text{otherwise.} \end{cases} \tag{3.29}$$

This has a clear physical interpretation. In $x > 0, y < 0$ to leading order there is no field as the cylinder will block out the incident field. This region is termed the *shadow*. Everywhere else (the *illuminated* region) the incident field exists along with a reflected field. The incident and reflected rays are illustrated in Figure 3.1. Note that the reflected field decays as $1/\sqrt{\tau}$. This results from the divergence of the ray tube described earlier.

The Neumann boundary condition problem is solved identically—the only change being that (3.18) becomes

$$\phi_r \;=\; e^{ikx}, \quad n = 0. \tag{3.30}$$

It follows straightaway that the only change is that the second part of (3.29) becomes

$$\phi \;=\; e^{ikx} + \left(\frac{\sin\psi}{\sin\psi - 2\tau\psi'}\right)^{\frac{1}{2}} e^{ikx_0 + ik\left((x-x_0)^2+(y-y_0)^2\right)^{1/2}}. \tag{3.31}$$

The change in (3.18) can be understood by noting that locally, the cylinder appears flat, so that the rays will reflect from a given point on the cylinder as if they had been reflected from a flat plate inclined at the requisite angle. The method of images tells

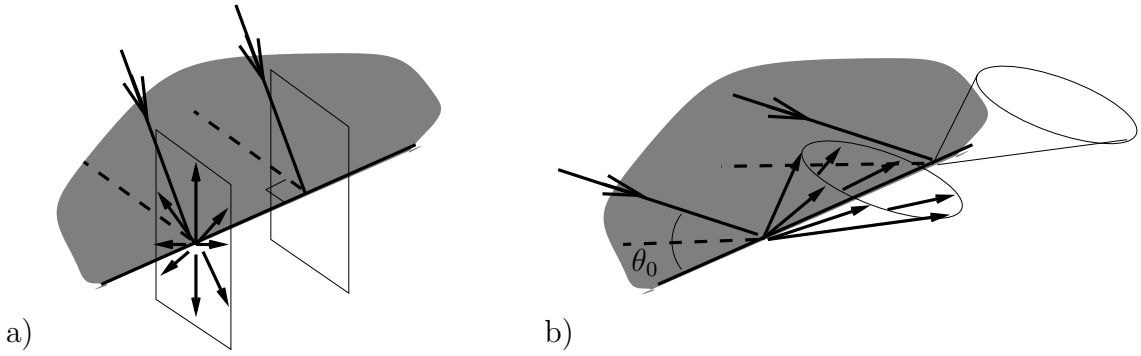
us that an incident field $\exp(ikx\cos\alpha - iky\sin\alpha)$ on an infinite plate, $y = 0$, with a Neumann boundary condition produces a reflected field $\exp(ikx\cos\alpha + iky\sin\alpha)$.

The geometrical optics solution described above can be seen to break down in two possible scenarios. The first is when we have a corner on the cylinder, *i.e.* a discontinuity in the tangent direction—what value do we take for ψ there? This singular behaviour will be investigated in §4. The second is when $\sin\psi - 2\tau\psi' = 0$. This occurs at tangency points—that is, where the incident rays are tangent to the cylinder—and at caustics of rays. The analysis at the tangency point will be described at greater length in §5. Caustics of rays occur frequently in ray tracing schemes for complex geometries (such as aircraft). As the techniques for dealing with caustics of rays are well-known (see e.g. [33]), we will not consider them further here.

3.2 Geometrical Theory of Diffraction

The Geometrical Theory of Diffraction (GTD) was developed by Keller [21], [22] in the 1950's to overcome the deficiencies of geometrical optics. Consider the examples listed in §1. The usual incident and reflected rays of geometrical optics do not explain these diffraction phenomena, defined in [21] as all those discrepancies between observations in the physical world and the predictions of geometrical optics. Since we know that an incident field on a smooth surface produces a well-behaved reflected field, it must be the case that the diffracted fields originate at the places where ray theory breaks down, such as edges, tangency points or caustics of rays. By exploiting the fact that diffraction is a local effect—*i.e.* the diffracted field produced by an incident field impinging on say an edge, is dependent solely on the nature of the edge and the value of the incident field *at* the edge—Keller describes a series of canonical diffraction problems that can be combined to produce a uniformly valid asymptotic solution to a general scattering problem. For each of the canonical problems GTD describes the diffracted rays that are set up. For a general problem we proceed as follows:

We trace the incident rays to calculate where they hit the scatterer. We then decide which local canonical problem is relevant to this ray/scatterer interaction—does it hit a smooth surface or an edge, etc? The solution to the appropriate canonical problem is used to launch diffracted rays from the interaction point. The amplitudes along these rays are determined by the canonical problem and the incident field. These rays must then be traced as they may interact further with the scatterer. A scattering problem that otherwise may only have been solved numerically has thus been reduced to a ray tracing problem.



a) b)

Figure 3.2: a) Diffracted rays when the incident ray is in a plane normal to the edge. b) Diffracted cone of rays when the incident field is in a plane oblique to the edge.

3.2.1 Edge Diffraction of a Plane Wave

Fermat's principle[2] tells us that light travelling from A to B takes the shortest possible route. In a homogenous medium there will generally be a direct straight line path. In the presence of a finite scatterer with an edge, there will also be a shortest path via the smooth part of the scatterer (corresponding to the reflected ray) and a shortest path via the edge of the scatterer (corresponding to an edge diffracted ray). In general the extremal reflected path will hit the scatterer at different places as we vary the observation point B, whereas the extremal edge diffracted path *must* go via the edge. Thus we expect a family of rays from each point on the edge. We look for an edge-diffracted field with the usual ray ansatz

$$\phi_d \sim \sum_{n=0}^{\infty} A_{d_n}(\mathbf{x})(ik)^{-n} e^{iku_d(\mathbf{x})}. \tag{3.32}$$

Remembering continuity of phase between the fields on the incident ray and diffracted rays at the edge $\mathbf{x} = \mathbf{x}(\gamma)$, we have

$$u_d(\mathbf{x}(\gamma)) = u_i(\mathbf{x}(\gamma)), \tag{3.33}$$

and hence

$$\nabla u_d \cdot \hat{\dot{\mathbf{x}}} = \nabla u_i \cdot \hat{\dot{\mathbf{x}}}, \tag{3.34}$$

where $\hat{\dot{\mathbf{x}}}$ is the unit tangent vector to the edge. We know that $|\nabla u_d| = |\nabla u_i| = 1$ as both u_d and u_i satisfy the eikonal equation. Therefore, if θ_0 and θ are the angles

[2] Although Fermat (1601-1655) originally formulated his principle to explain the laws of reflection and refraction, it is relatively straightforward to show that it is, in fact, equivalent to geometrical optics.

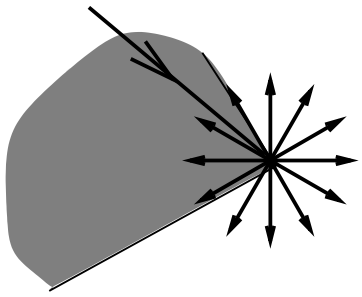


Figure 3.3: Diffraction by a conical tip.

between $\hat{\dot{\mathbf{x}}}$ and $\nabla u_i, \nabla u_d$, respectively, then

$$\cos\theta \;=\; \cos\theta_0. \tag{3.35}$$

That is to say that diffracted rays are launched at an angle θ_0 to the tangent vector. In general there are an infinite number of such directions and we will get a diffracted cone of rays from the edge—see Figure 3.2. Further details can be found in [6]. In §4 we will investigate the Sommerfeld problem in detail. This is a degenerate case of general plane wave incidence on an edge as illustrated in Figure 3.2a) where the incident rays are in a plane normal to the edge. The cone of diffracted rays flattens to become a plane.

For completeness we mention that a similar discussion is also needed to treat line discontinuities in the derivatives of the curvatures of a scattering surface (see [21]). The diffraction effects here are much smaller, and will not be considered in this thesis.

3.2.2 Conical Tips

An incident ray on a conical tip produces a spherically diffracted wavefront—*i.e.* an infinite two-parameter family of rays—from the tip, as in Figure 3.3. This can be justified again by consideration of Fermat's principle. There will be an extremal path from A to B that goes via the tip for all B exterior to the scatterer, and so we expect a diffracted ray in all directions from the tip. The problem of determining the amplitudes along the diffracted rays has not yet been solved analytically for a vertex of arbitrary cross section—although Smyshlyaev [36], [37], [38] has developed a numerical routine to evaluate the diffraction coefficients. Papers such as [27] have found the high frequency limit of the diffracted field for scattering by circular and elliptic cones, but the solution for cones of arbitrary cross section still eludes us.

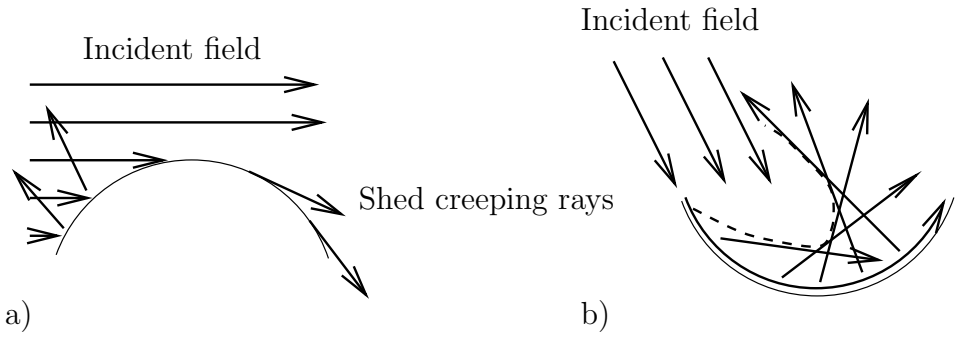


Figure 3.4: a) Diffraction by a convex scatterer. Creeping rays are shed into the shadow region. b) Diffraction by a concave scatterer. A surface field is set up close to the surface at the tangency point and follows the scatterer. The dashed line is a caustic of the reflected rays.

3.2.3 Grazing Rays

Another case where the ray theory of §3.1 breaks down is when an incident field is tangential to a scatterer. The relevant theory is covered in some detail in §5. In short, a surface field is induced close to the scatterer. On a convex body, this surface field sheds rays tangentially into the shadow region—hence the surface field decays as we travel away from the tangency point. On a concave surface, the surface field propagates along the boundary as in Figure 3.4. Importantly this surface field does not decay as we move along the boundary. Many authors have studied this area of diffraction, among them [2], [33] and [40].

3.2.4 Changes in the Material Properties

In the electromagnetic problem, a discontinuity in the permittivity or permeability of the medium results in a discontinuity in the nondimensional wave-number k. In this thesis we are only interested in the field exterior to a perfectly conducting scatterer (which means we have a zero E-M field inside the scatterer) and we found boundary conditions for the field external to the scatterer in §2.1.1. However, in general, a wave field incident on a discontinuity in a medium produces a reflected wave and a transmitted wave which travels in a different direction to the incident wave. In the case of total internal reflection the transmitted wave becomes parallel to the discontinuity and an evanescent wave field is also produced—see *e.g.* [29]. We will not go into details here, further information can be found in [6].

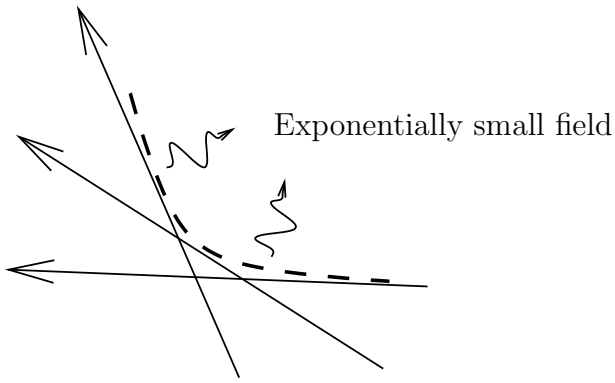


Figure 3.5: Rays passing through a caustic.

3.2.5 Caustics

We include caustics in this review of GTD as, although no scatterer is involved, a higher order diffracted field is produced that is not predicted by geometrical optics. As we approach a caustic of rays the Jacobian in (3.16) tends towards zero and so the ray solution breaks down. An inner expansion needs to be carried out around the caustic. This reveals that the amplitude along the ray remains unchanged on passing through the caustic, but that there is a $\pi/2$ jump in the phase. It also transpires that an exponentially small field exists on the other side of the caustic. This can be interpreted as *complex rays* intersecting real space on the dark side of the caustic. For a discussion of complex rays, see [9], [24]. Airy and Ludwig [25] were among the first to investigate the field at the caustic. The inner expansion about the caustic of [8] is summarised in [33].

The remainder of this thesis is devoted to working towards solving canonical source/ scatterer interaction problems which may be added to Keller's GTD as subroutines in a ray tracing solution of a general source/scatterer interaction problem.

Part II

Sources Remote from Structures

Chapter 4

Flat Structures

In §3.2.1 we described how, according to GTD, a planar wave field incident on an edge produces a conical family of rays from each point on the edge. In this chapter we will investigate this problem in more detail. We begin by reviewing the two-dimensional Sommerfeld problem of scattering of a plane wave by a semi-infinite plate. An asymptotic solution (valid for $kr \gg 1$ where r is the distance from the end of the plate) is obtained for the field in the case where the incident field is normal to the edge of the plate. We will introduce the concept of shadow boundary regions to ensure a smoothly varying field. We use this solution to construct an asymptotic description of the field scattered by a finite plate in two dimensions. The equivalence of scattering and radiation problems will be discussed before investigating a three-dimensional problem—radiation by a finite line source. We then look at extensions to the two-dimensional Sommerfeld problem—more specifically the structure of the shadow boundary regions when the illumination is due to a line source excitation at an $\mathcal{O}(1)$[1] distance from the source, and when a finite source is set up to focus its radiated energy at a point in space.

4.1 Sommerfeld Problem

This canonical problem addresses one of the areas cited in §3.1 where ray theory breaks down—that of a discontinuity in the boundary where we no longer have a well-defined tangent direction.

We consider an incident field $\phi_i = \exp(-ikr\cos(\theta-\alpha))$ impinging on the semi-infinite line $y < 0$, where r, θ are the usual polar coordinates. Imposing a homogenous

[1] In the context of the semi-infinite plate where there is no natural lengthscale, $\mathcal{O}(1)$ is taken to mean 'large compared to a wavelength.'

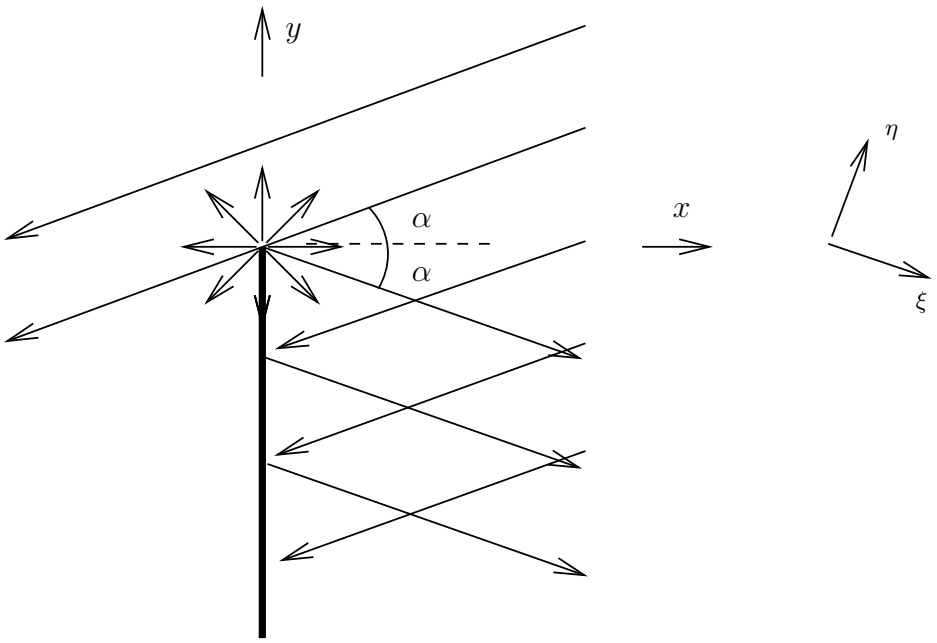


Figure 4.1: The Sommerfeld problem—incident plane wave $\exp(-ikr\cos(\theta-\alpha))$ on a half-line

Dirichlet boundary condition on the plate we are required to solve

$$\nabla^2\phi + k^2\phi = 0, \tag{4.1}$$

$$\phi = 0, \quad x = 0,\, y < 0, \tag{4.2}$$

along with an outgoing wave condition. Three possible solution techniques for this problem can be found in the literature[2]. The Wiener-Hopf technique can be used to deal with the discontinuity of the boundary data and is outlined in [4]. Sommerfeld's method involves the method of images on a two-sheeted Riemann surface and can be found in [32]. A more natural way to solve the problem is by employing the Kontorovich-Lebedev transform, see for example [28]. All three solution methods yield the result obtained by Sommerfeld, namely

$$\phi = \frac{e^{i\pi/4+ikr}}{2\sqrt{\pi}}\left(-\mathrm{Fr}\left(\sqrt{2kr}\cos\left(\frac{\theta+\alpha-\pi}{2}\right)\right)+\mathrm{Fr}\left(-\sqrt{2kr}\cos\left(\frac{\theta-\alpha}{2}\right)\right)\right), \tag{4.3}$$

where

$$\mathrm{Fr}(z) = e^{-iz^2}\int_z^\infty e^{iv^2}\,\mathrm{d}v, \tag{4.4}$$

is the Fresnel integral. This exact solution is valid for all values of kr.

[2]We remark that a fourth method, namely separation of coordinates in a parabolic coordinate system, is also at our disposal.

4.1.1 Solution Away from the Origin

For $kr \gg 1$, we can use the large argument expansions for the Fresnel integrals, see *e.g.* [1],

$$\mathrm{Fr}(z) \sim \frac{i}{2z} + O\left(\frac{1}{|z|^2}\right), \quad \mathrm{Re}(z) > 0, \tag{4.5}$$

$$\mathrm{Fr}(z) \sim \sqrt{\pi} e^{i\pi/4} e^{-iz^2} + \frac{i}{2z} + O\left(\frac{1}{|z|^2}\right), \quad \mathrm{Re}(z) < 0, \tag{4.6}$$

whereupon (4.3) can be approximated as

$$\phi \sim \begin{cases} e^{-ikr\cos(\theta-\alpha)} - e^{ikr\cos(\theta+\alpha)} + D(\theta)\dfrac{e^{ikr}}{\sqrt{kr}}, & -\pi/2 < \theta < -\alpha, \\ e^{-ikr\cos(\theta-\alpha)} + D(\theta)\dfrac{e^{ikr}}{\sqrt{kr}}, & -\alpha < \theta < \pi + \alpha, \\ D(\theta)\dfrac{e^{ikr}}{\sqrt{kr}}, & \pi + \alpha < \theta < 3\pi/2, \end{cases} \tag{4.7}$$

where

$$D(\theta) = \frac{e^{i\pi/4}}{2\sqrt{2\pi}} \left(\frac{1}{\cos\left((\theta - \alpha)/2\right)} + \frac{1}{\cos\left((\theta + \alpha - \pi)/2\right)} \right). \tag{4.8}$$

The three terms in (4.7) can be identified with the incident field, the reflected field and the diffracted field. The first two wave fields are $\mathcal{O}(1)$ plane waves. The diffracted field is $\mathcal{O}((kr)^{-1/2})$ and can be thought of as arising from a point source with non-uniform directivity placed at the origin. It can be seen that the expansion is non-uniform along the lines $\theta = -\alpha$ and $\theta = \pi + \alpha$ which are the reflected and incident *shadow boundaries* respectively. To investigate the behaviour of the field near these critical values of θ we consider the reflected shadow boundary at $\theta = -\alpha$. An identical procedure can be used to examine the incident shadow boundary at $\theta = \pi + \alpha$.

4.1.2 The Reflected Shadow Boundary Region

We wish to find a solution in the *reflected shadow boundary region*—a narrow region in the neighbourhood of the reflected shadow boundary—that provides a smooth transition between the incident and diffracted fields for $\theta > -\alpha$ and the incident, diffracted *and* reflected fields for $\theta < -\alpha$. Such a solution must exist as we know that solutions of the elliptic Helmholtz equation must be analytic away from any boundaries—*e.g.* [28].

Near the reflected shadow boundary we can write $\theta = -\alpha + \psi$, where ψ is small. We introduce the coordinates

$$\xi = x\cos\alpha - y\sin\alpha, \tag{4.9}$$

$$\eta = y\cos\alpha + x\sin\alpha. \tag{4.10}$$

The distance along the reflected shadow boundary is given by ξ and the perpendicular distance to the boundary is η. Under this transformation the homogenous Helmholtz equation becomes

$$\phi_{\xi\xi} + \phi_{\eta\eta} + k^2\phi = 0. \tag{4.11}$$

In the reflected shadow boundary region the incident field is still present and $r \sim \xi$ so we are motivated to try a solution of the form

$$\phi \sim e^{-ikr\cos(\theta-\alpha)} + A(\xi,\eta)e^{ik\xi}. \tag{4.12}$$

Substituting this into (4.11) gives us

$$A_{\xi\xi} + A_{\eta\eta} + 2ikA_\xi = 0. \tag{4.13}$$

This suggests the following scaling of η in the shadow boundary region

$$\eta = k^{-1/2}\tilde{\eta}, \tag{4.14}$$

which leads to the parabolic wave approximation in the inner shadow boundary region

$$A_{\tilde{\eta}\tilde{\eta}} + 2iA_\xi = 0. \tag{4.15}$$

To establish the matching conditions as $|\tilde{\eta}| \to \infty$, we need to write the outer solution (4.7) in terms of the inner variables $\xi, \tilde{\eta}$. When we are near the line $\theta = -\alpha$, providing $\alpha \neq \pi/2$, we can make the approximations

$$r \sim \xi + \frac{\eta^2}{2\xi}, \tag{4.16}$$

$$\cos\left(\frac{(\theta-\alpha)}{2}\right) = \mathcal{O}(1), \tag{4.17}$$

$$\cos\left(\frac{(\theta+\alpha-\pi)}{2}\right) \sim \frac{1}{2}\tan\psi = \frac{1}{2}\frac{\eta}{\xi}. \tag{4.18}$$

This gives us the matching conditions as

$$A \sim \begin{cases} -\dfrac{e^{i\tilde{\eta}^2/2\xi}}{\sqrt{2\pi}}\dfrac{\sqrt{\xi}}{\tilde{\eta}}, & \tilde{\eta} \to \infty, \\ -\dfrac{e^{i\tilde{\eta}^2/2\xi}}{\sqrt{2\pi}}\dfrac{\sqrt{\xi}}{\tilde{\eta}} - 1, & \tilde{\eta} \to -\infty. \end{cases}$$

Now (4.15) has a similarity solution

$$A = B + C\mathrm{erfc}\left(\frac{\tilde{\eta}e^{-i\pi/4}}{\sqrt{2\xi}}\right), \tag{4.19}$$

where $\mathrm{erfc}(z)$ is the complementary error function

$$\mathrm{erfc}(z) = \frac{2}{\sqrt{\pi}}\int_z^\infty e^{-t^2}\,\mathrm{d}t. \tag{4.20}$$

Using the asymptotics of $\mathrm{erfc}(z)$ for large values of the argument z

$$\mathrm{erfc}(z) \sim \begin{cases} \dfrac{e^{-z^2}}{z\sqrt{\pi}}, & z \to \infty, \\ 2 + \dfrac{e^{-z^2}}{z\sqrt{\pi}}, & z \to -\infty, \end{cases}$$

we must choose

$$B = 0, \tag{4.21}$$

$$C = -\frac{1}{2}, \tag{4.22}$$

to ensure that the two solutions match. As $\xi \to 0$ we can see that the shadow boundary field will also match to leading order with the 'initial data' given by the GO incident and reflected fields. Our shadow boundary solution is thus unique as it is the solution to a parabolic equation with initial and boundary conditions. We now have expressions for the field both away from and inside the reflected shadow boundary region. It is straightforward to confirm that (4.12), (4.19), (4.21) and (4.22) do actually give the correct solution in the shadow boundary region. We simply rewrite (4.3) in terms of $\xi, \hat{\eta}$. The first term of (4.3) becomes the complementary error function of (4.19) and the second term, upon expanding for large arguments, represents the incident field. A similar approach will remove the non-uniformity of (4.7) at the incident shadow boundary.

To solve the Sommerfeld problem with (4.2) replaced by the Neumann boudary condition

$$\frac{\partial\phi}{\partial n} = 0, \quad x = 0,\, y < 0, \tag{4.23}$$

we note that the two terms in (4.3) are both solutions of (4.1) and so we choose the linear combination that satisfies the boundary condition (4.23) on the plate—*i.e.*

$$\phi = \frac{e^{i\pi/4+ikr}}{\sqrt{\pi}}\left(\mathrm{Fr}\left(\sqrt{2kr}\cos\left(\frac{\theta+\alpha-\pi}{2}\right)\right) + \mathrm{Fr}\left(-\sqrt{2kr}\cos\left(\frac{\theta-\alpha}{2}\right)\right)\right). \tag{4.24}$$

Treatment of the shadow boundary regions will be exactly as before.

4.2 Field Due to an Excited Flat Plate

Consider a finite radiating source $x = 0$, $-1 \leq y \leq 0$ in two-dimensional space, and suppose that we wish to find the field ϕ in $x > 0$. We assume that the plate is uniformly excited along its length. This serves as a useful prototype for a distributed source which we shall consider later. We can formulate the problem as

$$\nabla^2\phi + k^2\phi = 0, \tag{4.25}$$

$$\phi = -1, \qquad x = 0,\ -1 \leq y \leq 0, \tag{4.26}$$

along with an outgoing wave condition.

We home in first on the origin, introducing an inner variable $\bar{r} = kr$. Under this length scale our finite plate looks like the semi-infinite plate of the Sommerfeld problem, and we observe that by writing $\phi = -\exp(-ikx) + \phi_s$ the problem reduces to (4.1) - (4.2) for ϕ_s. In general, a non-homogenous boundary condition on a surface is equivalent to the problem of scattering by some incident field. We can thus write

$$\phi = \frac{e^{i\pi/4+i\bar{r}}}{\sqrt{\pi}}\left(-\mathrm{Fr}\left(\sqrt{2\bar{r}}\cos\left(\frac{\theta-\pi}{2}\right)\right) + \mathrm{Fr}\left(-\sqrt{2\bar{r}}\cos\left(\frac{\theta}{2}\right)\right)\right) - e^{-ikx}. \tag{4.27}$$

If we now revert to our geometrical optics coordinate r, we can see that as we move away from the origin we will set up a shadow boundary region along the line $y = 0$, $x > 0$. A similar procedure—homing in on the lower end of the plate and introducing an inner variable here—again indicates that as we move away from the lower discontinuity into the geometrical optics field we will set up a shadow boundary layer emerging from the lower end of the plate parallel to the x-axis. Using the results from §4.1.2 and discounting the incident field we can write the solutions in the two shadow boundary regions emerging to the right as

$$\phi_u \sim -\frac{e^{ikx}}{2}\mathrm{erfc}\left(\sqrt{\frac{1}{2x}}\tilde{y}e^{-\frac{i\pi}{4}}\right), \tag{4.28}$$

$$\phi_l \sim -\frac{e^{ikx}}{2}\mathrm{erfc}\left(-\sqrt{\frac{1}{2x}}\tilde{y}_1 e^{-\frac{i\pi}{4}}\right), \tag{4.29}$$

where the subscripts represent *upper* and *lower* and

$$\tilde{y} = k^{1/2}y, \quad \tilde{y}_1 = k^{1/2}(y+1).$$

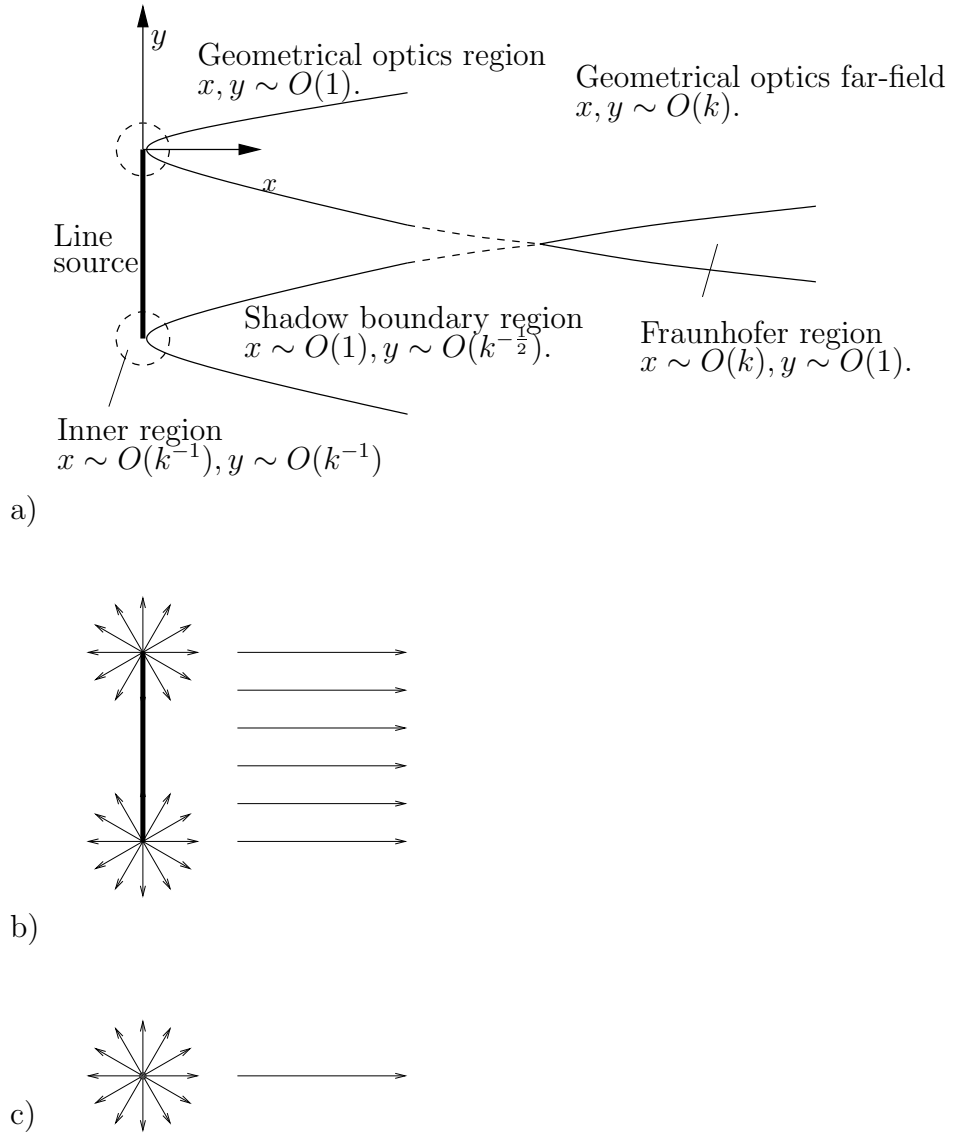


Figure 4.2: a) Asymptotic regions for the field generated by a flat plate. b) Ray picture in the geometrical optics region. c) Ray picture in the geometrical optics far-field.

4.2.1 Terminology

For a radiating source, the term 'shadow boundary' does not really make sense, as it was originally defined to be a region where the incident or reflected fields were switched off. For a radiating source there is no incident field! However, due to the equivalence of scattering and radiation problems, we will employ the term 'shadow boundary' in the context of radiating sources in the hope that this will not cause any confusion.

4.2.2 The Fraunhofer Region

The scalings of the transverse shadow boundary coordinates imply that the shadow boundary regions grow in width like $(x/k)^{1/2}$. When the shadow boundary regions have a width of $\mathcal{O}(1)$ they will merge to form what we shall refer to as the *Fraunhofer* region[3]. Writing the field in the Fraunhofer region as

$$\phi_f \quad = \quad e^{ik^2X}B(X,y), \tag{4.30}$$

where $X = x/k$ gives us the governing equation

$$B_{yy} + 2iB_X \quad = \quad 0. \tag{4.31}$$

'Initial data' is given by the outer limits of the GO and shadow boundary region solutions as $x \to \infty$. To leading order this gives

$$B(0,y) \quad = \quad \begin{cases} -1, & y \in (0,\infty), \\ -2, & y \in (-1,0), \\ -1, & y \in (-\infty,-1). \end{cases} \tag{4.32}$$

The field away from the x-axis for $X \sim \mathcal{O}(1)$ is just a diffracted field from each tip as we have discounted the incident field. This gives us the matching conditions that as $|y| \to \infty$

$$\phi_f \quad \sim \quad \frac{e^{ik^2R+i\pi/4}}{k\sqrt{2\pi R}}\left(\frac{1}{\cos\left(\frac{\theta}{2}\right)} + \frac{1}{\cos\left(\frac{\theta-\pi}{2}\right)}\right), \tag{4.33}$$

where $R = r/k$. We can check that the unique solution to (4.30), (4.31), (4.32) and (4.33) is

$$B \quad = \quad -\frac{1}{2}\left(\mathrm{erfc}\left(\sqrt{\frac{1}{2X}}ye^{-\frac{i\pi}{4}}\right) + \mathrm{erfc}\left(-\sqrt{\frac{1}{2X}}(y+1)e^{-\frac{i\pi}{4}}\right)\right) + 1. \tag{4.34}$$

[3]In the literature the term 'Fraunhofer diffraction' describes the field at distances from the scatterer/source that are large compared to the size of the scatterer/source. This is distinct from 'Fresnel diffraction' which describes the field at distances from the scatterer/source that are large compared to a wavelength of the radiation.

This is just the sum of the two shadow boundary fields with the incident field subtracted off to ensure that the initial data is satisfied.

For $X = \mathcal{O}(1)$, comparing (4.33) to (4.34) we see that the geometrical optics far-field decays like $1/\sqrt{R}$ except along the x-axis where we have a beam which is Gaussian in profile.

In the case that the excitation varies along the plate we can use the local effect of diffraction at each end of the plate to describe the fields. Provided that our boundary condition is of the form

$$\phi(y) \quad = \quad f(y)e^{ig(k,y)}, \quad x = 0, -1 \leq y \leq 0, \tag{4.35}$$

where either $g \sim o(k)$ or $g = k\hat{g}(y)$ for some $\hat{g}$, where $\hat{g}$ varies on an $\mathcal{O}(1)$ length scale with respect to y and $|\hat{g}'(0)| < 1$, we are able in principle to carry out the analysis at each end of the plate as described above. If $g \sim o(k)$ then in an $\mathcal{O}(k^{-1})$ region about the end of the plate the excitation will appear constant—that is to say that the inner region about the end of the plate will be exactly the Sommerfeld problem of §4.1. If $g = k\hat{g}(y)$ then in the inner-inner region around the tip, we may expand $\hat{g}$ to give

$$g(\bar{y}) \quad \sim \quad k\hat{g}(0) + \bar{y}\cos\alpha, \tag{4.36}$$

for some α, where $\bar{y} = ky$. This is just the Sommerfeld problem of §4.1. Thus a shadow boundary region will emerge to the right of the plate end at an angle of$-\pi/2 + \alpha$ to the positive x-axis. Obviously if the value of α is different at both ends of the plate we will not in general produce a Fraunhofer region as the two shadow boundaries will either diverge or converge and cross over. If $g(y) = k\hat{g}(y)$ with $|\hat{g}'(0)| > 1$ then the scattered field must be described in terms of complex rays—*i.e.* the angle α in (4.36) will necessarily be complex. See [9] for a discussion on complex rays.

The Neumann equivalent to (4.35) is identical except that we must now write

$$\phi \quad = \quad e^{-ikx} + \phi_s, \tag{4.37}$$

to reduce the problem to the Sommerfeld problem with a Neumann boundary condition for ϕ_s.

4.3 Ray Picture for a General Radiating Source

We have seen that a radiating source in free space is equivalent to a (possibly contrived!) scattering problem and so, calling upon the GTD of §3.2, we can describe

the ray picture for an arbitrary radiating body. In general, there will be a single ray launched from each interior point of the source corresponding to the reflected field of the scattering problem. In addition we have to launch a cone of rays from each point on any edges and a spherical family, or 'hedgehog', of rays from any vertices. See Figure 4.3. Line or point discontinuities of the source must be treated in the same way as edges and corners.

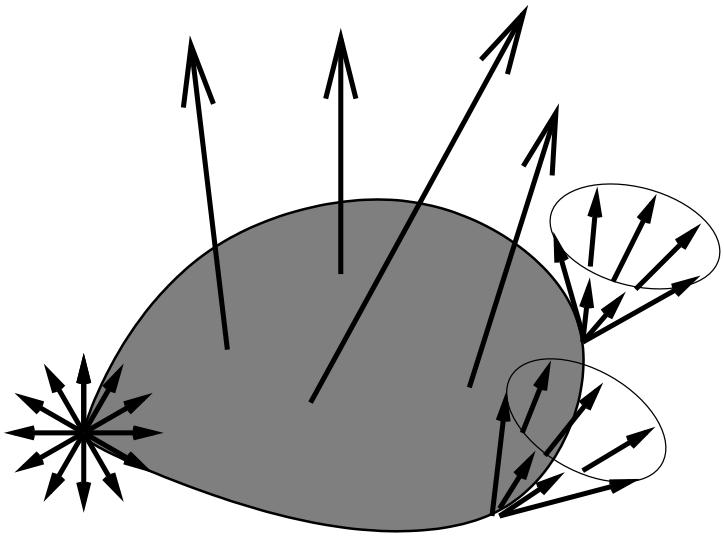


Figure 4.3: Ray picture for a radiating source. One ray is launched from each interior point, a cone of rays from each edge point and a spherical hedgehog from each corner.

4.4 Field Due to an Antenna in Three Dimensions

We can model many antennas much more realistically as line sources in three dimensions. Unfortunately the Sommerfeld problem is two-dimensional and so we must now use a different method to solve for ϕ. In addition, the comments in §2.3.4 concerning the decomposition of the E-M fields into two scalar fields do not apply in their present form to this problem. After dealing with the representation of this vector problem as a scalar one, we will follow the procedure of the last section. We will find an asymptotic representation of the field due to a semi-infinite line source and then, using the local effect of 'diffraction' at each tip, will be able to determine the field due to a finite line source in free space.

4.4.1 Axi-symmetric E-M Field

We will work in cylindrical coordinates r, θ, z with unit vectors $\mathbf{e}_{r,\theta,z}$ in the appropriate directions. Assuming no dependence on the angular coordinate, equations (2.27) -

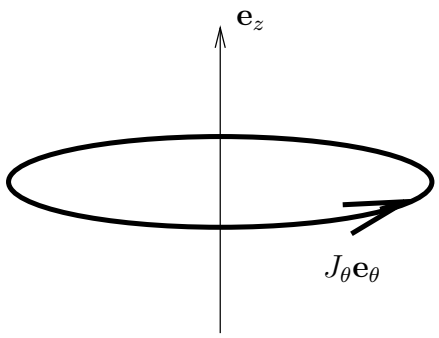


Figure 4.4: Infinitesimal current rings about the axis.

(2.28) yield

$$H_r = \frac{1}{ik}\frac{\partial E_\theta}{\partial z}, \tag{4.38}$$

$$H_z = \frac{1}{ik}\left(\frac{\partial E_\theta}{\partial r} + \frac{E_\theta}{r}\right), \tag{4.39}$$

$$E_r = \frac{1}{ik}\left(-\frac{\partial H_\theta}{\partial z} + J_r\right), \tag{4.40}$$

$$E_z = \frac{1}{ik}\left(-\frac{\partial H_\theta}{\partial r} + \frac{E_\theta}{r} + J_z\right). \tag{4.41}$$

That is to say that Maxwell's equations are reduced to solving for the components of the $\mathbf{E}, \mathbf{H}$ fields in the θ direction, namely

$$\nabla^2 E_\theta + k^2 E_\theta = -ikJ_\theta, \tag{4.42}$$

$$\nabla^2 H_\theta + k^2 H_\theta = \nabla \wedge \mathbf{J} \centerdot \mathbf{e}_\theta. \tag{4.43}$$

For the purposes of modelling an antenna the current is concentrated in a small region about an axis, say $r = 0$. Then (4.42), (4.43) correspond to solving for the angular components of the field due to infinitesimal current rings about the axis[4]—see Figure 4.4. We would then write

$$\mathbf{J} = J_\theta \mathbf{e}_\theta = J(z)\delta(r)\mathbf{e}_\theta, \tag{4.44}$$

for some $J(z)$. This will mean that the right-hand side of (4.43) is zero.

4.4.2 Semi-infinite Line Source

Let us take a semi-infinite line source on $z \geq 0, r = 0$, where $r = (x^2 + y^2)^{1/2}$, along with a prescribed source current excitation. From the arguments in section 4.4.1 it

[4]An infinitesimal current ring J_θ is equivalent to an infinitesimal 'magnetic current' M_z that is to be found in the engineering literature.

will be sufficient to solve

$$\nabla^2\phi + k^2\phi \;=\; \delta(r)H(z)e^{ikz\cos\alpha}, \tag{4.45}$$

along with an outgoing wave condition. This source is described as having a *phase coherence of* α.

Taking a Fourier transform[5]

$$\bar{\phi}(s) \;=\; \int_{-\infty}^{\infty}\phi(z)e^{isz}\,\mathrm{d}z, \tag{4.46}$$

of (4.45) yields

$$\bar{\phi}(r,s)_{rr}+\frac{1}{r}\bar{\phi}(r,s)_r+\frac{1}{r^2}\bar{\phi}(r,s)_{\theta\theta}+(k^2-s^2)\bar{\phi} = \delta(r)\Big(\frac{i}{s+k\cos\alpha}+\pi\delta(s+k\cos\alpha)\Big). \tag{4.47}$$

For a proof that

$$\overline{H(s)} \;=\; \frac{i}{s}+\pi\delta(s), \tag{4.48}$$

see Appendix A. The separable solution to (4.47) away from the forcing on the right hand side is

$$\bar{\phi} \;=\; \left(\sum_n A_n H_n^{(1)}\left(\left(k^2-s^2\right)^{\frac{1}{2}}r\right)+\sum_n B_n H_n^{(2)}\left(\left(k^2-s^2\right)^{\frac{1}{2}}r\right)\right)\cos n\theta, \tag{4.49}$$

where the $H_n^{(i)}$ are Hankel functions. To satisfy the outgoing wave condition we need first to look at the asymptotic representations of the Hankel functions for large argument z, namely

$$H_n^{(1)}(z) \;\sim\; \sqrt{\frac{2}{\pi z}}e^{i(z-n\pi/2-\pi/4)}, \tag{4.50}$$

$$H_n^{(2)}(z) \;\sim\; \sqrt{\frac{2}{\pi z}}e^{i(-z-n\pi/2-\pi/4)}. \tag{4.51}$$

Taking the branch cuts of $(k^2-s^2)^{1/2}$ to be $(-\infty,-k]$ and $[k,\infty)$ with $(k^2-s^2)^{1/2}=k$ when $s=0$, then to satisfy the outgoing wave condition we must set the B_n's equal

[5]In general, given a distributed source, the Fourier transform is a convenient method of obtaining the solution. Because we do not know the behaviour of the scattered field everywhere along the $y-$axis in advance, we were unable to use the Fourier transform to solve (4.1) - (4.2). Without knowledge of the field along the axis we are unable to specify the regions of the complex plane where the Fourier transform would be valid.

to zero. To calculate the A_n's we insert (4.49) into the left-hand side of (4.47) and integrate over a disc $r \leq \epsilon$ and then let $\epsilon \to 0$. To do this we need to use asymptotic representations of Hankel functions for small arguments, namely

$$H_n^{(1)}(z) \sim \begin{cases} \dfrac{2i}{\pi} \ln z, & n = 0, \\ -\dfrac{i\Gamma(n)}{\pi} \left(\dfrac{z}{2}\right)^{-n}, & n \neq 0. \end{cases}$$

To ensure convergence of the integral we must choose

$$A_n = \begin{cases} 0, & n \neq 0, \\ -\dfrac{i}{4} \left(\dfrac{i}{s + k\cos\alpha} + \pi\delta(s + k\cos\alpha) \right), & n = 0. \end{cases}$$

Upon inverting the Fourier transform and using (4.50) in place of the Hankel functions under the assumption that $r \sim \mathcal{O}(1)$, we obtain

$$\phi \;=\; -\frac{i\sqrt{2}e^{-i\pi/4}}{8\pi^{3/2}} \int_{-\infty}^{\infty} \Big(\frac{i}{s + k\cos\alpha} + \pi\delta(s + k\cos\alpha) \Big) \frac{e^{i(k^2 - s^2)^{1/2} - isz}}{(k^2 - s^2)^{1/4} r^{1/2}} \, \mathrm{d}s. \tag{4.52}$$

To ensure convergence of the (4.52) we take the contour of integration to come in from $-\infty$ above the left branch cut and to go out towards ∞ below the right branch cut.

We can directly evaluate the δ-function contribution in (4.52) and so will ignore it for the moment. Let ϕ' be ϕ with the δ-function contribution removed. If we make the change of variables $s = kt$ and in addition write

$$z \;=\; \rho\cos\psi, \tag{4.53}$$

$$r \;=\; \rho\sin\psi, \tag{4.54}$$

$$\rho^2 \;=\; r^2 + z^2, \tag{4.55}$$

then (4.52) becomes

$$\phi' \;\sim\; \frac{1}{4\sqrt{2}\pi^{\frac{3}{2}}} e^{\frac{i\pi}{4}} \int_{-\infty}^{\infty} \frac{\exp\left(ik\rho \left(\sqrt{1 - t^2}\sin\psi - t\cos\psi \right) \right) \, \mathrm{d}t}{t + \cos\alpha}, \tag{4.56}$$

which is in a suitable form to be evaluated via the method of steepest descents as $k \to \infty$—see *e.g.* [18]. The saddle point is at $t = -\cos\psi$ and the steepest descents contribution is

$$\phi_s \;\sim\; -\frac{e^{ik\rho}}{4k\rho\pi\left(\cos\psi - \cos\alpha\right)}. \tag{4.57}$$

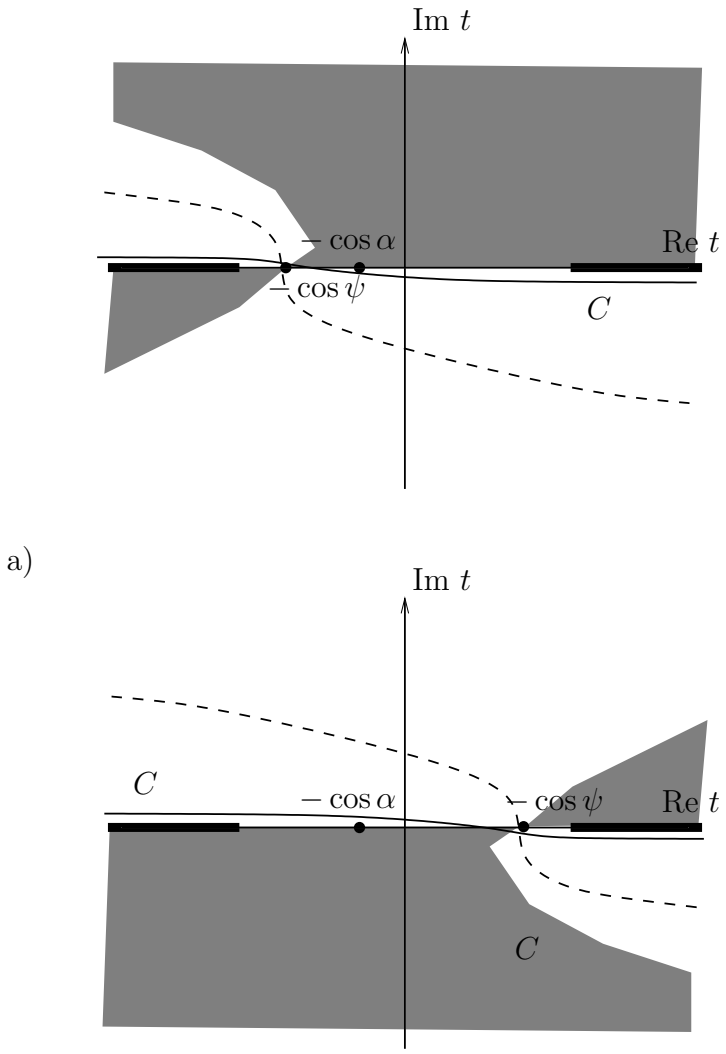


Figure 4.5: a) Contours of integration for (4.52) with $0 < \psi < \pi/2$. The dashed line is the steepest descents contour through $t = -k\cos\psi$. The shaded regions are the 'hills' of the exponent in the integrand in (4.52) with respect to the value at $-\cos\psi$. C is the contour obtained by initially deforming the real axis. b) As for a), but with $\pi/2 < \psi < \pi$.

Figure 4.5 shows the steepest descent contours along with the original integration path and the 'hills' of the exponent with respect to the saddle point. We now need to compare ϕ_s and ϕ. We look at the two possible ranges of the value of ψ.

a) $0 < \psi < \frac{\pi}{2}$

We first deform the integration contour into the steepest descents path going through the saddle point (see Figure 4.5). The pole contribution from $t = -\cos\alpha$ is enclosed in a positive sense—*i.e.* anticlockwise—if $\psi > \alpha$ and in a negative sense if $\psi < \alpha$. We can therefore say that

$$\begin{aligned} \phi &\sim \phi_s + (\delta - \text{function contribution}) \\ &\quad -(\pi i \times \text{residue from pole} \times \text{sgn}(\alpha - \psi)). \end{aligned} \tag{4.58}$$

This gives us ϕ in the geometrical optics region for $0 < \psi < \frac{\pi}{2}$ as

$$\phi \sim -\frac{i}{4}\sqrt{\frac{2}{\pi kr\sin\alpha}}e^{ikr\sin\alpha+\frac{i\pi}{4}}e^{ikz\cos\alpha} - \frac{ie^{ik\rho}}{4\pi k\rho\,(\cos\psi - \cos\alpha)}, \tag{4.59}$$

with the first term only present if $\alpha > \psi$.

b) $\frac{\pi}{2} < \psi < \pi$

We again deform the real axis into the steepest descents contour through the saddle point and consider the sense in which the poles are enclosed. We arrive at the same expression for ϕ as (4.59).

Equation (4.59) reveals that there is a conical wave launched at an angle α to the z-axis and a lower order spherically diffracted wavefront from the discontinuity at the origin—see Figure 4.6. Although (4.45) is not quite the three-dimensional equivalent of (4.1) - (4.2), there is a marked similarity between the forms of the two solutions. In both cases there is a leading order field from all points of the source and a higher order field from the end points or discontinuities. In the Sommerfeld problem the leading order field is a plane wave, whereas for the line source it is a cylindrical wave. The higher order diffracted field is a cylindrical wave for the Sommerfeld problem and a spherical wave for the line source. In §4.1.1 we also commented that the diffracted field from the edge of the semi-infinite plate could be viewed as the field due to a line source along the edge. This is substantiated here as the diffracted field for the Sommerfeld problem and the leading order field from the line source are both cylindrical wave fields.

We remark that the above analysis only holds for the case $\alpha > 0$. A canonical related problem for small α is considered in Appendix B for illustrative purposes.

4.4.3 Axi-symmetric Shadow Boundary Region

The expansion (4.59) becomes non-uniform when $\cos\psi - \cos\alpha = \mathcal{O}(k^{-1/2})$. As for the Sommerfeld problem, we require an expansion to examine this shadow boundary region, $\psi = \alpha$. From the arguments above, the analytical cause of this shadow boundary region is the coalescence of the pole and the saddle point in (4.56).

We proceed as in §4.1.2, first making the coordinate change

$$\xi = r\sin\alpha + z\cos\alpha, \tag{4.60}$$

$$\eta = z\sin\alpha - r\cos\alpha, \tag{4.61}$$

upon which the homogeneous Helmholtz equation becomes

$$\phi_{\xi\xi} + \phi_{\eta\eta} + \frac{\phi_\xi \sin\alpha - \phi_\eta\cos\alpha}{\xi\sin\alpha - \eta\cos\alpha} + k^2\phi = 0. \tag{4.62}$$

In the shadow boundary region, $r \sim \xi$. Anticipating a conical wave, we are motivated by our work in two-dimensions to look for a solution of the form

$$\phi \sim A(\xi,\eta)\frac{e^{ik\xi}}{\sqrt{\xi}}. \tag{4.63}$$

Putting this into (4.62) the sensible scaling in the shadow boundary region is

$$\eta = k^{-1/2}\tilde{\eta}. \tag{4.64}$$

This produces the leading order equation

$$A_{\tilde{\eta}\tilde{\eta}} + 2iA_\xi = 0. \tag{4.65}$$

As $k \to \infty$ the shadow boundary solution must match into (4.59), giving us the matching conditions

$$A \sim \begin{cases} -\dfrac{ie^{\frac{i\tilde{\eta}^2}{2\xi}}}{4\pi\sqrt{k}}\dfrac{\sqrt{\xi}}{\tilde{\eta}}, & \tilde{\eta}\to\infty, \\ -\dfrac{ie^{\frac{i\tilde{\eta}^2}{2\xi}}}{4\pi\sqrt{k}}\dfrac{\sqrt{\xi}}{\tilde{\eta}} - \dfrac{ie^{i\pi/4}}{4}\sqrt{\dfrac{2}{\pi k}}, & \tilde{\eta}\to-\infty. \end{cases}$$

As in §4.1.2 we have an error function solution to (4.65) and the matching conditions yield the final solution in the shadow boundary region as

$$\phi \sim \frac{e^{ik\xi+i\pi/4}}{8\sqrt{\xi}}\sqrt{\frac{2}{\pi}}\left(\operatorname{erfc}\left(\frac{\tilde{\eta}}{\sqrt{2\xi}}e^{-i\pi/4}\right) - 2\right). \tag{4.66}$$

The comments about uniqueness made in §4.1.2 also apply here. Since the field radiated by a semi-infinite line source has the same asymptotic structure as the scattered field in the Sommerfeld problem we expect a similar behaviour to §4.2 when we make our line source finite in length. We check the validity of this assumption next.

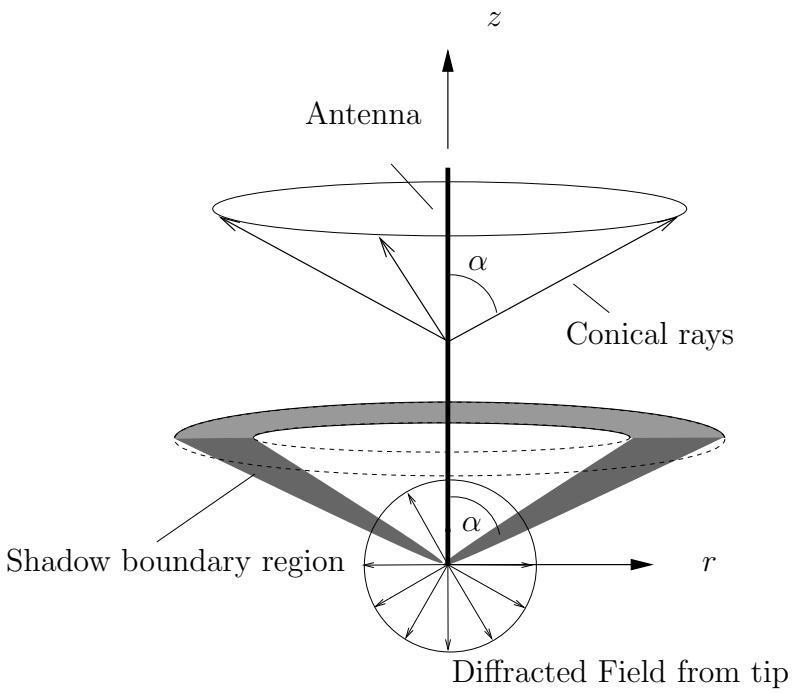


Figure 4.6: Ray picture for a semi-infinite antenna with phase coherence of α.

4.5 Field Due to a Finite Antenna

Let us take a line source between the points $(0,0,0)$ and $(0,0,1)$ with a uniform strength of 1—although we note that we can deal with non-constant excitation just as in §4.2.

As before, zooming in on an $\mathcal{O}(k^{-1})$ inner region around either end of the line source reduces the problem locally to each end to that of a semi-infinite line source. Section 4.4.2 predicts a shadow boundary perpendicular to the source emerging from each end in which the solutions can be written

$$\phi_u \sim \frac{\sqrt{2}e^{ikr+\frac{i\pi}{4}}}{4\sqrt{k\pi r}}\left(-1+\frac{1}{2}\mathrm{erfc}\left(\frac{\tilde{z}}{\sqrt{2r}}e^{-\frac{i\pi}{4}}\right)\right), \tag{4.67}$$

$$\phi_l \sim \frac{\sqrt{2}e^{ikr+\frac{i\pi}{4}}}{4\sqrt{k\pi r}}\left(-1+\frac{1}{2}\mathrm{erfc}\left(\frac{\tilde{z}_1}{\sqrt{2r}}e^{-\frac{i\pi}{4}}\right)\right), \tag{4.68}$$

where $\tilde{z}=k^{1/2}z$, $\tilde{z}_1=k^{1/2}(1-z)$. For general non-constant excitation of the source the shadow boundary regions emerging from each tip will be conical.

The asymptotics of §4.2 hold here and we can deduce the existence of a Fraunhofer region at an $\mathcal{O}(k)$ distance from the line source where the shadow boundaries merge. Once again the field will be strongest in the direction perpendicular to the source,

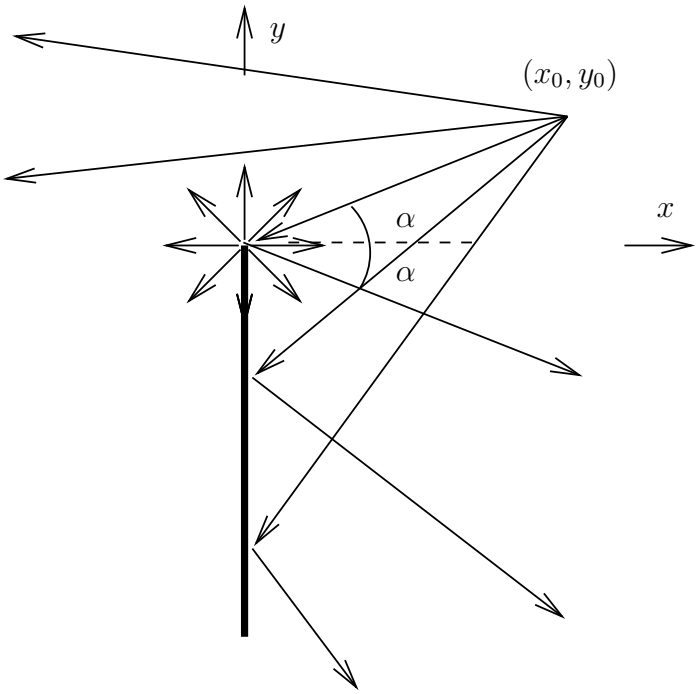


Figure 4.7: Scattered field due to a line source parallel to the edge of a semi-infinite plate.

but we have an additional $1/\sqrt{r}$ decay imposed on the field everywhere in the axi-symmetric Fraunhofer region over that in the Fraunhofer region of §4.2.2. Figure 4.2 is also valid for the axi-symmetric case provided that x, y are interpreted as r, z, respectively.

4.6 Sommerfeld Problem with Line Source Illumination

In §4.1 we investigated the asymptotic behaviour of the scattered field induced by an incident plane wave on a semi-infinite plate. We described the behaviour of the $\mathcal{O}(k^{-1/2})$ shadow boundary regions where there is an error function solution. We also observed that for the case of scattering by a finite plate the shadow boundaries from either end meet at an $\mathcal{O}(k)$ distance from the plate. We now consider the illumination of a semi-infinite plate by radiation from a line source parallel to the edge of the plate. We will assume that the line-source is of unit strength and at an $\mathcal{O}(1)$ distance from the edge. Jones, [19] investigates this problem, leaving the solution as an integral but says nothing about the shadow boundary regions that will necessarily exist and have a different behaviour from those found in §4.1.

4.6.1 Geometrical Optics Field

Our two-dimensional problem is

$$\nabla^2\phi + k^2\phi = -\delta(x-x_0)\delta(y-y_0), \tag{4.69}$$

$$\phi = 0, \quad x=0,\, y<0. \tag{4.70}$$

In the absence of the plate the solution to (4.69) that satisfies the radiation condition is

$$\phi_{inc} = \frac{i}{4}H_0^{(1)}\left(k\left((x-x_0)^2+(y-y_0)^2\right)^{1/2}\right). \tag{4.71}$$

Introducing inner coordinates at the origin

$$\bar{x} = kx, \quad \bar{y} = ky, \tag{4.72}$$

and using the assumption that the line source is an $\mathcal{O}(1)$ distance from the origin lets us write the incident field at the origin as

$$\phi_{inc} \sim \frac{i}{4}\sqrt{\frac{2}{k\pi r_0}}e^{-i\pi/4+ikr_0}e^{-ix_0\bar{x}-iy_0\bar{y}}, \tag{4.73}$$

$$r_0^2 = x_0^2+y_0^2. \tag{4.74}$$

This is a plane wave incident on the origin with an angle of incidence $\alpha = \arctan(y_0/x_0)$ to the positive x axis. This means that we can call upon §4.1 immediately to say that there will be an incident field in $-\pi/2 < \theta < \pi+\alpha$, a reflected field in $-\pi/2 < \theta < -\alpha$ and a diffracted field everywhere. Reflected rays can be drawn from every point of the plate away from the origin with the angle of reflection equal to the angle of incidence, and the method of images indicates that the solution along the reflected rays will be

$$\phi_r \sim -\frac{i}{4}\sqrt{\frac{2}{k\pi(r_0+\tau)}}e^{-i\pi/4+ik\tau_1}e^{ik\tau}, \tag{4.75}$$

where τ is the distance along the reflected ray. The diffracted field can be written down from (4.7) as

$$\phi_d = -\frac{ie^{i\pi/4+ikr_0+ikr}}{8k\pi\sqrt{r_0 r}}\left(\frac{1}{\cos((\theta-\alpha)/2)}+\frac{1}{\cos((\theta+\alpha-\pi)/2)}\right). \tag{4.76}$$

Unsurprisingly the expansion for the field will become non-uniform near $\theta = -\alpha$ and $\theta = \pi+\alpha$ which are the reflected and incident shadow boundaries respectively.

4.6.2 Reflected Shadow Boundary

To investigate the solution in the reflected shadow boundary region we first remove the incident field as it is present everywhere. We set $\alpha = 0$ by fixing $y_0 = 0$. Making the usual scaling in the shadow boundary region $\tilde{y} = k^{1/2}y$ and looking for a solution of the form $\phi = e^{ikx}A(x, \tilde{y})$ leaves us with the leading order shadow boundary problem

$$A_{\tilde{y}\tilde{y}} + 2iA_x = 0, \tag{4.77}$$

$$A(0, \tilde{y}) = \begin{cases} 0, & \tilde{y} > 0, \\ \dfrac{i}{4}\sqrt{\dfrac{2}{k\pi}}\dfrac{\exp\left(ik\left(x_0^2 + \frac{\tilde{y}^2}{k}\right)^{1/2}\right)}{\left(x_0^2 + \frac{\tilde{y}^2}{k}\right)^{1/4}}, & \tilde{y} < 0. \end{cases} \tag{4.78}$$

Taking a Fourier transform of (4.77) with respect to $\tilde{y}$ gives the solution to the transformed equation as

$$\bar{A}(s, \tilde{y}) = \bar{A}(0, \tilde{y})e^{-is^2/2}, \tag{4.79}$$

where s is the Fourier variable. To obtain the solution to the original problem we apply the convolution theorem to (4.79)

$$A = \int_{-\infty}^{\infty} A(0, \tilde{y} - s)f(x, s)\,\mathrm{d}s, \tag{4.80}$$

where

$$f(x, s) = \frac{1}{2\pi}\int_{-\infty}^{\infty} \exp\left(\frac{-is^2}{2} - is\tilde{y}\right)\,\mathrm{d}s. \tag{4.81}$$

After tedious calculations, we can rewrite (4.80) as

$$A = -\frac{i}{8}\sqrt{2\pi k}\frac{\exp\left(ikx + \frac{i\tilde{y}^2}{2(x+x_0)}\right)}{\sqrt{x + x_0}}\mathrm{erfc}\left(-\frac{\tilde{y}}{\sqrt{x + x_0}}\sqrt{\frac{x_0}{2x}}e^{-i\pi/4}\right). \tag{4.82}$$

Expanding (4.82) for large $\tilde{y}$, it is easy to check that this does in fact match into the outer geometrical optics solution. In addition, it is satisfying to note that if we let $x_0 \to \infty$ and scale the source strength by $\exp(ikx_0)/\sqrt{x_0}$ we recover the shadow boundary solution (4.19) for plane wave incidence.

For the case $\alpha \neq 0$ we replace x, y in (4.77) - (4.82) with ξ, η as defined in (4.9) - (4.10).

The incident shadow boundary can be dealt with identically. To solve the same problem with (4.70) replaced by

$$\frac{\partial\phi}{\partial x} = 0, \quad x = 0,\, y < 0, \tag{4.83}$$

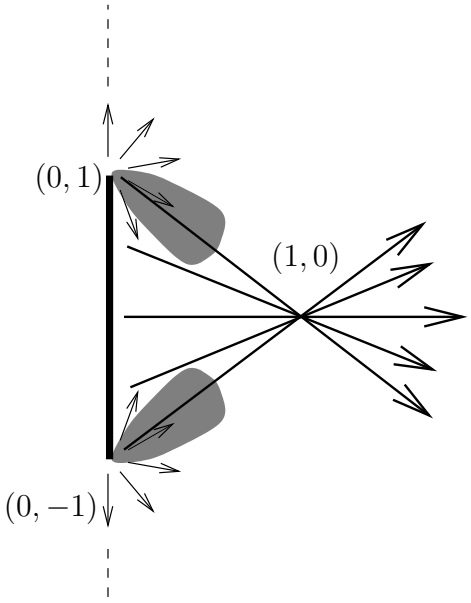


Figure 4.8: Leading order rays from the source all pass through the focal point $(1, 0)$.

the only change is the disappearance of the minus sign in front of (4.75). The rest of the analysis will carry through with the final solution being identical to (4.82) with no minus sign out in front.

Perhaps the biggest qualitative difference between the Sommerfeld problem for plane wave incidence and for line source illumination of a finite scatterer is that in the former, a Fraunhofer region is set up at an $\mathcal{O}(k)$ distance from the scatterer where the two parallel shadow boundary regions merge. This will not happen in the latter case as the two shadow boundary regions will diverge with an $\mathcal{O}(1)$ angle between them at infinity.

4.7 Converging Shadow Boundary Regions

It is possible for a suitably designed finite source to radiate in such a way that the shadow boundaries from each end meet at a point. We might expect the behaviour of the field in the vicinity of the singularity of the rays to depend on how far from the source we are—are we in the geometrical optics region or the geometrical optics far-field where the Fraunhofer region may already have been set up? We will not describe asymptotic solutions in this case; rather, we will use the exact solution for a line source in two dimensions formulated by consideration of an integral of the Green's function over the source. As we will only obtain a qualitative description of the behaviour of the shadow boundary regions here, we will investigate just the

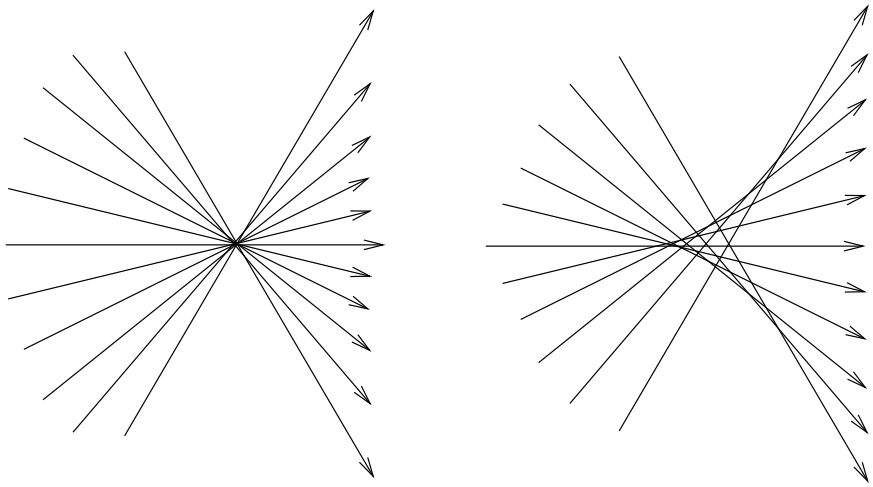


Figure 4.9: The point caustic formed when rays converge *at* a point and the line caustics arising when rays *almost* converge at a point.

Dirichlet boundary data problem.

Before doing so, we note that the cases where the rays converge *at* a point and where they *almost* converge at a point are very different. This is illustrated in Figure 4.9. In the first, the rays form a point caustic. In the second, line caustics and cusps occur. Saward, [33] investigates a specific example of the latter.

We first pose the problem

$$\nabla^2\phi + k^2\phi = 0, \tag{4.84}$$

$$\phi = \frac{e^{-ik(1+y^2)^{1/2}}}{(1+y^2)^{1/4}}, \quad x = 0,\ -1 \le y \le 1, \tag{4.85}$$

which corresponds to a line-source set up to focus its rays at the point $(1, 0)$. This can be verified by solving the ray equations of §3 and eliminating one set of solutions by invoking the outgoing wave condition. Using the large argument approximation for the Hankel function of the 1st kind—the Green's function for a point source in two dimensions—the radiated field can be written

$$\phi \sim -\frac{1}{4}\sqrt{\frac{2}{k\pi}}e^{i\pi/4}\int_{-1}^{1}\frac{e^{ik\left(x^2+(y-z)^2\right)^{1/2}}}{\left(x^2+(y-z)^2\right)^{1/4}}\frac{e^{-ik(1+z^2)^{1/2}}}{(1+z^2)^{1/4}}\,\mathrm{d}z. \tag{4.86}$$

Performing a stationary phase analysis on this integral yields

$$\phi \sim -\frac{e^{i\pi/4}}{2k}\frac{\left((x-1)^2+y^2\right)^{1/4}}{(x-1)}e^{\pm i\pi/4\mp ik\left((x-1)^2+y^2\right)^{1/2}}$$
$$+\frac{2^{1/4}}{\sqrt{\pi}}\frac{e^{-i\pi/4}}{4k^{3/2}}\frac{1}{g(1)}\frac{e^{ikf(1)}}{\left(x^2+(y-1)^2\right)^{1/4}} - \frac{2^{1/4}}{\sqrt{\pi}}\frac{e^{-i\pi/4}}{4k^{3/2}}\frac{1}{g(-1)}\frac{e^{ikf(-1)}}{\left(x^2+(y+1)^2\right)^{1/4}}, \tag{4.87}$$

where

$$f(z) = \left(x^2 + (y-z)^2\right)^{1/2} - \left(1+z^2\right)^{1/2}, \tag{4.88}$$

$$g(z) = -\frac{(y-z)}{(x^2+(y-z)^2)^{1/2}} - \frac{z}{(1+z^2)^{1/2}}, \tag{4.89}$$

and we take the upper sign in (4.87) for $x < 1$ and the lower sign for $x > 1$. The leading order term is only present in

$$-1 < \frac{y}{1-x} < 1.$$

This is clearly a ray picture—Figure 4.8. The dominant stationary phase contribution corresponds to rays from the centre of the source and the higher order terms to the diffracted rays from either end of the source. We note that there is a $\pi/2$ jump in the phase as the rays pass through the focal point. The expansion (4.87) is non-uniform when $g(\pm 1) = \mathcal{O}(k^{-1/2})$. Provided that we are an $\mathcal{O}(1)$ distance from the focal point, this occurs when $\pm y - x + 1 = \mathcal{O}(k^{-1/2})$. These are the shadow boundary regions introduced in §4.1. The discussions in §4.1 indicate that these shadow boundary regions will grow in width like $\mathcal{O}(k^{-1/2})$. We *expect* the shadow boundaries from either end of the source to meet at an $\mathcal{O}(k^{-1/2})$ distance from the point $(1,0)$ as there is an $\mathcal{O}(1)$ angle between them. Thus motivated, we make the scalings

$$\bar{x} = k^{1/2}(1-x), \quad \bar{x} > 0, \tag{4.90}$$

$$\bar{y} = k^{1/2} y, \tag{4.91}$$

whereupon (4.86) becomes

$$\phi = -\frac{e^{i\pi/4}}{4}\sqrt{\frac{2}{k\pi}}\int_{-1}^{1} \frac{\exp\left(-ik^{1/2}p(\bar{x},\bar{y},z) + iq(\bar{x},\bar{y},z)\right)}{(1+z^2)^{1/2}}\,\mathrm{d}z, \tag{4.92}$$

where

$$p(z) = \frac{(\bar{y}z + x)}{(1+z^2)^{1/2}}, \tag{4.93}$$

and q is $\mathcal{O}(1)$ and real. This is still in a form that can be evaluated via stationary phase to give a ray picture. We will obtain a leading order stationary phase contribution from $z_0 = -\bar{x}/\bar{y}$, provided that $-1 < -\bar{x}/\bar{y} < 1$, and endpoint contributions from $z = \pm 1$. Thus our assumption about the rate of growth of the shadow boundary regions for this source configuration is incorrect as we should not be able to talk about a ray solution where the shadow boundaries merge. Consideration of the standard

expressions for the stationary phase and endpoint contributions—*e.g.* [3]—reveals that the expansion will break down whenever

$$\frac{p'(\pm 1)}{p''(z_0)} \;=\; \mathcal{O}(k^{-1/4}). \tag{4.94}$$

This can be shown to occur wherever $(-\bar{y} \pm \bar{x}) \sim k^{1/4}$. *i.e.* when $(-y \pm x) \sim k^{-1/4}$. That is to say that the shadow boundary regions have shrunk in size due to the convergence of the rays. In fact, if we make the scalings

$$\bar{x} \;=\; k^{(n-1)/n}(1-x), \tag{4.95}$$

$$\bar{y} \;=\; k^{(n-1)/n}y, \tag{4.96}$$

for any $n > 0$, we find that we will always pick up the ray solution described above for $|\bar{y}|/\bar{x} < 1$, and that the ray solution breaks down when $(-y \pm x) \sim k^{-1+1/2n}$. This confirms that the shadow boundary regions shrink as we approach the caustic and that at an $\mathcal{O}(k^{-1})$ distance from the caustic we can no longer talk about ray regions and shadow boundary regions as these two regions are now the same size. In the $\mathcal{O}(k^{-1})$ caustic region the solution must be obtained numerically from (4.86).

The rays from the ends of the line source will obviously pass through the caustic and continue on the other side. The above analysis with $\bar{x} < 0$ indicates that to the right of the caustic we will get the usual ray picture for $|\bar{y}|/|\bar{x}| < 1$ with shadow boundaries that now grow as we move away from the caustic. In addition, the shadow boundaries know that they have originally come from the line source and *not* the caustic—*i.e.* once we are an $\mathcal{O}(1)$ distance, X say, to the right of the caustic the shadow boundaries will have a width like $\mathcal{O}((\sqrt{2}(1+X)/k)^{1/2})$. The $\sqrt{2}$ factor is there because the rays from the ends of the line source make an angle of $\pi/4$ to the horizontal. This can be deduced from a simple stationary phase analysis of (4.86) as follows. We investigate the shadow boundary near the line $y = x - 1$. We set

$$x \;=\; 1 + X, \tag{4.97}$$

$$y \;=\; X + k^{-1/2}(1+X)^{1/2}Y, \tag{4.98}$$

$$z \;=\; -1 + k^{-1/2}Z. \tag{4.99}$$

where X, Y, Z are $\mathcal{O}(1)$ and $X > 0$. The scaling on z is introduced as we know that the shadow boundary arises due to the coalescence of the stationary phase and end points of the integral. After some manipulation we are able to write (4.86) as

$$\phi \;=\; f(X,Y)\mathrm{erfc}\left(-\frac{Ye^{i\pi/4}}{2^{3/4}\sqrt{X}}\right). \tag{4.100}$$

This representation for the fields in the shadow boundary region is used provided the argument of the error function is $\mathcal{O}(1)$. This reveals that the shadow boundary to the right of the caustic grows in width like $\left(\sqrt{2}(1+X)/k\right)^{1/2}$ as required.

Having dealt with the case where the rays are focussed at an $\mathcal{O}(1)$ distance from the source, we now vary the distance to the focus, rewriting (4.85) as

$$\phi \;=\; \frac{e^{-ik(k^{2\alpha}+y^2)^{1/2}}}{(k^{2\alpha}+y^2)^{1/4}}, \quad x=0,\, -1\le y\le 1, \tag{4.101}$$

where $\alpha > 0$. This ensures the rays focus at a distance k^α from the source, where $\alpha > 0$. The field can now be written

$$\phi \;=\; -\frac{i}{4}\int_{-1}^{1} \frac{e^{ik\left(x^2+(y-z)^2\right)^{1/2}}}{\left(x^2+(y-z)^2\right)^{1/4}} \frac{e^{-ik(k^{2\alpha}+z^2)^{1/2}}}{(k^{2\alpha}+z^2)^{1/4}}\,\mathrm{d}z. \tag{4.102}$$

If we now look at the region where the rays from each end of the source converge by introducing the $\mathcal{O}(1)$ variable $\bar{x} = k^{-\alpha}x$, we can expand the exponents in (4.102) to produce

$$\phi \;\sim\; \frac{e^{ik^{1+\alpha}(\bar{x}-1)}}{k^\alpha\sqrt{\bar{x}}} \int_{-1}^{1} \exp\left(ik^{1-\alpha}\frac{(y-z)^2}{2\bar{x}} - ik^{1-\alpha}\frac{z^2}{2}\right)\,\mathrm{d}z. \tag{4.103}$$

For $0 < \alpha < 1$ we can perform stationary phase analysis to produce a ray picture and shadow boundary regions that shrink as they approach the caustic. For $\alpha = 1$ the integral can be rewritten as the sum of two error functions—*i.e.* we are in the Fraunhofer region of the problem. That is to say that to leading order the converging rays do not affect the usual ray picture described in §4.2. These results are consistent with the comments at the end of §4.2.2. For $\alpha > 1$ we can replace the exponent in the integral by zero, giving a weak $\exp(ikx)\sqrt{x}$ field propagating parallel to the x-axis.

Figure 4.7 is a schematic illustrating the behaviour of the shadow boundary regions for the two cases $\alpha = 0$ and $\alpha = 1$, in addition to an intermediate case $0 < \alpha < 1$.

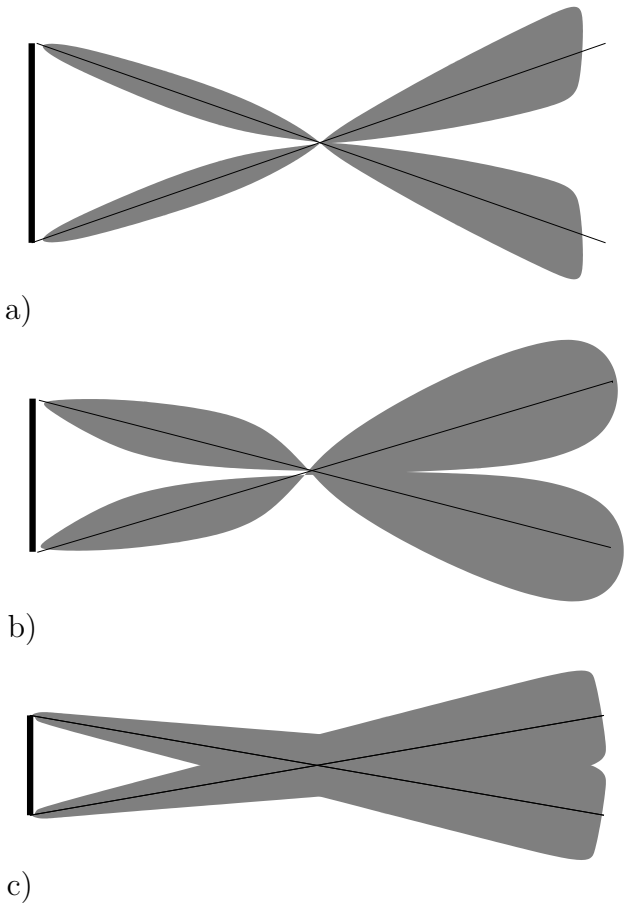


Figure 4.10: A plate of $\mathcal{O}(1)$ length set up to produce a converging ray picture. a) Rays converge at an $\mathcal{O}(1)$ distance from the source—convergence of rays dominates growth of shadow boundary regions. b) Rays converge at an $\mathcal{O}(k^\alpha)$ distance from the source, $0 < \alpha < 1$. c) Rays converge at an $\mathcal{O}(k)$ distance from the source—growth of shadow boundary regions dominates.

Chapter 5

Curved Structures

In this chapter we investigate one of the canonical diffraction problems of GTD. In the example of §3.1 we saw how the ray theory ansatz breaks down when the rays of an incident plane wave-field impinge tangentially on a scatterer. The diffraction phenomena that arise here will be fundamental to later chapters and a good understanding of them is required before tackling the harder problems that will follow. We restrict our attention almost entirely to convex surfaces. Many authors have investigated this problem—a comprehensive review of the extensive Russian literature on this area can be found in [2]. A complete asymptotic picture for the two-dimensional acoustic problem is given in [33], [35] and [40] for sound hard and sound soft boundary conditions. These papers extend the results of [2] for scattering by circular cylinders to cater for *arbitrary* convex scatterers. The solution to the corresponding E-M problem follows from the discussion in §2.3.4. In [33], the three-dimensional scalar problem is also solved asymptotically with a Neumann boundary condition on the scatterer, although no remarks are made concerning either its connection to the E-M problem or the shadow boundary structure that exists between the geometrical optics lit and shadow regions. The general three-dimensional scalar problem is also not considered, attention being restricted to the case where the incident rays are along the axis of a body of revolution. The literature reveals that close to the scatterer a surface field is induced that cannot be described by ray theory. *Creeping rays* are launched tangentially from this surface field into the geometrical optics shadow. Diffraction by a thin body introduces new complications because of the small aspect ratio, and is considered among others by [10]. This turns out to exhibit diffraction patterns characteristic of both smooth bodies and flat plates when appropriate limits are taken.

The aim of this chapter is to solve asymptotically, for short-wavelength irradiation, the electromagnetic problem for plane wave incidence on an arbitrary three-dimensional

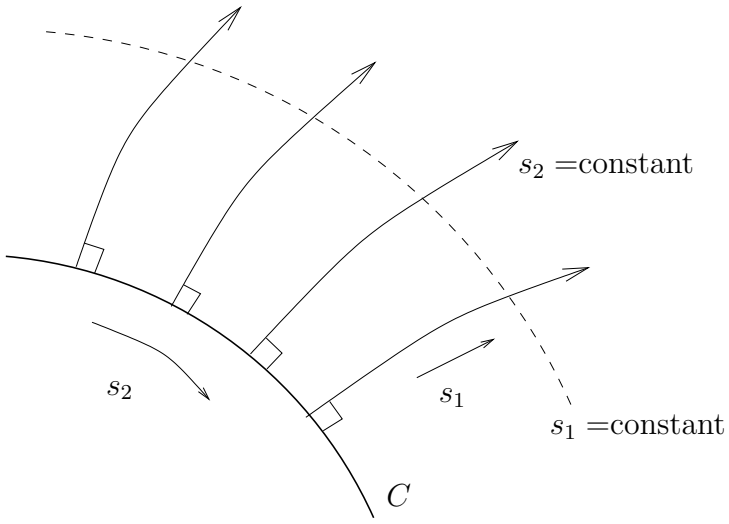


Figure 5.1: Geodesic normal coordinate system.

convex surface. In general we find that we can decompose the surface field into two components which can be solved via the scalar equations of [33]. We initially study the special case where the incident rays fall normally to the horizon as in Figure 5.2. This lets us establish the asymptotic structure without unecessary complications. We will also describe in detail the shadow boundary structure of this three-dimensional problem. The case where the incident rays fall obliquely on the tangency line will be dealt with by first considering a 'toy problem' to gain intuition. The toy problem is then used to relate this problem to that of normal incidence.

We will then consider some extensions to the original problem. We discuss the irradiation of a scatterer by a point source at an $\mathcal{O}(1)$ distance and provide a more complete asymptotic solution to the related two-dimensional canonical problem of the scattering by a cylinder of the field induced by a line source parallel to the axis of the cylinder.

We also discuss the analogue to creeping ray fields for concave surfaces, namely whispering gallery (WG) modes, and describe an open problem in this area which is of both academic and industrial importance.

5.1 Geodesic Normal Coordinates

The geodesic normal coordinate system s_1, s_2, s_3 that we will use in this section is illustrated in Figure 5.1. An initial line C on a surface is parametrised by s_2. We construct the geodesics in the surface normal to C, and measure the distance along

each geodesic, s_1. The distance normal to the surface is s_3. In general, this coordinate system will not be well-defined everywhere as geodesics may intersect. We will say more about this later. In addition, for a concave surface there is the possibility of intersecting normals at a point. But locally to the horizon, at least, the coordinate system *is* well-defined. If a surface $\mathcal{S}$ is given by $\mathbf{r} = \mathbf{R}(s_1, s_2)$ then a general position vector can be written

$$\mathbf{r} = \mathbf{R}(s_1, s_2) + s_3\mathbf{n}(s_1, s_2), \tag{5.1}$$

where $\mathbf{n}$ is the unit outward pointing normal to the surface. The unit vectors $\mathbf{e}_1, \mathbf{e}_2$ are in the directions $\partial\mathbf{R}/\partial s_1, \partial\mathbf{R}/\partial s_2$ respectively and $\mathbf{e}_3 = \mathbf{n}$. We introduce the first and second fundamental forms

$$\begin{aligned} E &= \frac{\partial\mathbf{R}}{\partial s_1}\cdot\frac{\partial\mathbf{R}}{\partial s_1}, \qquad F = \frac{\partial\mathbf{R}}{\partial s_1}\cdot\frac{\partial\mathbf{R}}{\partial s_2}, \qquad G = \frac{\partial\mathbf{R}}{\partial s_2}\cdot\frac{\partial\mathbf{R}}{\partial s_2}, \\ L &= \frac{\partial^2\mathbf{R}}{\partial s_1^2}\cdot\mathbf{n}, \qquad M = \frac{\partial^2\mathbf{R}}{\partial s_1\partial s_2}\cdot\mathbf{n}, \qquad N = \frac{\partial^2\mathbf{R}}{\partial s_2^2}\cdot\mathbf{n}. \end{aligned} \tag{5.2}$$

The distance $|\mathrm{d}\mathbf{R}|$ between two adjacent points on a surface is connected to the components of the first fundamental form by the relationship

$$|\mathrm{d}\mathbf{R}|^2 = E\mathrm{d}s_1^2 + 2F\mathrm{d}s_1\mathrm{d}s_2 + G\mathrm{d}s_2^2. \tag{5.3}$$

The components of the second fundamental form are related to the curvatures of the surface—see [41].

As the geodesics are parametrised by arclength, $E = 1$. It follows that

$$\frac{\partial^2\mathbf{R}}{\partial s_1 s_i}\cdot\frac{\partial\mathbf{R}}{\partial s_1} = 0, \quad i = 1, 2. \tag{5.4}$$

By definition, the derivative of the tangent to a geodesic is normal to the surface. Hence we may also say that

$$\frac{\partial^2\mathbf{R}}{\partial s_1^2}\cdot\frac{\partial\mathbf{R}}{\partial s_2} = 0. \tag{5.5}$$

Thus (5.4) and (5.5) imply

$$\frac{\partial F}{\partial s_1} = \frac{\partial^2\mathbf{R}}{\partial s_1^2}\cdot\frac{\partial\mathbf{R}}{\partial s_2} + \frac{\partial\mathbf{R}}{\partial s_1}\cdot\frac{\partial^2\mathbf{R}}{\partial s_1\partial s_2} = 0. \tag{5.6}$$

Hence $F = F(s_2)$, and so is constant along each geodesic. However, the definition of the coordinate system fixes $F = 0$ along each geodesic at $s_1 = 0$. Therefore $F \equiv 0$. Both G and the components of the second fundamental form still depend on the

coordinate position. In general $M \neq 0$. Therefore s_1, s_2, s_3 do not form an orthogonal coordinate system and we must be careful in writing down Maxwell's equations.

We comment that information about the two-dimensional problem can be extracted from what follows by setting $G = 1$, $\mathbf{R}(s_1, s_2) = \mathbf{R}(s_1)$. The solution is independent of the vector $\mathbf{e}_2$ which is now directed along the axis of symmetry. We can also relate L, the curvature along a geodesic, to the usual curvature κ via $L(s_1, s_2) = -\kappa(s_1)$. The minus sign arises from consideration of the Serret-Frenet formula applied to the right-handed set $\mathbf{e}_1, \mathbf{e}_3, \mathbf{e}_2$, corresponding to the tangent, normal and binormal vectors respectively. For our set of basis vectors $\mathbf{e}_1, \mathbf{e}_2, \mathbf{e}_3$ to be of the required form to apply the Serret-Frenet formulae, we must replace $\mathbf{e}_3$ with $-\mathbf{e}_3$. This result has the important consequence that $L < 0$ for convex surfaces.

The derivation of Maxwell's equations in the geodesic normal coordinate system is carried out in Appendix C with the results given by (C.17) - (C.22) and (C.35) - (C.38).

5.2 Surface Field Propagation along Geodesics

The acoustics literature—*e.g.* [33], [35], [40]—suggests that to investigate the surface field in the shadow we must scale $s_3 = k^{-2/3}\rho$. Motivated by results in the cited papers, we look for a solution of the form

$$\mathbf{F} = e^{iku(s_1,s_2)+ik^{1/3}v(s_1,s_2)} \sum_{n=0}^{\infty} \frac{\mathbf{F}^n(s_1, s_2, \rho)}{k^{n/3}}, \tag{5.7}$$

where $\mathbf{F}$ is to be read as either $\mathbf{E}$ or $\mathbf{H}$. Substituting this ansatz into Maxwell's equations (C.17) - (C.22) produces the leading order equation

$$\frac{1}{E}\left(\frac{\partial u}{\partial s_1}\right)^2 + \frac{1}{G}\left(\frac{\partial u}{\partial s_2}\right)^2 = 1, \tag{5.8}$$

which is the *surface eikonal equation* for the phase. Letting

$$p = \frac{\partial u}{\partial s_1}, \quad q = \frac{\partial u}{\partial s_2}, \tag{5.9}$$

we can write Charpit's equations for (5.8) as

$$\frac{\mathrm{d}s_1}{\mathrm{d}t} = \frac{p}{E}, \tag{5.10}$$

$$\frac{\mathrm{d}s_2}{\mathrm{d}t} = \frac{q}{G}, \tag{5.11}$$

$$\frac{\mathrm{d}p}{\mathrm{d}t} = \frac{1}{2}\left(\frac{p^2}{E^2}E_{s_1} + \frac{q^2}{G^2}G_{s_1}\right), \tag{5.12}$$

$$\frac{\mathrm{d}q}{\mathrm{d}t} = \frac{1}{2}\left(\frac{p^2}{E^2}E_{s_2} + \frac{q^2}{G^2}G_{s_2}\right), \tag{5.13}$$

$$\frac{\mathrm{d}u}{\mathrm{d}t} = 1, \tag{5.14}$$

where t is distance along a characteristic. Equation (5.14) tells us that the phase is equal to the distance along the characteristics. From [41], for a curve parametrised by arclength to be a geodesic, it must satisfy the geodesic equations, namely

$$\frac{\mathrm{d}}{\mathrm{d}t}\left(E\frac{\mathrm{d}s_1}{\mathrm{d}t}\right) = \frac{1}{2}\left(E_{s_1}\left(\frac{\mathrm{d}s_1}{\mathrm{d}t}\right)^2 + G_{s_1}\left(\frac{\mathrm{d}s_2}{\mathrm{d}t}\right)^2\right), \tag{5.15}$$

$$\frac{\mathrm{d}}{\mathrm{d}t}\left(G\frac{\mathrm{d}s_1}{\mathrm{d}t}\right) = \frac{1}{2}\left(E_{s_2}\left(\frac{\mathrm{d}s_1}{\mathrm{d}t}\right)^2 + G_{s_2}\left(\frac{\mathrm{d}s_2}{\mathrm{d}t}\right)^2\right). \tag{5.16}$$

Now (5.10), (5.11) along with either (5.12) or (5.13) imply that the characteristic curves satisfy (5.15) and (5.16) respectively. Therefore the characteristics *are* the geodesics on the surface.

5.3 Plane Wave-Field Incident Upon a Convex Scatterer

We consider a plane wave

$$\mathbf{E}^{inc} = \bar{\mathbf{E}}^{inc}\exp(i\mathbf{k}\,.\,\mathbf{r}), \tag{5.17}$$

$$\mathbf{H}^{inc} = \bar{\mathbf{H}}^{inc}\exp(i\mathbf{k}\,.\,\mathbf{r}), \tag{5.18}$$

incident upon a convex scatterer with an outward pointing unit normal $\mathbf{n}$. The wavefronts will be level sets of $\mathbf{k}\,.\,\mathbf{r}$, and the incident field will be tangent to the surface at points satisfying

$$\mathbf{k}\,.\,\mathbf{n}(s_1, s_2) = 0, \tag{5.19}$$

along a line C commonly referred to as the *horizon*. Geometrical optics breaks down here and we must carry out an expansion in the neighbourhood of C. We thus define

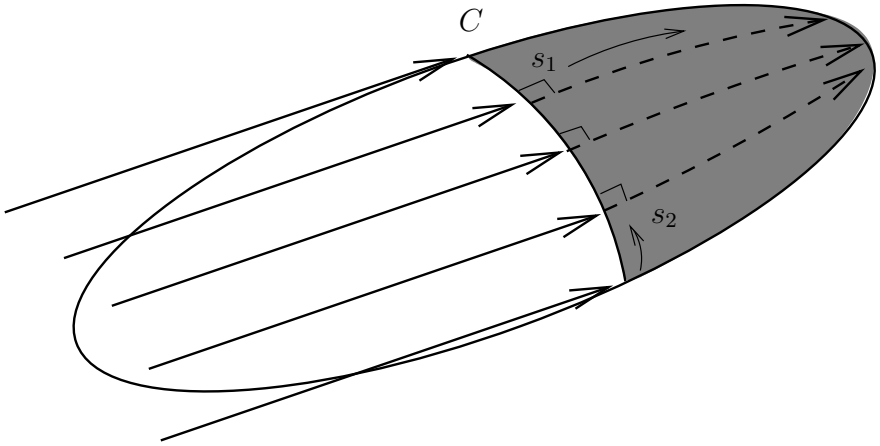


Figure 5.2: Plane wave-field incident on a convex scatterer. Shaded area is in shadow and cut off by the horizon C. The surface field propagates along the geodesics.

a system of geodesic normal coordinates based on C. The line C is parametrised by s_2 and the geodesics perpendicular to C by s_1. For the moment we restrict our attention to the case where the tangent rays impinge normally to C—*e.g.* a plane wave-field incident along an axis of an ellipsoid. This is the E-M analogue of the acoustic problem considered in [33].

5.3.1 The Airy Layer

We wish to find the surface field away from C and in shadow. We assume that s_1 is $\mathcal{O}(1)$ and positive. The ansatz (5.7) is introduced for both **E** and **H**.

Equation (5.14) leads to the assumption that $u(s_1, s_2) = s_1$. Then (C.17) - (C.22) yield the following sets of equations.

Terms of $\mathcal{O}(k)$:

$$H_1^0 = 0, \tag{5.20}$$

$$E_3^0 + H_2^0 = 0, \tag{5.21}$$

$$H_3^0 - E_2^0 = 0, \tag{5.22}$$

$$E_1^0 = 0, \tag{5.23}$$

$$H_3^0 - E_2^0 = 0, \tag{5.24}$$

$$E_3^0 + H_2^0 = 0. \tag{5.25}$$

Terms of $\mathcal{O}(k^{2/3})$:

$$
\begin{aligned}
-\frac{\partial E_2^0}{\partial \rho} - iH_1^1 &= 0, && (5.26)\\
-iE_3^1 - iH_2^1 &= 0, && (5.27)\\
iE_2^1 - iH_3^1 &= 0, && (5.28)\\
-\frac{\partial H_2^0}{\partial \rho} + iE_1^1 &= 0, && (5.29)\\
-iH_3^1 + iE_2^1 &= 0, && (5.30)\\
iH_2^1 + iE_3^1 &= 0. && (5.31)
\end{aligned}
$$

Terms of $\mathcal{O}(k^{1/3})$, upon employing (5.21), (5.26) and (5.29):

$$
\begin{aligned}
H_1^2 &= \frac{E_3^0}{\sqrt{G}}\frac{\partial v}{\partial s_2} + i\frac{\partial E_2^1}{\partial \rho}, && (5.32)\\
E_3^2 + H_2^2 &= -\frac{\partial^2 H_2^0}{\partial \rho^2} + \frac{\partial v}{\partial s_1}H_2^0 + \rho L H_2^0, && (5.33)\\
H_3^2 - E_2^2 &= \frac{\partial v}{\partial s_1}E_2^0 + \rho L E_2^0, && (5.34)\\
E_1^2 &= -\frac{H_3^0}{\sqrt{G}}\frac{\partial v}{\partial s_2} - i\frac{\partial H_2^1}{\partial \rho}, && (5.35)\\
H_3^2 - E_2^2 &= \frac{\partial^2 E_2^0}{\partial \rho^2} - \frac{\partial v}{\partial s_1}E_2^0 - \rho L E_2^0, && (5.36)\\
E_3^2 + H_2^2 &= -\frac{\partial v}{\partial s_1}H_2^0 - \rho L H_2^0. && (5.37)
\end{aligned}
$$

Combining equations (5.33) and (5.37) and equations (5.34) and (5.36) produces

$$
\begin{aligned}
\frac{\partial^2 H_2^0}{\partial \rho^2} - 2\frac{\partial v}{\partial s_1}H_2^0 - 2\rho L H_2^0 &= 0, && (5.38)\\
\frac{\partial^2 E_2^0}{\partial \rho^2} - 2\frac{\partial v}{\partial s_1}E_2^0 - 2\rho L E_2^0 &= 0. && (5.39)
\end{aligned}
$$

The perfectly conducting boundary condition (2.26) implies that the boundary condition for (5.39) is

$$
E_2^0 = 0 \quad \text{on } \rho = 0. \tag{5.40}
$$

Application of (5.29), along with the perfectly conducting boundary condition, tells us that the boundary condition for (5.38) is

$$
\frac{\partial H_2^0}{\partial \rho} = 0 \quad \text{on } \rho = 0. \tag{5.41}
$$

In addition, (5.38) and (5.39) must be accompanied by an outgoing wave condition as $\rho \to \infty$ to ensure that we match into an outgoing wave field.

We recall from §2.3.2 that if the wave-fronts of the $\mathbf{E}, \mathbf{H}$ fields are known, then in the high frequency limit, $\mathbf{E}$ and $\mathbf{H}$ will be parallel to the wave-fronts and perpendicular to each other. This is the case here as the field is known to propagate along geodesics. The wave-fronts are in the $s_2 - \rho$ plane. This allows the decomposition of the Airy Layer field into two perpendicular fields. We choose the polarisations as follows: the *magnetic* polarisation has the electric field entirely perpendicular to the surface. This forces $E_2^0 \equiv 0$. The *electric* polarisation has the magnetic field entirely perpendicular to the surface, which fixes $H_2^0 \equiv 0$. Each of these polarisations is solved separately in what is to follow. The linearity of Maxwell's equations allows the summation of the solutions for the two polarisations to yield the total field.

Magnetically Polarised Airy Layer

We set $E_2^0 \equiv 0$. Equations (5.20), (5.22) and (5.23) imply

$$E_2^0 \equiv E_1^0 \equiv H_1^0 \equiv H_3^0 \equiv 0.$$

Equation (5.21) gives us E_3^0 in terms of H_2^0. We therefore only need to solve (5.38) along with (5.41). The solution to this problem is described in detail in [33]. Briefly, the transformation

$$\eta = |L|^{-2/3} \left(\rho |L| - \frac{\partial v}{\partial s_1} \right) \tag{5.42}$$

reduces (5.38) to

$$\frac{\partial^2 H_2^0}{\partial \eta^2} + 2\eta H_2^0 = 0. \tag{5.43}$$

To satisfy the outgoing wave condition as $\rho \to \infty$ we must take

$$H_2^0 = \beta(s_1, s_2) \mathrm{Ai}(-\sqrt[3]{2} e^{2\pi i/3} \eta). \tag{5.44}$$

The boundary condition fixes

$$v = \frac{a_m' e^{-2\pi i/3}}{\sqrt[3]{2}} \int_0^{s_1} |L|^{2/3} \, d\lambda, \tag{5.45}$$

where the a_m' are the zeros of $\mathrm{Ai}'(z)$. This gives us an infinite set of solution modes. The $\mathcal{O}(1)$ Maxwell's equations—not listed here—give a solvability condition which

removes some of the indeterminacy in $\beta(s_1, s_2)$. This solvability condition is identical to that derived for the acoustic version of the problem in [33]. This leaves us with

$$\beta_m(s_1, s_2) \;=\; \beta_m(s_2)\frac{|L|^{1/6}}{G^{1/4}}, \tag{5.46}$$

where the $\beta_m(s_2)$ are to be determined via matching into the surface field *at* the horizon. Thus the solution in the Airy layer is

$$\begin{aligned}
\mathbf{E} &= -\phi_M \mathbf{e}_3, && (5.47)\\
\mathbf{H} &= \phi_M \mathbf{e}_2, && (5.48)\\
\phi_M &\sim \sum_{m=0}^{\infty} \frac{\beta_m(s_2)|L|^{1/6}}{G^{1/4}} \mathrm{Ai}\left(-\sqrt[3]{2}e^{2\pi i/3}|L|^{1/3}\rho + a'_m\right), \\
&\quad \times \exp\left(iks_1 + ik^{1/3}\frac{a'_m e^{-2\pi i/3}}{\sqrt[3]{2}}\int_0^{s_1} |L|^{2/3}\, d\lambda\right). && (5.49)
\end{aligned}$$

We remark that as the expansions for $\mathbf{E}, \mathbf{H}$ given by (5.7) are algebraic in negative powers of k, the exponentially subdominant terms in (5.49) may well be dominated by the second and subsequent terms in the expansions for $\mathbf{E}, \mathbf{H}$.

Electrically Polarised Airy Layer

We now set $H_2^0 \equiv 0$. From (5.20), (5.21) and (5.23) we have

$$H_2^0 \;\equiv\; H_1^0 \;\equiv\; E_1^0 \;\equiv\; E_3^0 \;\equiv\; 0.$$

To find E_2^0 and H_3^0 we must solve (5.39) along with (5.40). The result for this can be computed, using the same techniques as in [33], to be

$$\begin{aligned}
\mathbf{E} &= \phi_E \mathbf{e}_2, && (5.50)\\
\mathbf{H} &= \phi_E \mathbf{e}_3, && (5.51)\\
\phi_E &\sim \sum_{m=0}^{\infty} \frac{\gamma_m(s_2)|L|^{1/6}}{G^{1/4}} \mathrm{Ai}\left(-\sqrt[3]{2}e^{2\pi i/3}|L|^{1/3}\rho + a_m\right) \\
&\quad \times \exp\left(iks_1 + ik^{1/3}\frac{a_m e^{-2\pi i/3}}{\sqrt[3]{2}}\int_0^{s_1} |L|^{2/3}\, d\lambda\right), && (5.52)
\end{aligned}$$

where the a_m are the zeros of $\mathrm{Ai}(z)$ and the γ_m are again obtained by matching with the field at the horizon.

We note that the ordering

$$\begin{aligned}
0 > a_0 > a_1 > \ldots > a_n > \ldots, \\
0 > a'_0 > a'_1 > \ldots > a'_n > \ldots,
\end{aligned}$$

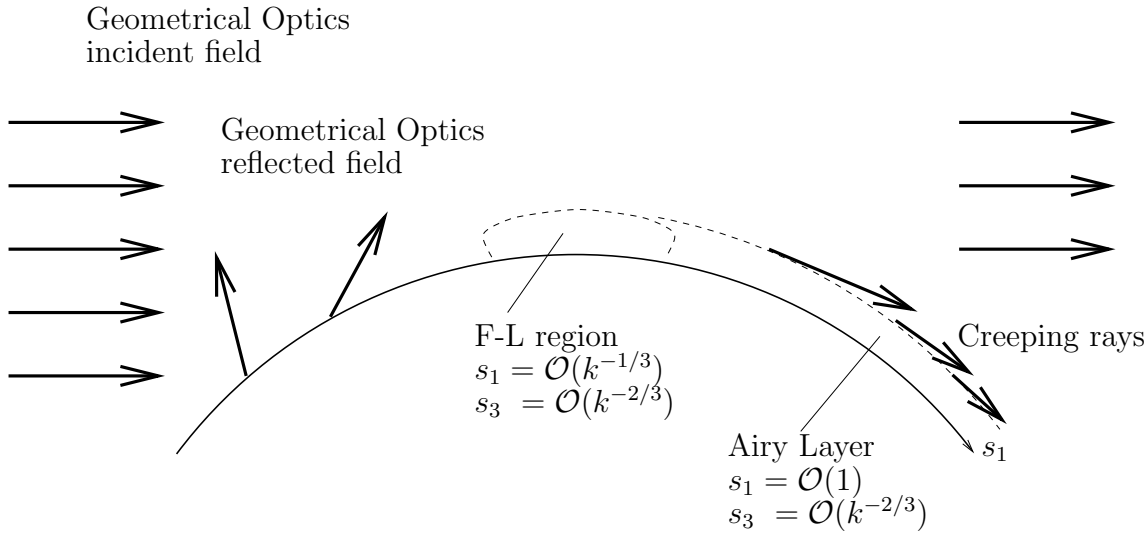


Figure 5.3: Ray picture for an incident plane wave-field impinging tangentially on a convex surface.

implies that there is exponential decay of both polarisations of the Airy layer field along each geodesic, and that in both cases the first mode would be a good approximation to the leading order solution. We also make the observation that because

$$a_0' \;>\; a_0,$$

the first magnetically polarised Airy layer mode will dominate the first electrically polarised mode.

5.3.2 Fock-Leontovič Region

In the Airy layer the electric and magnetic fields are known to within the functions $\beta_m(s_2), \gamma_m(s_2)$ which must be determined by considering the surface field at the horizon. To this end we examine the solution in the neighbourhood of the horizon. The diffraction problem in this region was originally solved by Fock and Leontovič, [17], hence the terminology *Fock-Leontovič* (or F-L) region. Their work motivates the scalings

$$\hat{s}_1 \;=\; k^{1/3} s_1, \tag{5.53}$$

$$\rho \;=\; k^{2/3} s_3. \tag{5.54}$$

The ansatz for the F-L solution is

$$\mathbf{F} \;=\; \bar{\mathbf{F}}^{inc} e^{i\mathbf{k}.\mathbf{r}} + e^{iks_1} \sum_{n=0}^{\infty} \frac{\mathbf{F}^n(\hat{s}_1, s_2, \rho)}{k^{n/3}}, \tag{5.55}$$

where **F** is to be read as **E** or **H**. Introducing the notation $L_0(s_2) = L(0, s_2)$, etc. our metrics (C.35) - (C.37) become

$$h_1^2 \sim 1 - 2k^{-2/3}\rho L_0(s_2), \tag{5.56}$$

$$h_2^2 \sim G_0(s_2) - 2k^{-2/3}\rho N_0(s_2), \tag{5.57}$$

$$h_3 = 1. \tag{5.58}$$

Substituting these scalings and metrics into Maxwell's equations, (C.17) - (C.22), produces $\mathcal{O}(k)$ and $\mathcal{O}(k^{2/3})$ equations identical to (5.20) - (5.25) and (5.26) - (5.31). On employing (5.20) - (5.23) the $\mathcal{O}(k^{1/3})$ equations become

$$H_1^2 = i\frac{\partial E_2^1}{\partial \rho}, \tag{5.59}$$

$$E_3^2 + H_2^2 = -\frac{\partial^2 H_2^0}{\partial \rho^2} - i\frac{\partial H_2^0}{\partial \hat{s}_1} + \rho L_0 H_2^0, \tag{5.60}$$

$$H_3^2 - E_2^2 = -i\frac{\partial E_2^0}{\partial \hat{s}_1} + \rho L E_2^0, \tag{5.61}$$

$$E_1^2 = -i\frac{\partial H_2^1}{\partial \rho}, \tag{5.62}$$

$$H_3^2 - E_2^2 = \frac{\partial^2 E_2^0}{\partial \rho^2} + i\frac{\partial E_2^0}{\partial \hat{s}_1} - \rho L_0 E_2^0, \tag{5.63}$$

$$H_2^2 + E_3^2 = i\frac{\partial H_2^0}{\partial \hat{s}_1} - \rho L H_2^0. \tag{5.64}$$

Combining (5.60) & (5.64) and (5.61) & (5.63) gives

$$\frac{\partial^2 H_2^0}{\partial \rho^2} + 2i\frac{\partial H_2^0}{\partial \hat{s}_1} - 2\rho L_0 H_2^0 = 0, \tag{5.65}$$

$$\frac{\partial^2 E_2^0}{\partial \rho^2} + 2i\frac{\partial E_2^0}{\partial \hat{s}_1} - 2\rho L_0 E_2^0 = 0, \tag{5.66}$$

which are the scalar F-L equations of [33] for $E_2^0,\ H_2^0$. The perfectly conducting boundary conditions and (5.55) imply that (5.65) and (5.66) must be accompanied by the boundary conditions

$$\frac{\partial H_2^0}{\partial \rho} \sim -\frac{\partial}{\partial \rho}\left(\bar{H}_2^{inc} e^{i\mathbf{k}.\mathbf{r}}\right) e^{-iks_1}, \qquad \rho = 0, \tag{5.67}$$

$$E_2^0 \sim -\bar{E}_2^{inc} e^{i\mathbf{k}.\mathbf{r}} e^{-iks_1}, \qquad \rho = 0. \tag{5.68}$$

As H_2^0, E_2^0 are independent of $\mathbf{k}$, we must first write (5.67) and (5.68) in a more suitable form. The definition of the geodesic normal coordinate system and (5.19) gives us

$$\mathbf{k} \cdot \mathbf{n}(0, s_2) = 0. \tag{5.69}$$

Expanding $\mathbf{r}(s_1, s_2, 0)$ and $\dfrac{\partial \mathbf{r}}{\partial \rho}(s_1, s_2, 0)$ for small s_1 and using (5.1) and (5.69) gives us

$$\begin{aligned}\frac{\partial H_2^0}{\partial \rho} \sim & -ik^{-1/2}\hat{s}_1 \mathbf{k} \cdot \frac{\partial \mathbf{n}}{\partial s_1}(0, s_2)\bar{H}_2^{inc} \\ & \times \exp\left(i\mathbf{k} \cdot \mathbf{R}(0, s_2) + ik^{-1/3}\hat{s}_1 \mathbf{k} \cdot \frac{\partial \mathbf{R}}{\partial \hat{s}_1}(0, s_2)\right) \\ & \times \exp\left(ik^{-2/3}\frac{\hat{s}_1^2}{2}\mathbf{k} \cdot \frac{\partial^2 \mathbf{R}}{\partial \hat{s}_1^2}(0, s_2) + ik^{-1}\mathbf{k} \cdot \frac{\hat{s}_1^3}{6}\frac{\partial^3 \mathbf{R}}{\partial \hat{s}_1^3}(0, s_2)\right). \qquad (5.70)\end{aligned}$$

The defining property of a geodesic is that the derivative of the unit tangent vector $\mathbf{t}$ along a geodesic is normal to the surface (*e.g.* [41]). Therefore we have

$$\frac{\partial \mathbf{t}}{\partial s_1} = \frac{\partial}{\partial s_1}\left(\frac{\partial \mathbf{R}}{\partial s_1}(s_1, s_2)\right) = L(s_1, s_2)\mathbf{n}, \qquad (5.71)$$

where $L(s_1, s_2)$ is the curvature along the geodesic $s_2 =$ constant. Using the Serret-Frenet formulae (see [30] for details) we have

$$\begin{aligned}\frac{\partial \mathbf{R}}{\partial s_1} &= \mathbf{t}, & (5.72)\\ \frac{\partial^2 \mathbf{R}}{\partial s_1^2} &= L(s_1, s_2)\mathbf{n}, & (5.73)\\ \frac{\partial^3 \mathbf{R}}{\partial s_1^3} &= \frac{\partial L}{\partial s_1}(s_1, s_2)\mathbf{n} - L^2(s_1, s_2)\mathbf{t} + \tau L(s_1, s_2)\mathbf{b}, & (5.74)\\ \frac{\partial \mathbf{n}}{\partial s_1} &= -L(s_1, s_2)\mathbf{t} + \tau \mathbf{b}, & (5.75)\end{aligned}$$

where $\mathbf{b} = \mathbf{t} \wedge \mathbf{n}$ is the binormal vector, and τ is the torsion of the geodesic. In terms of $\{\mathbf{e}_1, \mathbf{e}_2, \mathbf{n}\}$, we have

$$\begin{aligned}\mathbf{t}(0, s_2) &= \mathbf{e}_1(0, s_2), & (5.76)\\ \mathbf{b}(0, s_2) &= -\mathbf{e}_2(0, s_2), & (5.77)\\ \mathbf{k} &= k\mathbf{e}_1(0, s_2). & (5.78)\end{aligned}$$

Putting (5.72) - (5.78) into (5.70) gives us

$$\frac{\partial H_2^0}{\partial \rho} = ik^{2/3}\bar{H}_2^{inc} L_0(s_2)\,\hat{s}_1 \exp\left(ik\mathbf{e}_1 \cdot \mathbf{R}(0, s_2) - i\frac{L_0^2(s_2)\hat{s}_1^3}{6}\right), \qquad \rho = 0. \quad (5.79)$$

Likewise, (5.68) is rewritten

$$E_2^0 = -\bar{E}_2^{inc} \exp\left(ik\mathbf{e}_1 \cdot \mathbf{R}(0, s_2) - i\frac{L_0^2(s_2)\hat{s}_1^3}{6}\right), \qquad \rho = 0. \quad (5.80)$$

We define

$$F^{inc^*} \quad = \quad \bar{F}^{inc}\exp\left(ik\mathbf{e}_1 \,.\, \mathbf{R}(0,s_2)\right), \tag{5.81}$$

which is just the value of the incident field F^{inc} *at* the horizon. Upon doing so (5.79) and (5.80) are seen to be independent of k as required. Similarly to the Airy layer problem we can decompose the F-L field into magnetically and electrically polarised components. The unknown functions $\beta_m(s_2)$ will be obtained by matching the magnetically polarised Airy layer solution with the magnetically polarised F-L solution. Likewise, the $\gamma_m(s_2)$ will be determined via matching between the corresponding electrically polarised solutions.

Magnetically Polarised Fock-Leontovič Solution

For the magnetically polarised F-L problem we take $E_2^0 \equiv 0$. The leading order equations (5.20) - (5.23) imply

$$H_1^0 \quad \equiv \quad H_3^0 \quad \equiv \quad E_1^0 \quad \equiv \quad 0, \tag{5.82}$$

with E_3^0 given in terms of H_2^0. It therefore remains to solve (5.65) with (5.79). Saward derives the solution as

$$\begin{aligned} H_2^0 \quad &= \quad -\sqrt[3]{2}e^{-2\pi i/3}|L_0|^{-2/3}H_2^{inc^*} \\ &\quad \times \int_{-\infty}^{\infty}\left\{\frac{\mathrm{Ai}'[-\sqrt[3]{2}|L_0|^{-2/3}\lambda]}{\mathrm{Ai}'[-\sqrt[3]{2}|L_0|^{-2/3}\lambda e^{2\pi i/3}]}\mathrm{Ai}[-\sqrt[3]{2}e^{2\pi i/3}|L_0|^{-2/3}(|L_0|\rho+\lambda)]\right\}e^{-i\lambda\hat{s}_1}\,\mathrm{d}\lambda. \end{aligned} \tag{5.83}$$

The matching between the Airy Layer and F-L solutions is carried out in Saward and the β_m of (5.46) found to be

$$\beta_m(s_2) \quad = \quad 2\pi H_2^{inc^*}G_0^{1/4}|L_0(s_2)|^{-1/6}e^{i\pi/6}\frac{\mathrm{Ai}'[e^{-2\pi i/3}a_m']}{\mathrm{Ai}''[a_m']}. \tag{5.84}$$

As each mode is exponentially dominated by the previous one, Stokes' phenomenon (*e.g.* [9]) may cause multiples of the higher order modes to be switched on or off at various points in the Airy layer. This has two important consequences. The first is that while (5.84) determines β_0 everywhere, the coefficients for $m > 0$ are only valid close to $s_1 = 0$. The second is that should there be jumps in the coefficients of the higher order modes in the Airy layer, an exponentially small backscattered field will be generated. This field, although small, could have important implications and merits future investigation.

Electrically Polarised Fock-Leontovič Solution

We take $H_2^0 \equiv 0$. Equations (5.20) - (5.23) imply

$$H_1^0 \equiv E_1^0 \equiv E_3^0 \equiv 0, \tag{5.85}$$

with H_3^0 given in terms of E_2^0. Therefore we need to solve (5.66) along with (5.80). Again following the methodology of Saward, it is straightforward to calculate the solution as

$$\begin{aligned} E_2^0 &= \sqrt[3]{2}|L_0(s_2)|^{-2/3} E_2^{inc^*} \\ &\times \int_{-\infty}^{\infty} \left\{ \frac{\mathrm{Ai}[-\sqrt[3]{2}|L_0|^{-2/3}\lambda]}{\mathrm{Ai}[-\sqrt[3]{2}|L_0|^{-2/3}\lambda e^{2\pi i/3}]} \mathrm{Ai}[-\sqrt[3]{2}e^{2\pi i/3}|L_0|^{-2/3}(|L_0|\rho+\lambda)] \right\} e^{-i\lambda \hat{s}_1}\, \mathrm{d}\lambda. \end{aligned} \tag{5.86}$$

The matching follows as before, with the γ_m of (5.52) forced to be

$$\gamma_m(s_2) = 2\pi e^{-5\pi i/6} E_2^{inc^*} G_0^{1/4} |L_0(s_2)|^{-1/6} \frac{\mathrm{Ai}[e^{-2\pi i/3} a_m]}{\mathrm{Ai}'[a_m]}. \tag{5.87}$$

Again, Stokes' phenomenon means that we are unable to determine the coefficients of the subdominant modes away from $s_1 = 0$.

We remark that the dependence of the surface fields on the parameter s_2 is through the value of the incident field—$\mathbf{E}^{inc^*}(s_2), \mathbf{H}^{inc^*}(s_2)$—at the horizon, and the curvature of the surface—$L_0(s_2)$—at the horizon.

We are now in a position to describe how to calculate the magnetic and electric surface fields due to an incident plane wave in the high frequency limit. We first construct the geodesic normal coordinate system outlined earlier. Along the horizon we decompose the incoming field $\mathbf{E}^{inc}$, $\mathbf{H}^{inc}$ into two components—$\mathbf{E}_M^{inc}$, $\mathbf{H}_M^{inc}$ and $\mathbf{E}_E^{inc}$, $\mathbf{H}_E^{inc}$. The first of these has the magnetic field parallel to the surface and the electric field perpendicular to the surface. This sets up *magnetically polarised* F-L and Airy layer fields. The second has the electric field parallel to the surface with the magnetic field perpendicular to the surface and sets up *electrically polarised* F-L and Airy layer fields. Knowing $\mathbf{E}_{M,E}^{inc}$, $\mathbf{H}_{M,E}^{inc}$ along C lets us write down the two polarisations of the Airy layer field via (5.49), (5.52), (5.84) and (5.87). The field in the Airy layer is seen to be entirely dependent on the geometry of the surface and the value of the incident field *at* the point of tangency which emphasises the locality of GTD. We stress that the coupling between the incident and surface fields occurs only at the point of tangency and that the information flows from the tangency point along the geodesics which are the characteristics of the system.

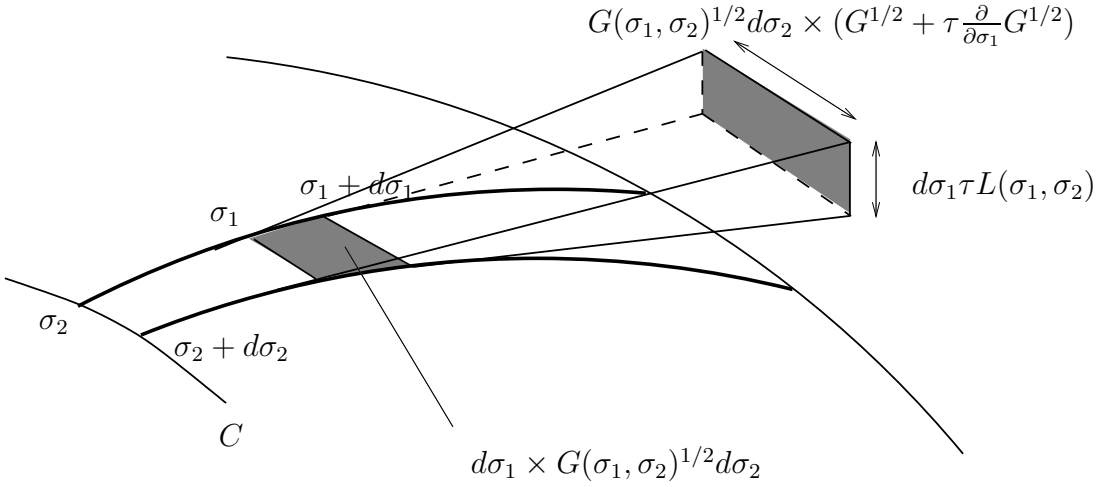


Figure 5.4: Raytube of Creeping Rays

5.3.3 Shed Creeping Ray Field

As the surface field propagates around the scatterer it sheds energy into the shadow region (this is associated with the exponential decay along a geodesic). Consideration of the form of the solution in the Airy layer would suggest that these rays are launched tangentially to the scatterer. Motivated by the scalar work of [40] in two dimensions and our knowledge of the behaviour of ray tubes outlined in §3, we pose an ansatz

$$\mathbf{E} = k^{\nu_E}\left|\frac{J(\sigma_1,\sigma_2,0)}{J(\sigma_1,\sigma_2,\tau)}\right|^{1/2}\sum_{m=0}^{\infty}\mathbf{f}_m(\sigma_1,\sigma_2)\exp\left(ik(\sigma_1+\tau)+ik^{1/3}u_m(\sigma_1)\right), \quad (5.88)$$

$$\mathbf{H} = k^{\nu_H}\left|\frac{J(\sigma_1,\sigma_2,0)}{J(\sigma_1,\sigma_2,\tau)}\right|^{1/2}\sum_{m=0}^{\infty}\mathbf{g}_m(\sigma_1,\sigma_2)\exp\left(ik(\sigma_1+\tau)+ik^{1/3}v_m(\sigma_1)\right), \quad (5.89)$$

where σ_1, σ_2 are the geodesic normal coordinates at the launch point of the creeping ray, and τ is the distance along a creeping ray. Figure 5.4 gives the geometrical interpretation of the relation

$$\left|\frac{J(\sigma_1,\sigma_2,\tau)}{J(\sigma_1,\sigma_2,0)}\right| = \tau L(\sigma_1,\sigma_2)\left(G(\sigma_1,\sigma_2)^{1/2}+\tau\frac{\partial}{\partial\sigma_1}G(\sigma_1,\sigma_2)^{1/2}\right). \quad (5.90)$$

As we have two polarisations of the surface field, and because the creeping rays are launched from the surface field, we now define correspondingly polarised creeping rays.

Magnetically Polarised Creeping Rays

Calling upon the detailed matching of [33] and the results for the magnetically polarised surface field (5.49), we can deduce that

$$\begin{aligned} k^{\nu_E} &= k^{\nu_H} = -\frac{1}{6}, \\ u_m &= v_m = \frac{a'_m e^{-2\pi i/3}}{\sqrt[3]{2}} \int_0^{\sigma_1} |L|^{2/3}\,\mathrm{d}\lambda, \\ \mathbf{f}_m &= -\beta_m |L(\sigma_1,\sigma_2)|^{1/3} \frac{2^{-5/6}}{\sqrt{\pi}} e^{\pi i/12} \mathbf{e}_3(\sigma_1,\sigma_2,0), \\ \mathbf{g}_m &= \beta_m |L(\sigma_1,\sigma_2)|^{1/3} \frac{2^{-5/6}}{\sqrt{\pi}} e^{\pi i/12} \mathbf{e}_2(\sigma_1,\sigma_2,0), \end{aligned} \tag{5.91}$$

where the β_m are given by (5.84).

Electrically Polarised Creeping Rays

Similarly, we can write down the electrically polarised creeping ray fields as

$$\begin{aligned} k^{\nu_E} &= k^{\nu_H} = -\frac{1}{6}, \\ u_m &= v_m = \frac{a_m e^{-2\pi i/3}}{\sqrt[3]{2}} \int_0^{\sigma_1} |L|^{2/3}\,\mathrm{d}\lambda, \\ \mathbf{f}_m &= \gamma_m |L(\sigma_1,\sigma_2)|^{1/3} \frac{2^{-5/6}}{\sqrt{\pi}} e^{\pi i/12} \mathbf{e}_2(\sigma_1,\sigma_2,0), \\ \mathbf{g}_m &= \gamma_m |L(\sigma_1,\sigma_2)|^{1/3} \frac{2^{-5/6}}{\sqrt{\pi}} e^{\pi i/12} \mathbf{e}_3(\sigma_1,\sigma_2,0). \end{aligned} \tag{5.92}$$

Figure 5.3 is a cross-section of our arbitrary surface along one of the geodesics s_2 =constant. The geometrical optics and creeping rays are marked, as are the F-L and Airy Layers.

5.3.4 Shadow Boundary Structure

Outside the cylinder formed by the grazing incident rays we have the incident and reflected geometrical optics fields and inside the cylinder the creeping ray field—Figure 5.3. There is thus a discontinuity in the leading order field across this cylinder. We require a smoothly varying field and so need to investigate the structure of the field near this surface. Ray theory breaks down here and, strictly speaking, we are unable to talk about 'rays' in this region, although we will discuss this point later. The two polarisations of the field necessitate the consideration of the shadow boundary solution for magnetic and electric polarisations respectively. While the shadow boundary

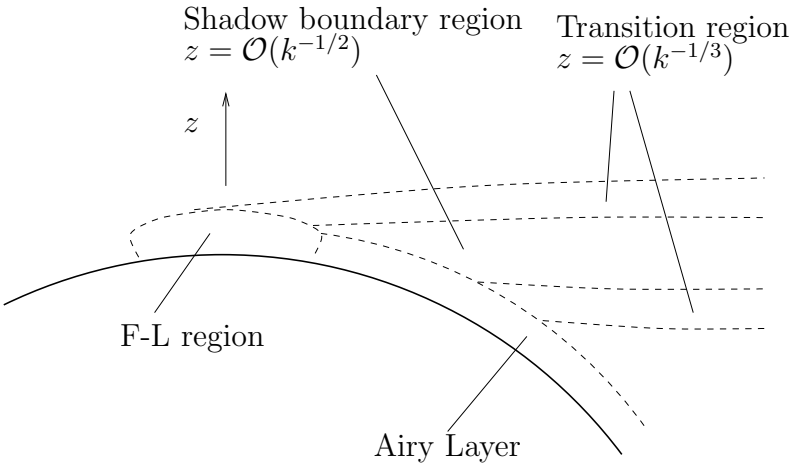


Figure 5.5: Shadow boundary structure for a plane wave-field tangent on a cylinder.

structure for two-dimensional acoustic problems is well understood, neither the three-dimensional acoustic nor the the E-M shadow boundary structure has previously been investigated in detail. We introduce the following coordinate system—see Figure 5.6. The s_2 coordinate parametrises the horizon C. The distance along the grazing incident ray is given by x and the normal distance to the cylinder with cross-section bounded by the horizon is denoted by r. As this is an orthogonal coordinate system we can use (C.17) - (C.22) with $\gamma = \pi/2$. We associate s_1, s_2, s_3 of (C.17) - (C.22) with x, s_2, r. As we are interested in small r we can approximate the metrics by

$$\begin{aligned} h_1^2 &= 1, && (5.93)\\ h_2^2 &\sim G(0, s_2) - 2rN(0, s_2) && (5.94)\\ h_3^2 &= 1, && (5.95)\\ \gamma &= \pi/2, && (5.96) \end{aligned}$$

In the same vein as §4.1.2, we make the scaling $R = k^{1/2}r$ and look for a solution of the form

$$\mathbf{F} = e^{ikx} \sum_{n=0}^{\infty} \frac{\mathbf{F}^n(x, s_2, R)}{k^{n/2}}, \tag{5.97}$$

where $\mathbf{F}$ is to be read as either $\mathbf{E}$ or $\mathbf{H}$. We insert (5.97) into (C.17) - (C.22). The $\mathcal{O}(k)$ equations are identical to (5.20) - (5.25). It is necessary to obtain terms of $\mathcal{O}(k^{1/2})$ and $\mathcal{O}(1)$. It can then easily be shown that these imply

$$\begin{aligned} \frac{\partial^2 E_2^0}{\partial R^2} + 2i\frac{\partial E_2^0}{\partial x} &= 0, && (5.98)\\ \frac{\partial^2 H_2^0}{\partial R^2} + 2i\frac{\partial H_2^0}{\partial x} &= 0. && (5.99) \end{aligned}$$

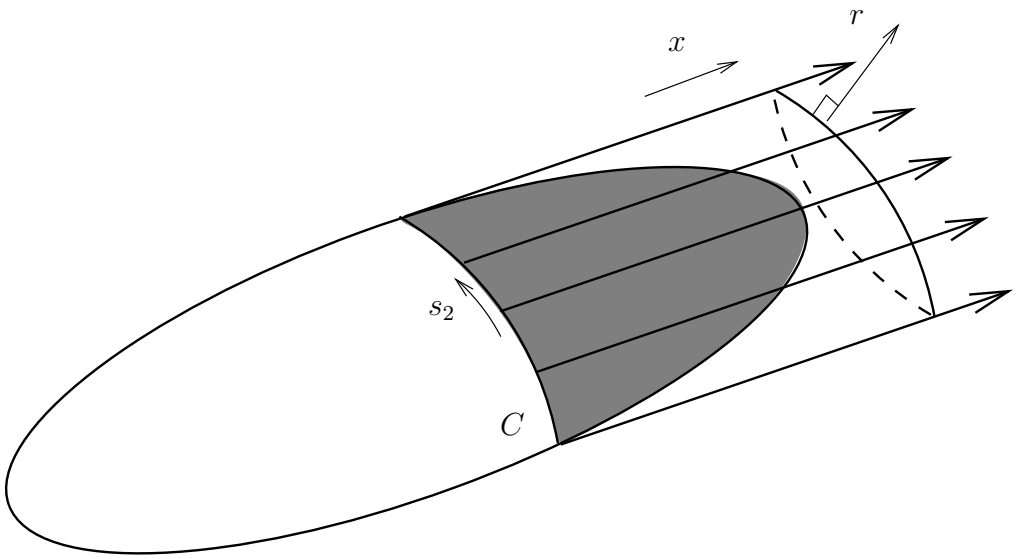


Figure 5.6: Coordinate system used to examine the shadow boundary structure for grazing incidence. Shaded area is in shadow.

Equations (C.17) - (C.22) imply that $E_1^0 \equiv H_1^0 \equiv 0$, and that E_3^0 and H_3^0 may be obtained from H_2^0 and E_2^0 respectively. We thus once again consider magnetically and electrically polarised shadow boundary solutions that will hopefully match into the correspondingly polarised geometrical optics and creeping ray fields.

Magnetically Polarised Shadow Boundary

We set $E_2^0 \equiv 0$. Equations (5.20) - (5.23) imply

$$E_1 \equiv E_2^0 \equiv H_1^0 \equiv H_3^0 \equiv 0, \tag{5.100}$$

and that $E_3^0 = -H_2^0$. The solution to (5.99) which matches into the leading order incident field must satisfy the condition

$$H_2^0 = \begin{cases} \bar{H}_2^{inc}(s_2), & R \to \infty, \\ 0, & R \to -\infty. \end{cases} \tag{5.101}$$

The relevant solution is

$$H_2^0(x, s_2, R) = \frac{\bar{H}_2^{inc}(s_2)}{2} \mathrm{erfc}\left(-\frac{e^{-i\pi/4}R}{\sqrt{2x}}\right). \tag{5.102}$$

However we see that (5.102) is incomplete when we consider the matching into the magnetically polarised reflected geometrical optics field as $R \to \infty$. We must first define what we mean by the magnetically polarised geometrical optics field.

At each point of the illuminated part of the scatterer we define $\tilde{\mathbf{e}}_2$ to be a unit vector tangent to the scatterer and perpendicular to the incident ray. We then split the incident field into two components as usual. The magnetically/electrically polarised incident field has the magnetic/electric field in the $\tilde{\mathbf{e}}_2$ direction. By considering reflection as a local effect for each polarisation, this will give rise to a magnetically/electrically polarised reflected ray (whose angle of reflection is equal to the angle of incidence) along which the magnetic/electric field is also in the $\tilde{\mathbf{e}}_2$ direction. Naturally $\tilde{\mathbf{e}}_2$ is a function of σ_1, σ_2 which are the values of s_1, s_2 at the launchpoint of the reflected ray. Using the results of §3.1 and in particular (3.31) we may write the magnetically polarised reflected field as

$$\mathbf{H} \;=\; H_{\tilde{2}}^{inc^*}(\sigma_1,\sigma_2)\left(G^{1/2}+\tau\frac{\partial}{\partial\sigma_1}G^{1/2}\right)^{-1/2}\left|\frac{\sin\psi}{\sin\psi-2\tau|L|}\right|^{1/2}e^{ik\tau}\tilde{\mathbf{e}}_2 \quad (5.103)$$

The extra geometrical factor in the reflected field that does not appear in (3.31) accounts for the spreading of the reflected ray tube in three dimensions. The distance along a reflected ray is τ and ψ is the angle the incident ray makes with the tangent plane at the point of incidence. The quantities G and L are evaluated at the point of incidence. $H_{\tilde{2}}^{inc^*}$ is the value of the component of $\mathbf{H}$ in the $\tilde{\mathbf{e}}_2$ direction evaluated at the point of incidence.

To investigate the limiting reflected ray to which the shadow boundary solution must match, we write (5.103) in terms of the shadow boundary coordinates and let $k \to \infty$. In addition, as the limiting reflected ray is launched at an $\mathcal{O}(1)$ distance from the horizon, we take $\sigma_1 = 0$—*i.e.* we evaluate G and L on the horizon. It also follows that $H_{\tilde{2}} \sim H_2$. Smith [35] shows that provided that we are close to the line $r = 0$, then we may make the following approximations

$$\tau \;\sim\; x, \quad (5.104)$$

$$\sin\psi \;\sim\; \frac{r}{2x}. \quad (5.105)$$

All of this tells us that the inner limit of the reflected field in shadow boundary coordinates is

$$H_2^0 \sim H_2^{inc}(0,s_2,0)\left(G_0^{1/2}(s_2)+x\frac{\partial G_0^{1/2}}{\partial\sigma_1}(s_2)\right)^{-1/2}\left(\frac{R}{k|L_0(s_2)|}\right)^{1/2}\frac{1}{2x}e^{ikx+iR^2/2x}. \quad (5.106)$$

Using the large argument asymptotics of the error function, the outer limit of (5.102) as $R \to \infty$ is

$$H_2^0 \;\sim\; H_2^{inc}(s_2)\left(1-\sqrt{\frac{x}{2\pi}}\frac{e^{iR^2/2x}}{R}\right)e^{ikx}. \quad (5.107)$$

It can be seen that the shadow boundary solution does not match successfully into the reflected field. A similar problem arises when we attempt to match the shadow boundary field to the creeping ray solution. Intermediate asymptotic layers must be constructed to ensure a smooth matching process.

Magnetically Polarised Transition Region

The 'last' reflected ray, as we approach the cylinder $R = 0$, $x > 0$ from above, comes from a point on the boundary just outside the F-L region, that is to say, an $\mathcal{O}(k^{-1/3})$ distance to the left of the horizon. Similarly, the 'last' creeping ray is launched from a point an $\mathcal{O}(k^{-1/3})$ distance to the right of the horizon. This motivates the scaling

$$\hat{r} \quad = \quad k^{1/3} r. \tag{5.108}$$

Motivated by the two-dimensional acoustic results of [40] we take the ansatz

$$\mathbf{F} \quad = \quad e^{ikx + ik^{1/3} u(x,\hat{r})} \sum_{n=0}^{\infty} \frac{\mathbf{F}^n(x, s_2, \hat{r})}{k^{n/3}}, \tag{5.109}$$

for the fields, where $\mathbf{F}$ is to be read as either $\mathbf{E}$ or $\mathbf{H}$. Maxwell's equations (C.17) - (C.22) give us the usual $\mathcal{O}(k)$ equations, but to solve for the leading order transition region fields we must consider also the next three higher order equations. These give us terms of $\mathcal{O}(k^{2/3})$:

$$-iE_2^0 \frac{\partial u}{\partial \hat{r}} - iH_1^1 \quad = \quad 0, \tag{5.110}$$

$$iE_1^0 \frac{\partial u}{\partial \hat{r}} - iE_3^1 - iH_2^1 \quad = \quad 0, \tag{5.111}$$

$$iE_2^1 - iH_3^1 \quad = \quad 0, \tag{5.112}$$

$$-iH_2^0 \frac{\partial u}{\partial \hat{r}} + iE_1^1 \quad = \quad 0, \tag{5.113}$$

$$iH_1^0 \frac{\partial u}{\partial \hat{r}} + iH_3^1 + iE_2^1 \quad = \quad 0, \tag{5.114}$$

$$iH_2^1 + iE_3^1 \quad = \quad 0, \tag{5.115}$$

terms of $\mathcal{O}(k^{1/3})$:

$$-\frac{\partial E_2^0}{\partial \hat{r}} - iE_2^1\frac{\partial u}{\partial \hat{r}} - iH_1^2 = 0, \tag{5.116}$$

$$\frac{\partial E_1^0}{\partial \hat{r}} + iE_1^1\frac{\partial u}{\partial \hat{r}} - iE_3^2 - iE_3^0\frac{\partial u}{\partial x} - iH_2^2 = 0, \tag{5.117}$$

$$iE_2^2 + iE_2^0\frac{\partial u}{\partial x} - iH_3^2 = 0, \tag{5.118}$$

$$-\frac{\partial H_2^0}{\partial \hat{r}} - iH_2^1\frac{\partial u}{\partial \hat{r}} + iE_1^2 = 0, \tag{5.119}$$

$$\frac{\partial H_1^0}{\partial \hat{r}} + iH_1^1\frac{\partial u}{\partial \hat{r}} - iH_3^2 - iH_3^0\frac{\partial u}{\partial x} + iE_2^2 = 0, \tag{5.120}$$

$$iH_2^2 + iH_2^0\frac{\partial u}{\partial x} + iE_3^2 = 0. \tag{5.121}$$

and terms of $\mathcal{O}(1)$:

$$\frac{1}{\sqrt{G}}\frac{\partial E_3^0}{\partial s_2} - \frac{\partial E_2^1}{\partial \hat{r}} - iE_2^2\frac{\partial u}{\partial \hat{r}} - iH_1^3 = 0, \tag{5.122}$$

$$\frac{\partial E_1^1}{\partial \hat{r}} + iE_1^2\frac{\partial u}{\partial \hat{r}} - iE_3^3 - \frac{\partial E_3^0}{\partial x} - iE_3^1\frac{\partial u}{\partial x} - iH_2^3 = 0, \tag{5.123}$$

$$\frac{\partial E_2^0}{\partial x} + iE_2^3 + iE_2^1\frac{\partial u}{\partial \hat{r}} - iH_3^3 = 0, \tag{5.124}$$

$$\frac{1}{\sqrt{G}}\frac{\partial H_3^0}{\partial s_2} - \frac{\partial H_2^1}{\partial \hat{r}} - iH_2^2\frac{\partial u}{\partial \hat{r}} + iE_1^3 = 0, \tag{5.125}$$

$$\frac{\partial H_1^1}{\partial \hat{r}} + iH_1^2\frac{\partial u}{\partial \hat{r}} - iH_3^3 - \frac{\partial H_3^0}{\partial x} - iH_3^1\frac{\partial u}{\partial x} + iE_2^3 = 0, \tag{5.126}$$

$$\frac{\partial H_2^0}{\partial x} + iH_2^3 + iH_2^1\frac{\partial u}{\partial \hat{r}} + iE_3^3 = 0. \tag{5.127}$$

Equating (5.118) and (5.120) and using (5.110) to eliminate H_1^1 gives us an equation for the phase

$$\left(\frac{\partial u}{\partial \hat{r}}\right)^2 + 2\frac{\partial u}{\partial x} = 0. \tag{5.128}$$

We then equate (5.123) and (5.127). Use of (5.119) and (5.128) yields

$$2\frac{\partial H_2^0}{\partial \hat{r}}\frac{\partial u}{\partial \hat{r}} + 2\frac{\partial H_2^0}{\partial x} + H_2^0\frac{\partial^2 u}{\partial \hat{r}^2} = 0. \tag{5.129}$$

Equations (5.128) and (5.129) are accompanied by the matching conditions that as $\hat{r} \to \pm\infty$ the transition region field must match into the the geometrical optics reflected field and the creeping ray field respectively. The first of these matching conditions can be written as

$$H_2 \sim H_2^{inc^*}\left(G_0^{1/2}(s_2) + x\frac{\partial G_0^{1/2}}{\partial \sigma_1}(s_2)\right)^{-1/2}\left(\frac{\hat{r}}{|L_0(s_2)|}\right)^{1/2}\frac{1}{k^{1/6}x}e^{ikx+ik^{1/3}\hat{r}^2/2x}, \quad \hat{r}\to\infty, \tag{5.130}$$

To obtain the second condition requires us first to write the creeping ray coordinates σ, τ in terms of the transition region coordinates. For small σ we can say

$$x \sim \tau + k^{-1/3}\hat{\sigma} - k^{-2/3}\tau\hat{\sigma}^2\frac{|L_0|^2}{2} - k^{-1}\hat{\sigma}^3\frac{|L_0|^2}{6}, \tag{5.131}$$

$$\hat{r} \sim -\tau\hat{\sigma}|L_0| - k^{-1/3}\hat{\sigma}^2\frac{|L_0|}{2} + k^{-2/3}\tau\hat{\sigma}^3\frac{|L_0|^3}{6}, \tag{5.132}$$

where $\hat{\sigma} = k^{1/3}\sigma_1$. These can be solved to give

$$\hat{\sigma} \sim -\frac{\hat{r}}{x|L_0|} + k^{-1/3}\frac{\hat{r}^2}{2x^3|L_0|^2}, \tag{5.133}$$

$$\tau \sim x + k^{-1/3}\frac{\hat{r}}{x|L_0|} + k^{-2/3}\left(\frac{\hat{r}^2|L_0|}{2x} - \frac{\hat{r}^2}{2x^3|L_0|^2}\right). \tag{5.134}$$

Using the results of §5.3.3 we can then write the second matching condition as

$$H_2 \sim \frac{H_2^{inc^*}2^{1/6}e^{-3\pi i/4}\sqrt{\pi}G_0^{1/4}}{k^{1/6}\sqrt{\tau}|L_0|^{1/3}\left(G_0^{1/2} + \frac{\partial}{\partial\sigma}G_0^{1/2}\right)^{1/2}}\frac{\mathrm{Ai}'\left(e^{-2\pi i/3}a_m'\right)}{\mathrm{Ai}''(a_m')}$$
$$\times\exp\left(ikx + ik^{1/3}\frac{\hat{r}^2}{2x} + i\frac{a_m'e^{-2\pi i/3}}{\sqrt[3]{2}}\hat{\sigma}_1|L_0|^{2/3}\right), \qquad \hat{r}\to-\infty. \tag{5.135}$$

Equations (5.128), (5.130) and (5.135) trivially fix

$$u = \frac{\hat{r}^2}{2x}. \tag{5.136}$$

The similarity solution

$$H_2^0(x,\hat{r}) = \frac{1}{\sqrt{x}}g\left(\frac{\hat{r}}{x}\right), \tag{5.137}$$

satisfies (5.129), but leaves us with no further equations for g. The unknown function g is found by observing that the outer limit of the F-L solution written in the transition region coordinates actually satisfies (5.130) and (5.135), in addition to being a similarity solution of the required form. The details can be found in [35] for the two-dimensional acoustic case. For the three-dimensional problem that we are considering, there is an additional $\left(G_0(s_2)^{1/2} + \frac{\partial}{\partial\sigma_1}G_0(s_2)^{1/2}\right)^{-1/2}$ factor that appears in the inner limits of the geometrical optics reflected and creeping ray fields. To deal with this we note that we can take $G_0(s_2) = 1$ as we may parametrise the horizon

C by arclength. In addition, we can say that $\frac{\partial}{\partial\sigma_1}G_0(s_2) = 0$[1] at the horizon. This reduces our matching to exactly that which is carried out for the two-dimensional problem in [35]. To rewrite the F-L solution (5.83) in transition region coordinates $x, \hat{r}$, we first note that

$$x \sim k^{-1/3}\hat{s_1} + k^{-1}(\hat{\rho}\hat{s_1}|L_0(s_2)| - \frac{1}{6}\hat{s_1}^3|L_0(s_2)|^2), \tag{5.138}$$

$$r \sim k^{-2/3}|L_0(s_2)|^{-1/3}(\hat{\rho} - \frac{x^2|L_0(s_2)|}{2}). \tag{5.139}$$

in the neighbourhood of the horizon. Using the large argument expansion for the Airy function

$$\mathrm{Ai}(z) \sim \frac{\exp\left(-\frac{2}{3}z^{3/2}\right)}{2\sqrt{\pi}z^{1/4}}, \tag{5.140}$$

and tedious algebra, we finally obtain the magnetically polarised upper transition region solution as

$$g = \frac{\sqrt{2}e^{-\pi i/12}\bar{H}_2^{inc}(s_2)}{\sqrt{\pi}|L_0|k^{1/6}}\int_{-\infty}^{\infty}\frac{\mathrm{Ai}'[-\sqrt[3]{2}|L_0|^{-2/3}\lambda]}{\mathrm{Ai}'[-\sqrt[3]{2}|L_0|^{-2/3}\lambda e^{2\pi i/3}]}\exp\left(\frac{-i\hat{r}\lambda}{|L_0|x} - \frac{i\hat{r}^3}{6|L_0|x^3}\right)\mathrm{d}\lambda, \tag{5.141}$$

Electrically Polarised Shadow Boundary Structure

The analysis follows through identically to §5.3.4. Specifically, for the electrically polarised shadow boundary solution we take (5.97) as an ansatz. The solution is

$$\begin{aligned} E_1 \equiv E_3^0 \equiv H_1^0 \equiv H_2^0 &\equiv 0, \\ H_3^0 \equiv E_2^0 &= \frac{\bar{E}_2^{inc}(s_2)}{2}\mathrm{erfc}\left(-\frac{e^{-i\pi/4}R}{\sqrt{2x}}\right). \end{aligned} \tag{5.142}$$

[1] At the horizon $\frac{\partial\mathbf{R}}{\partial s_1} = \mathbf{k} = $ constant as the incident field is a plane wave. Thus, *at the horizon,*

$$\begin{aligned} \frac{\partial G}{\partial s_1} &= 2\frac{\partial\mathbf{R}}{\partial s_2}\cdot\frac{\partial^2\mathbf{R}}{\partial s_1\partial s_2}, \\ &= 2\frac{\partial}{\partial s_2}\left(\frac{\partial\mathbf{R}}{\partial s_1}\cdot\frac{\partial\mathbf{R}}{\partial s_2}\right) - 2\frac{\partial\mathbf{R}}{\partial s_1}\cdot\frac{\partial^2\mathbf{R}}{\partial s_2^2}, \\ &= 2\frac{\partial}{\partial s_2}\left(\mathbf{k}\cdot\frac{\partial\mathbf{R}}{\partial s_2}\right) - 2\mathbf{k}\cdot\frac{\partial^2\mathbf{R}}{\partial s_2^2}, \\ &= 0. \end{aligned}$$

For the electrically polarised transition region solution we take the ansatz (5.109). The solution is obtained as

$$\begin{aligned} E_1 \equiv E_3^0 \equiv H_1^0 \equiv H_2^0 &\equiv 0, \\ H_3^0 \equiv E_2^0 &= \frac{1}{\sqrt{x}} h\left(\frac{\hat{r}}{x}\right) \\ u &= \frac{\hat{r}^2}{2x} \end{aligned} \tag{5.143}$$

where

$$h = -\frac{\sqrt{2}e^{11\pi i/12}\bar{H}_2^{inc}(s_2)}{|L_0|k^{1/6}} \int_{-\infty}^{\infty} \frac{\mathrm{Ai}[-\sqrt[3]{2}|L_0|^{-2/3}\lambda]}{\mathrm{Ai}[-\sqrt[3]{2}|L_0|^{-2/3}\lambda e^{2\pi i/3}]} \exp\left(\frac{-i\hat{r}\lambda}{|L_0|x} - \frac{i\hat{r}^3}{6|L_0|x^3}\right) \mathrm{d}\lambda, \tag{5.144}$$

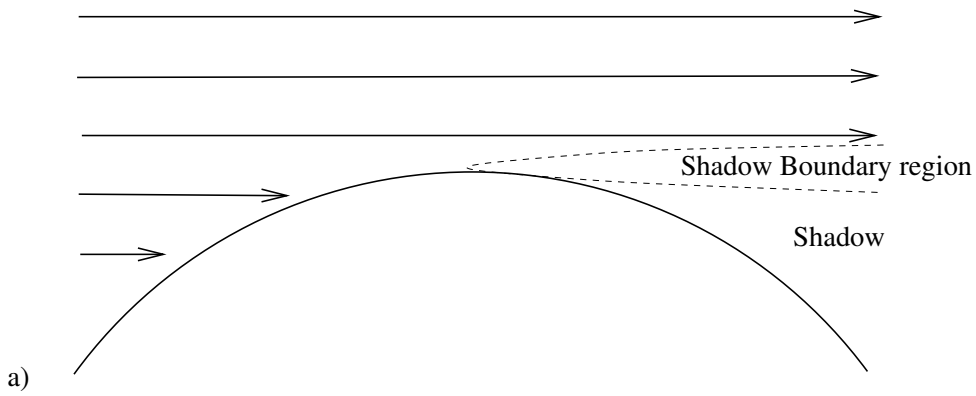
To summarise, the $\mathcal{O}(k^{-1/2})$ shadow boundary region smoothly switches the incident field off as we cross from the geometrical optics lit region into shadow. The $\mathcal{O}(k^{-1/3})$ transition region provides a match between the geometrical optics reflected and creeping ray fields. Figure 5.7 shows the ray picture and associated asymptotic structure for both the incident and scattered fields.

5.3.5 Finite Bodies

In §4.2.2 we saw how the two shadow boundaries generated by a radiating flat plate meet at an $\mathcal{O}(k)$ distance from the plate, and that here the error-function profiles characteristic of the shadow boundary regions are no longer valid. If we have a finite convex scatterer illuminated by plane-wave radiation, we would anticipate that the shadow boundaries and transition regions will similarly merge at $\mathcal{O}(k)$ and $\mathcal{O}(k^{1/3})$ distances from the horizon, respectively. This is discussed at greater length in [40]. In addition, the geodesics will perform multiple revolutions of a finite body. Thus creeping rays will repeatedly circulate the body. However, the exponential decay of the surface field from which the creeping rays are launched means that to leading order we do not need to consider the creeping rays arising from multiple revolutions.

5.3.6 Ray Solutions

We can only talk about ray solutions if we have an eikonal equation for the phase from which we can construct the wavefronts. Thus in the geometrical optics and creeping ray regions we can construct rays along which we know the solution. In the other asymptotic regions considered we did not have an eikonal equation for the phase because we assumed *a priori* an $\exp(ikx)$ or $\exp(iks_1)$ factor in the solution. These



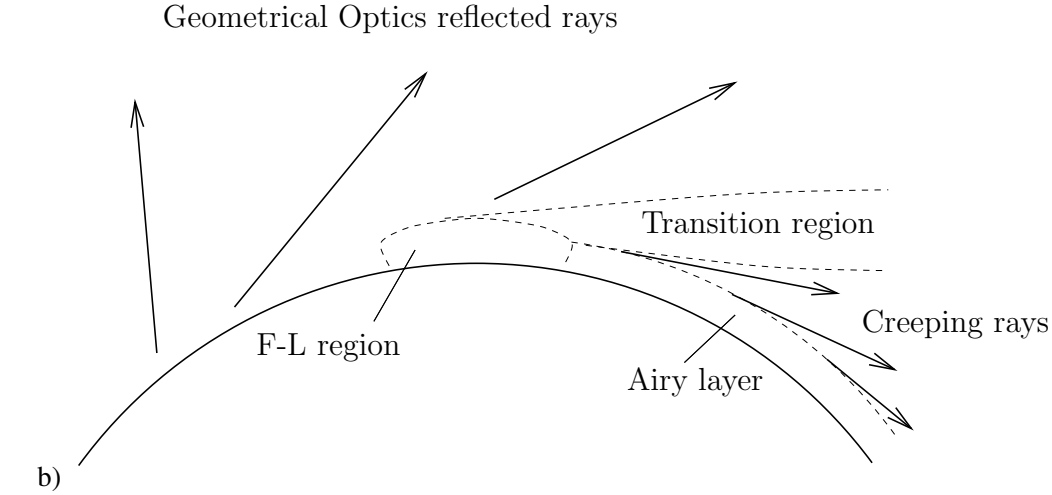
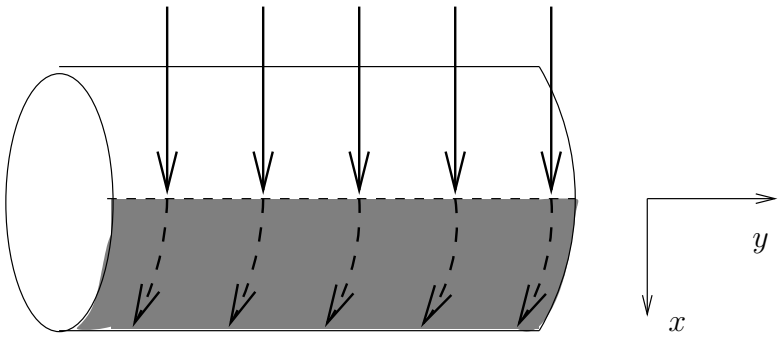
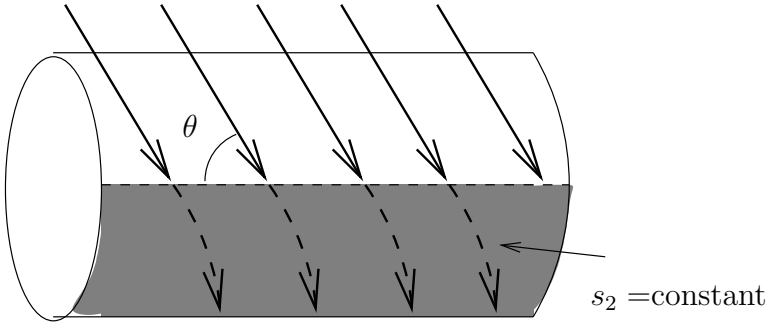


Figure 5.7: a) Incident field and associated shadow boundary region. b) Scattered field and associated asymptotic structure.



a)



b)

Figure 5.8: Plane wave incident a) perpendicular to the horizon, b) obliquely to the horizon.

phases satisfy the leading order eikonal equation which means that the higher order equations for the amplitudes become the leading order equations in these regions. Thus for a numerical ray tracing scheme the solutions in the F-L region and Airy layer could be constructed along rays in the s_1 direction. In the shadow boundary and transition regions we could construct rays in the x direction.

5.4 Oblique Plane Wave Incidence

Having set up the asymptotic structure for the simplest three-dimensional problem, we now generalise it to the case where the tangent rays are no longer perpendicular to the horizon C. Although our aim is ultimately to write down the surface field, as in the previous section we must consider an F-L region near C. Before doing this for general geometries we consider a toy problem that will give us an idea of what to expect.

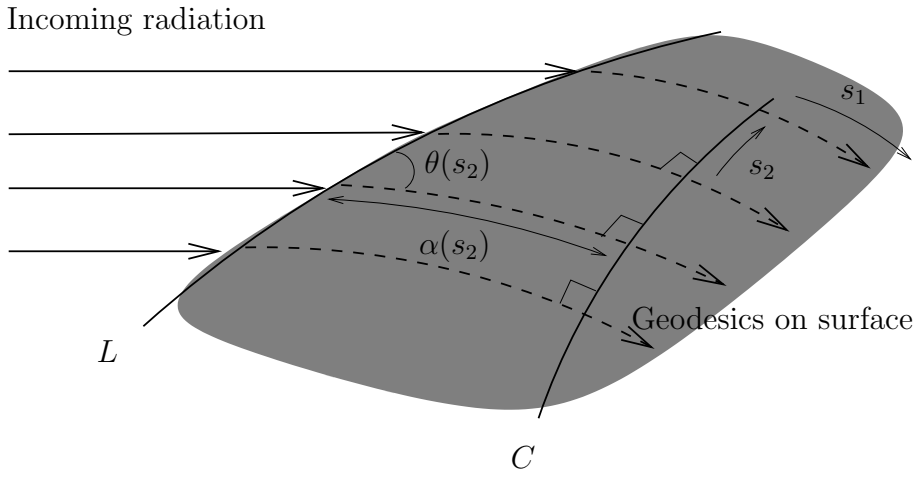


Figure 5.9: Geodesic normal coordinate system for oblique incidence.

5.4.1 Fock-Leontovič Region

As each component of the $\mathbf{E}, \mathbf{H}$ fields satisfies the Helmholtz equation we consider an acoustic problem for simplicity. Consider the two-dimensional problem of a plane wave-field impinging on a cylinder with either a sound hard or soft boundary condition as in Figure 5.8a). Instead of working in s, n coordinates we carry out a local expansion about the horizon in terms of the scaled coordinates

$$\hat{x} \;=\; k^{1/3}x, \quad \hat{z} \;=\; k^{2/3}z. \tag{5.145}$$

Taking an ansatz

$$\phi \;=\; A(\hat{x}, \hat{z})e^{ikx}, \tag{5.146}$$

the Helmholtz equation for ϕ yields the leading order equation

$$\frac{\partial^2 A}{\partial \hat{z}^2} + 2i\frac{\partial A}{\partial \hat{x}} \;=\; 0, \tag{5.147}$$

along with either a Neumann or a Dirichlet boundary condition on $\hat{z} = -\kappa_0 \hat{x}^2/2$. Solving (5.147) yields the same solution in the F-L region that we obtained earlier—see [35] for details.

We now consider the plane wave-field $\exp(ikx\sin\theta \;+\; iky\cos\theta)$ illuminating the same cylinder, for some $\theta = \mathcal{O}(1)$ as in Figure 5.8b). If $\theta = \mathcal{O}(k^{-1/3})$ then the normal curvature of the geodesics will not get into the leading order problem. We introduce the variable

$$\eta \;=\; x\sin\theta + y\cos\theta, \tag{5.148}$$

and the ansatz

$$\phi \;=\; B(\eta, z, s_2)e^{ik\eta}, \tag{5.149}$$

where s_2 indicates which geodesic we are on. The scalings

$$\hat{\eta} \;=\; k^{1/3}\eta, \quad \hat{z} \;=\; k^{2/3}z, \tag{5.150}$$

give us the leading order F-L equation

$$\frac{\partial^2 B}{\partial \hat{z}^2} + 2i\frac{\partial B}{\partial \hat{\eta}} \;=\; 0, \tag{5.151}$$

with either a Neumann or a Dirichlet condition on the line $\hat{z} = -|L_0|\left(\hat{\eta} - \hat{\eta}(s_2)\right)^2/2$, where the horizon is given by $\hat{\eta} = \hat{\eta}(s_2)$. Here L_0 is the normal curvature along the geodesic $s_2 = \text{constant}$ *at* the point of tangency. The solutions in this F-L region can thus be obtained from those for the two-dimensional problem. The geodesic *normal* coordinate s_1 in (5.83) and (5.86) is simply replaced by the corresponding geodesic *oblique* coordinate η.

We now consider the E-M problem of plane wave incidence on a general convex surface. We use the geodesic normal coordinate system illustrated in Figure 5.9. We construct the geodesics on the surface that are the continuations of the incident rays. We take C to be an arbitrary curve on the surface that is perpendicular to these geodesics. This curve then acts as the initial line for a geodesic normal coordinate system—i.e. C is parametrised by s_2 and s_1 measures the distance along the geodesics from C. The normal distance to the surface is given by s_3. The function $\alpha(s_2)$ measures the distance between C and the horizon L. Each geodesic makes an angle $\theta(s_2)$ with L. Motivated by our toy problem, we pose the ansatz

$$\mathbf{F} \;=\; \bar{\mathbf{F}}^{inc}e^{i\mathbf{k}.\mathbf{r}} + e^{iks_1}\sum_{n=0}^{\infty}\frac{\mathbf{F}^n(\hat{s}_1^*, s_2, \rho)}{k^{n/3}}, \tag{5.152}$$

where

$$\hat{s}_1^* \;=\; k^{1/3}(s_1 + \alpha(s_2)), \quad \hat{\rho} \;=\; k^{2/3}s_3, \tag{5.153}$$

and $\mathbf{F}$ is to be read as either $\mathbf{E}$ or $\mathbf{H}$. Using the representation of Maxwell's equations given by (C.17) - (C.22) and noting that we must now replace

$$\frac{\partial}{\partial s_2} \;\rightarrow\; \frac{\partial}{\partial s_2} + \alpha'(s_2)\frac{\partial}{\partial s_1}, \tag{5.154}$$

we find that subject to to the constraints that $\alpha'(s_2) \ll k^{2/3}$—in other words α varies with respect to s_2 on a length scale D where $D \gg k^{-1/3}$—and that $\theta(s_2) = \mathcal{O}(1)$ we may derive the F-L equations (5.65) - (5.66) for H_2^0 and E_2^0 with s_1 replaced by s_1^*. The boundary conditions on $\rho = 0$ given by (5.79) - (5.80) change to

$$\begin{aligned}
\frac{\partial H_2^0}{\partial \rho} &= ik^{2/3}\bar{H}_2^{inc} L(-\alpha(s_2), s_2)\hat{s}_1^* \\
&\quad \times \exp\left(ik\mathbf{e}_1 \centerdot \mathbf{R}\left(-\alpha(s_2), s_2\right) + ik\alpha(s_2) - iL^2\left(-\alpha(s_2), s_2\right)\frac{\hat{s}_1^*}{6}\right), \quad (5.155) \\
E_2^0 &= -\bar{E}_2^{inc} \exp\left(ik\mathbf{e}_1 \centerdot \mathbf{R}\left(-\alpha(s_2), s_2\right) + ik\alpha(s_2) - iL^2\left(-\alpha(s_2), s_2\right)\frac{\hat{s}_1^*}{6}\right), \quad (5.156)
\end{aligned}$$

as we have expanded about $s_1 = -\alpha(s_2)$ rather than about $s_1 = 0$ as was the case for normal incidence. Again using the notation

$$F^{inc^*} = \bar{F}^{inc} \exp\left(ik\mathbf{e}_1 \centerdot \mathbf{R}(0, s_2)\right), \quad (5.157)$$

where F^{inc^*} is the value of the incident field F^{inc} at the horizon, (5.155) - (5.156) may be written

$$\begin{aligned}
\frac{\partial H_2^0}{\partial \rho} &= ik^{2/3} H_2^{inc^*} L(-\alpha(s_2), s_2)\hat{s}_1^* \exp\left(ik\alpha(s_2) - iL^2\left(-\alpha(s_2), s_2\right)\frac{\hat{s}_1^*}{6}\right), \quad (5.158) \\
E_2^0 &= -E_2^{inc^*} \exp\left(ik\alpha(s_2) - iL^2\left(-\alpha(s_2), s_2\right)\frac{\hat{s}_1^*}{6}\right), \quad (5.159)
\end{aligned}$$

Using the results from §5.3.2 the magnetically polarised solution in the F-L region may thus be written

$$E_1 \sim E_2 \sim H_1 \sim H_3 \sim 0, \quad (5.160)$$

with

$$\begin{aligned}
H_2 \sim -E_3 &\sim -\sqrt[3]{2}e^{-2\pi i/3}|L_0|^{-2/3} H_2^{inc^*} e^{iks_1^*} \quad (5.161) \\
&\times \int_{-\infty}^{\infty} \left\{ \frac{\mathrm{Ai}'[-\sqrt[3]{2}|L_0|^{-2/3}\lambda]}{\mathrm{Ai}'[-\sqrt[3]{2}|L_0|^{-2/3}\lambda e^{2\pi i/3}]} \mathrm{Ai}[-\sqrt[3]{2}e^{2\pi i/3}|L_0|^{-2/3}(|L_0|\rho + \lambda)] \right\} e^{-i\lambda\hat{s}_1^*} \, \mathrm{d}\lambda.
\end{aligned}$$

Thus the magnetically polarised F-L solution is exactly the same as the F-L solution for normal incidence but with the normal geodesic coordinate s_1 replaced everywhere by the geodesic coordinate. Similarly with the electrically polarised F-L field.

5.4.2 Airy Layer Field

Using the results of §5.3.1 the magnetically polarised field in the Airy layer is

$$\begin{aligned}\mathbf{E} \sim & -\sum_{m=0}^{\infty} \frac{\beta_m(s_2)|L|^{1/6}}{G^{1/4}} \mathrm{Ai}\left(-\sqrt[3]{2}e^{2\pi i/3}|L|^{1/3}\rho + a'_m\right) \\ & \times \exp\left(iks_1 + ik^{1/3}\frac{a'_m e^{-2\pi i/3}}{\sqrt[3]{2}}\int_0^{s_1}|L|^{2/3}\,\mathrm{d}\lambda\right)\mathbf{e}_3, \qquad (5.162) \\ \mathbf{H} \sim & \sum_{m=0}^{\infty} \frac{\beta_m(s_2)|L|^{1/6}}{G^{1/4}} \mathrm{Ai}\left(-\sqrt[3]{2}e^{2\pi i/3}|L|^{1/3}\rho + a'_m\right) \\ & \times \exp\left(iks_1 + ik^{1/3}\frac{a'_m e^{-2\pi i/3}}{\sqrt[3]{2}}\int_0^{s_1}|L|^{2/3}\,\mathrm{d}\lambda\right)\mathbf{e}_2, \qquad (5.163)\end{aligned}$$

where we have to fix the $\beta_m(s_2)$. Matching the fields as $s_1 \to -\alpha(s_2)$, (5.84) implies that

$$\begin{aligned}\beta_m(s_2) = & \ 2\pi H_2^{inc^*} G_0^{1/4}|L_0(s_2)|^{-1/6}e^{i\pi/6}\frac{\mathrm{Ai}'[e^{-2\pi i/3}a'_m]}{\mathrm{Ai}''[a'_m]} \\ & \times \exp\left(ik\alpha(s_2) + ik^{1/3}\frac{a'_m e^{-2\pi i/3}}{\sqrt[3]{2}}\int_{-\alpha(s_2)}^{0}|L|^{2/3}\,\mathrm{d}\lambda\right). \qquad (5.164)\end{aligned}$$

We may thus rewrite (5.162) and (5.163) as

$$\begin{aligned}\mathbf{E} \sim & -\sum_{m=0}^{\infty} \frac{\beta_m(s_2)|L|^{1/6}}{G^{1/4}} \mathrm{Ai}\left(-\sqrt[3]{2}e^{2\pi i/3}|L|^{1/3}\rho + a'_m\right) \\ & \times \exp\left(iks_1^* + ik^{1/3}\frac{a'_m e^{-2\pi i/3}}{\sqrt[3]{2}}\int_0^{s_1^*}|L|^{2/3}\,\mathrm{d}\lambda\right)\mathbf{e}_3, \qquad (5.165) \\ \mathbf{H} \sim & \sum_{m=0}^{\infty} \frac{\beta_m(s_2)|L|^{1/6}}{G^{1/4}} \mathrm{Ai}\left(-\sqrt[3]{2}e^{2\pi i/3}|L|^{1/3}\rho + a'_m\right) \\ & \times \exp\left(iks_1^* + ik^{1/3}\frac{a'_m e^{-2\pi i/3}}{\sqrt[3]{2}}\int_0^{s_1^*}|L|^{2/3}\,\mathrm{d}\lambda\right)\mathbf{e}_2, \qquad (5.166)\end{aligned}$$

with the $\beta_m(s_2)$ given by (5.84).

The determination of the creeping ray fields relies solely on the outer limit of the Airy layer field. Thus the solutions along the creeping rays will be exactly the same as those already obtained in §5.3.3.

Similar calculations can be carried out for the electrically polarised surface fields with the same result—namely identical solutions to those already obtained for tangent rays normal to C.

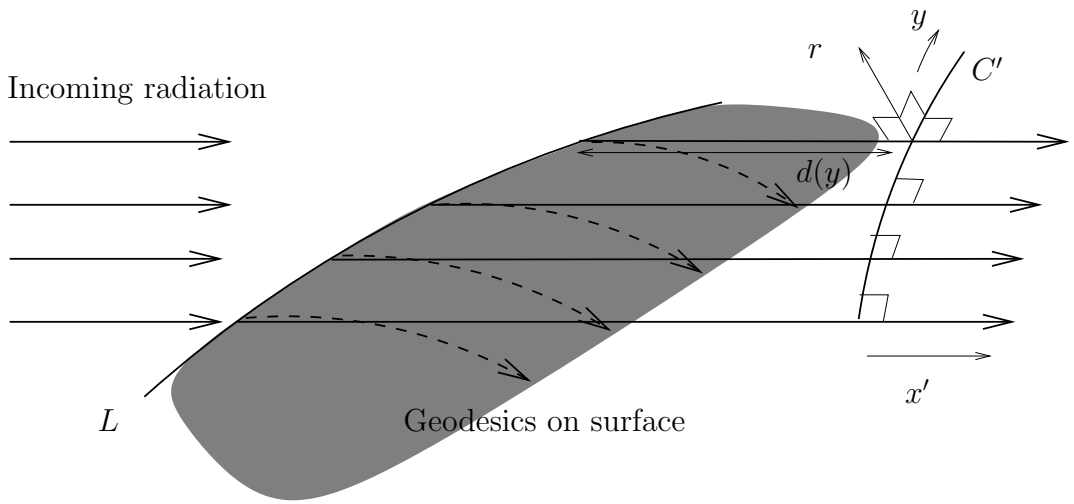


Figure 5.10: Coordinate system for the shadow boundary regions formed by obliquely tangent rays.

5.4.3 Shadow Boundary Structure

In light of §5.3.4 it should come as no surprise that we must introduce asymptotic regions to deal with the discontinuity between the leading order geometrical optics incident and reflected fields on one side of the surface formed by the grazing incident rays, and the creeping ray field on the other. We again introduce a cylindrical coordinate system as in Figure 5.10. Unit vectors $\hat{\mathbf{e}}_1, \hat{\mathbf{e}}_2, \hat{\mathbf{e}}_3$ are in the directions of maximum increase of x', y, r. The coordinate x' represents the distance from an arbitrarily chosen line C' that is normal to and intersects all the grazing rays, y indicates which grazing ray we are on and r is the normal distance to the surface formed by the grazing rays. The quantity $d(y)$ is the distance from C' to the horizon along the ray y = constant. This is an orthogonal coordinate system and so we may use the metrics (5.93) - (5.96). We make the scaling $\tilde{r} = k^{1/2} r$ and take the ansatz

$$\mathbf{F} \;=\; e^{ikx'} \sum_{n=0}^{\infty} \frac{\mathbf{F}_n(x', y, \tilde{r})}{k^{n/2}}, \tag{5.167}$$

for the fields $\mathbf{E}, \mathbf{H}$. Section 5.3.4 immediately implies that to lowest order the fields satisfy equations (5.20) - (5.25) and that going to higher orders we obtain the familiar parabolic wave approximation, namely

$$\frac{\partial^2 E_2^0}{\partial \tilde{r}^2} + 2i \frac{\partial E_2^0}{\partial x'} \;=\; 0, \tag{5.168}$$

$$\frac{\partial^2 H_2^0}{\partial \tilde{r}^2} + 2i \frac{\partial H_2^0}{\partial x'} \;=\; 0. \tag{5.169}$$

To investigate the matching we consider just the magnetically polarised shadow boundary solution. We set $H_3^0 \equiv 0$ and solve (5.169) along with the matching condition

$$H_2^0 \;\rightarrow\; \begin{cases} H_2^{inc^*}(y), & \tilde{r} > 0, \\ 0, & \tilde{r} < 0, \end{cases} \tag{5.170}$$

as $x' \rightarrow -d(y)$. This has the solution

$$H_2^0(x', y, \tilde{r}) \;=\; \frac{H_2^{inc^*}(y)}{2} e^{ikd(y)} \mathrm{erfc}\left(-\frac{e^{-i\pi/4}\tilde{r}}{\sqrt{2\left(x' + d(y)\right)}} \right). \tag{5.171}$$

If we introduce $x = x' + d(y)$, we may rewrite the non-zero component of the magnetic field in the shadow boundary region as

$$H_2 \;=\; H_2^{inc^*} e^{ikx} \mathrm{erfc}\left(-\frac{e^{-i\pi/4}\tilde{r}}{\sqrt{2x}} \right). \tag{5.172}$$

Exactly as before, this does not match successfully into either the reflected geometrical optics or the creeping ray fields and so a transition region must be considered.

We look at just the magnetically polarised transition region. We work with the orthogonal co-ordinates x', y, r illustrated in Figure 5.10. Again we introduce the $\mathcal{O}(1)$ variable $\hat{r} = k^{1/3} r$ and take the usual ansatz for the transition region fields, namely

$$\mathbf{F} \;=\; e^{ikx' + ik^{1/3} u(x', \hat{r})} \sum_{n=0}^{\infty} \frac{\mathbf{F}^n(x', s_2, \hat{r})}{k^{n/3}}. \tag{5.173}$$

This yields equations (5.128) and (5.129) for the phase and leading order amplitude respectively—with any occurences of x replaced by x'—in addition to the usual lowest order equations for the fields (5.20) - (5.25). To obtain the transition region solution we again take the F-L solution and write it in terms of our transition region coordinates and vectors. It is straightforward to see that this is a similarity solution of the correct form and that it will also match into the inner limits of the reflected geometrical optics and creeping ray fields in the same way as occurred for the case when $\theta(s_2) \equiv \pi/2$. The footnote on page 80 is still valid.

The electrically polarised solutions in the shadow boundary and transition regions are identical to those obtained in §5.3.4.

We are thus in the agreeable situation where the angle of the incident rays to the horizon does not affect either the solution structure or form. A cross section taken along any incident ray still reveals the same asymptotic structure as illustrated in Figures 5.3 and 5.5.

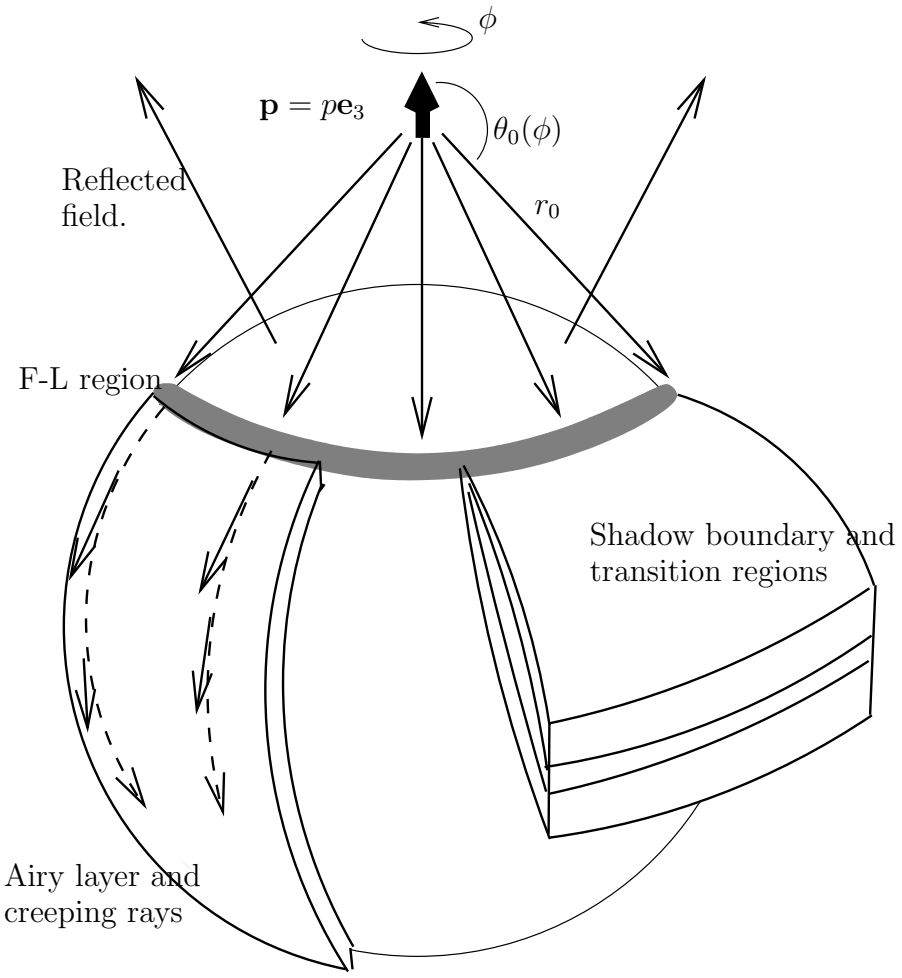


Figure 5.11: Dipole at an $\mathcal{O}(1)$ distance from a convex scatterer.

5.5 A Dipole at an $\mathcal{O}(1)$ Distance from a Perfectly Conducting Convex Surface

The plane wave incidence problem considered thus far can be considered as the irradiation of the scatterer by a source at infinity. In many applications we will wish to know the scattered field due to a source at an $\mathcal{O}(1)$ distance from the scatterer. We are unable to obtain the complete asymptotic solution for this problem, but there are certain things that we are able to say. The associated two-dimensional problem—a line source at an $\mathcal{O}(1)$ distance from and parallel to a perfectly conducting cylinder—is more tractable and is investigated in §5.6.

We do know that the structure of the solution must be as illustrated in Figure 5.11. That is, there will be an F-L region in the neighbourhood of the horizon, an Airy layer close to the surface in shadow, creeping rays launched tangentially from the Airy

layer, and shadow boundary and transition regions to match smoothly between the GO incident and reflected fields and the creeping ray field. It is also straightforward to write down the asymptotic fields in the F-L, Airy layer and creeping ray regions. At each point along the horizon we decouple the field into magnetically and electrically polarised components. They will each set up correspondingly polarised F-L, Airy and shed creeping ray fields. We will just investigate the magnetically polarised fields here—the analysis for the electrically polarised fields is no different. We parametrise the horizon by the polar angle ϕ, and construct the geodesics on the scatterer which are the continuations of the grazing rays. The dipole has a moment $\mathbf{p} = p\mathbf{e}_3$. Taking s_1^* to be the distance along these geodesics we can write down the F-L solution using the results of §5.4.1. We take the usual F-L ansatz

$$\mathbf{F} \quad = \quad \bar{\mathbf{F}}^{inc} e^{i\mathbf{k}.\mathbf{r}} + e^{iks_1^*} \sum_{n=0}^{\infty} \frac{\mathbf{F}^n(\hat{s}_1^*, \phi, \rho)}{k^{n/3}}. \tag{5.174}$$

Expanding the incident field close to the tangency point yields

$$H_2^{inc^*} \quad = \quad -p^* k \frac{e^{ikr_0}}{4\pi r_0}, \tag{5.175}$$

where $r_0(\phi)$ is the distance from the source to the horizon. p^* is to be calculated from (2.54) and knowledge of the geometry of the convex scatterer in the neighbourhood of the horizon. As the source approaches the surface we see that $p^* \to p$. Thus, §5.4.1 and in particular (5.161) implies that the solution in the F-L region is given by

$$E_1^0 \equiv E_2^0 \equiv H_1^0 \equiv H_3^0 \quad \equiv \quad 0, \tag{5.176}$$

$$H_2^0 \equiv -E_3^0 \quad = \quad -\sqrt[3]{2} e^{\pi i/3} |L_0|^{-2/3} p^* k \frac{e^{ikr_0}}{4\pi r_0} \tag{5.177}$$

$$\times \int_{-\infty}^{\infty} \left\{ \frac{\mathrm{Ai}'[-\sqrt[3]{2}|L_0|^{-2/3}\lambda]}{\mathrm{Ai}'[-\sqrt[3]{2}|L_0|^{-2/3}\lambda e^{2\pi i/3}]} \mathrm{Ai}[-\sqrt[3]{2} e^{2\pi i/3} |L_0|^{-2/3} (|L_0|\rho + \lambda)] \right\} e^{-i\lambda \hat{s}_1^*} \, \mathrm{d}\lambda.$$

The ansatz for the Airy layer field is

$$\mathbf{F} \quad = \quad e^{iks_1^* + ik^{1/3} u(s_1^*, \phi)} \sum_{n=0}^{\infty} \frac{\mathbf{F}^n(s_1^*, \phi, \rho)}{k^{n/3}}. \tag{5.178}$$

The solution follows from §5.4.2, namely

$$E_1^0 \equiv E_2^0 \equiv H_1^0 \equiv H_3^0 \quad \equiv \quad 0, \tag{5.179}$$

$$H_2^0 \equiv -E_3^0 \quad = \quad p^* k \frac{e^{ikr_0}}{2r_0} G_0^{1/4}(\phi) |L_0(\phi)|^{-1/6} e^{\pi i/6} \frac{\mathrm{Ai}'[e^{-2\pi i/3} a_m']}{\mathrm{Ai}''[a_m']}$$

$$\times \sum_{m=0}^{\infty} \frac{|L|^{1/6}}{G^{1/4}} \mathrm{Ai}\left(-\sqrt[3]{2} e^{2\pi i/3} |L|^{1/3} \rho + a_m' \right), \tag{5.180}$$

$$u(s_1^*, \phi) \quad = \quad \frac{a_m' e^{-2\pi i/3}}{\sqrt[3]{2}} \int_0^{s_1^*} |L|^{2/3} \, d\lambda. \tag{5.181}$$

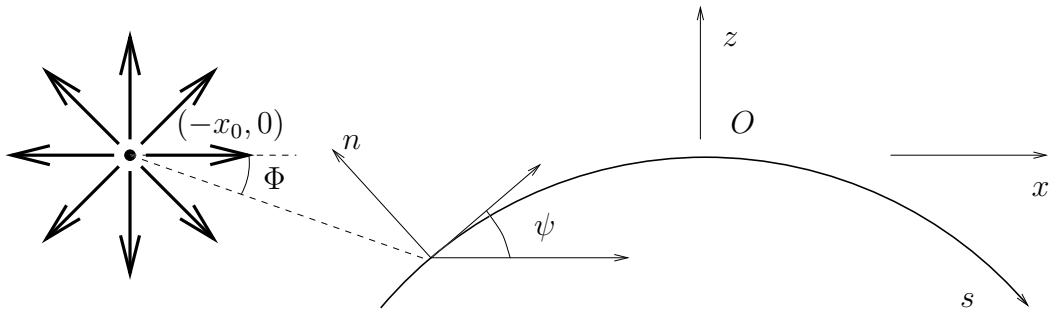


Figure 5.12: Coordinate system for problem of a line source at $(-x_0, 0)$ radiating in the presence of a cylinder.

We must however be careful in our interpretation of the components of the first fundamental form. In §5.4.2 we parameterised the horizon by arclength, whereas now it is parameterised by ϕ. Thus, for example, $G_0(\phi) = \sqrt{r_0(\phi)}$.

It is straightforward to write down the geometrical optics incident and reflected fields via ray theory. This means that we have an asymptotic solution everywhere apart from the transition and shadow boundary regions. Thus far, asymptotic solutions in these latter two regions have eluded us. The behaviour of the solutions in both of these regions in the limit as the source goes to infinity is known since a detailed analysis was provided earlier in this chapter for the plane wave incidence case. In §7 we will derive a complete asymptotic solution for the case where the source is an $\mathcal{O}(k^{-2/3})$ distance from the scatterer. This will provide information about the limiting behaviour of the shadow boundary and transition regions as $r_0 \to 0$. To gain insight at this stage, we consider a simpler problem for which we *are* able to calculate asymptotic solutions in both the shadow boundary and transition regions.

5.6 Illumination by a Field from a Line Source

We now consider the related two-dimensional problem of calculating the scattered field due to a current line source parallel to a perfectly conducting convex cylinder. This problem was tackled by Jones, [19] for the circular cylinder. He obtains the field using an eigenfunction expansion and then expands this exact solution asymptotically to calculate the surface fields. However, in the shadow boundary region where we expect a rich asymptotic structure, the solution is left in the form of an integral. In addition, no generalisation is made to a line source parallel to convex cylinders of arbitrary cross-section. We will carry out this generalisation as well as constructing a complete asymptotic picture similar to that described in §5.3.

We use the same cylinder as in §3.1 with s parametrising the cylinder. An electric current source of strength $1/k$ at $(-x_0, 0)$ directed along $\mathbf{e}_2$ means we need to solve

$$\begin{aligned} \nabla^2\mathbf{E} + k^2\mathbf{E} &= -i\delta(x+x_0)\delta(z)\mathbf{e}_2, && (5.182)\\ \mathbf{E}\,.\,\mathbf{t} &= 0 \quad \text{on the cylinder,} && (5.183) \end{aligned}$$

along with a radiation condition at infinity. The magnetic field $\mathbf{H}$ is then obtained from Maxwell's equations.

5.6.1 Geometrical Optics Field

We introduce the angle $\Phi(s)$ as in Figure 5.12 to represent the angle between the line source and the point $(x(s), z(s))$ on the cylinder. In addition, we assume that the line source is an $\mathcal{O}(1)$ distance from the cylinder. As we are only interested in the field arising *due to* the presence of the line source, the problem becomes

$$\begin{aligned} E_1 &= 0, && (5.184)\\ E_3 &= 0, && (5.185)\\ \nabla^2 E_2 + k^2 E_2 &= -i\delta(x+x_0)\delta(z) && (5.186)\\ E_2 &= 0 \quad \text{on the cylinder,} && (5.187) \end{aligned}$$

along with a radiation condition. In the absence of the cylinder we have a field

$$-\frac{1}{4}H_0^{(1)}\left(k\left((x+x_0)^2+z^2\right)^{1/2}\right). \qquad (5.188)$$

Thus, locally to the cylinder, we have (5.188) incident on the cylinder in the absence of sources. Therefore, dropping subscripts and using the assumption that the line source is an $\mathcal{O}(1)$ distance from the cylinder, we need only solve

$$\begin{aligned} \nabla^2 E + k^2 E &= 0, && (5.189)\\ E &= -\frac{1}{4}\sqrt{\frac{2}{k\pi r_0(s)}}e^{i\pi/4+ikr_0(s)}, \quad \text{on the cylinder,} && (5.190)\\ r_0(s) &= \left((x(s)+x_0)^2 + z(s)^2\right)^{1/2}, && (5.191) \end{aligned}$$

with an outgoing wave condition at infinity. Following the ray theory technique of §3 we find the solutions along two ray families, namely those associated with the incident and reflected rays. The first set of rays is

$$\mathbf{x}(s,\tau) = (x(s) + \tau\cos\Phi(s), y(s) - \tau\sin\Phi(s)). \qquad (5.192)$$

The field is given by

$$\phi_i \;=\; -\frac{1}{4}\sqrt{\frac{2}{k\pi r_0(s)}}e^{-i\pi/4+ikr_0(s)+ik\tau}\left|\frac{-\sin(\psi+\Phi)\psi'}{-\sin(\psi+\Phi)\psi'+\tau\Phi'}\right|^{1/2}, \quad (5.193)$$

where τ is the distance along a ray and $'$ is differentiation with respect to s. This corresponds to the incident field. The formulae for the second family of rays are

$$\mathbf{x}(s,\tau) \;=\; (x(s)+\tau\cos(2\psi(s)+\Phi(s)), y(s)+\tau\sin(2\psi(s)+\Phi(s))), \quad (5.194)$$

$$\phi_r \;=\; \frac{1}{4}\sqrt{\frac{2}{k\pi r_0(s)}}e^{-i\pi/4+ikr_0(s)+ik\tau}\left|\frac{-\sin(\psi+\Phi)\psi'}{-\sin(\psi+\Phi)\psi'+\tau(2\psi'+\Phi')}\right|^{1/2}. \quad (5.195)$$

This corresponds to the reflected field.

Inspection of (5.193) and (5.195) reveals that both families of ray solutions are singular when

$$\begin{array}{lll}\tau=0, & \psi=0, & \Phi=0,\\ \tau=0, & \psi+\Phi=\pi. & \end{array} \quad (5.196)$$

These points are the upper and lower tangency points respectively. Hence both ray fields are confined to rays leaving either the lit or the shadow sides of the cylinder. Adding back in the incident field and consideration of the outgoing wave condition gives us the solution as

$$E \;=\; \phi_i+\phi_r, \quad (5.197)$$

for $\Phi_0<\Phi<2\pi$ where Φ_0 is the value of Φ at the lower tangency point, and also in the region bounded by the cylinder and the lines $\Phi=0$ and $\Phi=\Phi_0$. Everywhere else the leading order field is zero. We will concentrate our efforts on the breakdown of the solution at the upper tangency point.

5.6.2 Fock-Leontovic, Airy Layer and Creeping Ray Fields

To investigate the solution in the neighbourhood of the upper tangency point we make the usual F-L scalings and pose an ansatz for the *scattered* field

$$E \;=\; A(\hat{n},\hat{s})e^{iks}, \quad (5.198)$$

where

$$\hat{s} \;=\; k^{1/3}s, \quad \hat{n} \;=\; k^{2/3}n. \quad (5.199)$$

This leaves us with Maxwell's equations and the Dirichlet boundary condition on the cylinder in the form

$$\frac{\partial^2 A}{\partial \hat{n}^2} + 2i\frac{\partial A}{\partial \hat{s}} - 2\hat{n}A\frac{\partial^2 A}{\partial \hat{n}^2} = 0, \quad \hat{n} > 0, \tag{5.200}$$

$$A = \frac{e^{ikr_0(s)-iks-i\pi/4}}{2\sqrt{2\pi k r_0(s)}}, \quad \hat{n} = 0. \tag{5.201}$$

Expanding the cartesian coordinates locally

$$x \sim s + k^{-1}\left(\hat{n}\hat{s} - \frac{1}{6}\hat{s}^3\right), \tag{5.202}$$

$$y \sim k^{-2/3}\left(\hat{n} - \frac{1}{2}\hat{s}^2\right), \tag{5.203}$$

we are able to rewrite the boundary condition (5.201) as

$$A \sim \frac{e^{ikx_0 - i\hat{s}^3/6 - i\pi/4}}{2\sqrt{2\pi k x_0}}, \quad \hat{n} = 0. \tag{5.204}$$

This turns out to be (5.68) with $\bar{E}_2^{inc} = -\exp(ikx_0 - i\pi/4)/2\sqrt{2\pi k x_0}$. This means we can immediately write down the fields in the F-L and Airy regions from (5.52), (5.86) and (5.87). The creeping ray field follows from (5.88) and (5.92).

We remark that this problem configuration excites only electrically polarised scattered fields. This should be apparent by noting that the magnetically polarised component of the incident field is zero.

The most interesting matching however involves the shadow boundary structure which we outline in some detail here.

5.6.3 Shadow Boundary Region

As in §5.3.4, to leading order, the incident field is 'switched off' as we cross the line $z = 0$, $x > 0$. To obtain a smoothly varying field in this region we make the usual scaling, $\tilde{z} = k^{1/2}z$ and try the ansatz

$$E = A(x, \tilde{z})e^{ikx}. \tag{5.205}$$

This reduces the problem to the by-now-familiar parabolic wave equation

$$A_{\tilde{z}\tilde{z}} + 2iA_x = 0, \tag{5.206}$$

along with the matching condition as $x \to 0$ that

$$A \;\to\; \begin{cases} \frac{1}{4}\sqrt{\frac{2}{k\pi x_0}}e^{ikx_0+i\tilde{z}^2/2x+i\pi/4}, & \tilde{z} > 0, \\ 0, & \tilde{z} < 0. \end{cases} \tag{5.207}$$

As in §4.6 we solve (5.206) and (5.207) via a Fourier transform. This gives us

$$A(x,\tilde{z}) \;=\; -\frac{\exp\left(ikx_0 - \frac{i\pi}{4} + i\frac{\tilde{z}^2}{2x} - \frac{i\tilde{z}^2 x_0}{2x(x+x_0)}\right)}{4\sqrt{2\pi k(x+x_0)}}\mathrm{erfc}\left(\frac{e^{-i\pi/4}\tilde{z}}{\sqrt{2(x+x_0)}}\sqrt{\frac{x_0}{x}}\right). \tag{5.208}$$

We see that as $x_0 \to \infty$, (5.208) tends towards the shadow boundary solution for plane wave incidence. In a similar fashion to §5.3.4 the matching into the reflected field as $\tilde{z} \to \infty$ and the creeping ray field as $\tilde{z} \to -\infty$ does not work. We again need to introduce a transition region to ensure smooth matching.

5.6.4 Transition Region

The limiting reflected and creeping rays will originate from the edges of the F-L region. This motivates the familiar scalings

$$x \;=\; \mathcal{O}(1), \quad \hat{z} \;=\; k^{1/3}z \tag{5.209}$$

in the transition region. As is §5.3.4, we take the ansatz

$$E \;=\; A(x,\hat{z})e^{ikx+ik^{1/3}u(x,\hat{z})}. \tag{5.210}$$

This yields identical equations to (5.128) and (5.129) for the phase and amplitude, namely

$$\left(\frac{\partial u}{\partial \hat{z}}\right)^2 + 2\frac{\partial u}{\partial x} \;=\; 0, \tag{5.211}$$

$$2\frac{\partial A}{\partial \hat{z}}\frac{\partial u}{\partial \hat{z}} + 2\frac{\partial A}{\partial x} + A\frac{\partial^2 u}{\partial \hat{z}^2} \;=\; 0. \tag{5.212}$$

We must accompany these equations with matching conditions as $\hat{z} \to \pm\infty$. To find the inner limit of the reflected field we first introduce the ray coordinates σ, τ. The value of s at the ray launch point is specified by σ and the distance along the ray by τ. As the limiting reflected ray will come from the left hand edge of the F-L region we scale

$$\hat{\sigma} \;=\; k^{1/3}\sigma, \quad \tau \;=\; \mathcal{O}(1). \tag{5.213}$$

For small σ we can make the approximations

$$\psi(\sigma) = \frac{\psi_0'}{k^{1/3}}\hat{\sigma} + \frac{\psi_0''}{2k^{2/3}}\hat{\sigma}^2 + \mathcal{O}(k^{-1}), \tag{5.214}$$

$$\Phi(\sigma) = \Phi_0 + \frac{\Phi_0'}{k^{1/3}}\hat{\sigma} + \frac{\Phi_0''}{2k^{2/3}}\hat{\sigma}^2 + \mathcal{O}(k^{-1}), \tag{5.215}$$

where f_0 is the value of f at $\sigma = 0$. Our definition of Φ implies $\Phi_0 = \Phi_0' = 0$. Substituting these expansions into the ray equation for the reflected field, (5.194), we find

$$x(\hat{\sigma},\tau) \sim \frac{\hat{\sigma}}{k^{1/3}} + \tau\left(1 - \frac{1}{2}\left(\frac{2\psi_0'}{k^{1/3}}\hat{\sigma} + \frac{\psi_0''}{k^{2/3}}\hat{\sigma}^2 + \frac{\Phi_0''}{2k^{2/3}}\hat{\sigma}^2\right)\right), \tag{5.216}$$

$$z(\hat{\sigma},\tau) \sim \frac{\psi_0'}{2k^{2/3}}\hat{\sigma}^2 + \tau\left(\frac{2\psi_0'}{k^{1/3}}\hat{\sigma} + \frac{\psi_0''}{k^{2/3}}\hat{\sigma}^2 + \frac{\Phi_0''\hat{\sigma}^2}{2k^{2/3}}\right). \tag{5.217}$$

For a leading order balance to occur in (5.217) we must scale $\hat{z} = k^{1/3}z$. So as to be able to match the limiting ray solution to the transition region close to $z = 0$, we must be able to write $\hat{\sigma}$, τ in terms of the transition regions coordinates x, z. We use (5.216) to write

$$\tau \sim x - \frac{\hat{\sigma}}{k^{1/3}} + \frac{2\psi_0'\hat{\sigma}^2 x}{k^{2/3}}. \tag{5.218}$$

Looking for an expansion

$$\hat{\sigma} = \sigma_0 + \frac{\sigma_1}{k^{1/3}} + \frac{\sigma_2}{k^{2/3}} + \ldots, \tag{5.219}$$

we can use (5.217) and then (5.218) to say

$$\sigma_0 = \frac{\hat{z}}{2\psi_0' x}, \tag{5.220}$$

$$\sigma_1 = \frac{3\hat{z}^2}{16{\psi_0'}^2 x^3} - \frac{\psi_0''\hat{z}^2}{8{\psi_0'}^3 x^2} - \frac{\Phi_0''\hat{z}^2}{16{\psi_0'}^3 x^2}, \tag{5.221}$$

$$\tau \sim x - \frac{1}{k^{1/3}}\frac{\hat{z}}{2\psi_0' x} + \frac{1}{k^{2/3}}\left(\frac{\hat{z}^2}{2x} - \frac{3\hat{z}^2}{16{\psi_0'}^2 x^3} + \frac{\psi_0''\hat{z}^2}{8{\psi_0'}^3 x^2} + \frac{\Phi_0''\hat{z}^2}{16{\psi_0'}^3 x^2}\right). \tag{5.222}$$

Substituting for ψ, Φ, σ, τ in (5.195), we find the inner limit of the reflected field is

$$E \sim \frac{1}{4k^{2/3}}\sqrt{\frac{\hat{z}}{2\pi\kappa_0 x_0 x^2}}\exp\left(ik(x + x_0) + \frac{ik^{1/3}\hat{z}^2}{2x} - i\pi/4\right), \tag{5.223}$$

where we have used the fact that $|\psi'| = \kappa$. The inner limit of the creeping ray field can trivially be written down as being equal to the right-hand side of (5.135) with $H_2^{inc^*}$ replaced by $-\exp(ikx_0 - i\pi/4)/2\sqrt{2\pi k x_0}$. The scaling for the transition

region for this problem is the same as that for the transition region for plane wave incidence, and we note that both (5.223) and the inner limit of the creeping ray field are the same as the corresponding limits for the plane wave-field incidence problems with $\bar{E}_2^{inc} = -\exp(ikx_0 - i\pi/4)/2\sqrt{2\pi k x_0}$. Hence we have found the solution in the transition region.

We have thus constructed a complete asymptotic picture for the scattered field due to a radiating line source parallel to a perfectly conducting convex cylinder. The asymptotic structure associated with the scattered field is exactly the same as for the problem of plane wave incidence. The asymptotic solutions associated with the incident field are different. It is straightforward to see that if we let $x_0 \to \infty$, the scattered field tends towards that due to an incident plane wave. The case where $x_0 \to 0$ will be dealt with in detail in §6. We will find that the asymptotic structure changes as the source approaches the scatterer.

5.7 Concave Surfaces

The previous sections describe the surface fields on a convex body. It is perfectly reasonable to ask about surface fields on concave boundaries. The generation of these fields by tangential incident radiation is more complicated as we will also generate a diffracted field from the surface discontinuity. Other possible causes of surface fields on concave structures are creeping rays passing through an inflexion point of the surface, or a point source on the surface—this will be discussed in §6. These scenarios are illustrated in Figure 5.13. While the energy of the surface field on a convex surface is shed as creeping rays, we anticipate on geometric grounds that there will be no decay in the amplitude of the surface field on a concave surface. Considerable attention is given to calculating the surface field on concave surfaces in the *IEEE* literature—[12], [13], [14] to cite but a few. There, though, the solution is typically obtained exactly for the special geometry of the interior of a circular cylinder. Asymptotics are then carried out on the exact solution. This precludes a systematic method of dealing with arbitrary concave geometries which our asymptotic framework allows. In addition, the circular cylinder is a bad paradigm as we expect further exponentially small backscattered surface fields due to changes in the curvature—*e.g.* [10].

5.7.1 Whispering Gallery Modes

To add mathematical substance to the paragraph above, we once again take the ansatz (5.7) for the field and consider (5.38) with (5.41). For a concave surface,

$L > 0$. Making the substitution

$$\eta \;=\; L^{-2/3}\left(L\rho + \frac{\partial v_0}{\partial s_1}\right), \tag{5.224}$$

and considering the magnetic WG modes only, gives us the leading order equation for the amplitude as

$$\frac{\partial^2 H_0^2}{\partial \eta^2} - 2\eta H_0^2 \;=\; 0. \tag{5.225}$$

As we expect the WG wave-field to be concentrated near to the surface, we require the solution to decay as $\eta \to \infty$. This forces us to take the solution to (5.225) as

$$H_0^2 \;=\; \beta(s_1,\, s_2)\mathrm{Ai}(\sqrt[3]{2}\eta). \tag{5.226}$$

The boundary condition (5.41) implies

$$v_0(s_1,\, s_2) \;=\; \frac{a'_m}{\sqrt[3]{2}}\int_0^{s_1} L^{2/3}\,\mathrm{d}t. \tag{5.227}$$

The solvability condition obtained from the higher order terms of Maxwell's equations gives us the surface field as

$$H_2^0 = \sum_{m=0}^{\infty} \frac{\delta_m(s_2)L^{1/6}}{G^{1/4}}\mathrm{Ai}\left(\sqrt[3]{2}L^{1/3}\rho + a'_m\right)\exp\left(iks_1 + ik^{1/3}\frac{a'_m}{\sqrt[3]{2}}\int_0^{s_1} L^{2/3}\,\mathrm{d}t\right). \tag{5.228}$$

Each term in the sum is referred to as a *whispering gallery* (WG) mode. The δ_m are to be determined by matching into a region in the neighbourhood of either the source or of the inflexion point. Comparison of (5.228) with (5.49) reveals that WG modes do not exhibit exponential decay along geodesics. Moreover, WG modes can be thought of as an analytic continuation of the Airy layer field.

5.7.2 Open Problem

We mentioned that a possible cause of WG modes was an inflexion point on a surface—Figure 5.13. An incoming creeping ray will excite WG modes close to the concave part of the surface. To date this transition problem remains unsolved. It is however of special interest to the aerospace industry, and so we will describe the problem formulation due to [36].

We revert to a two-dimensional problem with s, n being the tangential and normal coordinates of the surface. Section 2.3.4 implies that we only need solve the Helmholtz

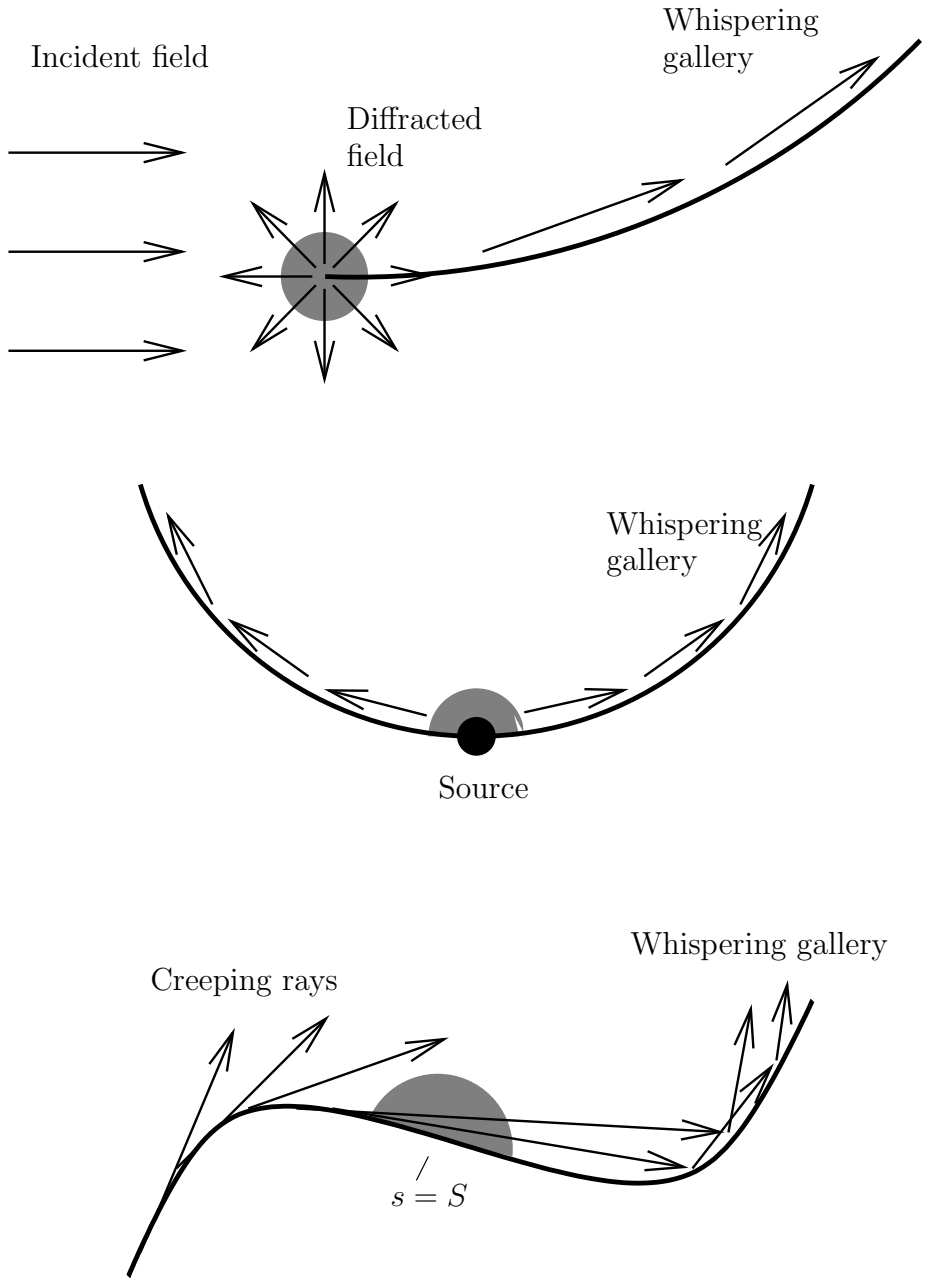


Figure 5.13: Whispering gallery modes due to incident tangent radiation, a point source on a concave surface and creeping rays passing through an inflexion point. Shaded areas represent inner regions into which WG modes must match.

equation for E_2 and H_2 with homogenous Dirichlet or Neumann boundary conditions on the surface respectively. In s, n coordinates this requires the solution of

$$\frac{1}{(1+n\kappa)^2}\frac{\partial^2\phi}{\partial s^2}+\frac{\partial^2\phi}{\partial n^2}-\frac{n\kappa'}{(1+n\kappa)^3}\frac{\partial\phi}{\partial s}+\frac{\kappa}{(1+n\kappa)}\frac{\partial\phi}{\partial n}+k^2\phi \;=\; 0, \quad (5.229)$$

along with either homogenous Neumann or Dirichlet boundary data respectively.

The inflexion point is at $s = S$. Near the inflexion point we take $\kappa(s) = \kappa_0(s-S)^N$, for some N and κ_0 is a constant. As we expect the rays at the inflexion point to be almost tangent to the surface we look for a solution $\phi = A(s,n)e^{iks}$. Looking for an inner transition region at the inflexion point we make the scalings

$$n \;=\; k^{-\alpha}\bar{n}, \quad (5.230)$$

$$s \;=\; S + k^{-\beta}\bar{s}. \quad (5.231)$$

The leading order balance yields

$$\frac{\partial^2 A}{\partial\bar{n}^2}+2i\frac{\partial A}{\partial\bar{s}}+2\kappa_0\bar{n}\bar{s}^N A \;=\; 0, \quad (5.232)$$

along with either a Dirichlet or a Neumann boundary condition on $\bar{n} = 0$, where

$$\alpha \;=\; \frac{N+2}{3+2N}, \quad \beta \;=\; \frac{1}{3+2N}. \quad (5.233)$$

We must also provide the matching conditions that as $\bar{s} \to -\infty$ the solution matches into a known creeping ray field, and as $\bar{s} \to \infty$ we hope there will be a successful match into an unknown WG field-*i.e.*

$$A \;\to\; \begin{cases} C\bar{s}^{N/6}\mathrm{Ai}\left(-\sqrt[3]{2}e^{2\pi i/3}\kappa_0^{1/3}\bar{n}+a'_m\right)\exp\left(D\kappa_0^{2/3}\bar{s}^{2N/3+1}\right), & \bar{s}\to-\infty, \\ \sum_{n=0}^{\infty} C_n\bar{s}^{N/6}\mathrm{Ai}\left(-\sqrt[3]{2}e^{2\pi i/3}|\kappa_0|^{1/3}\bar{n}+a'_m\right)\exp\left(D_n|\kappa_0|^{2/3}\bar{s}^{2N/3+1}\right), & \bar{s}\to\infty. \end{cases}$$

The aim is to establish a connection condition between the known constant C and the as yet unknown C_n. Equation (5.232) has not been solved except for the case $N = 0$ where there is no inflexion point anyway. The solution in the limit as $N \to \infty$ should reproduce the field for a source on an infinite plane. Later in this thesis we will discuss the surface fields arising due to a point source placed at an inflexion point of a cylinder. It may be possible to shed some light on the open creeping ray—WG mode problem using reciprocity (Appendix D) and the results of this discussion.

5.8 Discussion

In this chapter we have outlined the asymptotic structure of the fields when a plane wave-field is incident on an arbitrary convex scatterer. We have built on acoustic results and extended them to cater for the E-M problem. In particular, we have described the decomposition of the incident and diffracted fields into magnetically and electrically polarised modes. The former are equivalent to solving the associated acoustic problems with a Neumann boundary condition and the latter are equivalent to the acoustic version with a Dirichlet boundary condition. We have paid special attention to the shadow boundary structure that allows a smooth transition between the fields in the geometrical optics lit and shadow regions. The problem of illumination of a general body by a point source was discussed and a complete asymptotic solution obtained for the two-dimensional version of this problem.

While we have not considered the corresponding problems for concave surfaces, it is relatively easy to generalize all the results of this chapter to concave surfaces. The discussion concerning WG modes gives an indication of how we do this.

Chapter 6 extends these results to the diffracted fields produced by a source sited on the surface. The asymptotic structure for this problem is similar to that developed in this chapter although, as will be seen, there are some vital differences.

Part III

Sources Close to Structures

Chapter 6

Point Sources on a Convex Surface

Having dealt with the surface and creeping ray fields set up by an incident wave field impinging tangentially on a convex surface, we now investigate the corresponding fields due to a point source that lies on the surface. This will let us establish the basic asymptotic structure so that in later chapters we will be able to consider more general line-source configurations. More is known about scattering problems involving point sources far from a scatterer than when the source is nearby. The texts that do exist are also mainly concerned with the specific geometry of a circular cylinder.[1] We will solve the three-dimensional electromagnetic problem asymptotically by extending the acoustic theory developed in [33]. In addition, we will also say something about the structure of the shadow boundary which provides a smooth transition between the geometrical optics and creeping ray fields. To date this has not been systematically studied. These results will all be valid for convex surfaces with positive $\mathcal{O}(1)$ principal curvatures everywhere (we remind the reader that this means our convex body has typical principal radii of curvature much larger than the wavelength of the radiation), but will not hold for objects such as cylinders which, although convex, do not possess positive principal curvatures everywhere—one principal curvature is zero along the generator of a cylinder. We conclude the chapter by resolving this omission.

6.1 Geodesic Polar Coordinates

When representing the surface fields for this problem, the natural coordinate system is a polar coordinate system on the surface with the origin at the point source location.

[1] Felsen, [14] and [15], investigates a line source on the interior of a perfectly conducting circular cylinder using an eigenfunction expansion. He obtains a WG solution close to the boundary. Although we will restrict ourselves to convex surfaces, we remark that the discussions in chapter 5 indicate that it should be straightforward to extend our results to sources on concave surfaces.

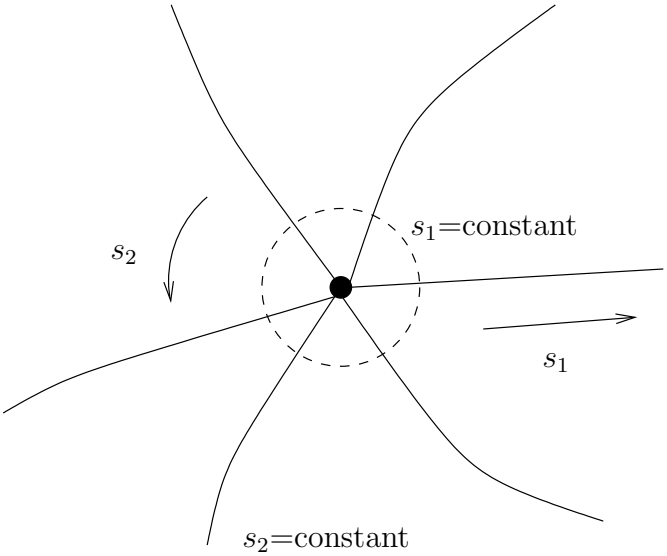


Figure 6.1: Geodesic polar coordinate system.

We construct the geodesics on the surface passing through the origin. The coordinate s_2 tells us which geodesic we are on (the sensible parametrisation is chosen—as we approach the origin s_2 becomes the usual polar coordinate), s_1 is the distance along a geodesic and s_3 is the normal distance to the surface (see Figure 6.1).

As discussed in §2.3.3, by a point source, we mean a dipole with a dipole moment $\mathbf{p}$. In addition we showed how no field was radiated by dipoles where $\mathbf{p}$ was parallel to the surface and so we take

$$\mathbf{p} \quad = \quad p\mathbf{e}_3, \tag{6.1}$$

where $\mathbf{e}_3$ is the unit vector normal to the surface.

We will begin by looking for an Airy layer solution close to the surface of the scatterer. This will yield a degree of indeterminacy which is only resolved by consideration of a (Fock-Leontovič) region in the neighbourhood of the source and then a further *inner-F-L* region even closer to the source. The geometrical optics and creeping ray solutions will then be calculated. In the light of §5 we anticipate a discontinuity between the geometrical optics and creeping ray fields that are launched from the Airy layer. We thus expect to require some kind of shadow boundary structure so as to ensure a smoothly varying field.

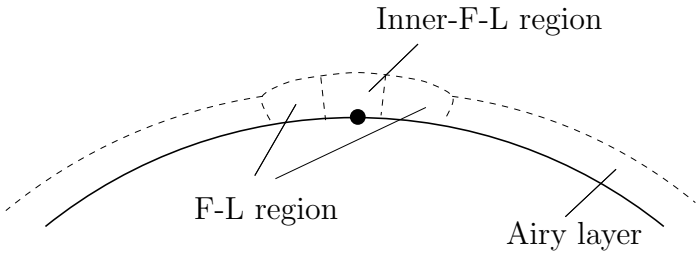


Figure 6.2: Point source on a surface.

6.2 Airy Layer

Close to the surface, when $s_1 = \mathcal{O}(1)$, we are away from the coordinate singularity and so can use the representations of the metrics (C.35) - (C.38). The analysis of §5.3.1 can be repeated, including the decomposition of the field into *magnetic* and *electric* polarisations. The results of §5.3.1 then imply that the magnetically polarised Airy layer field is given by

$$\begin{aligned}
\mathbf{E} &= -\phi_M(s_1, s_2, \rho)\mathbf{e}_3, && (6.2)\\
\mathbf{H} &= \phi_M(s_1, s_2, \rho)\mathbf{e}_2, && (6.3)\\
\phi_M &= \sum_{m=0}^{\infty} \frac{\beta_m(s_2)|L|^{1/6}}{G^{1/4}} \mathrm{Ai}\left(-\sqrt[3]{2}e^{2\pi i/3}\rho|L|^{1/3} + a'_m\right) \\
&\quad \times \exp\left(iks_1 + ik^{1/3}\frac{a'_m e^{-2\pi i/3}}{\sqrt[3]{2}}\int_0^{s_1} |L(t, s_2)|^{2/3}\,\mathrm{d}t\right), && (6.4)
\end{aligned}$$

where

$$\rho = k^{2/3}s_3. \qquad (6.5)$$

The electrically polarised field is given by

$$\begin{aligned}
\mathbf{E} &= \phi_E\mathbf{e}_2, && (6.6)\\
\mathbf{H} &= \phi_E\mathbf{e}_3, && (6.7)\\
\phi_E &= \sum_{m=0}^{\infty} \frac{\gamma_m(s_2)|L|^{1/6}}{G^{1/4}} \mathrm{Ai}\left(-\sqrt[3]{2}e^{2\pi i/3}\rho|L|^{1/3} + a_m\right) \\
&\quad \times \exp\left(iks_1 + ik^{1/3}\frac{a_m e^{-2\pi i/3}}{\sqrt[3]{2}}\int_0^{s_1} |L(t, s_2)|^{2/3}\,\mathrm{d}t\right), && (6.8)
\end{aligned}$$

The unknown functions $\beta_m(s_2)$, $\gamma_m(s_2)$ need to be fixed by matching into a region closer to the source. It can be seen that the dominant effect of the azimuthal variation is in the exponential decay as we travel along geodesics. The larger the normal curvature along a geodesic (as a function of s_2), the faster the surface field will decay.

6.3 Fock-Leontovič Region

Under the Fock-Leontovič scalings,

$$\hat{s}_1 \;=\; k^{1/3}s_1, \quad \rho \;=\; k^{2/3}s_3. \tag{6.9}$$

the metrics for the geodesic polar coordinate system become

$$h_1^2 \;\sim\; 1 - 2k^{-2/3}\rho L(0, s_2), \tag{6.10}$$
$$h_2^2 \;\sim\; k^{-2/3}\hat{s}_1^2 G(0, s_2), \tag{6.11}$$
$$h_3^2 \;=\; 1. \tag{6.12}$$

We try the usual F-L ansatz for the fields

$$\mathbf{F} \;=\; e^{iks_1}\sum_{n=0}^{\infty}\frac{\mathbf{F}^n(\hat{s}_1, s_2, \rho)}{k^{n/3}}, \tag{6.13}$$

where $\mathbf{F}$ is to be read as either $\mathbf{E}$ or $\mathbf{H}$. We insert (6.13) into Maxwell's equations written in the geodesic coordinate system. Instead of solving Maxwell's equations with a source at the origin, we will solve them in the absence of sources and use a matching condition which governs the behaviour of our solution as we approach the origin.

Terms of $\mathcal{O}(k)$ and $\mathcal{O}(k^{2/3})$ are identical to (5.20) - (5.25) and (5.26) - (5.31) respectively. That is to say that they are the same as in the F-L region for an incident plane wave. The difference comes in the $\mathcal{O}(k^{1/3})$ equations and is due to the coordinate singularity at $s_1 = 0$. We obtain

$$H_1^2 \;=\; i\frac{\partial E_2^1}{\partial \rho} - \frac{i}{\hat{s}_1 G_0^{1/2}}\frac{\partial E_3^0}{\partial s_2}, \tag{6.14}$$
$$E_3^2 + H_2^2 \;=\; -\frac{\partial^2 H_2^0}{\partial \rho^2} - i\frac{\partial H_2^0}{\partial \hat{S}_1} + \rho L H_2^0, \tag{6.15}$$
$$H_3^2 - E_2^2 \;=\; -i\frac{\partial E_2^0}{\partial \hat{s}_1} + \rho L E_2^0 - i\frac{E_2^0}{\hat{s}_1}, \tag{6.16}$$
$$E_1^2 \;=\; i\frac{\partial H_2^1}{\partial \rho} + \frac{i}{\hat{s}_1 G_0^{1/2}}\frac{\partial H_3^0}{\partial s_2}, \tag{6.17}$$
$$E_2^2 - H_3^2 \;=\; -\frac{\partial^2 E_2^0}{\partial \rho^2} - i\frac{\partial H_2^0}{\partial \hat{s}_1} + \rho L E_2^0, \tag{6.18}$$
$$E_3^2 + H_2^2 \;=\; i\frac{\partial H_2^0}{\partial \hat{s}_1} - \rho L H_2^0 + i\frac{H_2^0}{\hat{s}_1}. \tag{6.19}$$

Equating (6.15) and (6.16) with (6.19) and (6.18) yields

$$\frac{\partial^2 H_2^0}{\partial \rho^2} + 2i\frac{\partial H_2^0}{\partial \hat{s}_1} - 2\rho L H_2^0 + \frac{i}{\hat{s}_1} H_2^0 = 0, \tag{6.20}$$

$$\frac{\partial^2 E_2^0}{\partial \rho^2} + 2i\frac{\partial E_2^0}{\partial \hat{s}_1} - 2\rho L E_2^0 + \frac{i}{\hat{s}_1} E_2^0 = 0. \tag{6.21}$$

The perfectly conducting boundary conditions and lower order equations imply that we are required to solve (6.20) and (6.21) along with the boundary conditions

$$\frac{\partial H_2^0}{\partial \rho} = 0, \tag{6.22}$$

$$E_2^0 = 0, \tag{6.23}$$

on $\rho = 0$. As before these correspond to magnetically and electrically polarised F-L solutions.

For the magnetically polarised field we take $E_2^0 \equiv 0$, whereupon the solutions satisfy

$$E_1^0 \equiv E_2^0 \equiv H_1^0 \equiv H_3^0 \equiv 0, \tag{6.24}$$

$$H_2^0 = -E_3^0 = \frac{A}{\sqrt{\hat{s}_1}}, \tag{6.25}$$

$$\frac{\partial^2 A}{\partial \rho^2} + 2i\frac{\partial A}{\partial \hat{s}_1} - 2\rho L A = 0, \tag{6.26}$$

$$\frac{\partial A}{\partial \rho} = 0, \quad \rho = 0. \tag{6.27}$$

Taking the Laplace transform of (6.26) - (6.27) gives us

$$\frac{\partial^2 \hat{A}}{\partial \rho^2} + 2i\lambda \hat{A} + 2|L(0, s_2)|\rho \hat{A} = F(\epsilon, \rho), \quad \rho > 0, \tag{6.28}$$

$$\frac{\partial \hat{A}}{\partial \rho} = 0, \quad \rho = 0, \tag{6.29}$$

where $\hat{f}$ is the Laplace transform of f,

$$\hat{f}(\lambda) = \int_0^\infty f(s_1) e^{-\lambda s_1} \, \mathrm{d}s_1. \tag{6.30}$$

In (6.28) $F(\epsilon, \rho) = 2iA(\epsilon, \rho)$ is effectively a matching condition that must be established before proceeding further. We obtain the functions F in §6.4 by consideration of an inner-F-L region around the origin. Equations (6.28) - (6.29) will then be solved in §6.5 in the limit as $\epsilon \to 0$. It can be seen that s_2 will only appear as a parameter in the solution.

For the electrically polarised field we specify $H_2^0 \equiv 0$ and proceed as before, whereupon

$$E_1^0 \equiv E_3^0 \equiv H_1^0 \equiv H_2^0 \equiv 0, \tag{6.31}$$

$$E_2^0 = H_3^0 = \frac{A}{\sqrt{\hat{s}_1}}, \tag{6.32}$$

$$\frac{\partial^2 \hat{A}}{\partial \rho^2} + 2i\lambda \hat{A} + 2|L(0, s_2)|\rho \hat{A} = F(\epsilon, \rho), \quad \rho > 0, \tag{6.33}$$

$$\hat{A} = 0, \quad \rho = 0. \tag{6.34}$$

Once again, the $F(\epsilon, \rho)$ is to be found via an inner-F-L region and (6.33) - (6.34) solved in the limit as $\epsilon \to 0$.

6.4 Inner-Fock-Leontovič Region

We consider an inner-F-L region around the origin. The correct scalings are

$$S_1 = k^{2/3} s_1, \quad \rho = k^{2/3} s_3. \tag{6.35}$$

To leading order, the fields do not see the curvature of the surface within this region. The inner-F-L problem is thus equivalent to that of §2.3.3 with k replaced by $k^{1/3}$. Introducing spherical polar coordinates R, ϕ, θ where

$$R = k^{2/3} r, \tag{6.36}$$

and ϕ is such that the lines $\phi = 0$ and $s_2 = 0$ coincide. From §2.3.3 the inner-F-L solution, to leading order, is

$$\begin{aligned} H_r &= 0, \quad H_\phi = -\frac{pk^{5/3} \sin\theta}{2\pi R} e^{ik^{1/3}R}, \quad H_\theta = 0, \\ E_r &= 0, \quad E_\phi = 0, \qquad\qquad\quad E_\theta = -\frac{pk^{5/3} \sin\theta}{2\pi R} e^{ik^{1/3}R}. \end{aligned} \tag{6.37}$$

The exponent of k is $5/3$ as the rescaling of Maxwell's equations in the inner-F-L region leaves us with an *effective* dipole moment of $\mathcal{O}(k^{4/3})$. Writing this in F-L coordinates, we have

$$\begin{aligned} H_\phi &= H_2 = -\frac{pk^{4/3}}{2\pi \hat{s}_1} e^{ik^{2/3}\hat{s}_1 + i\rho^2/2\hat{s}_1}, \\ E_\theta &= -E_3 = -\frac{pk^{4/3}}{2\pi \hat{s}_1} e^{ik^{2/3}\hat{s}_1 + i\rho^2/2\hat{s}_1}, \end{aligned} \tag{6.38}$$

with all other components zero to leading order. The ansatz (6.13) then implies that the function F appearing on the right-hand side of (6.28) is

$$F(\epsilon,\rho) \;=\; -\frac{ipk^{4/3}}{\pi}\frac{e^{i\rho^2/2\epsilon}}{\sqrt{\epsilon}}, \tag{6.39}$$

and that the F appearing in (6.33) is identically zero. As we are only interested in the radiated fields, we require just the particular solutions of (6.28) and (6.33). This implies that the γ_m of (6.8) are zero and gives us the important result that a current source of the form considered on a perfect conductor cannot excite electrically polarised surface fields. Thus the radiated fields are completely specified by consideration of H_2.

6.5 Fock-Leontovič Region Solution

Saward carries out the procedure of solving (6.28) - (6.29) in the limit as $\epsilon \to 0$. We describe the method here as we will have recourse to it later, with some slight alterations, in §7. We first make the variable change

$$\eta \;=\; -\tau + \rho|L_0|^{1/3}, \tag{6.40}$$

$$\tau \;=\; -i\lambda|L_0|^{-2/3}, \tag{6.41}$$

resulting in the new problem

$$\frac{\partial^2\bar{A}}{\partial\eta^2} + 2\eta\bar{A} \;=\; |L_0|^{-2/3}F\left(\frac{\eta+\tau}{|L_0|^{1/3}},\epsilon\right), \quad \eta > -\tau, \tag{6.42}$$

$$\frac{\partial\bar{A}}{\partial\eta} \;=\; 0, \quad \eta = -\tau, \tag{6.43}$$

along with the condition that we must match into an outgoing solution as $\eta \to \infty$. The solution to (6.42) - (6.43) can be written down using the method of variation of parameters as

$$\bar{A}(\eta,\tau) \;=\; |L_0|^{-2/3}\int_{-\tau}^{\infty} G(\eta,t)F\left(\frac{\tau+t}{|L_0|^{1/3}},\epsilon\right)\,\mathrm{d}t. \tag{6.44}$$

The Green's function G is defined as

$$G(\eta,t) \;=\; \begin{cases} \dfrac{A_1(\eta)A_2(t)}{W(t)}, & -\tau < \eta < t < \infty, \\ \dfrac{A_2(\eta)A_1(t)}{W(t)}, & -\tau < t < \eta < \infty, \end{cases} \tag{6.45}$$

where $A_1(\eta)$ satisfies the boundary condition (6.43) and $A_2(\eta)$ satisfies the matching condition as $\eta \to \infty$. $W(t)$ is the Wronskian of A_1 and A_2. Suitable choices for A_1, A_2 are

$$A_1(\eta) = \mathrm{Ai}\left(-\sqrt[3]{2}\eta\right) - e^{-2\pi i/3}\frac{\mathrm{Ai}'\left(\sqrt[3]{2}\tau\right)}{\mathrm{Ai}'\left(\sqrt[3]{2}e^{2\pi i/3}\tau\right)}\mathrm{Ai}\left(-\sqrt[3]{2}e^{2\pi i/3}\eta\right), \quad (6.46)$$

$$A_2(\eta) = \mathrm{Ai}\left(-\sqrt[3]{2}e^{2\pi i/3}\eta\right). \quad (6.47)$$

Using an identity on Airy functions, [1], we have

$$W(t) = W = -\frac{e^{-i\pi/6}}{2^{2/3}\pi}. \quad (6.48)$$

Thus

$$\bar{A} = -\frac{ipk^{4/3}|L_0|^{-2/3}}{\pi W\sqrt{\epsilon}}\left\{A_1(\eta)\int_\eta^\infty A_2(t)\exp\left(\frac{i}{2\epsilon}\left(\frac{\tau+t}{|L_0|^{1/3}}\right)^2\right)\,\mathrm{d}t \right. \\ \left. + A_2(\eta)\int_{-\tau}^\eta A_1(t)\exp\left(\frac{i}{2\epsilon}\left(\frac{\tau+t}{|L_0|^{1/3}}\right)^2\right)\,\mathrm{d}t\right\}. \quad (6.49)$$

Letting $\epsilon \to 0$ we can evaluate both integrals via the method of stationary phase. The first integral does not provide a leading order contribution as the stationary phase point is not in the range of the integral. The second integral gives us

$$\bar{A} \sim \frac{ipk^{4/3}e^{5\pi i/4}|L_0|^{-1/3}}{\sqrt{2\pi}W}A_2(\eta)A_1(-\tau). \quad (6.50)$$

An identity on Airy functions, [1], lets us write

$$A_1(-\tau) = \frac{e^{-5\pi i/6}}{2\pi\mathrm{Ai}'\left(\sqrt[3]{2}e^{2\pi i/3}\tau\right)}. \quad (6.51)$$

Inverting the Laplace transform then gives

$$A(\hat{s}_1, s_2, \rho) = \frac{pk^{4/3}e^{\pi i/12}}{2^{11/6}\pi^{3/2}}|L_0(s_2)|^{1/3}\int_{-\infty}^\infty \frac{\mathrm{Ai}\left(\sqrt[3]{2}e^{2\pi i/3}\left(\tau - |L_0|^{1/3}\rho\right)\right)}{\mathrm{Ai}'\left(\sqrt[3]{2}e^{2\pi i/3}\tau\right)}e^{i\tau|L_0|^{2/3}\hat{s}_1}\,\mathrm{d}\tau. \quad (6.52)$$

To match with the field in the Airy layer we invert the scaling on s_1 and evaluate the integral via Cauchy's residue theorem. We also need to use the fact that for small s_1 we have

$$G(s_1, s_2) \sim G_0 s_1^2. \quad (6.53)$$

It follows that the β_m of (6.4) are

$$\beta_m(s_2) = \frac{pk^{7/6}e^{-\pi i/12}|L_0(s_2)|^{1/6}G_0^{1/4}}{2^{7/6}\sqrt{\pi}\mathrm{Ai}''(a'_m)}. \tag{6.54}$$

The field in the Airy layer is thus the magnetically polarised mode

$$\mathbf{H} = \phi_M \mathbf{e}_2, \tag{6.55}$$

$$\mathbf{E} = -\phi_M \mathbf{e}_3, \tag{6.56}$$

where

$$\phi_M = \sum_{m=0}^{\infty} \frac{pk^{7/6}e^{-\pi i/12}|L_0(s_2)|^{1/6}G_0^{1/4}|L|^{1/6}}{2^{7/6}\sqrt{\pi}\mathrm{Ai}''(a'_m)G(s_1,s_2)^{1/4}} \tag{6.57}$$

$$\times \mathrm{Ai}\left(-\sqrt[3]{2}e^{2\pi i/3}\rho|L|^{1/3} + a'_m\right) \exp\left(iks_1 + ik^{1/3}\frac{a'_m e^{-2\pi i/3}}{\sqrt[3]{2}}\int_0^{s_1}|L(t,s_2)|^{2/3}\mathrm{d}t\right).$$

It remains now to complete the picture by investigating the creeping ray fields that are launched from the Airy layer and the shadow boundary structure that we expect to exist between the geometrical optics lit and shadow regions. As the point source generates just magnetically polarised surface fields we only have half the work that was needed for plane wave incidence, where we had to consider the field in shadow due to both magnetic *and* electric polarisations of the fields. First though, we calculate the geometrical optics field.

6.6 Geometrical Optics Field

For the problem of plane wave incidence the geometrical optics field was specified by considering the incident and reflected fields. When we have a point source on the surface we do not have a prescribed GO field. We expect the field in the geometrical optics lit region to resemble that due to a dipole in free space. Working in the same spherical polar coordinates r, ϕ, θ that we used in §6.4 we try, to lowest order

$$\begin{aligned} H_r &= 0, \quad H_\phi = \chi(s_1,s_2,\rho)\sin\theta\frac{e^{ikr}}{r}, \quad H_\theta = 0, \\ E_r &= 0, \quad E_\phi = 0, \qquad\qquad\quad E_\theta = \chi(s_1,s_2,\rho)\sin\theta\frac{e^{ikr}}{r} \end{aligned} \tag{6.58}$$

where χ is to be found. Matching with the inner-F-L solution reveals that

$$\chi(s_1,s_2,s_3) = -\frac{pk}{2\pi}. \tag{6.59}$$

We now check that the F-L solution matches with the GO field given by (6.58) - (6.59).

The inner limit of (6.58) written in F-L coordinates is

$$H_2 \sim \frac{\chi k^{4/3}}{\hat{s}_1} e^{ik^{2/3}\hat{s}_1 + i\rho^2/2\hat{s}_1}. \tag{6.60}$$

We split the integral in (6.52) at the origin and change variables to write it as

$$\begin{aligned} A &= \alpha |L_0(s_2)|^{1/3} \int_0^\infty \frac{\mathrm{Ai}\left(\sqrt[3]{2}e^{2\pi i/3}(\tau - |L_0|^{1/3}\rho)\right)}{\mathrm{Ai}'\left(\sqrt[3]{2}e^{2\pi i/3}\tau\right)} e^{i\tau|L_0|^{2/3}\hat{s}_1}\,\mathrm{d}\tau \\ &\quad + \alpha |L_0(s_2)|^{1/3} \int_0^\infty \frac{\mathrm{Ai}\left(\sqrt[3]{2}e^{-\pi i/3}(\omega + |L_0|^{1/3}\rho)\right)}{\mathrm{Ai}'\left(\sqrt[3]{2}e^{-\pi i/3}\omega\right)} e^{i\omega|L_0|^{2/3}\hat{s}_1}\,\mathrm{d}\omega, \end{aligned} \tag{6.61}$$

$$\alpha = \frac{pk^{4/3}e^{\pi i/12}}{2^{11/6}\pi^{3/2}}. \tag{6.62}$$

We set $\tau = k^{2/3}\bar{\tau}, \omega = k^{2/3}\bar{\omega}$ and expand the Airy functions for large argument. Reverting to GO coordinates s_1, s_3, the first integral has a steepest descents contribution which is exponentially small in comparison with the stationary phase contribution of the second integral. The second integral thus dominates. Evaluating the stationary phase contribution yields

$$A \sim -\frac{pke^{iks_3^2/2s_1}}{2\pi\sqrt{s_1}}, \tag{6.63}$$

as required.

6.7 Creeping Ray Field

We introduce the creeping ray coordinates σ_1, σ_2, τ. The distance along a creeping ray is τ and the values of s_1, s_2 at the launchpoint of the creeping ray are given by σ_1, σ_2. We take the ansatz for the magnetically polarised creeping ray field given by (5.88) - (5.89), namely

$$\mathbf{E} = k^{\nu_E}\left|\frac{J(\sigma_1,\sigma_2,0)}{J(\sigma_1,\sigma_2,\tau)}\right|^{1/2} \sum_{m=0}^{\infty} \mathbf{f}_m(\sigma_1,\sigma_2)\exp\left(ik(\sigma_1+\tau) + ik^{1/3}u_m(\sigma_1)\right), \tag{6.64}$$

$$\mathbf{H} = k^{\nu_H}\left|\frac{J(\sigma_1,\sigma_2,0)}{J(\sigma_1,\sigma_2,\tau)}\right|^{1/2} \sum_{m=0}^{\infty} \mathbf{g}_m(\sigma_1,\sigma_2)\exp\left(ik(\sigma_1+\tau) + ik^{1/3}v_m(\sigma_1)\right). \tag{6.65}$$

The factor involving the Jacobians is, as before

$$\left|\frac{J(\sigma_1,\sigma_2,\tau)}{J(\sigma_1,\sigma_2,0)}\right| = \tau L(\sigma_1,\sigma_2)\left(G(\sigma_1,\sigma_2)^{1/2} + \tau\frac{\partial}{\partial\sigma_1}G(\sigma_1,\sigma_2)^{1/2}\right). \tag{6.66}$$

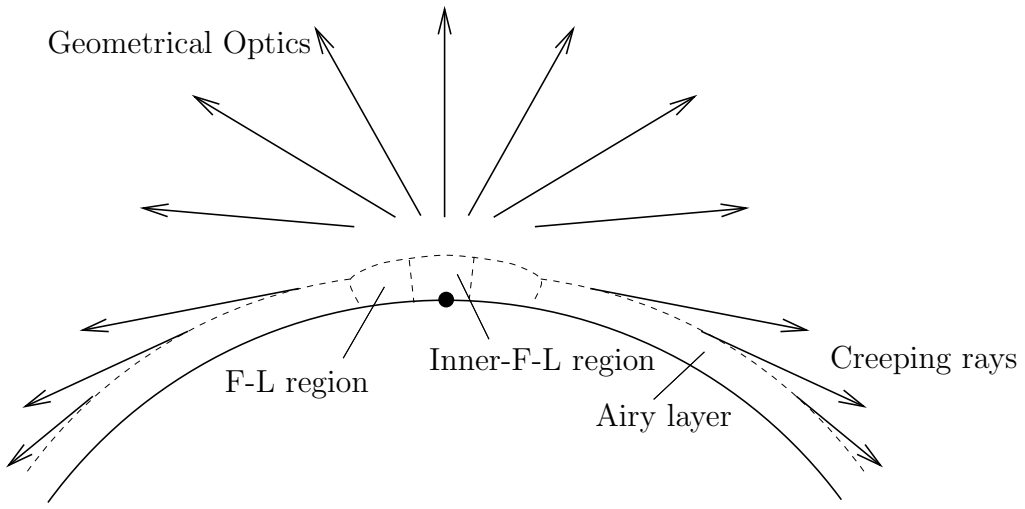


Figure 6.3: Geometrical Optics rays and Creeping rays due to a source on a convex surface.

To match between the Airy layer and creeping ray fields we first write the Airy layer coordinates in terms of the creeping ray coordinates. We have

$$\rho \sim \frac{1}{2}L(\sigma_1,\sigma_2)\bar{\tau}^2 + \frac{1}{6}k^{-1/3}\frac{\partial L(\sigma_1,\sigma_2)}{\partial \sigma_1}\bar{\tau}^3, \tag{6.67}$$

$$s_1 \sim \sigma_1 + k^{-1/3}\bar{\tau} - \frac{1}{3}k^{-1}L^2(\sigma_1,\sigma_2)\bar{\tau}^3, \tag{6.68}$$

where

$$\bar{\tau} = k^{1/3}\tau, \tag{6.69}$$

is $\mathcal{O}(1)$ inside the Airy layer. The Airy layer solution (6.57) is expanded for large ρ. We rewrite this expansion in terms of σ_1, σ_2 and $\bar{\tau}$ and invert the scaling on $\bar{\tau}$. This gives us the outer limit of the Airy layer solution in terms of creeping ray coordinates as

$$\mathbf{E} \sim -\phi_c(\sigma_1,\sigma_2,\tau)\mathbf{e}_3, \tag{6.70}$$

$$\mathbf{H} \sim \phi_c(\sigma_1,\sigma_2,\tau)\mathbf{e}_2, \tag{6.71}$$

where

$$\begin{aligned}\phi_c(\sigma_1,\sigma_2,\tau) &= \sum_{m=0}^{\infty}\frac{pk}{4\pi \mathrm{Ai}''(a'_m)}\frac{G_0^{1/4}}{G^{1/4}}\frac{|L_0|^{1/6}}{|L|^{1/6}\sqrt{\tau}} \\ &\quad\times\exp\left(ik(\sigma_1+\tau) + ik^{1/3}\frac{a'_m e^{-2\pi i/3}}{\sqrt[3]{2}}\int_0^{\sigma_1}|L(t,\sigma_2)|^{2/3}\mathrm{d}t\right).\end{aligned} \tag{6.72}$$

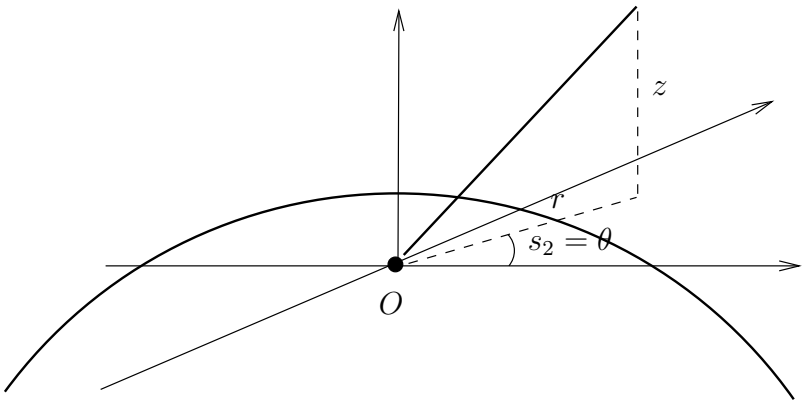


Figure 6.4: Cylindrical polar coordinate system.

It is straightforward to see that

$$\begin{aligned} k^{\nu_E} &= k^{\nu_H} = 1, \\ u_m &= v_m = \frac{a'_m e^{-2\pi i/3}}{\sqrt[3]{2}} \int_0^{\sigma_1} |L(t,\sigma_2)|^{2/3}\,\mathrm{d}t, \\ \mathbf{f}_m &= \frac{pG_0^{1/4}}{4\pi \mathrm{Ai}''(a'_m)} |L_0(\sigma_2)|^{1/6} |L(\sigma_1,\sigma_2)|^{1/3} \mathbf{e}_3(\sigma_1,\sigma_2,0), \\ \mathbf{g}_m &= -\frac{pG_0^{1/4}}{4\pi \mathrm{Ai}''(a'_m)} |L_0(\sigma_2)|^{1/6} |L(\sigma_1,\sigma_2)|^{1/3} \mathbf{e}_2(\sigma_1,\sigma_2,0). \end{aligned} \quad . \tag{6.73}$$

We are now in the position illustrated in Figure 6.3. We next look at the shadow boundary that must exist to provide a smooth transition between the creeping ray and GO fields.

6.8 Shadow Boundary Structure

We first introduce the cylindrical polar coordinate system illustrated in Figure 6.4. The coordinates r, ϕ are in the tangent plane, and the distance normal to the tangent plane is given by z. The plane $\phi = 0$ is chosen so that $\phi = s_2$ at the origin. For the plane wave incidence problem the $\mathcal{O}(k^{-1/2})$ shadow boundary region existed to switch the incident field on and off and the $\mathcal{O}(k^{-1/3})$ transition regions provided a smooth match between the reflected field in the lit region and the creeping ray field in the shadow. When the source is located on the surface we do not have an incident field and it may be the case that the matching between the GO and creeping ray fields can be carried out using just the transition region—*i.e.* without requiring an $\mathcal{O}(k^{-1/2})$ shadow boundary. Another argument in favour of the omission of the

shadow boundary region is the following. Taking the ansatz

$$\mathbf{F} = e^{ikr}\sum_{n=0}^{\infty} k^{-n/2}\mathbf{F}^n(r,\phi,\tilde{z}), \tag{6.74}$$

for the fields, where $\tilde{z} = k^{1/2}z$, we eventually obtain the general solution

$$E_r^0 \equiv E_\phi^0 \equiv H_r^0 \equiv H_z^0, \tag{6.75}$$

$$H_\phi^0 = -E_z^0 = \frac{1}{\sqrt{r}}\left(B(\phi) + C(\phi)\exp\left(e^{-i\pi/4}\frac{\tilde{z}}{\sqrt{2r}}\right)\right). \tag{6.76}$$

There is no way that this can match into the leading order GO field which has the form $\exp(ikr + i\tilde{z}^2/2r)/r$. At this level, there appears to be no purpose in having an $\mathcal{O}(k^{-1/2})$ shadow boundary region.

To investigate the transition regions, which we anticipate will take care of the matching, we scale $\hat{z} = k^{1/3}z$ and take the ansatz

$$\mathbf{F} = e^{ikr+ik^{1/3}u(r,\hat{z})}\sum_{n=0}^{\infty} k^{-n/3}\mathbf{F}^n(r,\phi,\hat{z}). \tag{6.77}$$

Maxwell's equations yield equations (5.20) - (5.25) at $\mathcal{O}(k)$. We also obtain terms of $\mathcal{O}(k^{2/3})$:

$$-\frac{\partial u}{\partial \hat{z}}E_\phi^0 - H_r^1 = 0, \tag{6.78}$$

$$-E_z^1 + \frac{\partial u}{\partial \hat{z}}E_r^0 - H_\phi^1 = 0, \tag{6.79}$$

$$E_\phi^1 - H_z^1 = 0, \tag{6.80}$$

$$-\frac{\partial u}{\partial \hat{z}}H_\phi^0 + E_r^1 = 0, \tag{6.81}$$

$$-H_z^1 + \frac{\partial u}{\partial \hat{z}}H_r^0 + E_\phi^1 = 0, \tag{6.82}$$

$$H_\phi^1 + E_z^1 = 0, \tag{6.83}$$

terms of $\mathcal{O}(k^{1/3})$:

$$-i\frac{\partial u}{\partial \hat{z}}E_\phi^1 - \frac{\partial E_\phi^0}{\partial \hat{z}} - iH_r^2 = 0, \tag{6.84}$$

$$i\frac{\partial u}{\partial \hat{z}}E_r^1 - \frac{\partial E_r^0}{\partial \hat{z}} - iE_z^2 - i\frac{\partial u}{\partial r}E_z^0 - iH_\phi^2 = 0, \tag{6.85}$$

$$E_\phi^2 + \frac{\partial u}{\partial r}E_\phi^0 - H_z^2 = 0, \tag{6.86}$$

$$-i\frac{\partial u}{\partial \hat{z}}H_\phi^1 - \frac{\partial H_\phi^0}{\partial \hat{z}} + iE_r^2 = 0, \tag{6.87}$$

$$i\frac{\partial u}{\partial \hat{z}}H_r^1 - \frac{\partial H_r^0}{\partial \hat{z}} - iH_z^2 - i\frac{\partial u}{\partial r}H_z^0 + iE_\phi^2 = 0, \tag{6.88}$$

$$H_\phi^2 + \frac{\partial u}{\partial r}H_\phi^0 + E_z^2 = 0, \tag{6.89}$$

and terms of $\mathcal{O}(1)$:

$$\frac{1}{r}\frac{\partial E_z^0}{\partial \phi} - i\frac{\partial u}{\partial \hat{z}}E_\phi^2 - \frac{\partial E_\phi^1}{\partial \hat{z}} - iH_r^3 = 0, \tag{6.90}$$

$$i\frac{\partial u}{\partial \hat{z}}E_r^2 + \frac{\partial E_r^1}{\partial \hat{z}} - iE_z^3 - i\frac{\partial u}{\partial r}E_z^1 - \frac{\partial E_z^0}{\partial r} - iH_\phi^3 = 0, \tag{6.91}$$

$$\frac{E_\phi^0}{r} + iE_\phi^3 + i\frac{\partial u}{\partial r}E_\phi^1 + \frac{\partial E_\phi^0}{\partial r} - \frac{1}{r}\frac{\partial E_r^0}{\partial \phi} - iH_z^3 = 0, \tag{6.92}$$

$$\frac{1}{r}\frac{\partial H_z^0}{\partial \phi} - i\frac{\partial u}{\partial \hat{z}}H_\phi^2 - \frac{\partial H_\phi^1}{\partial \hat{z}} + iE_r^3 = 0, \tag{6.93}$$

$$i\frac{\partial u}{\partial \hat{z}}H_r^2 + \frac{\partial H_r^1}{\partial \hat{z}} - iH_z^3 - i\frac{\partial u}{\partial r}H_z^1 - \frac{\partial H_z^0}{\partial r} + iE_\phi^3 = 0, \tag{6.94}$$

$$\frac{H_\phi^0}{r} + iH_\phi^3 + i\frac{\partial u}{\partial r}H_\phi^1 + \frac{\partial H_\phi^0}{\partial r} - \frac{1}{r}\frac{\partial H_r^0}{\partial \phi} + iE_z^3 = 0. \tag{6.95}$$

Equating (6.86) and (6.88) gives us an equation for the phase function identical to that obtained for the plane wave incidence problem, namely

$$\left(\frac{\partial u}{\partial \hat{z}}\right)^2 + 2\left(\frac{\partial u}{\partial r}\right) = 0. \tag{6.96}$$

Equating (6.91) and (6.95) and using the lower order terms to eliminate variables, eventually leads to

$$\frac{\partial^2 u}{\partial \hat{z}^2}H_\phi^0 + 2\frac{\partial u}{\partial \hat{z}}\frac{\partial H_\phi^0}{\partial \hat{z}} + 2\frac{\partial H_\phi^0}{\partial r} + \frac{H_\phi^0}{r} = 0. \tag{6.97}$$

Setting $H_\phi^0 = A(r, \phi, \hat{z})/\sqrt{r}$ reduces (6.97) to (5.129) for A. We can thus use the results of section 5.3.4 to say that there is a similarity solution of the form

$$u(r, \hat{z}) = u(\hat{z}^2/r), \tag{6.98}$$

$$H_\phi^0 = \frac{1}{r}g\left(\frac{\hat{z}}{r}\right). \tag{6.99}$$

For the plane wave incidence problem in §5.3.4 we re-wrote the F-L solution in terms of the transition region coordinates and showed that not only was it a similarity solution of the correct form, but that it also matched succesfully into the reflected and creeping ray fields. We follow this same procedure here.

The transition region and F-L coordinates are related by

$$r \sim k^{-1/3}\hat{s}_1 + k^{-1}\left(\rho\hat{s}_1|L_0(s_2)| - \frac{1}{6}\hat{s}_1^3|L_0(s_2)|^2\right), \tag{6.100}$$

$$\phi = s_2, \tag{6.101}$$

$$\hat{z} \sim \frac{k^{-1/3}}{|L_0|^{1/3}}\left(\rho - \frac{\hat{s}_1^2|L_0(s_2)|}{2}\right). \tag{6.102}$$

Solving (6.100) and (6.102) for $\hat{s}_1, \rho$ lets us write the F-L solution in terms of $r, \hat{z}$ as

$$H_2 \sim \frac{\beta}{\sqrt{r}}e^{ikr+ik^{2/3}\hat{z}r|L_0(s_2)|-ir^3|L_0(s_2)|^2/3} \tag{6.103}$$
$$\times\int_{-\infty}^{\infty}\mathrm{Ai}\left(\sqrt[3]{2}e^{2\pi i/3}\left(\tau - |L_0|^{1/3}\left(k^{1/3}\hat{z} + k^{2/3}\frac{r^2|L_0|}{2}\right)\right)\right)\frac{e^{i\tau|L_0|^{2/3}k^{1/3}r}}{\mathrm{Ai}'\left(\sqrt[3]{2}e^{2\pi i/3}\tau\right)}\,\mathrm{d}\tau,$$

$$\beta = \frac{pk^{7/6}e^{\pi i/12}}{2^{11/6}\pi^{3/2}}. \tag{6.104}$$

Expanding the Airy function for large argument yields

$$g = \frac{\beta e^{\pi i/12}}{k^{1/6}2^{5/6}\sqrt{\pi}|L_0|^{1/3}}\int_{-\infty}^{\infty}\frac{e^{-i\frac{\hat{z}}{r}|L_0|^{-1/3}\tau - \frac{i}{6}\frac{\hat{z}^3}{r^3}|L_0|^{-1}}}{\mathrm{Ai}'\left(\sqrt[3]{2}e^{2\pi i/3}\tau\right)}\,\mathrm{d}\tau, \tag{6.105}$$

which is indeed of the required form. We now need to show that this matches successfully into the GO and creeping ray fields.

We first check the matching into the GO field. That is, we look at the limit of (6.77) and (6.105) as $\hat{z}/r \to \infty$. We first split the range of integration, so that

$$H_2 \sim \frac{\beta e^{\pi i/12}}{k^{1/6}r2^{5/6}\sqrt{\pi}|L_0|^{1/3}}e^{ikr+ik^{1/3}\hat{z}^2/2r}$$
$$\times\left\{\int_0^{\infty}\frac{e^{-i\frac{\hat{z}}{r}|L_0|^{-1/3}\tau - \frac{i}{6}\frac{\hat{z}^3}{r^3}|L_0|^{-1}}}{\mathrm{Ai}'\left(\sqrt[3]{2}e^{2\pi i/3}\tau\right)}\,\mathrm{d}\tau + \int_0^{\infty}\frac{e^{i\frac{\hat{z}}{r}|L_0|^{-1/3}\omega - \frac{i}{6}\frac{\hat{z}^3}{r^3}|L_0|^{-1}}}{\mathrm{Ai}'\left(\sqrt[3]{2}e^{-\pi i/3}\omega\right)}\,\mathrm{d}\omega\right\}. \tag{6.106}$$

We set $\tau = (\hat{z}/r)^2\bar{\tau}, \omega = (\hat{z}/r)^2\bar{\omega}$ and expand Ai' for large arguments. The first integral has an exponentially small steepest descents contribution and the second a stationary phase point at $\bar{\omega} = |L_0|^{-2/3}/2$. The stationary phase contribution dominates and we can write down the far-field of the transition region as $\hat{z}/r \to \infty$ as

$$H_2^0 \sim \frac{pk}{2\pi r}e^{ikr+ik^{1/3}\hat{z}^2/2r}. \tag{6.107}$$

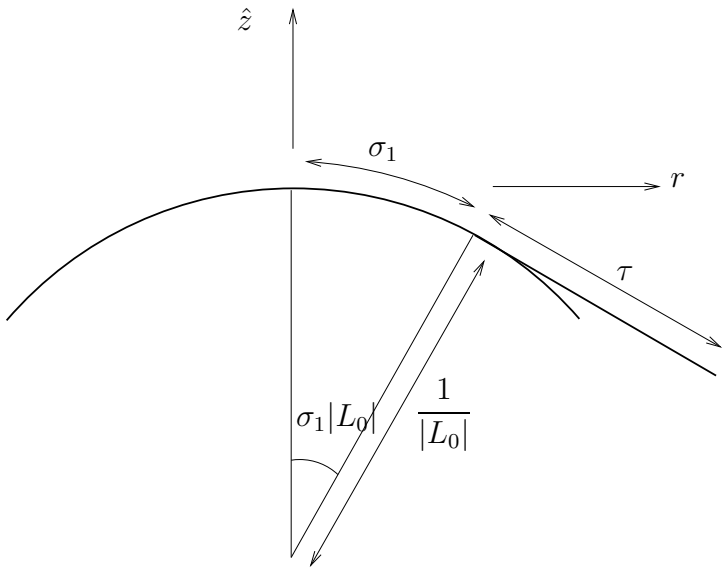


Figure 6.5: Relationship between the creeping ray and transition region coordinates.

This matches with the GO field.

To match to the creeping ray field we look at the behaviour of (6.105) as $\hat{z}/r \to -\infty$. This time, however, upon splitting the integral and scaling τ, ω as before, we find that the stationary phase point is no longer in the range of either integral. This means that the integral is dominated by the pole contributions, and using Cauchy's residue theorem, can be evaluated as

$$H_2 \sim \frac{\beta\pi e^{-\pi i/12}}{2^{1/6}\sqrt{\pi}|L_0|^{1/3}k^{1/6}r} e^{ikr+ik^{1/3}\frac{\hat{z}^2}{2r}-i\frac{\hat{z}^3}{6r^3}|L_0|^{-1}} \sum_{m=0}^{\infty} \frac{1}{\mathrm{Ai}''(a'_m)} e^{-i\frac{\hat{z}}{r}\frac{|L_0|^{-1/3}}{\sqrt[3]{2}}a'_m e^{-2\pi i/3}} \quad (6.108)$$

To show that this is a successful match, we need to write the transition region coordinates in terms of the creeping ray coordinates. Figure 6.5 gives the relationships

$$r = \tau\cos(\sigma_1|L_0|) + \frac{1}{|L_0|}\sin(\sigma_1|L_0|), \quad (6.109)$$

$$z = \frac{1}{|L_0|}(\cos(\sigma_1|L_0|) - 1) - \tau\sin(\sigma_1|L_0|), \quad (6.110)$$

for small σ_1. The transition region coordinate is $\hat{z} = k^{1/3}z$. For a balance to occur in (6.110) we must scale $\hat{\sigma}_1 = k^{1/3}\sigma_1$. Thus (6.109) - (6.110) can be approximated by

$$r \sim \tau + k^{-1/3}\hat{\sigma}_1 - k^{-2/3}|L_0|^2\frac{\hat{\sigma}_1^2}{2}\tau - k^{-1}|L_0|^2\frac{\hat{\sigma}_1^3}{6}, \quad (6.111)$$

$$\hat{z} \sim -|L_0|\tau\hat{\sigma}_1 - k^{-1/3}|L_0|\frac{\hat{\sigma}_1^2}{2}. \quad (6.112)$$

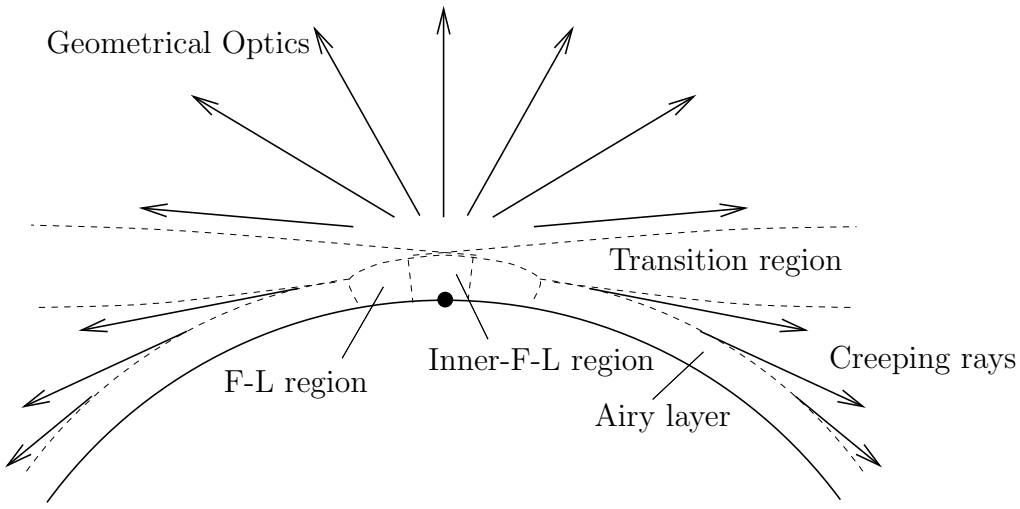


Figure 6.6: A cross-section of the complete asymptotic structure for a point source on a convex scatterer.

It is then easy to see that we can indeed match the transition region and the creeping ray fields.

The ray picture, along with the complete asymptotic structure, is illustrated in Figure 6.6. The fundamental differences between the asymptotic structures for a source at an $\mathcal{O}(1)$ distance from the surface and a source on the surface are the absence of the $\mathcal{O}(k^{-1/2})$ shadow boundary region and the necessity for an inner-F-L region in the neighbourhood of the source for the latter case. The shadow boundary region is no longer needed as there is not an incident field to switch on and off and the inner-F-L region is needed to fix the solution in the F-L region.

It is worth briefly discussing the dependence of the various fields on the azimuthal coordinate s_2 which appears as a parameter in our solutions. In the GO and inner-F-L regions, to lowest order, we have a point source on a half space which experiences no azimuthal variation. We have already remarked that, although there is an algebraic dependence on $L(s_1, s_2)$ in the Airy layer field, the main influence of s_2 comes in the decay factor $k^{1/3} \int_0^{s_1} |L(t, s_2)|^{2/3} \, \mathrm{d}t$ in the exponent. Thus, along geodesics with larger normal curvatures we will see an exponentially more rapid decay of the surface fields (and hence also more rapid decay of the creeping ray field).

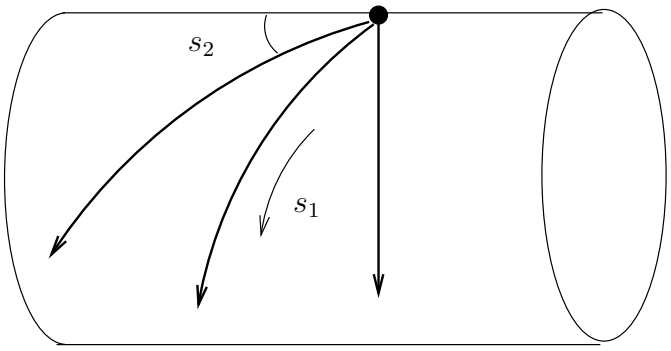


Figure 6.7: Point source on a cylinder

6.9 Surface Fields Due to a Point Source on a Circular Cylinder

The analysis carried out above is only valid provided the normal curvature L along the geodesics is $\mathcal{O}(1)$. If $L \ll 1$ the term involving the curvature will not appear in the Airy layer equation. This naturally precludes certain geometries such as a cylinder because $L \to 0$ as we approach the generator. To calculate exactly where the Airy layer solution breaks down we proceed as follows. We take a cylinder of unit radius as illustrated in Figure 6.7. The origin of the geodesic polar system is located at the source and $s_2 = 0$ corresponds to one of the geodesics along the axis of the cylinder. Consideration of the ansatz for the Airy layer solution, namely

$$\mathbf{F} \;=\; e^{iks_1 + ik^{1/3}v(s_1,s_2)} \sum_{n=0}^{\infty} \frac{\mathbf{F}^n(s_1,s_2,\rho)}{k^{n/3}}, \tag{6.113}$$

indicates that the Airy layer solution breaks down when $v = \mathcal{O}(k^{-1/3})$. From earlier results we know that

$$v(s_1,s_2) \;=\; \frac{a'_m e^{-2\pi i/3}}{\sqrt[3]{2}} \int_0^{s_1} |L(t,s_2)|^{2/3}\,\mathrm{d}t. \tag{6.114}$$

For a unit cylinder whose geodesics are parametrised by arclength the parametrisation of the surface is given by

$$\mathbf{R}(s_1,s_2) \;=\; (s_1\cos s_2, \cos(s_1\sin s_2), -\sin(s_1\sin s_2))\,, \tag{6.115}$$

with the first and second fundamental forms given by

$$\begin{array}{rclrclrcl} E &=& 1, & F &=& 0, & G &=& s_1^2, \\ L &=& -\sin^2 s_2, & M &=& s_1 \sin s_2 \cos s_2, & N &=& -s_1^2\cos^2 s_2. \end{array} \tag{6.116}$$

Thus, as we approach the generator for $s_1 = \mathcal{O}(1)$, the Airy layer solution breaks down when $s_2 = \mathcal{O}(k^{-1/4})$. We need to investigate the field in this region (which we shall term the F-L^1 region)[2].

To obtain the scaling on s_3 in the F-L^1 region we insert the ansatz

$$\mathbf{F} \quad = \quad e^{iks_1} \sum_{n=0}^{\infty} \frac{\mathbf{F}^n(s_1, \breve{s}_2, \breve{s}_3)}{k^{n/3}}, \tag{6.117}$$

into Maxwell's equations. A leading order balance occurs if we take the $\mathcal{O}(1)$ coordinates

$$\breve{s}_2 \quad = \quad k^{1/4} s_2, \quad \breve{s}_3 \quad = \quad k^{1/2} s_3. \tag{6.118}$$

We find that, as usual, we may decouple the field into magnetically and electrically polarised modes. The lowest order magnetically polarised mode satisfies

$$E_1^0 \equiv E_2^0 \equiv H_1^0 \equiv H_3^0 \quad \equiv \quad 0, \tag{6.119}$$

$$H_2^0 = -E_3^0 \quad = \quad \frac{A}{\sqrt{s_1}}, \tag{6.120}$$

$$\frac{\partial^2 A}{\partial \breve{s}_3^2} + 2i \frac{\partial A}{\partial s_1} + 2\breve{s}_3 \breve{s}_2^2 A \quad = \quad 0, \tag{6.121}$$

$$\frac{\partial A}{\partial \breve{s}_3} \quad = \quad 0, \quad \breve{s}_3 = 0, \tag{6.122}$$

and the lowest order electrically polarised mode satisfies

$$E_1^0 \equiv E_3^0 \equiv H_1^0 \equiv H_3^0 \quad \equiv \quad 0, \tag{6.123}$$

$$H_3^0 = E_2^0 \quad = \quad \frac{A}{\sqrt{s_1}}, \tag{6.124}$$

$$\frac{\partial^2 A}{\partial \breve{s}_3^2} + 2i \frac{\partial A}{\partial s_1} + 2\breve{s}_3 \breve{s}_2^2 A \quad = \quad 0, \tag{6.125}$$

$$A \quad = \quad 0, \quad \breve{s}_3 = 0. \tag{6.126}$$

The solution method for (6.121) - (6.122) and (6.125) - (6.126) is exactly the same as for (6.26) - (6.27). That is, we must consider an inner-F-L^1 region closer to the source.

The $\mathcal{O}(1)$ coordinates in the inner-F-L^1 region are

$$\bar{s}_1 \quad = \quad k^{1/2} s_1, \quad \breve{s}_2 \quad = \quad k^{1/4} s_2, \quad \breve{s}_3 \quad = \quad k^{1/2} s_3. \tag{6.127}$$

[2]In general the Airy layer solution breaks down when $k^{1/3} s_1 s_2^{4/3} = \mathcal{O}(1)$. In terms of cartesian coordinates close to the generator we have $x = s_1$, $y = s_1 s_2$. This means that the F-L^1 region is $ky^4/x = \mathcal{O}(1)$. Thus the width of the F-L^1 region is $\mathcal{O}(k^{-1/4})$.

Using the results of §6.4 we can immediately write down the field in the inner-F-L^1 region as

$$H_r \equiv H_\theta \equiv E_r \equiv E_\phi \equiv 0, \tag{6.128}$$

$$H_\phi \equiv E_\theta = -\frac{pk^{3/2}\sin\theta}{2\pi\left(\bar{s}_1^2+\breve{s}_3^2\right)^{1/2}} e^{ik^{1/2}\left(\bar{s}_1^2+\breve{s}_3^2\right)^{1/2}}, \tag{6.129}$$

where θ is the spherical polar angle to the vertical at the origin. The solution technique of §6.5 may be applied to show that no electrically polarised modes are excited in the F-L^1 region and that the magnetically polarised F-L^1 field is given by

$$A(s_1,\breve{s}_2,\breve{s}_3) \sim \frac{pke^{\pi i/12}}{2^{11/6}\pi^{3/2}}\breve{s}_2^{2/3}\int_{-\infty}^{\infty}\frac{\mathrm{Ai}\left(\sqrt[3]{2}e^{2\pi i/3}\left(\tau-\breve{s}_2^{2/3}\breve{s}_3\right)\right)}{\mathrm{Ai}'\left(\sqrt[3]{2}e^{2\pi i/3}\tau\right)}e^{i\tau\breve{s}_2^{4/3}s_1}\,\mathrm{d}\tau. \tag{6.130}$$

Figure 6.8 is a schematic of the asymptotic regions involved. To check that we have a smoothly varying solution we see that we must check that we must be able to carry out matching between the following pairs of regions.

a) inner-F-L region and F-L region.

b) F-L region and Airy layer.

c) inner-F-L^1 region and F-L^1 region.

d) inner-F-L^1 region and inner-F-L region.

e) inner-F-L^1 region and F-L region.

f) F-L^1 region and F-L region.

g) F-L^1 region and Airy layer.

The matching required for a) - c) has already been carried out at various stages in the derivation of the solutions. It may also be seen that the matching needed for d) and f) is trivial. We will now briefly verify the remaining two cases.

Case e).

We write the F-L solution (6.130) in terms of the inner-F-L^1 coordinates $\bar{s}_1,\breve{s}_2,\breve{s}_3$, to get

$$H_2 \sim \frac{pk^{5/4}\breve{s}_2^{2/3}e^{ik^{1/2}\bar{s}_1+i\pi/12}}{2^{11/6}\pi^{3/2}\sqrt{\bar{s}_1}}\int_{-\infty}^{\infty}\frac{\mathrm{Ai}\left(\sqrt[3]{2}e^{2\pi i/3}\left(\tau-\breve{s}_3\breve{s}_2^{2/3}\right)\right)}{\mathrm{Ai}'\left(\sqrt[3]{2}e^{2\pi i/3}\tau\right)}e^{ik^{-1/2}\tau\bar{s}_1\breve{s}_2^{4/3}}. \tag{6.131}$$

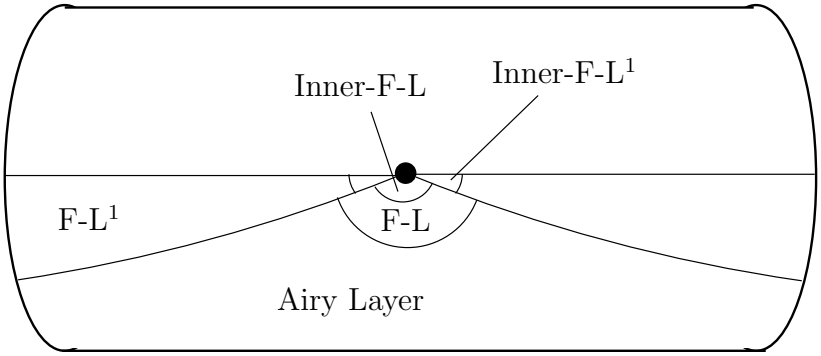


Figure 6.8: Asymptotic regions along the axis of the cylinder.

We scale $\tau = k\omega$, and then expand the Airy functions for large arguments, whereupon (6.131) becomes

$$H_2 \sim \frac{pk^2 \breve{s}_2^{2/3} e^{ik^{1/2}\bar{s}_1 + 3\pi i/4}}{4\pi^{3/2}\sqrt{\bar{s}_1}} \int_{-\infty}^{\infty} \frac{\exp\left(-k^{1/2}\sqrt{2\omega}\breve{s}_3\breve{s}_2^{2/3} + ik^{1/2}\omega\bar{s}_1\breve{s}_2^{4/3}\right)}{\sqrt{\omega}}\,\mathrm{d}\omega. \quad (6.132)$$

This may be further manipulated to yield an error function. Eventually this gives

$$H_2 \sim -\frac{pk^{3/2}e^{ik^{1/2}\bar{s}_1 + \frac{i\breve{s}_3^2}{2\bar{s}_1}}}{2\pi\bar{s}_1}. \quad (6.133)$$

This is exactly the outer limit of the inner-F-L^1 solution as required.

Case g).

We write the magnetically polarised F-L^1 field in terms of s_1, s_2, ρ, namely

$$H_2 \sim \frac{e^{iks_1}}{\sqrt{s_1}} \frac{pk^{7/6}e^{i\pi/12}s_2^{2/3}}{2^{11/6}\pi^{3/2}} \int_{-\infty}^{\infty} \frac{\mathrm{Ai}\left(\sqrt[3]{2}e^{2\pi i/3}\left(\tau - \rho s_2^{2/3}\right)\right)}{\mathrm{Ai}'\left(\sqrt[3]{2}e^{2\pi i/3}\tau\right)} e^{ik^{1/3}\tau s_2^{1/3}s_1}\,\mathrm{d}\tau. \quad (6.134)$$

Remembering that $G \sim s_1^2$ and $|L| \sim s_2^2$ for small s_2 it is straightforward to see that the evaluation of (6.134) via Cauchy's Residue Theorem gives rise to an *outer limit of the inner* (F-L^1) *solution* that is equal to the *inner limit of the outer* (Airy) *solution.*

At first sight, (6.130) seems to imply that the field is zero along $\breve{s}_2 = 0$. This is counterintuitive as we would expect the field to decay *least* rapidly in this direction. A little analysis will allay our fears. We consider (6.130) for small values of $\breve{s}_2$. We make the substitutions

$$\tau = M^4 T, \quad \breve{s}_2 = M^{-3} S, \quad (6.135)$$

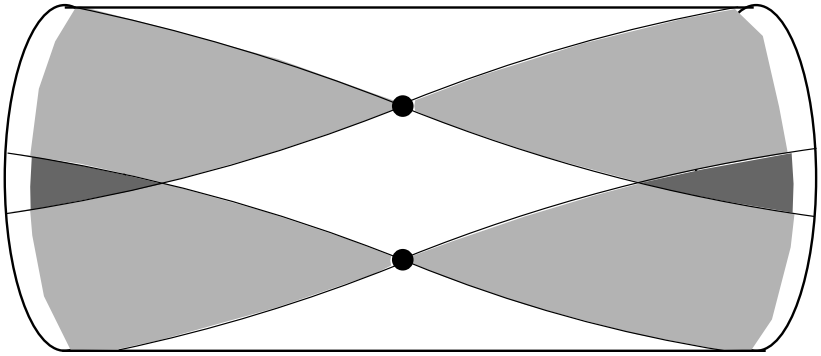


Figure 6.9: F-L^1 regions arising due to two sources on a cylinder. These regions overlap at an $\mathcal{O}(k)$ distance from the sources.

where M is large. We then expand Ai and Ai$'$ for large arguments. A little manipulation then gives us the limit of (6.130) as $\breve{s}_2 \to 0$ as

$$A(s_1, \breve{s}_2, \breve{s}_3) \quad \sim \quad -\frac{pke^{i\frac{\breve{s}_3^2}{2s_1}}}{2\pi\sqrt{s}_1}. \tag{6.136}$$

Equations (6.117), (6.120) and (6.136) then indicate that as we approach the generator the surface field tends towards the surface field obtained were we to place a dipole source on an infinite flat perfect conductor.

As an interesting extension to this problem (not considered here) consider a cylinder with two point sources as in Figure 6.9. The linearity of the governing equations allows independent consideration of the surface fields due to each source. Along the generators through each source we will need to introduce F-L^1 regions. These will grow in width as we travel away from the source. When the F-L^1 regions become $\mathcal{O}(1)$ in width they will overlap and extra care will be needed. For the F-L^1 region to have an $\mathcal{O}(1)$ width we require

$$s_1 s_2 \quad = \quad \mathcal{O}(1). \tag{6.137}$$

But the F-L^1 region is defined as being where

$$s_1 s_2^{4/3} \quad = \quad \mathcal{O}(k^{-1/3}). \tag{6.138}$$

Thus, (6.137) - (6.138) imply that the two F-L^1 regions will meet when $s_1 = \mathcal{O}(k)$.

6.10 Sources at Inflexion Points

Consider the cylinder illustrated in Figure 6.10. A point source is placed on the line of inflexion. Consider the two parametrisations of the surface that are illustrated.

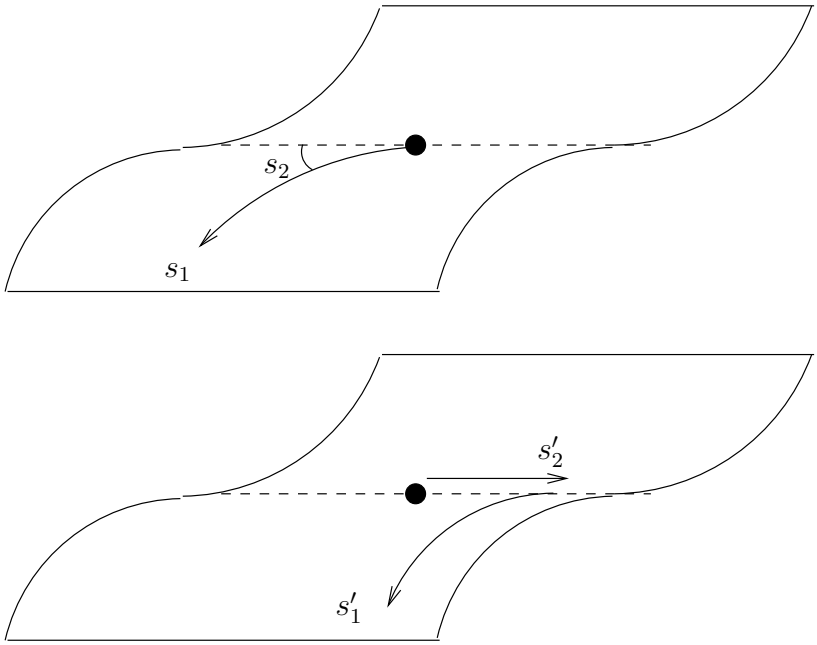


Figure 6.10: A source on the line of inflexion of a cylinder, along with the geodesic polar and geodesic normal coordinate systems.

The coordinates s_1, s_2, s_3 are the usual geodesic polar coordinates based at the source and with $s_2 = 0$ coinciding with the line of inflexion. The coordinates s_1', s_2', s_3 form a geodesic normal coordinate system with the origin again at the source. The distance along the line of inflexion is given by s_2' and the distance around the cylinder from the line of inflexion is given by s_1'. We know that away from the line of inflexion there will be a creeping ray field set up in the convex section and a whispering gallery field in the concave section. As in §6.9 the Airy layer field will break down when $v = \mathcal{O}(k^{-1/3})$. Explicitly, this occurs when

$$\int_0^{s_1} |L(t, s_2)|^{2/3} \, \mathrm{d}t \;\; = \;\; \mathcal{O}(k^{-1/3}). \tag{6.139}$$

A new region in the neighbourhood of the line of inflexion will then need to be considered. To obtain the scalings for this region, we must first find an expression for the behaviour of $L(s_1, s_2)$ as we approach the line of inflexion. If we define L', M', N' to be the components of the second fundamental form associated with s_1', s_2' we have that close to the line of inflexion

$$L' \;\; \sim \;\; s_1', \quad M' \;\; = \;\; 0, \quad N' \;\; = \;\; 0. \tag{6.140}$$

The standard definition of curvature in a given direction then gives us

$$L \;\; = \;\; L' \left(\frac{\mathrm{d}s_1'}{\mathrm{d}s_1} \right)^2 + 2M' \left(\frac{\mathrm{d}s_1'}{\mathrm{d}s_1} \right) \left(\frac{\mathrm{d}s_2'}{\mathrm{d}s_1} \right) + N' \left(\frac{\mathrm{d}s_2'}{\mathrm{d}s_1} \right)^2 . \tag{6.141}$$

This reveals that as we approach the line of inflexion we have

$$L \sim s_1 s_2 \left(\sin s_2\right)^2 \quad \sim \quad s_1 s_2^3. \tag{6.142}$$

Upon taking $s_1 = \mathcal{O}(1)$, equations (6.139) and (6.142) imply that the Airy layer solution breaks down when $s_2 = \mathcal{O}(k^{-1/6})$. Introducing the $\mathcal{O}(1)$ variables

$$\breve{s}_2 \quad = \quad k^{1/6} s_2, \quad \breve{s}_3 \quad = \quad k^{1/2} s_3, \tag{6.143}$$

we obtain the now familiar F-L equations for the two polarisations of the field, namely

$$E_1^0 \equiv E_2^0 \equiv H_1^0 \equiv H_3^0 \quad \equiv \quad 0, \tag{6.144}$$

$$H_2^0 = -E_3^0 \quad = \quad \frac{A}{\sqrt{s_1}}, \tag{6.145}$$

$$\frac{\partial^2 A}{\partial \breve{s}_3^2} + 2i \frac{\partial A}{\partial s_1} - 2\breve{s}_3 s_1 \breve{s}_2^3 A \quad = \quad 0, \tag{6.146}$$

$$\frac{\partial A}{\partial \breve{s}_3} \quad = \quad 0, \quad \breve{s}_3 = 0, \tag{6.147}$$

for the magnetically polarised field and

$$E_1^0 \equiv E_3^0 \equiv H_1^0 \equiv H_2^0 \quad \equiv \quad 0, \tag{6.148}$$

$$H_3^0 = E_2^0 \quad = \quad \frac{A}{\sqrt{s_1}}, \tag{6.149}$$

$$\frac{\partial^2 A}{\partial \breve{s}_3^2} + 2i \frac{\partial A}{\partial s_1} - 2\breve{s}_3 s_1 \breve{s}_2^3 A \quad = \quad 0, \tag{6.150}$$

$$A \quad = \quad 0, \quad \breve{s}_3 = 0, \tag{6.151}$$

for the electrically polarised field. For both polarisations we must include the conditions that the field matches into the creeping ray/whispering gallery fields as $\breve{s}_2 \to \pm\infty$. The fact that $L(s_1, s_2)$ is now a non-trivial function of s_1 means that we are unable to solve (6.146) and (6.150) using a Laplace transform as we were able to do in §6.3. We comment on the similarity between (6.146) and (6.150) and (5.232). This is not altogether surprising as the geometry of the two problems is the same.

6.11 Sources on Saddle Points

We now consider the case where the source is located at a saddle point of the surface. We work in a geodesic polar coordinate system s_1, s_2, s_3 based at the saddle point and construct the two geodesics C_1, C_2 that pass through the saddle point and that have zero normal curvature. These split the surface into convex and concave sections.

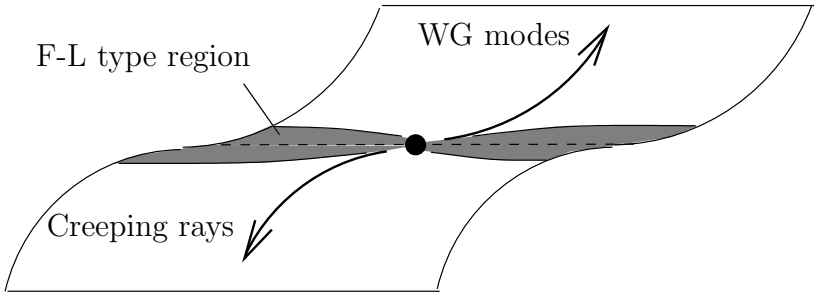


Figure 6.11: Asymptotic regions for a source located on a line of inflexion

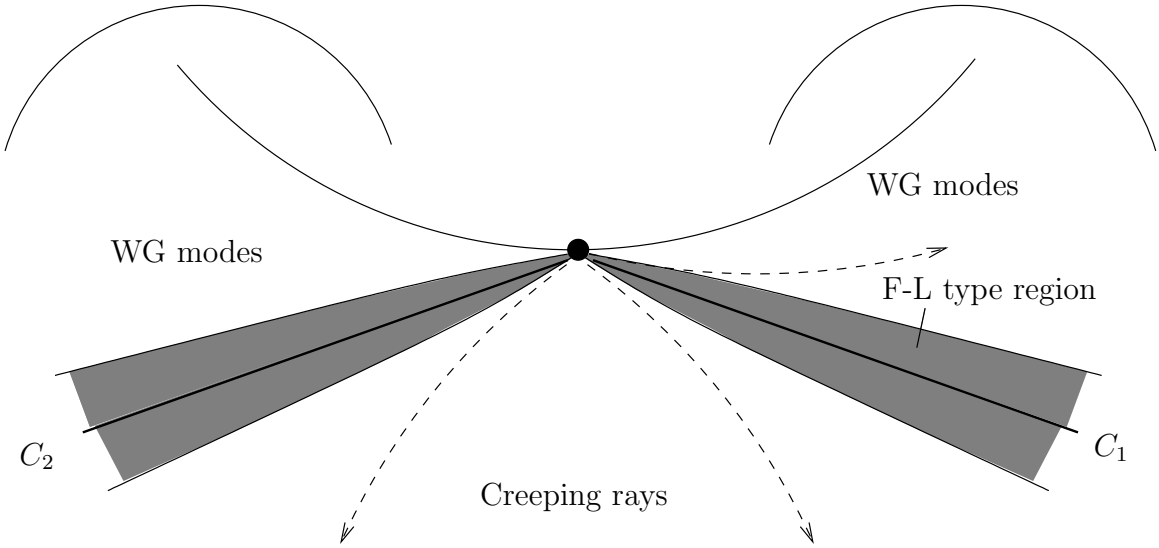


Figure 6.12: Source on a saddle point.

In the convex sections a creeping ray field will be set up and in the concave regions whispering gallery modes will propagate. As we approach C_1, C_2 the expansions for the surface fields will break down and a new asymptotic region close to each line of zero curvature will need to be introduced. Although we do not consider this problem in detail here, we postulate that there will be an F-L type region in the neighbourhood of C_1, C_2, and that we will face the same problems when trying to solve this F-L equation as in §6.10—namely that $L(s_1, s_2)$ is a non-trivial function of s_1 as we approach the lines of zero curvature.

Chapter 7

Sources Close to a Convex Surface

We have now dealt with the cases where our point source is at infinity (plane wave incidence), at an $\mathcal{O}(1)$ distance from the surface and actually on the surface of the scatterer. The one case we have omitted so far is when the source is close to but not on the surface. The canonical problem is a source at an $\mathcal{O}(k^{-2/3})$ distance from the surface. The solution technique will follow §6.2 - §6.8 with some small adjustments. The major difference will be that the source is now able to excite both magnetically *and* electrically polarised surface and shed ray fields. We will work in a geodesic polar coordinate system with the source located at $s_1 = 0, s_3 = s_{3_0} = k^{-2/3}\rho_0$ for some $\rho_0 = \mathcal{O}(1)$. The analysis in the Airy layer and F-L regions carries through as earlier in §6. That is to say, in the Airy layer we have solutions

$$\mathbf{F} \quad = \quad e^{iks_1 + ik^{1/3}u(s_1,s_2)} \sum_{n=0}^{\infty} \frac{\mathbf{F}^n(s_1, s_2, \rho)}{k^{n/3}}. \tag{7.1}$$

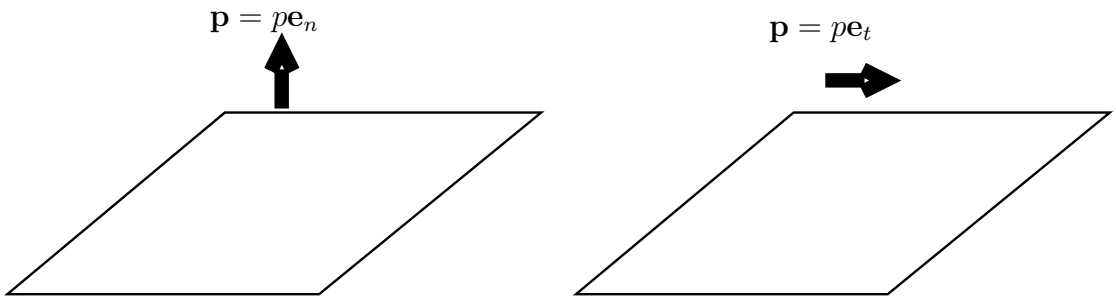


Figure 7.1: Orientations of an electric dipole close to the surface. The first excites magnetically polarised solutions, the second electrically polarised solutions.

The magnetically polarised modes are given by

$$E_1^0 \equiv E_2^0 \equiv H_1^0 \equiv H_3^0 \equiv 0, \tag{7.2}$$

$$H_2^0 = -E_3^0 = \sum_{m=0}^{\infty} \frac{\beta_m(s_2)|L|^{1/6}}{G^{1/4}} \mathrm{Ai}\left(-\sqrt[3]{2}e^{2\pi i/3}|L|^{1/3}\rho + a'_m\right), \tag{7.3}$$

$$u(s_1, s_2) = \frac{a'_m e^{-2\pi i/3}}{\sqrt[3]{2}} \int_0^{s_1} |L(\lambda, s_2)|^{2/3}\, \mathrm{d}\lambda. \tag{7.4}$$

The electrically polarised solutions may be obtained in the same way as

$$E_1^0 \equiv E_3^0 \equiv H_1^0 \equiv H_2^0 \equiv 0, \tag{7.5}$$

$$E_2^0 = H_3^0 = \sum_{m=0}^{\infty} \frac{\gamma_m(s_2)|L|^{1/6}}{G^{1/4}} \mathrm{Ai}\left(-\sqrt[3]{2}e^{2\pi i/3}|L|^{1/3}\rho + a_m\right), \tag{7.6}$$

$$u(s_1, s_2) = \frac{a_m e^{-2\pi i/3}}{\sqrt[3]{2}} \int_0^{s_1} |L(\lambda, s_2)|^{2/3}\, \mathrm{d}\lambda. \tag{7.7}$$

The unknown functions $\beta_m(s_2), \gamma_m(s_2)$ are determined via consideration of the solution in an F-L region in the neighbourhood of the source.

The solution in the F-L region is

$$\mathbf{F} = e^{iks_1} \sum_{n=0}^{\infty} \frac{\mathbf{F}^n(\hat{s}_1, s_2, \rho)}{k^{n/3}}. \tag{7.8}$$

The magnetically polarised modes satisfy

$$E_1^0 \equiv E_2^0 \equiv H_1^0 \equiv H_3^0 \equiv 0, \tag{7.9}$$

$$H_2^0 = -E_3^0 = \frac{A}{\sqrt{\hat{s}_1}}, \tag{7.10}$$

$$\frac{\partial^2 \bar{A}}{\partial \rho^2} + 2i\lambda\bar{A} + 2|L(0, s_2)|\rho\bar{A} = F(\epsilon, \rho), \quad \rho > 0, \tag{7.11}$$

$$\frac{\partial \bar{A}}{\partial \rho} = 0, \quad \rho = 0. \tag{7.12}$$

For the electric polarisation, the F-L solution satisfies

$$E_1^0 \equiv E_3^0 \equiv H_1^0 \equiv H_2^0 \equiv 0, \tag{7.13}$$

$$E_2^0 = H_3^0 = \frac{A}{\sqrt{\hat{s}_1}}, \tag{7.14}$$

$$\frac{\partial^2 \bar{A}}{\partial \rho^2} + 2i\lambda\bar{A} + 2|L(0, s_2)|\rho\bar{A} = F(\epsilon, \rho), \quad \rho > 0, \tag{7.15}$$

$$\bar{A} = 0, \quad \rho = 0. \tag{7.16}$$

The function $F(\epsilon, \rho) = 2iA(\rho, \epsilon)$ is found by consideration of an inner-F-L region around the source.

7.1 Magnetically Polarised Solutions

We first consider an electric dipole with moment

$$\mathbf{p} \;=\; p\delta(\rho-\rho_0)\delta(s_1)\mathbf{e}_3, \tag{7.17}$$

where ρ is the usual $\mathcal{O}(1)$ F-L variable.

Inner-F-L Solution

As discussed in §2.3.3 we introduce an image dipole

$$\mathbf{p} \;=\; p\delta(\rho+\rho_0)\delta(s_1)\mathbf{e}_3, \tag{7.18}$$

to ensure that the perfectly conducting boundary conditions are satisfied. Section §2.3.3 implies that the solution in the inner-F-L region due to the original dipole is

$$\begin{aligned} H_r &= 0, \quad H_\phi = -\frac{pk^{5/3}\sin\theta}{4\pi R}e^{ik^{1/3}R}, \quad H_\theta = 0, \\ E_r &= 0, \quad E_\phi = 0, \qquad\qquad\quad E_\theta = -\frac{pk^{5/3}\sin\theta}{4\pi R}e^{ik^{1/3}R}, \end{aligned} \tag{7.19}$$

where r,ϕ,θ are spherical polars based at the dipole with $\theta=0$ corresponding to the direction $\mathbf{e}_3$ and $R=k^{2/3}r$. The field due to the image source is identical to (7.19) with the spherical polar coordinates now based at the image source. The outer limit of the inner-F-L solution in terms of the F-L coordinates $\hat{s}_1,\rho$ is

$$\begin{aligned} H_\phi &= H_2 \;\sim\; -\frac{pk^{4/3}}{4\pi\hat{s}_1}e^{ik^{2/3}\hat{s}_1}\left(e^{i(\rho-\rho_0)^2/2\hat{s}_1}+e^{i(\rho+\rho_0)^2/2\hat{s}_1}\right), \\ E_\theta &\sim -E_3 \;\sim\; -\frac{pk^{4/3}}{4\pi\hat{s}_1}e^{ik^{2/3}\hat{s}_1}\left(e^{i(\rho-\rho_0)^2/2\hat{s}_1}+e^{i(\rho+\rho_0)^2/2\hat{s}_1}\right). \end{aligned} \tag{7.20}$$

Thus, the function F of (7.11) is given by

$$F(\epsilon,\rho) \;=\; -\frac{ipk^{4/3}}{2\pi\sqrt{\epsilon}}\left(e^{i(\rho-\rho_0)^2/2\epsilon}+e^{i(\rho+\rho_0)^2/2\epsilon}\right). \tag{7.21}$$

Fock-Leontovič Region Solution

Using the expression (6.44) for the solution with $G(\eta,\tau)$ given by (6.45), (6.46) - (6.47) gives the solution in the F-L region as

$$A \;=\; \begin{cases} \zeta\displaystyle\int_{-\infty}^{\infty} A_2(\eta)A_1(-\tau+\rho_0|L_0|^{1/3})e^{i\tau|L_0|^{2/3}\hat{s}_1}\,\mathrm{d}\tau, & \rho>\rho_0, \\ \zeta\displaystyle\int_{-\infty}^{\infty} A_1(\eta)A_2(-\tau+\rho_0|L_0|^{1/3})e^{i\tau|L_0|^{2/3}\hat{s}_1}\,\mathrm{d}\tau, & \rho<\rho_0, \end{cases} \tag{7.22}$$

$$\zeta \;=\; \frac{e^{11\pi i/12}pk^{4/3}|L_0|^{1/3}}{2^{5/6}\sqrt{\pi}}. \tag{7.23}$$

If we exchange the roles of ρ and ρ_0 it is easy to see that reciprocity—Appendix D—is satisfied.

Geometrical Optics Field

We anticipate a solution of the form

$$H_2 = \chi_+ \frac{\sin\theta_+}{r_+} e^{ikr_+} + \chi_- \frac{\sin\theta_-}{r_-} e^{ikr_-}, \tag{7.24}$$

$$\sim \chi_+ \frac{\sin\theta}{r} e^{ikr - ik^{1/3}\rho_0 \sin\theta} + \chi_- \frac{\sin\theta}{r} e^{ikr + ik^{1/3}\rho_0 \sin\theta}, \tag{7.25}$$

where $r_\pm$ are the distances to the source and image source respectively and $\theta_\pm$ are the spherical polar angles of the observation point to the vertical at the source and image source. The distance to the origin is given by r and θ is the spherical polar angle of the observation point to the vertical at the origin. Matching with the inner-F-L region fixes

$$\chi_+ = \chi_- = \frac{pk}{4\pi}. \tag{7.26}$$

We must now check that the F-L solution matches with the GO field given by (7.24) - (7.26). We take the form of the F-L solution for $\rho > \rho_0$, and make the variable change $\tau = k^{2/3}\bar{\tau}$. We then split the F-L integral into four parts, namely

$$\begin{aligned}
A = \; & k^{2/3}\zeta \int_0^\infty \mathrm{Ai}\big(\sqrt[3]{2}e^{2\pi i/3}\big(k^{2/3}\bar{\tau} - \rho|L_0|^{1/3}\big)\big)\mathrm{Ai}\big(\sqrt[3]{2}\big(k^{2/3}\bar{\tau} - \rho_0|L_0|^{1/3}\big)\big) e^{ik^{2/3}\bar{\tau}|L_0|^{2/3}\hat{s}_1}\,\mathrm{d}\bar{\tau} \\
& + k^{2/3}\zeta \int_0^\infty \mathrm{Ai}\big(\sqrt[3]{2}e^{-\pi i/3}\big(k^{2/3}\bar{\omega} + \rho|L_0|^{1/3}\big)\big)\mathrm{Ai}\big(-\sqrt[3]{2}\big(k^{2/3}\bar{\omega} + \rho_0|L_0|^{1/3}\big)\big) e^{-ik^{2/3}\bar{\omega}|L_0|^{2/3}\hat{s}_1}\,\mathrm{d}\bar{\omega} \\
& - k^{2/3}e^{-2\pi i/3}\zeta \int_0^\infty \mathrm{Ai}\big(\sqrt[3]{2}e^{2\pi i/3}\big(k^{2/3}\bar{\tau} - \rho|L_0|^{1/3}\big)\big) \frac{\mathrm{Ai}'\big(\sqrt[3]{2}\bar{\tau}k^{2/3}\big)}{\mathrm{Ai}'\big(\sqrt[3]{2}e^{2\pi i/3}\bar{\tau}k^{2/3}\big)} \\
& \qquad \times \mathrm{Ai}\big(\sqrt[3]{2}e^{2\pi i/3}\big(k^{2/3}\bar{\tau} - \rho_0|L_0|^{1/3}\big)\big) e^{ik^{2/3}\bar{\tau}|L_0|^{2/3}\hat{s}_1}\,\mathrm{d}\bar{\tau} \\
& - k^{2/3}e^{-2\pi i/3}\zeta \int_0^\infty \mathrm{Ai}\big(\sqrt[3]{2}e^{-\pi i/3}\big(k^{2/3}\bar{\omega} + \rho|L_0|^{1/3}\big)\big) \frac{\mathrm{Ai}'\big(-\sqrt[3]{2}\bar{\omega}k^{2/3}\big)}{\mathrm{Ai}'\big(\sqrt[3]{2}e^{-\pi i/3}\bar{\omega}k^{2/3}\big)} \\
& \qquad \times \mathrm{Ai}\big(\sqrt[3]{2}e^{-\pi i/3}\big(k^{2/3}\bar{\omega} + \rho_0|L_0|^{1/3}\big)\big) e^{-ik^{2/3}\bar{\omega}|L_0|^{2/3}\hat{s}_1}\,\mathrm{d}\bar{\omega}.
\end{aligned} \tag{7.27}$$

In each of these integrals we must use different large argument expansions of the Airy functions. For each integral we expand the Airy functions for large argument and then rewrite everything in terms of the geometrical optics coordinates s_1, s_3.

The first integral gives exponentially small contributions as $\rho > \rho_0$.

The second integral gives us two stationary phase contributions, namely

$$-\frac{pk^{7/6}}{4\pi\sqrt{s_1}} e^{iks_3^2/2s_1 - ik^{1/3}\rho_0 s_3/s_1} + \vartheta(s_1, s_2, s_3).$$

The third integral also yields an exponentially small contribution.

The fourth integral will give two stationary phase contributions,

$$-\frac{pk^{7/6}}{4\pi\sqrt{s}_1}e^{iks_3^2/2s_1+ik^{1/3}\rho_0 s_3/s_1}-\vartheta(s_1,s_2,s_3).$$

It is straightforward to verify that this is equal to the inner limit of the outer (GO) solution as required.

Airy Layer Field

To match into the Airy layer we rewrite (7.22) in terms of the Airy layer coordinates. For $\rho<\rho_0$ this gives us

$$\begin{aligned}A \;\rightarrow\; & \zeta\int_{\infty}^{\infty}\mathrm{Ai}\left(-\sqrt[3]{2}e^{2\pi i/3}\left(|L_0|^{1/3}\rho-\tau\right)\right)\mathrm{Ai}\left(-\sqrt[3]{2}\left(|L_0|^{1/3}\rho_0-\tau\right)\right)e^{ik^{1/3}\tau|L_0|^{2/3}s_1}\mathrm{d}\tau,\\ & -\zeta e^{-2\pi i/3}\int_{-\infty}^{-\infty}\mathrm{Ai}\left(-\sqrt[3]{2}e^{2\pi i/3}\left(|L_0|^{1/3}\rho-\tau\right)\right)\frac{\mathrm{Ai}'\left(\sqrt[3]{2}\tau\right)}{\mathrm{Ai}'\left(\sqrt[3]{2}e^{2\pi i/3}\tau\right)}\\ & \qquad\times\mathrm{Ai}\left(-\sqrt[3]{2}e^{2\pi i/3}\left(|L_0|^{1/3}\rho_0-\tau\right)\right)e^{ik^{1/3}\tau|L_0|^{2/3}s_1}\,\mathrm{d}\tau. \qquad (7.28)\end{aligned}$$

The first integral is oscillatory and so gives no dominant contribution. The second integral has poles along the line $\arg(\tau)=2\pi/3$. Closing the contour in the upper half-plane gives

$$\begin{aligned}A \;\rightarrow\; & 2^{2/3}\pi e^{\pi i/6}\zeta\sum_{m=0}^{\infty}\frac{\mathrm{Ai}'\left(a_m'e^{-2\pi i/3}\right)}{\mathrm{Ai}''(a_m')}\\ & \qquad\times\mathrm{Ai}\left(-\sqrt[3]{2}e^{2\pi i/3}|L_0|^{1/3}\rho+a_m'\right)\mathrm{Ai}\left(-\sqrt[3]{2}e^{2\pi i/3}|L_0|^{1/3}\rho_0+a_m'\right). \qquad (7.29)\end{aligned}$$

The same limit is obtained for $\rho>\rho_0$. This fixes

$$\begin{aligned}\alpha_m(s_2) \;=\; & -\frac{\sqrt{\pi}e^{\pi i/12}pk^{7/6}}{2^{1/6}}\frac{\mathrm{Ai}'\left(a_m'e^{-2\pi i/3}\right)}{\mathrm{Ai}''(a_m')}G_0(s_2)^{1/4}|L_0(s_2)|^{1/6}\\ & \qquad\times\mathrm{Ai}\left(-\sqrt[3]{2}e^{2\pi i/3}|L_0|^{1/3}\rho_0+a_m'\right). \qquad (7.30)\end{aligned}$$

The only difference between this solution and that for the point source *on* the surface is the value of the constant $\alpha_m(s_2)$. Thus it is trivial to write down the associated creeping ray fields. The comments regarding the dependence of the surface and shed creeping ray fields on s_2 at the end of §6.8 are also still valid. Reassuringly, the Airy layer field is seen to satisfy reciprocity if we exchange the roles of ρ and ρ_0.

Transition Region Solution

Once again there is a discontinuity in the leading order field as we pass from the GO lit region into the creeping ray field. From our work earlier we first look for a solution in an $\mathcal{O}(k^{-1/3})$ transition region in the hope that it will provide a complete match. We introduce the coordinate system r, θ, z as in §6.8. Scaling $\hat{z} = k^{1/3}z$, and taking the ansatz (6.77) for the fields yields the same equations, namely (5.20) - (5.25) and (6.78) - (6.95). Thus once again we require a solution of the form

$$u = \frac{\hat{z}^2}{2r}, \tag{7.31}$$

$$H_2^0 = \frac{1}{r} g\left(\frac{\hat{z}}{r}\right), \tag{7.32}$$

where g must match successfully into the geometrical optics and creeping ray fields. We follow the same procedure as before. Writing the F-L solution in terms of the transition region coordinates gives us a similarity solution of the correct form, namely

$$g = \frac{\zeta e^{\pi i/12}}{2^{5/6}\sqrt{\pi}|L_0|^{1/3}k^{1/6}} \int_{-\infty}^{\infty} e^{-\frac{\hat{z}}{r}|L_0|^{-1/3}\tau - \frac{i}{6}\frac{\hat{z}^3}{r^3}|L_0|^{-1}} \tag{7.33}$$

$$\times \left\{ \mathrm{Ai}\left(\sqrt[3]{2}\left(\tau - \rho_0|L_0|^{1/3}\right)\right) - e^{-2\pi i/3}\frac{\mathrm{Ai}'\left(\sqrt[3]{2}\tau\right)}{\mathrm{Ai}'\left(\sqrt[3]{2}e^{2\pi i/3}\tau\right)}\mathrm{Ai}\left(\sqrt[3]{2}e^{2\pi i/3}\left(\tau - \rho_0|L_0|^{1/3}\right)\right)\right\} \mathrm{d}\tau.$$

We must now show that this provides a successful match as $\hat{z} \to \pm\infty$. Here, we will only outline this somewhat tedious calculation.

To verify that we can match (7.33) into the reflected field we first set $\tau = \frac{\hat{z}}{r}\bar{\tau}$ and split (7.33) into four integrals as we did earlier in this section. In each of these integrals we must be careful to use the correct expansion for the Airy functions. This eventually gives the limit of (7.33) as $\hat{z}/r \to \infty$ as

$$g \sim -\frac{pk}{4\pi r}\left(e^{i\rho_0\hat{z}/r} + e^{-i\rho_0\hat{z}/r}\right). \tag{7.34}$$

It can easily be checked that this is the inner limit of the GO solution.

For the matching into the creeping ray field we again scale $\tau = \frac{\hat{z}}{r}\bar{\tau}$ in (7.33) and look at the limit as $\hat{z}/r \to -\infty$. We again split the integral into four parts corresponding to the four integrals in (7.27). The first and second integrals produce stationary phase contributions which cancel each other out. The third integral is entirely oscillatory and thus does not contribute to leading order. The fourth integral gives a stationary phase contribution which evaluates as zero. The integral is thus dominated by its pole contributions. We close the contour in the upper half plane and sum the residue

series. It can be checked that this matches with the creeping ray field. Again, the comments at the end of §6.8 regarding the dependence of the transition region field on s_2 are still valid here.

7.2 Electrically Polarised Solutions

We now consider the electric dipole with moment

$$\mathbf{p} \;=\; p\delta(s_1)\delta(\rho-\rho_0)\mathbf{e}_t, \tag{7.35}$$

where $\mathbf{e}_t$ is some vector tangent to the surface.

Inner-F-L Solution

Without loss of generality we take $\mathbf{e}_t$ to be in the direction $s_2 = 0$ at the origin. Section 2.3.3 indicates that we must include an image dipole

$$\mathbf{p} \;=\; -p\delta(s_1)\delta(\rho+\rho_0)\mathbf{e}_t, \tag{7.36}$$

to satisfy the perfectly conducting boundary conditions. The inner-F-L solution due to the original source is

$$\begin{array}{lllllllll} H_r &=& 0, & H_\phi &=& -\dfrac{pk^{5/3}\sin\theta}{4\pi R}e^{ik^{1/3}R}, & H_\theta &=& 0, \\ E_r &=& 0, & E_\phi &=& 0, & E_\theta &=& -\dfrac{pk^{5/3}\sin\theta}{4\pi R}e^{ik^{1/3}R}, \end{array} \tag{7.37}$$

where r,ϕ,θ are now spherical polar coordinates at the source with $\theta = 0$ in the direction of $\mathbf{e}_t$ and again $R = k^{2/3}r$. The field due to the image dipole is identical to (7.37) with p replaced by $-p$ and with the spherical polars defined with respect to $\mathbf{e}_t$ at the image source. By symmetry we will just consider the surface fields for $0 < s_2 < \pi$. The outer limit of the inner-F-L solution written in F-L coordinates is

$$\begin{array}{lllllll} H_\phi &\sim& H_3 &\sim& -\dfrac{pk^{4/3}\sin s_2}{4\pi\hat{s}_1}e^{ik^{2/3}\hat{s}_1}\left(e^{i(\rho-\rho_0)^2/2\hat{s}_1}-e^{i(\rho+\rho_0)^2/2\hat{s}_1}\right), \\ E_\theta &=& E_2 &\sim& -\dfrac{pk^{4/3}\sin s_2}{4\pi\hat{s}_1}e^{ik^{2/3}\hat{s}_1}\left(e^{i(\rho-\rho_0)^2/2\hat{s}_1}-e^{i(\rho+\rho_0)^2/2\hat{s}_1}\right). \end{array} \tag{7.38}$$

It follows immediately that the function F of (7.15) is

$$F(\epsilon,\rho) \;=\; -\frac{ipk^{2/3}}{2\pi\sqrt{\epsilon}}\sin s_2\left(e^{i(\rho-\rho_0)^2/2\epsilon}-e^{i(\rho+\rho_0)^2/2\epsilon}\right). \tag{7.39}$$

Fock-Leontovič Region Solution

The solution in the F-L region is obtained exactly as before, this time with A_1 given by

$$A_1(\eta) = \mathrm{Ai}\left(-\sqrt[3]{2}\eta\right) - \frac{\mathrm{Ai}\left(\sqrt[3]{2}\tau\right)}{\mathrm{Ai}\left(\sqrt[3]{2}e^{2\pi i/3}\tau\right)}\mathrm{Ai}\left(-\sqrt[3]{2}e^{2\pi i/3}\eta\right). \tag{7.40}$$

Reciprocity will be satisfied by the solution.

Geometrical Optics Field

We try an ansatz

$$E_2^0 = \Upsilon_+\frac{\sin\theta_+}{r_+}e^{ikr_+} + \Upsilon_-\frac{\sin\theta_-}{r_-}\frac{e^{ikr_-}}{r_-}, \tag{7.41}$$

$$\sim \Upsilon_+\frac{\sin\theta}{r}e^{ikr-ik^{1/3}\rho_0\sin\theta} + \Upsilon_-\frac{\sin\theta}{r}e^{ikr+ik^{1/3}\rho_0\sin\theta}. \tag{7.42}$$

Matching with the inner-F-L solution yields

$$\Upsilon_+ = -\Upsilon_- = \frac{pk}{4\pi}. \tag{7.43}$$

Again, we must verify the matching between the F-L and GO solutions. The outer limit of the F-L region is calculated in the same way as in §7.1. The differences between the two F-L solutions are the $e^{-2\pi i/3}$ factor and the derivatives of the Airy functions in the second term of A_1. Consideration of the large argument behaviours of Ai and Ai$'$ makes it clear that the analysis of §7.1 still requires the examinination of four separate integrals and that the final outcome is as required.

Airy Layer Solution

The analysis carries through as before, eventually yielding

$$\beta_m(s_2) = \frac{\sqrt{\pi}e^{-\pi i/4}pk^{7/6}}{2^{1/6}}\frac{\mathrm{Ai}\left(a_m e^{-2\pi i/3}\right)}{\mathrm{Ai}'(a_m)}G_0(s_2)^{1/4}|L_0(s_2)|^{1/6}$$
$$\times\mathrm{Ai}\left(-\sqrt[3]{2}e^{2\pi i/3}|L_0|^{1/3}\rho_0 + a_m\right)\sin s_2. \tag{7.44}$$

Again, reciprocity is satisfied.

Transition Region

The usual arguments mean that we have a solution

$$E_2 \;=\; e^{ikx+ik^{1/3}\hat{z}^2/2r}\frac{1}{r}g\left(\frac{\hat{z}}{r}\right). \tag{7.45}$$

Again we take g to be the F-L region solution written in terms of the transition coordinates, namely

$$\begin{aligned} g \;&=\; -\frac{\zeta e^{\pi i/12}\sin s_2}{2^{5/6}\sqrt{\pi}|L_0|^{1/3}k^{1/6}}\int_{-\infty}^{\infty} e^{-\frac{\hat{z}}{r}|L_0|^{-1/3}\tau-\frac{i}{6}\frac{\hat{z}^3}{r^3}|L_0|^{-1}} \\ &\times\left\{\mathrm{Ai}\left(\sqrt[3]{2}\left(\tau-\rho_0|L_0|^{1/3}\right)\right)-\frac{\mathrm{Ai}\left(\sqrt[3]{2}\tau\right)}{\mathrm{Ai}\left(\sqrt[3]{2}e^{2\pi i/3}\tau\right)}\mathrm{Ai}\left(\sqrt[3]{2}e^{2\pi i/3}\left(\tau-\rho_0|L_0|^{1/3}\right)\right)\right\}\mathrm{d}\tau, \end{aligned} \tag{7.46}$$

where ζ is given by (7.23). Following the matching methodolgies of §7.1 it should be apparent without going into further detail that we obtain successful matches with the GO and creeping ray fields.

The dependence of the electrically polarised solutions on the parameter s_2 is more interesting than for the magnetically polarised fields. In addition to the dependence on the curvatures there is an extra $\sin s_2$ factor. This means that there are two null directions (parallel to the direction of the source) in which no surface field propagates. This could be an important consideration in choosing an antenna site.

7.3 Limiting Cases

We hope that our solutions for a source at an $\mathcal{O}(k^{-2/3})$ distance from the boundary are consisent with our other results, namely that as $\rho_0 \to 0, \infty$ we would like to retrieve the results for a source *on* the surface and at an $\mathcal{O}(1)$ distance from the surface respectively.

Case: $\rho_0 \to 0$—Source on the Surface

We consider the magnetically polarised solutions first.

As $\rho_0 \to 0$ the inner-F-L region solution will tend towards

$$H_\phi \;=\; E_\theta \;=\; -\frac{pk^{5/3}}{2\pi R}\sin\theta e^{ik^{1/3}R}, \tag{7.47}$$

where r, ϕ, θ are spherical polars based at the origin and $R = k^{2/3}r$. This is exactly the inner-F-L region solution for a point source on a surface. Similarly with the GO

fields.

The functions A_1, A_2 used to calcuate the F-L and transition region solutions for a source an $\mathcal{O}(k^{-2/3})$ distance from the boundary also tend towards the corresponding functions for the source on the boundary as $\rho_0 \to 0$.

For the Airy layer field due to a point source just off the surface, the constant given in (7.30) tends towards

$$\frac{\sqrt{\pi}e^{-11\pi i/12}pk^{7/6}}{2^{1/6}}\frac{\mathrm{Ai}'\left(a'_m e^{-2\pi i/3}\right)}{\mathrm{Ai}''(a'_m)}G_0(s_2)^{1/4}|L_0(s_2)|^{1/6}\mathrm{Ai}\left(a'_m\right) \qquad \text{as } \rho_0 \to 0.$$

Using the identity

$$\mathrm{Ai}\left(xe^{-2\pi i/3}\right)\mathrm{Ai}'(x) - e^{-2\pi i/3}\mathrm{Ai}'\left(xe^{-2\pi i/3}\right)\mathrm{Ai}\left(x\right) \;=\; \frac{e^{-5\pi i/6}}{2\pi}, \tag{7.48}$$

see [1], this is exactly equal to the corresponding constant for the source on the surface given by (6.54). A similar result holds for the creeping ray fields associated with the two problems.

Thus the asymptotic solutions in all the regions tend towards those for the point source on the surface as $\rho_0 \to 0$.

For the electric solutions things are easier as we just need to check that all the asymptotic solutions for a source an $\mathcal{O}(k^{-2/3})$ distance from the source tend towards zero as $\rho_0 \to 0$. This is straightforward for all the asymptotic regions.

Case: $\rho_0 \to \infty$—Source an $\mathcal{O}(1)$ distance from the Surface

In §5.5 we calculated the magnetically polarised F-L and Airy layer fields when the irradiation was due to a point source at an $\mathcal{O}(1)$ distance. As we let $\rho_0 \to \infty$ we hope that the solutions for a magnetically polarised source will tend towards those obtained in §5.5. That is, we must show that (7.22) and (7.3) tend towards (5.177) and (5.180) respectively as $\rho_0 \to \infty$.

We fix the value of s_2 and define the ϕ of §5.5 such that $s_2 = \phi$. For small s_{3_0} the s_1 of (7.22), (7.3) and the s_1^* of (5.177) and (5.180) satisfy

$$s_1 \;=\; s_1^* + \sigma, \tag{7.49}$$

as illustrated in Figure 7.2. We can derive

$$\sigma \;\sim\; r_0 - \frac{4}{3}\sqrt{\frac{|L_0|}{2}}s_{3_0}^{3/2}, \tag{7.50}$$

$$r_0 \;\sim\; \sqrt{\frac{2}{|L_0|}}s_{3_0}^{1/2} + \frac{1}{2}\sqrt{\frac{|L_0|}{2}}s_{3_0}^{3/2}. \tag{7.51}$$

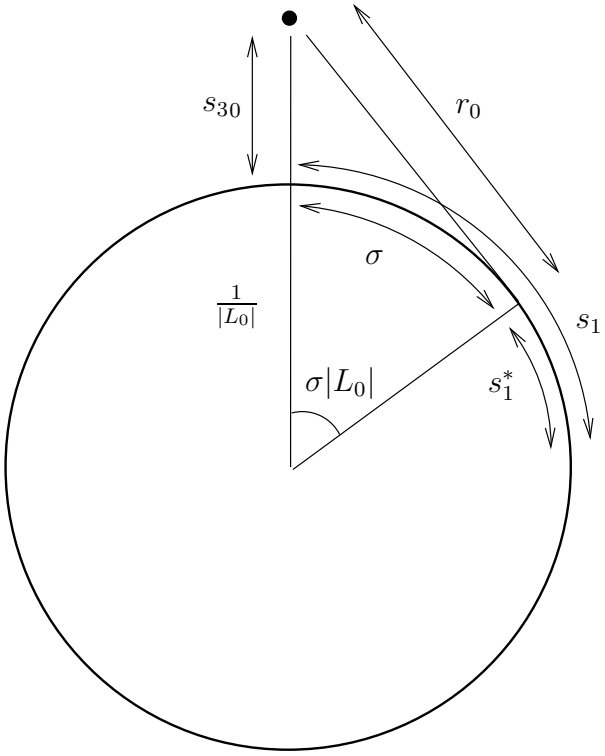


Figure 7.2:

To check that (7.3) tends towards (5.180) as $\rho_0 \to \infty$ we expand (7.3) for large ρ_0 and then rewrite in terms of s_1^*, ϕ, noting that

$$G_0(s_2) \;\sim\; \frac{G_0(\phi)}{r_0^2} \tag{7.52}$$

for small r_0. This gives us a successful match.

To check that (7.22) tends towards (5.177) as $\rho_0 \to \infty$ we expand (7.22) for $\rho < \rho_0$ for large ρ_0 and then rewrite in terms of s_1^*, ϕ. This tells us that

$$H_2 \;\to\; \frac{\sqrt[3]{2}pk}{4\pi r_0} e^{iks_1^* + ikr_0} \int_{-\infty}^{\infty} A_1(\eta) e^{i\tau|L_0|^{2/3}\hat{s}_1^*}\, \mathrm{d}\tau, \quad \rho_0 \to \infty. \tag{7.53}$$

There are two terms in A_1—see (6.46). The second of these can be seen to match perfectly with (5.177). The first term is associated with the incident field—see [35].

To show that the electrically polarised fields match as $\rho_0 \to \infty$ we carry out the same procedure. The electrically polarised versions of (5.177) and (5.180) are easy to calculate and there is a successful match.

Chapter 8

Arrays of Localised Sources

Arrays of excited apertures or current elements are often found on aircraft structures as part of the onboard antenna systems. They have the advantage over singly mounted antennas in that you can construct complicated, highly directive far field patterns. Much work has been done on the inverse problem of beam synthesis—*i.e.* given an array size and restrictions on the far field pattern, such as nulls at certain angles or sidelobes of a specified gain, we wish to find excitations of the array elements which will produce the desired field. A glance at the numerical results in any of the papers on this subject will reveal just how versatile arrays can be. We cite [26] and [34] as just two of many examples. Our aim will be to apply asymptotic techniques to the direct problem: given an array of a large number of elements, can we use asymptotic techniques to make time savings in the calculation of the far field?

We begin by comparing exact and asymptotic solutions for the simplest possible arrays. Good agreement here will then give us the confidence to apply our asymptotic methods to more general arrays.

8.1 Exact Solutions for Arrays of Point Sources

8.1.1 One-dimensional Arrays

We consider a linear array of $N+1$ elements on a flat, perfectly conducting surface in two-dimensional space as in Figure 8.1. The left hand edge of the array is taken to be the origin and the element spacing to be d/k where $d = \mathcal{O}(1)$. We will use cartesian coordinates with x directed along the array, z normal to the surface and $\partial/\partial y = 0$. The perfect conductor occupies $z < 0$. The sth array element is a dipole with moment $\mathbf{p} = p_s \mathbf{e}_z$ for some p_s. We can use §2.3.3 and the method of stationary

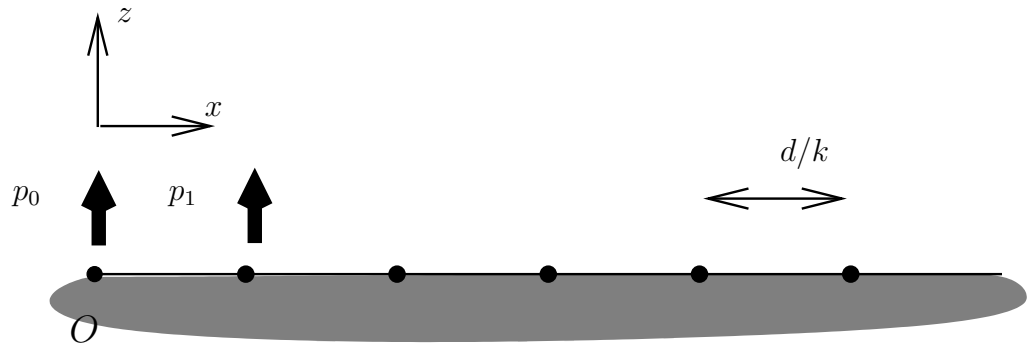


Figure 8.1: One-dimensional array of point sources on a perfectly conducting surface.

phase to calculate the Hertz vector for each array element, namely

$$\mathbf{\Pi}_s \sim -\frac{p_s}{\sqrt{2\pi k r_s}} e^{ikr_s + i\pi/4} \mathbf{e}_z, \tag{8.1}$$

$$r_s = \left((y - sd/k)^2 + z^2\right)^{1/2}. \tag{8.2}$$

For the simplest possible array we set $p_s = 1, \forall s$. Insisting that $N = o(k)$ lets us make the approximation

$$r_s \sim r - \frac{sd}{k}\cos\theta, \tag{8.3}$$

where r, θ are the usual polar coordinates based at the origin in the x, z plane. Summing over all the array elements yields the Hertz vector for the whole array

$$\mathbf{\Pi} \sim -\frac{1}{\sqrt{2\pi kr}} \frac{\sin\left(\frac{d}{2}(N+1)\cos\theta\right)}{\sin\left(\frac{d}{2}\cos\theta\right)} \exp\left(ikr - i\pi/4 - \frac{iNd}{2}\cos\theta\right)\mathbf{e}_z. \tag{8.4}$$

The diffraction pattern—Figure 8.2—has a maximum at $\theta = \pi/2$ with smaller amplitude side-lobes. We note that a diffraction pattern with the main lobe in the direction $\theta = \alpha$ can be obtained by setting $p_s = \exp(isd\cos\alpha)$. This ultimately yields an identical field pattern to (8.4) with $\cos\theta$ replaced everywhere by $\cos\theta - \cos\alpha$. The term *phased array* is often used to describe such an array of localised sources for which we are able to change the direction of the diffraction pattern by altering the phase of the element excitations.

8.1.2 Two-dimensional Arrays

We now consider an array of $N+1$ by $M+1$ elements on a perfect conductor occupying $z < 0$—Figure 8.3. The 'bottom left' element of the array is at the origin. The elements are separated in the x and y directions by distances u/k, v/k respectively,

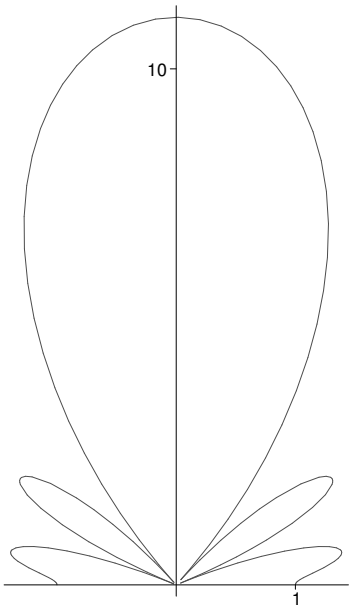


Figure 8.2: Diffraction pattern given by (8.4) with $d = \pi/2, N = 10$.

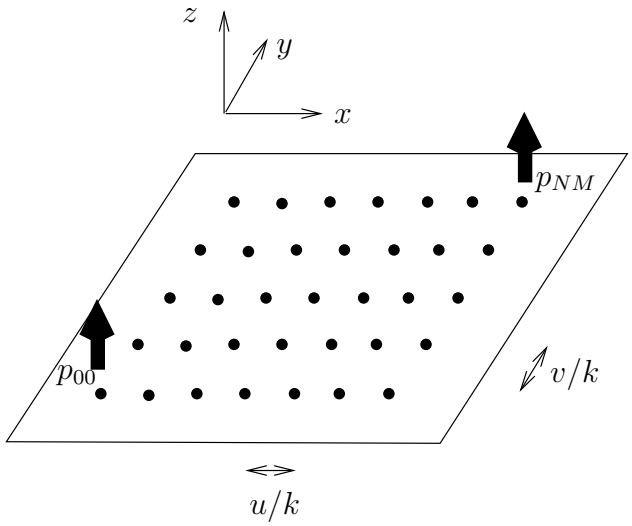


Figure 8.3: Two-dimensional array on a perfect conductor.

where $u, v = \mathcal{O}(1)$. Similarly to §8.1.1 the stth element is a dipole with moment $\mathbf{p}_{st} = p_{st}\mathbf{e}_z$ for some p_{st}. The Hertz vector for each array element is

$$\begin{aligned} \mathbf{\Pi}_{st} &= -\frac{p_{st}e^{ikr_{st}}}{2\pi k r_{st}}\mathbf{e}_z, & (8.5)\\ r_{st} &= \left((x - su/k)^2 + (y - tv/k)^2 + z^2\right)^{1/2}. & (8.6) \end{aligned}$$

To examine the simplest possible array, we set $p_{st} = 1$, $\forall s, t$. We assume that $N, M = o(k)$ which lets us make a similar approximation to (8.3). Summing (8.5) over all the array elements yields the Hertz vector for the entire array as

$$\begin{aligned} \mathbf{\Pi} &= \frac{1}{2\pi kr}\frac{\sin\left(\frac{u}{2}(N+1)\frac{x}{r}\right)\sin\left(\frac{v}{2}(M+1)\frac{y}{r}\right)}{\sin\left(\frac{u}{2}\frac{x}{r}\right)\sin\left(\frac{v}{2}\frac{y}{r}\right)} \\ &\quad \times\exp\left(ikr - \frac{iNu}{2}\frac{x}{r} - \frac{iMv}{2}\frac{y}{r}\right)\mathbf{e}_z, \qquad (8.7) \end{aligned}$$

where r is now the three-dimensional radial distance from the origin.

We would like to consider the possibility that our array is placed on a curved structure. We recall that the inner-F-L region first introduced in §6.4 is flat to lowest order. For the configuration described above to be the inner-F-L region of a larger problem we require $N, M \sim \mathcal{O}(k^{1/3})$. This guarantees that the lengthscale of the array is $\mathcal{O}(k^{-2/3})$ which is the scaling of the inner-F-L region. On aircraft, the arrays are generally sited on structures with large radii of curvature. Thus the case $N, M = \mathcal{O}(k^{1/3})$ will cover the majority of situations requiring modelling. In what follows we will investigate the asymptotics specifically for this case.

8.2 Asymptotic Solutions for Arrays of Point Sources

8.2.1 One-dimensional Arrays

In §8.1.1 we are required to evaluate

$$\begin{aligned} \mathbf{\Pi} &= \sum_{s=0}^{N} f(s)\mathbf{e}_z, & (8.8)\\ f(s) &= -\frac{p_s}{\sqrt{2\pi k}}\frac{\exp\left(ik\left((x - sd/k)^2 + y^2\right)^{1/2} + i\pi/4\right)}{\left((x - sd/k)^2 + y^2\right)^{1/4}}. & (8.9) \end{aligned}$$

Taking $N = \mathcal{O}(k^{1/3})$, this is suitable for employment of the Euler-Maclaurin summation formula. This states, as $N \to \infty$,

$$\mathbf{\Pi} \sim \frac{1}{2}\left(f(0) + f(N)\right) + \int_0^N f(t)\,\mathrm{d}t \tag{8.10}$$
$$+ \lim_{m\to\infty}\left\{\sum_{j=1}^{m}(-1)^j \frac{B_{j+1}}{(j+1)!}\left(f^{(j)}(0) – f^{(j)}(N)\right) + \frac{(-1)^m}{(m+1)!}\int_0^N B_{m+1}\left(t-[t]\right) f^{(m+1)}(t)\mathrm{d}t\right\}\mathbf{e}_z,$$

provided f is sufficiently smooth. The B_j and $B_j(t)$ are the Bernoulli numbers and polynomials defined in [3]. We investigate (8.10) with a view to comparing it to the results in §8.1.1.

Evaluating the first integral in (8.10) for $N = \mathcal{O}(k^{1/3})$, we must make the substitution $t = kT$ to eliminate the movable saddle point. We are then integrating a function of the form $g(T)\exp(kh(T))$ over a region of width $\mathcal{O}(k^{-2/3})$. This yields just endpoint contributions. We combine these endpoint contributions with the first term of (8.10) and the summation term involving the derivatives of f. This provides us with a solution consisting of a contribution from the two end elements of the array,

$$\mathbf{\Pi}_0 \sim p_0 \frac{e^{ikr+i\pi/4}}{\sqrt{2\pi kr}}\left(\frac{ie^{-id\cos\theta/2}}{2\sin(d\cos\theta/2)} - 1\right)\mathbf{e}_z, \tag{8.11}$$

$$\mathbf{\Pi}_N \sim -p_N \frac{e^{ikr_N+i\pi/4}}{\sqrt{2\pi kr}}\frac{ie^{-id\cos\theta/2}}{\sin(d\cos\theta/2)}\mathbf{e}_z. \tag{8.12}$$

To obtain these simplified expressions we have used the identity

$$\sum_{m=0}^{\infty} B_m \frac{t^m}{m!} = \frac{t}{e^t - 1}, \tag{8.13}$$

and $B_0 = 1, B_1 = -1/2$—see [3]. The second integral in (8.10) is ignored. We add together (8.11) and (8.12) to obtain the leading order Euler-Maclaurin approximation for the field. In Figure 8.4 we compare the modulus of the solution obtained by summing terms of the form (8.1) - (8.2) with that of the solution given by (8.11) - (8.12). We see that for industrially relevant values of N and d there is good agreement. Figure 8.4 a) and b) are for $N = 10, d = \pi/2$ and c),d) are for $N = 20, d = \pi/2$. Figures a) and c) are for the case $p_s = 1$, $\forall s$, and b) and d) are for the case where

$$p_s = \begin{cases} 1, & s = 0, N, \\ 1 + \frac{1}{N}c(s), & \text{otherwise} \end{cases} \tag{8.14}$$

where $c(s)$ is normally distributed with mean 0 and variance 1. For larger values of N the approximation improves apart from an increasingly small range of θ near 0 and

π where it deteriorates slightly. However, we are more interested in the actual $\mathbf{E}, \mathbf{H}$ fields than in $\mathbf{\Pi}$. It will be sufficient to consider just the magnetic field. Using §2.3.3 it transpires that the magnetic field is

$$\mathbf{H} \sim \left(\frac{1}{r} \frac{\partial}{\partial \theta} (\Pi_z \sin\theta) - \frac{\partial}{\partial r} (\Pi_z \cos\theta) \right) \mathbf{e}_y. \tag{8.15}$$

To leading order this is just

$$\mathbf{H} \sim -ik\Pi_z \cos\theta \mathbf{e}_y. \tag{8.16}$$

The plots in Figure 8.4 show good agreement between the exact solution and Euler-Maclaurin approximations for Π_z. Thus there will be an equally good agreement between the actual magnetic field and its Euler-Maclaurin approximation.

We also note that in the limit as $d \to 0$, the sum of (8.11) and (8.12) for $p_s = 1$, $\forall s$ becomes

$$\mathbf{\Pi} \sim -\frac{2e^{ikr - iNd\cos\theta/2 + i\pi/4}}{\sqrt{2\pi kr}} \frac{\sin(Nd\cos\theta/2)}{d\cos\theta} \mathbf{e}_z, \tag{8.17}$$

which gives good agreement with (8.4) close to the main beam $\theta = \pi/2$.

8.2.2 Two-dimensional Arrays

Although more complicated, we can apply the Euler-Maclaurin summation formula twice to obtain an approximation for the field due to a two-dimensional array. For the case $N, M = \mathcal{O}(k^{1/3})$, examination of the first integral in (8.10) reveals that integration with respect to both N and M yields no stationary phase contributions. Two applications of (8.10) thus produce four 'corner' contributions, namely

$$\mathbf{\Pi}_{00} \sim -\frac{p_{00}e^{ikr}}{2\pi kr} \quad A(\phi,\theta;u) \quad B(\phi,\theta;v)\mathbf{e}_z, \tag{8.18}$$

$$\mathbf{\Pi}_{0M} \sim -\frac{p_{0M}e^{ikr_{0M}}}{2\pi kr} \quad A(\phi,\theta;u) \quad (B(\phi,\theta;v) - 1)\,\mathbf{e}_z, \tag{8.19}$$

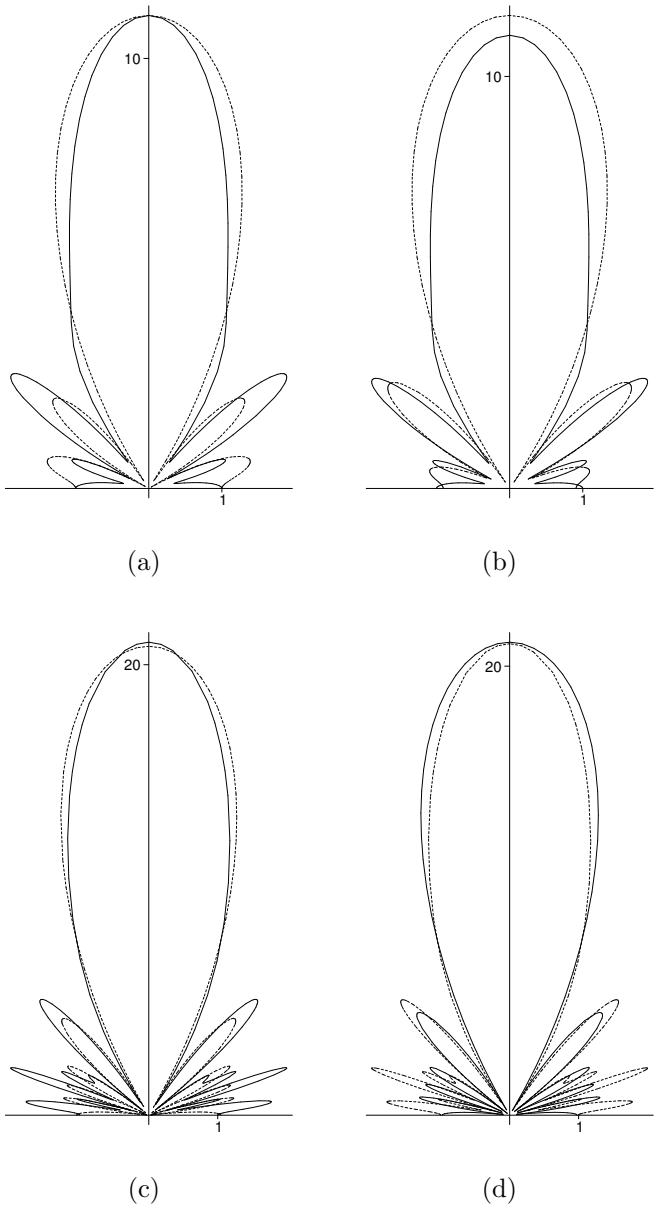
$$\mathbf{\Pi}_{N0} \sim -\frac{p_{N0}e^{ikr_{N0}}}{2\pi kr} \quad (A(\phi,\theta;u) - 1) \quad B(\phi,\theta;v)\mathbf{e}_z, \tag{8.20}$$

$$\mathbf{\Pi}_{NM} \sim -\frac{p_{NM}e^{ikr_{NM}}}{2\pi kr} (A(\phi,\theta;u) - 1)\,(B(\phi,\theta;v) - 1)\,\mathbf{e}_z, \tag{8.21}$$

where

$$A(\phi,\theta;s) = \frac{ie^{-is\cos\phi\sin\theta}}{2\sin(s\cos\phi\sin\theta/2)}, \tag{8.22}$$

$$B(\phi,\theta;s) = \frac{ie^{-is\cos\theta}}{2\sin(s\cos\theta/2)}, \tag{8.23}$$



(a) (b)

(c) (d)

Figure 8.4: Conventional summation (solid) versus Euler-Maclarin (dashed) approximation for $d = \pi/2$. a) $N = 10$, uniform element excitation, b) $N = 10$, random element excitation, c) $N = 20$, uniform element exciation, d) $N = 20$, random element excitation.

where r, ϕ, θ are the usual spherical polar angles centred at the origin. The factors multiplying the Green's function for each corner element can be seen to be the three-dimensional versions of the equivalent factors in (8.11) and (8.12). Setting $p_{st} = 1$, $\forall s, t$, and letting $u, v \to 0$, gives us the total field as a sum of (8.18) - (8.21) as

$$\begin{aligned} \mathbf{\Pi} \;\sim\; & \frac{2}{k\pi uvr} \frac{\sin\left(Nu\cos\psi\sin\theta/2\right)\sin\left(Mv\cos\theta/2\right)}{\cos\theta\sin\theta\cos\psi} \\ & \times\exp\left(ikr - \frac{iNu}{2}\cos\psi\sin\theta - \frac{iMv}{2}\cos\theta\right)\mathbf{e}_z. \end{aligned} \tag{8.24}$$

In the limit $u, v \to 0$, the asymptotic solution (8.24) provides a good approximation almost everywhere to the corresponding limit of the exact solution (8.7).

Although the use of the Euler-Maclarin formula requires considerable labour, the outcome is an asymptotic description of the field due to fairly general arrays. Our only stipulation is that the excitation of the elements varies by an $\mathcal{O}(1)$ amount over the array. In addition, the asymptotic contributions to the field give us insight into which array elements have the greatest impact on the field pattern.

8.3 Arrays of Continuously Distributed Sources

The arrays found on military aircraft are not particularly well modelled by point source arrays. Dimensionally, both the array elements and the element spacing are typically $\mathcal{O}(\lambda)$ as illustrated in Figure 8.5. Thus a non-dimensional element spacing of $\mathcal{O}(k^{-1})$ is fine, but the representation of the array elements as point sources is not yet entirely accurate.

We will start by considering an arbitrary excitation of a single line element with end-points at $(0,0,0)$ and $(0,w/k,0)$ on a perfectly conducting surface where $w = \mathcal{O}(1)$. The source is taken to have a dipole moment $\mathbf{p} = p(y)\mathbf{e}_z$ where

$$p(y) \;=\; \sum_{n=0}^{\infty} a_n \sin\left(\frac{2n\pi ky}{w}\right) + b_n \cos\left(\frac{2n\pi ky}{w}\right), \tag{8.25}$$

for some a_n, b_n. We remark that, although we assume that the a_n, b_n are known *a priori,* the determination of these constants for real antennas sited on aircraft poses significant difficulties. The Hertz vector for this element is

$$\mathbf{\Pi} \;=\; -\int_0^{w/k} p(y')\frac{e^{ikr(y')}}{2\pi kr(y')}\,\mathrm{d}y', \tag{8.26}$$

$$r(y') \;=\; \left(x^2 + (y-y')^2 + z^2\right)^{1/2}\mathbf{e}_z. \tag{8.27}$$

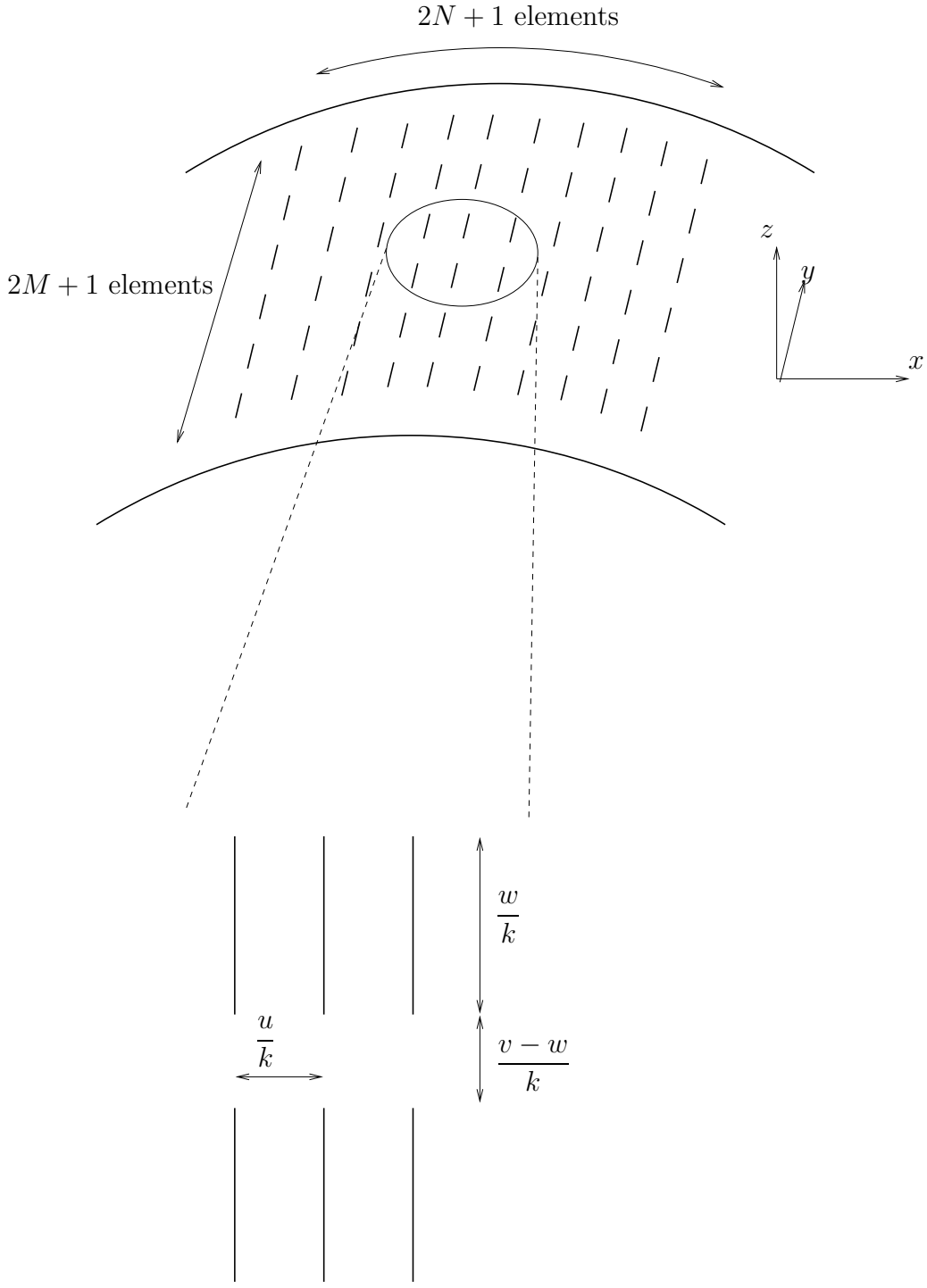


Figure 8.5: More general two-dimensional array of line sources.

We can evaluate the integral asymptotically as $k \to \infty$. This yields endpoint contributions

$$\begin{aligned} \mathbf{\Pi} &\sim -\sum_{n=0}^{\infty} \frac{ie^{ikr}}{2\pi ky} b_n \left(e^{iyw/r} - 1\right), \\ &= \frac{e^{ikr}}{2\pi kr} f(\theta, \phi) \sum_{n=0}^{\infty} b_n, \end{aligned} \tag{8.28}$$

where

$$f(\theta, \phi) - \frac{\sin\left(\omega \sin\phi \sin\theta\right)}{\sin\phi \sin\theta} e^{i\omega \sin\phi \sin\theta/2} \tag{8.29}$$

where r, ϕ and θ are the usual spherical polar coordinates centred at the origin. This is just the field due to a dipole, multiplied by a directivity factor dependent on the b_n's. This fact can be exploited to write down the field due to an array of arbitrarily excited line source elements (provided that the amplitudes b_n change slowly from element to element) in the following way:

- Consider an array of line source elements depending just on the first excitation mode $(b_0)_{st}$. This is asymptotically equivalent to an array of point sources of strength $f(\theta, \psi)(b_0)_{st}$. We can write down an asymptotic representation of the field due to such an array of point sources using (8.18) - (8.21).

- Now consider an array of line source elements excited only by the first harmonic $(b_1)_{st}$. This can again be asymptotically treated as an array of point sources of strength $f(\theta, \psi)(b_1)_{st}$ and we can again write down an asymptotic representation of the field due to this array of point sources.

- Repeat this process for the higher modes of excitation.

- Add the resultant fields due to each of these 'point source' arrays.

It is apparent from what has come before that for $N, M = \mathcal{O}(k^{1/3})$, and for smoothly varying b_n, the geometrical optics field will depend entirely on the four corner elements of the line source array.

8.4 Comparison of Arrays with Unperforated Continuously Distributed Sources

We will now compare the fields obtained in §8.2.1 and §8.2.2 with those radiated by unperforated continuously distributed sources of the same size. In what follows the

perfect conductor will occupy $z < 0$ and the source is taken to have a dipole moment $\mathbf{p} = p(x, y)\mathbf{e}_z$. For comparison with the asymptotic results we have already obtained we set $p = 1$.

8.4.1 One-dimensional Arrays

To obtain the Hertz vector we are required to solve

$$\nabla^2\mathbf{\Pi} + k^2\mathbf{\Pi} \;=\; \chi_{[0,L]}(x)\mathbf{e}_z, \tag{8.30}$$

along with a radiation condition at infinity. The characteristic function χ is defined by

$$\chi_{[a,b]}(z) = \begin{cases} 1, & a \le z \le b, \\ 0, & \text{o.w.}, \end{cases}$$

and $L = Nd$. We integrate the Greens function, $-\frac{i}{2}H_0^{(1)}(kr)$, over the source. This yields just end point contributions which can be evaluated and summed to give

$$\mathbf{\Pi} \;\sim\; -\frac{e^{ikr - iNd/2\cos\theta + i\pi/4}}{k\cos\theta}\sqrt{\frac{2}{\pi kr}}\sin(Nd/2\cos\theta)\mathbf{e}_z. \tag{8.31}$$

This agrees exactly with (8.17) if we scale the unperforated distributed source strength by k/d. This is physically intuitive as being necessary to ensure that the same amount of energy is being used to excite the two configurations.

8.4.2 Two-dimensional Arrays

We consider the two-dimensional equivalent of (8.30), namely

$$\nabla^2\mathbf{\Pi} + k^2\mathbf{\Pi} \;=\; \chi_{[0,a]}(x)\chi_{[0,b]}(y)\mathbf{e}_z, \tag{8.32}$$

along with a radiation condition at infinity. For comparison with the results in §8.2.2 we take $a = Nu, b = Mv$. We use the three-dimensional Green's function to write the solution as

$$\mathbf{\Pi} \;=\; -\int_0^{Mv}\int_0^{Nu}\frac{1}{2k\pi}\frac{e^{ik\left((x-s)^2+(y-t)^2+z^2\right)^{1/2}}}{\left((x-s)^2+(y-t)^2+z^2\right)^{1/2}}\,\mathrm{d}s\,\mathrm{d}t\mathbf{e}_z. \tag{8.33}$$

We can calculate the four end point contributions from (8.33) and sum them to give

$$\mathbf{\Pi} \;=\; \frac{2re^{ikr}}{k^3\pi}\frac{\sin\left(Nukx/2r\right)\sin\left(Mvkz/2r\right)}{xz}e^{-ikNux - ikMvz}\mathbf{e}_z. \tag{8.34}$$

Upon writing x, z in terms of the spherical polar coordinates r, ϕ, θ, (8.34) is seen to be uv/k^2 times the asymptotic solution (8.24) in the limit as $u, v \to 0$. As in the one-dimensional case, the scaling factor guarantees that the same amount of energy is being put into both configurations.

8.5 Larger Arrays

We briefly consider arrays where $N, M = \mathcal{O}(k)$. These have $\mathcal{O}(1)$ non-dimensional lengthscales.

We first note that the results of §8.1.1 - 8.1.2 are not valid as we may no longer use (8.3) to approximate r_s nor a similar formula for r_{st}.

For one-dimensional arrays we may still use the Euler-Maclaurin summation formula (8.10). In addition to the end-point contributions (8.11) - (8.12), the first integral in (8.10) yields a stationary phase contribution. If $p_s = 1, \forall s$, this contribution is $-id^{-1}\exp(ikz)$ for $0 < x < Nd$ and zero otherwise. In light of §4.7 the array appears to be behaving in the same way as a continuously distributed source with an $\mathcal{O}(1)$ lengthscale—*i.e.* there is a leading order contribution from the interior of the source and higher order contributions from each end. This can easily be confirmed by working through §8.4.1 with $N = \mathcal{O}(k)$. The integral over the source now yields a stationary phase contribution $-ike^{ikz}$ for $0 < x < Nd$ and zero otherwise. Scaling the source strength by k/d so that the same amount of energy is used to excite the two configurations, the two problems yield identical fields.

For two-dimensional arrays with $N, M = \mathcal{O}(k)$ we can apply the Euler-Maclaurin formula twice. Careful examination reveals that this will yield nine contributions to the field. It can be checked that there is a one-to-one correspondence between these nine terms and the nine terms that arise upon asymptotically evaluating (8.33). The leading order term corresponds to the stationary phase/stationary phase contribution from (8.33). The four second order terms correspond to the stationary phase/endpoint contributions to (8.33) which are the edge diffracted fields from the continuously distributed source. The four higher order terms are equivalent to the endpoint/endpoint terms of (8.33) which are the corner diffracted fields of the source.

We have thus seen that our asymptotic techniques provide excellent agreement for simple one and two-dimensional arrays of point sources. More complicated arrays can be dealt with by simply extending the theory for point source arrays. Our asymptotic method is supported by the fact that our solutions tend towards the results obtained for unperforated continuously distributed sources if we let the element separation tend towards zero.

Chapter 9

Conformal Antennas on Curved Surfaces

A large number of the antennas sited on aircraft cannot be satisfactorily dealt with using the basic models of either a point source or an array of point sources on a surface. In this chapter we will extend our theory to cater for fairly arbitrary line sources lying in the surface. We will begin by describing how to deal with closed line sources. The asymptotic structure for point sources on a surface developed in §6 indicates that we may expect different asymptotic behaviour depending on the length scale of the line source. For example, it is likely that a source with a lengthscale of $\mathcal{O}(k^{-2/3})$ that fits entirely into a flat inner-F-L region will behave in a very different way to a source whose lengthscale is the same as the radii of curvature of the surface on which it is sited. We will investigate each of the four lengthscales that give rise to qualitatively different radiated fields. For open antennas, additional higher order diffraction effects must be considered. These are similar to those encountered when dealing with finite line sources in free space—see §4. We will introduce *surface fresnel* regions to provide a smooth surface field. These are the analogue for surface fields of the shadow boundaries of §4. We will then extend our work on shadow boundary interactions—§4.7—to cover sources on a surface. Here, the focussing effects will arise from the convergence of the geodesics, rather than as a result of some cunning source specification as in §4.7. We will conclude with a discussion of a spiral antenna on a perfectly conducting surface, which is a problem of particular interest to BAe Systems.

The general configuration is a line source Γ lying on a smooth, convex, perfectly conducting surface. The source is parametrised by $0 < s_2 < t$ for some t and has coordinates $\mathbf{x}_0(s_2)$. The source has dipole moment $\mathbf{p} = p(\mathbf{x}_0)\mathbf{e}_3(\mathbf{x}_0)$. The discussions of §2.3.3 indicate that this is the only orientation of the dipoles that can radiate in

the presence of a perfect conductor. We also assume that p is slowly varying with respect to the wave-length of the radiation. For the moment we will also assume that the source is excited in phase—*i.e.* $\arctan\left(\mathrm{Im}\left(p(\mathbf{x}_0)\right)/\mathrm{Re}\left(p(\mathbf{x}_0)\right)\right)$ is constant.

9.1 Closed Line Sources

We impose the restriction that the line source is closed. There are four length scales that we must discuss separately so as to provide an asymptotic description of the fields radiated by a general closed line source. These are: $\mathcal{O}(1)$, corresponding to sources of the same size as the radii of curvature of the surface; $\mathcal{O}(k^{-1/3})$, where the lengthscale of the source is the same as that of the F-L region; $\mathcal{O}(k^{-2/3})$, where the lengthscale is equal to that of the inner-F-L region and $\leq \mathcal{O}(k^{-1})$ where the source is smaller than a wavelength of the radiation. These canonical scalings for line sources on a surface are illustrated in Figure 9.1. In §6 we demonstrated that a source on a perfectly conducting boundary could not excite electrically polarised fields. We will therefore consider just the magnetically polarised solutions.

9.1.1 Sources of $\mathcal{O}(1)$ Size

We expand upon the idea outlined by Saward [33]. The solution technique is exactly the same as for a point source on a surface, §6. We now take s_1 to be the distance along geodesics normal to Γ and s_3 to be the normal distance to the surface. Thus s_1, s_2, s_3 form a geodesic normal coordinate system. The Airy layer solution can be derived (as in §6) to be

$$\mathbf{E} \sim -\phi_M(s_1, s_2, \rho)\mathbf{e}_3, \tag{9.1}$$

$$\mathbf{H} \sim \pm\phi_M(s_1, s_2, \rho)\mathbf{e}_2, \tag{9.2}$$

$$\begin{aligned}\phi_M = &\sum_{m=0}^{\infty} \frac{\beta_m(s_2)|L|^{1/6}}{G^{1/4}} \mathrm{Ai}\left(-\sqrt[3]{2}e^{2\pi i/3}\rho|L|^{1/3} + a'_m\right) \\ &\times \exp\left(iks_1 + ik^{1/3}\frac{a'_m e^{-2\pi i/3}}{\sqrt[3]{2}}\int_0^{s_1} |L(t, s_2)|^{2/3}\,\mathrm{d}t\right),\end{aligned} \tag{9.3}$$

where $\rho = k^{2/3}s_3$ and we take the upper/lower sign in (9.2) if s_1, s_2, s_3 form a right/left-handed set, and the $\beta_m(s_2)$ are to be determined. We also take the familiar ansatz for the F-L solution, namely

$$\mathbf{F} = e^{iks_1}\sum_{n=0}^{\infty} \frac{\mathbf{F}^n(\hat{s}_1, s_2, \rho)}{k^{n/3}}, \tag{9.4}$$

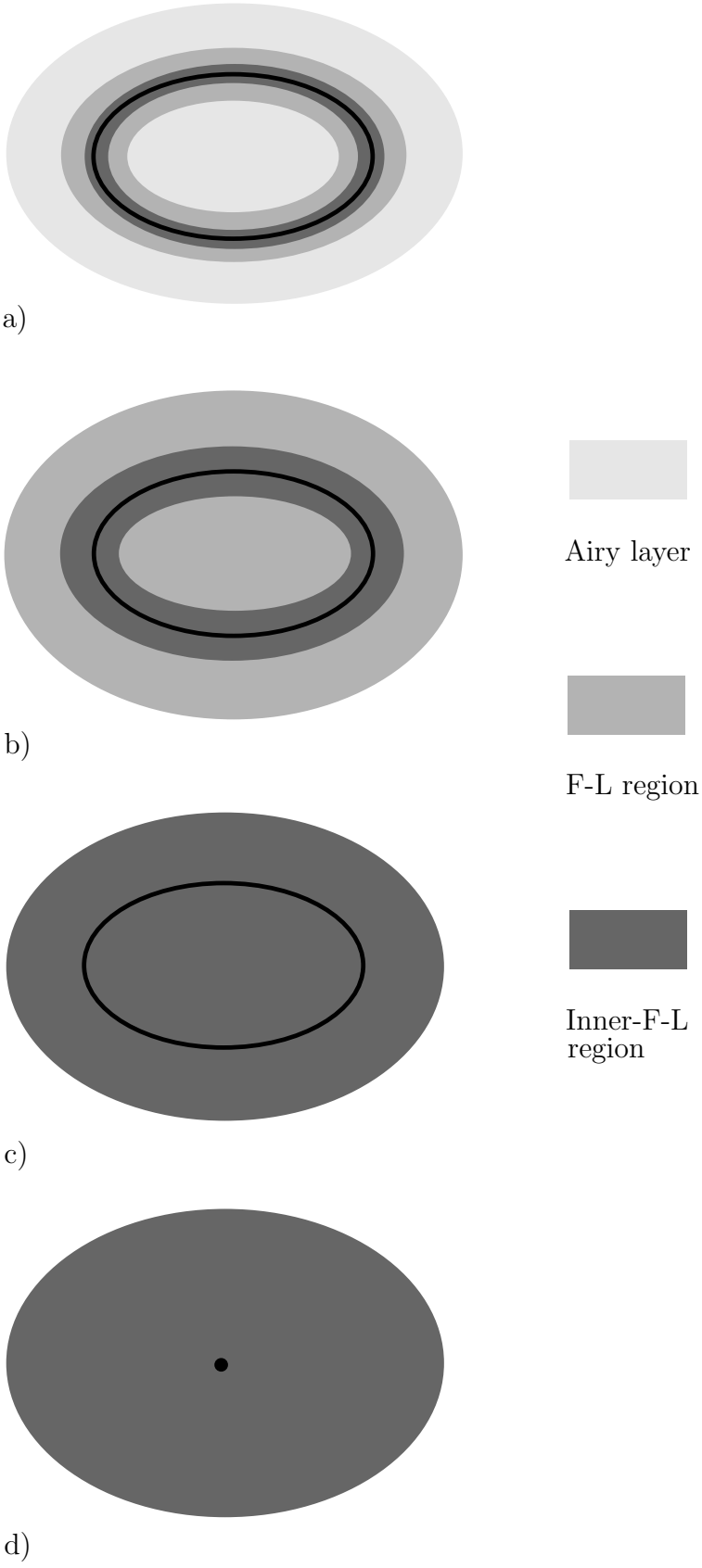


Figure 9.1: Canonical scalings for line soures on a convex surface. Source of size a) $\mathcal{O}(1)$, b) $\mathcal{O}(k^{-1/3})$, c) $\mathcal{O}(k^{-2/3})$, d) $\mathcal{O}(k^{-1})$.

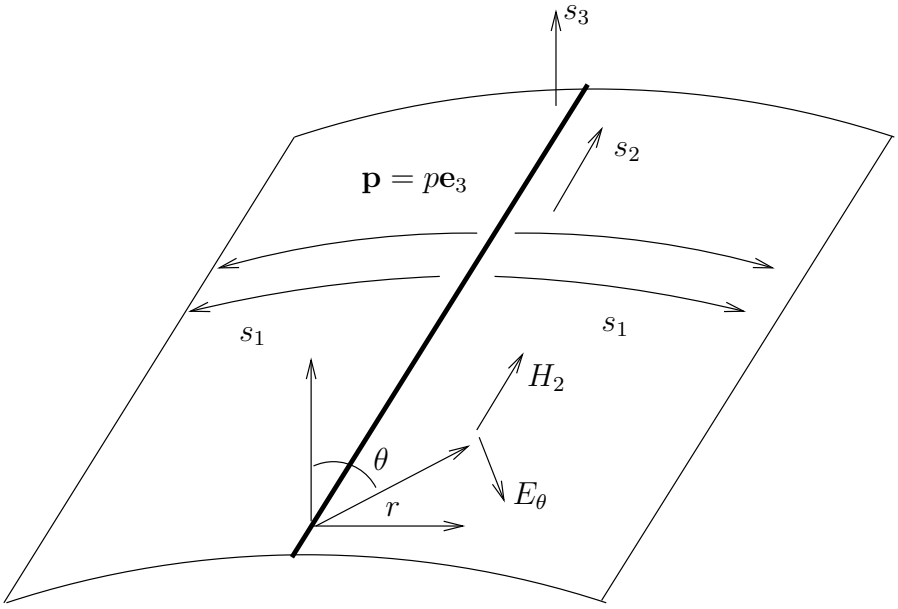


Figure 9.2: Inner-F-L region problem is two dimensional. To the right of the source, s_1, s_2, s_3 form a right-handed set and to the left they form a left-handed set.

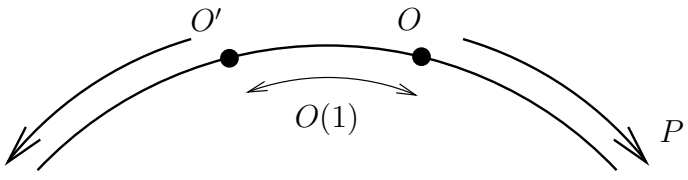


Figure 9.3: Surface field at P dominated by contribution from O.

where $\hat{s}_1 = k^{1/3} s_1$. We recall that in §6.3 we solved the F-L problem in the absence of sources. We first took the Laplace transform of the problem which introduced $F(\epsilon, \rho) = 2iH_2^0(\epsilon, \rho)$. We then had to solve an inner-F-L region around the source to obtain F. The function F then acted as a matching condition between the F-L and inner-F-L regions. We do the same here, to obtain

$$\begin{aligned} E_1^0 \equiv E_2^0 \equiv H_1^0 \equiv H_3^0 &\equiv 0, && (9.5)\\ E_3^0 &= \mp H_2^0, && (9.6)\\ \frac{\partial^2 \hat{H}_2^0}{\partial \rho^2} + 2i\lambda \hat{H}_2^0 + 2|L(0, s_2)|\rho \hat{H}_2^0 &= F(\epsilon, \rho), \quad \rho > 0, && (9.7)\\ \frac{\partial \hat{H}_2^0}{\partial \rho} &= 0, \quad \rho = 0, && (9.8) \end{aligned}$$

where the upper/lower sign in (9.6) is taken if s_1, s_2, s_3 form a right/left-handed set. The Laplace transform of H_2^0 with respect to $\hat{s}_1$ is denoted by $\hat{H}_2^0$ and the Laplace variable is λ. To lowest order the inner-F-L region problem is two-dimensional—a line source of dipoles along the axis of a cylinder. Using the results of §2.3.3, in particular applying the method of stationary phase to (2.52), yields the leading order inner-F-L solution

$$\begin{aligned} H_r \equiv H_\theta \equiv E_r \equiv E_2 &\equiv 0, && (9.9)\\ E_\theta &\sim -\frac{p(s_2) k^{5/6}}{2\pi} \sqrt{\frac{2\pi}{R}} \sin\theta e^{ik^{1/3}R + i\pi/4}, && (9.10)\\ H_2 &\sim \mp \frac{p(s_2) k^{5/6}}{2\pi} \sqrt{\frac{2\pi}{R}} \sin\theta e^{ik^{1/3}R + i\pi/4}, && (9.11) \end{aligned}$$

as in Figure 9.2, where $R = k^{2/3}(s_1^2 + \rho^2)^{1/2}$ is $\mathcal{O}(1)$ in the inner-F-L region. We take the minus sign in (9.11) to the right of the source in Figure 9.2 and the plus sign when we are to the left. For now we restrict our attention to the fields to the right of the source. The far field of this written in F-L coordinates is

$$\begin{aligned} E_\theta = -E_3 &\sim -\frac{p(s_2) k^{2/3}}{2\pi} \sqrt{\frac{2\pi}{\hat{s}_1}} e^{ik^{2/3}\hat{s}_1 + i\rho^2/2\hat{s}_1 + i\pi/4},\\ H_2 &= -\frac{p(s_2) k^{2/3}}{2\pi} \sqrt{\frac{2\pi}{\hat{s}_1}} e^{ik^{2/3}\hat{s}_1 + i\rho^2/2\hat{s}_1 + i\pi/4}. \end{aligned} \qquad (9.12)$$

To see the similarities between this problem and that in §6 the reader should compare (9.5) - (9.8) and (9.12) with (6.24) - (6.29) and (6.38). The matching arguments of §6 can be followed. As we are dealing with a geodesic normal coordinate system here,

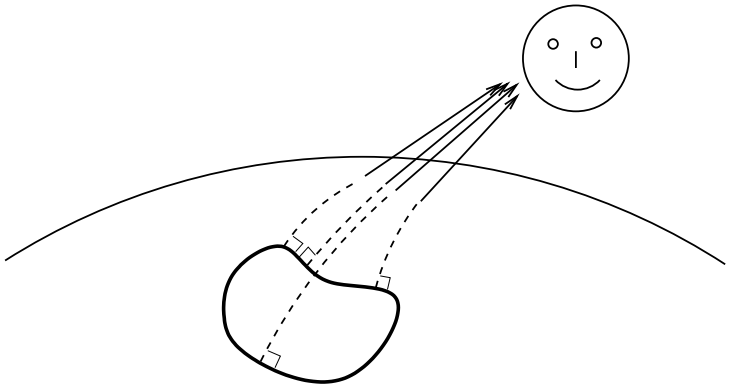


Figure 9.4: Contributions to the observed creeping ray field from a closed source lying in a convex surface. Dashed lines are geodesics on the surface normal to the source and the solid lines are shed creeping rays.

and not geodesic polars as in §6, we must replace the right-hand side of (6.53) with G_0. Finally (6.54) fixes the unknown β_m in the expression for the Airy layer field as

$$\beta_m(s_2) \quad = \quad \frac{p(\mathbf{x}_0(s_2))k^{2/3}e^{\pi i/6}|L_0(s_2)|^{1/6}G_0(s_2)^{1/4}}{2^{2/3}\mathrm{Ai}''(a'_m)}. \tag{9.13}$$

We conclude with the following remark. Take a point O on the source and construct the normal geodesic through O. Suppose this geodesic intersects the source again at O' and that we observe the surface field at a point P on this geodesic that is closer to O than to O'—Figure 9.3. As the surface field propagates along geodesics normal to the source, there will be contributions to the surface field at P from both O and O'. However, because $|OO'| = \mathcal{O}(1)$, the $k^{1/3}s_1$ exponential decay of the surface field along the normal geodesics ensures that the field at P will be dominated by the contribution from O. To leading order we can ignore the contribution from O'.

Sources of size $\mathcal{O}(k^{-1/3})$ have the same length scale as the F-L region. Thus we may not use the arguments of §9.1.1 to describe the surface fields. However, we may consider sources of size $\mathcal{O}(k^{-1/3})$ as being the limits of sources of size $\mathcal{O}(1)$ and $\mathcal{O}(k^{-2/3})$ as the source size tends towards zero and infinity respectively. We will come back to sources of size $\mathcal{O}(k^{-1/3})$ in section §9.1.3.

9.1.2 Sources of Size $k^{-2/3}$.

The source now lies entirely within an appropriate inner-F-L region. By finding the outer limit of the inner-F-L solution we will be able to obtain the function $F(\epsilon, \rho)$ on the right-hand side of (6.28). We then have the machinery in place to calculate the surface fields which should resemble those due to an anisotropic source at the origin.

The inner-F-L region is a half space with the source and observation points having position vectors $(X_0(s_2), Y_0(s_2), 0)$ and (X, Y, ρ) respectively, where X_0, Y_0, X, Y, ρ are $\mathcal{O}(1)$ variables in the inner-F-L region. Using the results of §2.3.3 we can write down the Hertz vector as

$$\mathbf{\Pi} = \frac{i}{2\pi k^{1/3}} \int_0^t \mathbf{p} \frac{e^{ik^{1/3}\left((X-X_0)^2+(Y-Y_0)^2+\rho^2\right)^{1/2}}}{((X-X_0)^2+(Y-Y_0)^2+\rho^2)^{1/2}} \, \mathrm{d}t'. \tag{9.14}$$

We make the substitution $\tau = k^{1/3}t'$ (so that variations in the source occur on the same length scale as the source itself). Re-writing (9.14) in terms of the usual F-L coordinates

$$X = k^{1/3}\hat{s}_1 \cos s_2^*, \quad Y = k^{1/3}\hat{s}_1 \sin s_2^*, \tag{9.15}$$

gives us

$$\mathbf{\Pi} = \frac{ie^{ik^{1/3}\hat{s}_1 + i\rho^2/2\hat{s}_1}}{2\pi k\hat{s}_1} \int_0^{k^{1/3}t} \mathbf{p} e^{-ik^{1/3}\left(\cos s_2^* X_0(\tau) + \sin s_2^* Y_0(\tau)\right)}, \, \mathrm{d}\tau, \tag{9.16}$$

where the integration is now over an interval of $\mathcal{O}(1)$ length. Stationary phase analysis yields contributions from points (X_0, Y_0) satisfying

$$\frac{Y_0'(s_2)}{X_0'(s_2)} = -\cot s_2^*. \tag{9.17}$$

The normal vector to the line source that lies in the tangent plane to the surface at the point (X_0, Y_0) has a gradient of $-X_0'(s_2)/Y_0'(s_2)$. Thus we get a stationary phase contribution from each point on the source which has a normal plane containing the observation point. Using §2.3.3 to calculate the magnetic and electric fields then gives the function $F(\epsilon, \rho)$ used to calculate the F-L solution as

$$F(\epsilon, \rho) \sim \sum_n i\sqrt{\frac{2}{\epsilon\pi}} \frac{p(s_{2n})}{k^{7/6}} \frac{e^{i\rho^2/2\hat{s}_1 - ik^{1/3}R_0(s_{2n}) + \mu_n i\pi/4}}{\sqrt{|\cos s_2 X_0''(s_{2n}) + \sin s_2 Y_0''(s_{2n})|}}, \tag{9.18}$$

$$\mu = \operatorname{sgn}\left(-\cos s_2 X_0''(s_{2n}) - \sin s_2 Y_0''(s_{2n})\right), \tag{9.19}$$

where $R_0^2 = X_0^2 + Y_0^2$ and the s_{2n} are the stationary phase points. It follows that the Airy layer and creeping ray fields at any point will consist of contributions from points on the source from which the normal geodesics either pass through the observation point (Airy layer) or form part of the extremal geodesic/creeping ray combination (creeping ray field).

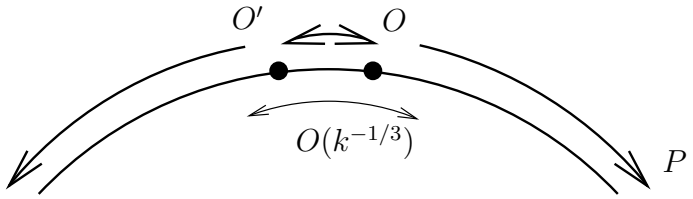


Figure 9.5: Contributions to surface field at P from O and O' are of equal magnitude.

9.1.3 Sources of Size $k^{-1/3}$

Treating sources of this size as the limits of sources of size $\mathcal{O}(1)$ and $\mathcal{O}(k^{-2/3})$ as the source size tends towards zero and infinity respectively, we may deduce that the Airy layer field will consist of contributions from points on the source whose normal geodesics pass through the observation point. Similarly for the creeping ray fields. The contributions are given by the representations in §9.1.1 and §9.1.2. The key observation for sources of size $\mathcal{O}(k^{-1/3})$ concerns the size of the creeping ray fields emanating from different locations on the source. Consider the setup described at the end of §9.1.1. As the source has a lengthscale $\mathcal{O}(k^{-1/3})$ we can say that now $|OO'| = \mathcal{O}(k^{-1/3})$—Figure 9.5. The extra decay factor in the exponent of the surface field from O' arising due to the additional distance travelled to P is now $\mathcal{O}(1)$. Thus O and O' contribute equally to the surface field at P.

9.1.4 Smaller Sources

Letting the source decrease further in size will not invalidate (9.14) as a representation of the field. If the source is $\mathcal{O}(k^m)$ in size where $m \leq -1$ then the outer limit of (9.14) written in F-L coordinates is

$$\mathbf{\Pi} \sim \frac{i}{2\pi k^{1/3}} \frac{e^{ik^{2/3}\hat{s}_1 + i\rho^2/2\hat{s}_1}}{\hat{s}_1} \int_0^t \mathbf{p}(t')\,\mathrm{d}t'. \tag{9.20}$$

By comparison with (6.38), the asymptotic solution will everywhere be equivalent to that due to a dipole at the origin whose moment is the integral of $\mathbf{p}$ over the source.

If we now generalise $p(s_2)$ slightly, allowing an oscillatory factor $\exp(iks_2\cos\alpha)$, then it is easy to adapt the above results as follows.

For sources of size $\mathcal{O}(1)$ and $\mathcal{O}(k^{-2/3})$ we take s_1 to be the distance along the geodesics at an angle $\pi/2-\alpha$ to the direction of increasing s_2. All the results hold as long as we interpret the fundamental forms of the surface consistently with the new coordinate system.

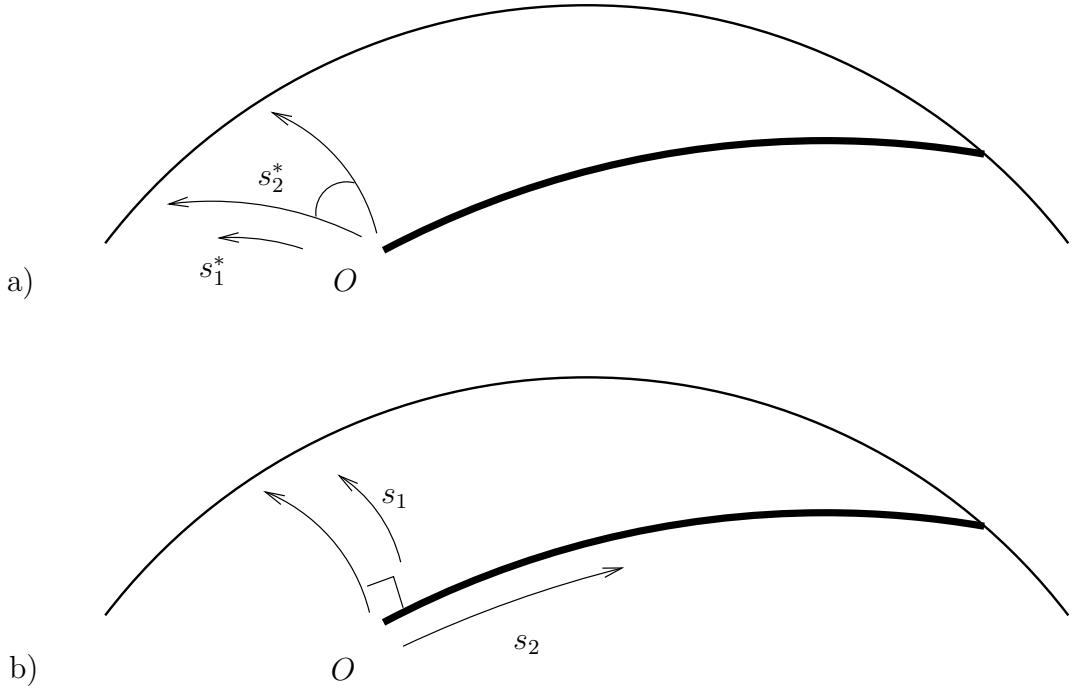


Figure 9.6:

Sources of size $\mathcal{O}(k^{-1/3})$, again treated as the limit of larger and smaller sources, will similarly produce leading order contributions to the fields which propagate along the geodesics at an angle $\pi/2 - \alpha$ to the direction of increasing s_2.

There will be no change for sources of size $\mathcal{O}(k^{-1})$ or smaller.

9.2 Semi-infinite Sources

In §4.1 we showed that a semi-infinite line source that is excited in phase produces a leading order field propagating along rays perpendicular to the source and also a higher-order field that is radially diffracted from the tip. A shadow boundary region of width $\mathcal{O}(k^{-1/2})$ was introduced to remove the non-uniformity in the ray expansion. In addition, we know that a source placed on a convex surface produces a surface field that decays exponentially along geodesics. Hence, if we place a semi-infinite line source on the surface—Figure 9.6—we expect both of these characteristic behaviours to be exhibited in some form.

We consider a 'semi-infinite' source with unit dipole moment $\mathbf{p} = \mathbf{e}_3$ lying on a convex surface. By this we really mean that, provided the dipole moment p is slowly varying, we rely on the locality of diffraction to consider the diffraction effects of each end of a line source with an $\mathcal{O}(1)$ length in isolation. For simplicity we will assume that the

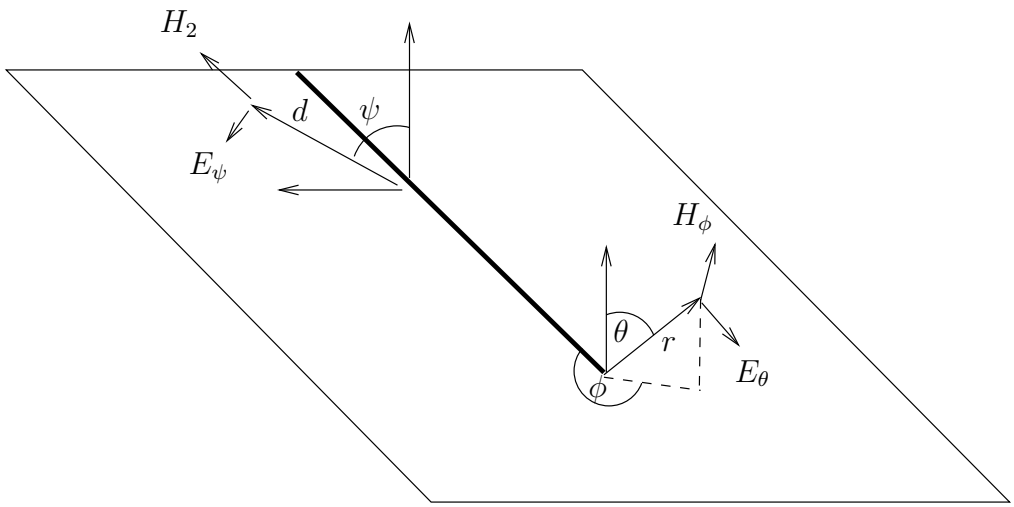


Figure 9.7: Components of **E** and **H** fields arising from a stationary phase analysis of the inner-F-L problem.

source is excited in phase.

When we are away from the tip we can deal with the radiated surface fields as described in §9.1.1. The leading order surface field will propagate along the geodesics perpendicular to the line source. Anticipating some kind of radially diffracted surface field from the tip, we consider radial F-L and inner-F-L regions around the tip as in §6.3 - 6.4. We expect two surface fields to be produced—a leading order field propagating along geodesics perpendicular to the source and a radially diffracted field from the tip. This means it will be convenient to use the following two coordinate systems. We will take s_1^*, s_2^*, s_3^* to be the geodesic polars, with the origin at the tip of the source and s_1, s_2, s_3 to be geodesic normal coordinates with the origin again at the tip of the source and s_2 increasing along the source. The coordinate systems are set up so that the lines $s_2 = 0$ and $s_2^* = 0$ coincide. See Figure 9.6a) and b) respectively.

9.2.1 Inner-Fock-Leontovič Region

We scale $S_1 = k^{2/3}s_1, S_1^* = k^{2/3}s_1^*, S_2 = k^{2/3}s_2$. Section 2.3.3 allows us to calculate the leading order fields in the inner-F-L region via applying the method of stationary

phase to (2.52). We will get a stationary phase contribution for $S_2 > 0$, namely

$$H_d \equiv H_\psi \equiv E_d \equiv E_2 \equiv 0, \tag{9.21}$$

$$H_2 = \mp \frac{k^{5/6}}{\sqrt{2\pi}} \frac{\sin\psi}{(S_1^2+\rho^2)^{1/4}} e^{ik^{1/3}\left(S_1^2+\rho^2\right)^{1/2}+i\pi/4}, \tag{9.22}$$

$$E_\psi = -\frac{k^{5/6}}{\sqrt{2\pi}} \frac{\sin\psi}{(S_1^2+\rho^2)^{1/4}} e^{ik^{1/3}\left(S_1^2+\rho^2\right)^{1/2}+i\pi/4}, \tag{9.23}$$

where the components of $\mathbf{E}, \mathbf{H}$ are indicated in Figure 9.7 and

$$\sin\psi = \frac{S_1}{(S_1^2+\rho^2)^{1/2}}. \tag{9.24}$$

The upper sign in H_2 is taken when we are to the right of the source and the lower when we are to the left. The stationary phase analysis also yields an end-point contribution, namely

$$H_r \equiv H_\theta \equiv E_r \equiv E_\phi \equiv 0, \tag{9.25}$$

$$H_\phi = \frac{ik^{2/3}\sin\theta}{2\pi} \frac{e^{ik^{1/3}\left(S_1^{*2}+\rho^2\right)^{1/2}}}{S_2}, \tag{9.26}$$

$$E_\theta = \frac{ik^{2/3}\sin\theta}{2\pi} \frac{e^{ik^{1/3}\left(S_1^{*2}+\rho^2\right)^{1/2}}}{S_2}, \tag{9.27}$$

where the components of $\mathbf{E}, \mathbf{H}$ are shown in Figure 9.7. In obtaining both the endpoint and stationary phase contributions, care has had to be taken in dealing with the delta functions associated with the source to arrive at the correct exponent for k. As usual we write this solution in terms of the F-L coordinates. We consider the field to the left of the source, thus the stationary phase contribution (written in F-L coordinates) is

$$H_2 \sim \frac{ik^{2/3}}{\sqrt{2\pi\hat{s}_1}} e^{ik^{2/3}\hat{s}_1+i\rho^2/2\hat{s}_1+i\pi/4}, \tag{9.28}$$

$$E_3 \equiv -E_\psi \sim \frac{ik^{2/3}}{\sqrt{2\pi\hat{s}_1}} e^{ik^{2/3}\hat{s}_1+i\rho^2/2\hat{s}_1+i\pi/4}, \tag{9.29}$$

where E_3 is the component of $\mathbf{E}$ in the $\mathbf{e}_3$ direction. These fields are identical to (9.12) with $p = 1$. Thus from §9.1.1 we know there is a surface field propagating along the geodesics corresponding to constant s_2 for $s_2 > 0$, namely

$$E_1 \equiv E_2 \equiv H_1 \equiv H_3 \equiv 0, \tag{9.30}$$

with

$$H_2 = E_3 \sim \sum_{m=0}^{\infty} \frac{k^{2/3} e^{\pi i/6} |L_0(s_2)|^{1/6} |L(s_1,s_2)|^{1/6} G_0(s_2)^{1/4}}{2^{2/3} G(s_1,s_2)^{1/4} \mathrm{Ai}''(a'_m)} \tag{9.31}$$
$$\times \mathrm{Ai}\left(-\sqrt[3]{2} e^{2\pi i/3} \rho |L(s_1,s_2)|^{1/3} + a'_m\right) \exp\left(iks_1 + ik^{1/3} \frac{a'_m e^{-2\pi i/3}}{\sqrt[3]{2}} \int_0^{s_1} |L_0(t,s_2)|^{2/3}\, \mathrm{d}t\right).$$

Writing the end-point contribution (9.25) - (9.27) in terms of the F-L coordinates yields

$$\begin{aligned} H_\phi = H_2 &\sim -\frac{ik^{1/3}}{2\pi} \frac{e^{ik^{2/3}\hat{s}_1^* + i\rho^2/2\hat{s}_1^*}}{\hat{s}_1^* \sin s_2^*}, \\ E_\theta \sim -E_3 &\sim -\frac{ik^{1/3}}{2\pi} \frac{e^{ik^{2/3}\hat{s}_1^* + i\rho^2/2\hat{s}_1^*}}{\hat{s}_1^* \sin s_2^*}, \end{aligned} \tag{9.32}$$

where H_2 now denotes the component of $\mathbf{H}$ in the direction of increasing s_2^*. By comparison with (6.38) we can say that there will be a surface field propagating along the geodesics associated with constant s_2^*. Equations (6.55) - (6.57) let us write down the leading order field in the Airy layer due to the endpoint contribution as

$$E_1 \equiv E_2 \equiv H_1 \equiv H_3 \equiv 0, \tag{9.33}$$

with

$$H_2 \sim -E_3 \sim \sum_{m=0}^{\infty} \frac{k^{1/6} e^{5\pi i/12} |L_0(s_2^*)|^{1/6} G_0(s_2^*)^{1/4} |L(s_1^*,s_2^*)|^{1/6}}{2^{7/6}\sqrt{\pi}\mathrm{Ai}''(a'_m) G(s_1^*,s_2^*)^{1/4} \sin s_2^*} \tag{9.34}$$
$$\times \mathrm{Ai}\left(-\sqrt[3]{2} e^{2\pi i/3} \rho |L(s_1^*,s_2^*)|^{1/3} + a'_m\right) \exp\left(iks_1^* + ik^{1/3} \frac{a'_m e^{-2\pi i/3}}{\sqrt[3]{2}} \int_0^{s_1^*} |L(t,s_2^*)|^{2/3} \mathrm{d}t\right).$$

Looking at the expansion for the total field in the Airy layer, given by adding the fields given by (9.31) and (9.34), we see that it breaks down when $s_2^* = \mathcal{O}(k^{-1/2})$. We introduce a *surface fresnel region* to remove this non-uniformity.

9.2.2 Surface Fresnel Region

We work in the geodesic normal coordinate system s_1, s_2, s_3. We make the scaling $\tilde{s}_2 = k^{1/2} s_2$, and take the ansatz

$$\mathbf{F} = e^{iks_1 + ik^{1/3} v(s_1)} \left(\mathbf{F}^0(s_1,\tilde{s}_2) + \frac{\mathbf{F}^1}{k^{1/3}} + \frac{\mathbf{F}^2}{k^{1/2}} + \frac{\mathbf{F}^3}{k^{2/3}} + \frac{\mathbf{F}^4}{k^{5/6}} + \frac{\mathbf{F}^5}{k} + \dots\right), \tag{9.35}$$

for the field. This ansatz is chosen as the field in the surface fresnel region must match into the Airy layer field on either side. The first five terms of Maxwell's

equations are listed in Appendix E. The $\mathcal{O}(k), \mathcal{O}(k^{2/3})$ and $\mathcal{O}(k^{1/3})$ equations imply the existence of magnetically and electrically polarised solutions obeying the usual Airy layer equations

$$\begin{aligned} E_1^0 \equiv E_2^0 \equiv H_1^0 \equiv H_3^0 &\equiv 0, && (9.36)\\ E_3 &= -H_2^0, && (9.37)\\ \frac{\partial^2 H_2^0}{\partial \rho^2} - 2\frac{\partial v}{\partial s_1} H_2^0 + 2\rho |L| H_2^0 &= 0, && (9.38) \end{aligned}$$

and

$$\begin{aligned} E_1^0 \equiv E_3^0 \equiv H_1^0 \equiv H_2^0 &\equiv 0, && (9.39)\\ H_3 &= E_2^0, && (9.40)\\ \frac{\partial^2 E_2^0}{\partial \rho^2} - 2\frac{\partial v}{\partial s_1} E_2^0 + 2\rho |L| E_2^0 &= 0, && (9.41) \end{aligned}$$

respectively, along with the conditions

$$\begin{aligned} \frac{\partial H_2^0}{\partial \rho} &= 0, \qquad \rho = 0, && (9.42)\\ E_2^0 &= 0, \qquad \rho = 0. && (9.43) \end{aligned}$$

Equating (E.33), (E.34) with (E.37) and (E.36) respectively, and using the lower order equations, we are able to deduce

$$\begin{aligned} &\frac{\partial^2 H_2^1}{\partial \rho^2} - 2\frac{\partial v}{\partial s_1} H_2^1 + 2\rho |L(s_1,0)| H_2^1 \\ &\qquad = -\frac{1}{G(s_1,0)} \frac{\partial^2 H_2^0}{\partial \tilde{s}_2^2} - 2i \frac{\partial H_2^0}{\partial s_1} - \frac{i H_2^0}{2} \frac{\partial (\ln G)}{\partial s_1} + i \frac{2M}{\sqrt{G}} E_2^0, && (9.44)\\ &\frac{\partial^2 E_2^1}{\partial \rho^2} - 2\frac{\partial v}{\partial s_1} E_2^1 + 2\rho |L(s_1,0)| E_2^1 \\ &\qquad = -\frac{1}{G(s_1,0)} \frac{\partial^2 E_2^0}{\partial \tilde{s}_2^2} - 2i \frac{\partial E_2^0}{\partial s_1} - \frac{i E_2^0}{2} \frac{\partial (\ln G)}{\partial s_1} - i \frac{2M}{\sqrt{G}} H_2^0, && (9.45) \end{aligned}$$

along with the boundary conditions

$$\begin{aligned} \frac{\partial H_2^1}{\partial \rho} &= 0, \quad \rho = 0, && (9.46)\\ E_2^1 &= 0, \quad \rho = 0. && (9.47) \end{aligned}$$

We remark that at $\mathcal{O}(k^{-1/3})$ we are no longer able to talk about magnetically and electrically polarised solutions as mode conversion between the two occurs at this order. As a point source on a surface is unable to excite electrically polarised surface

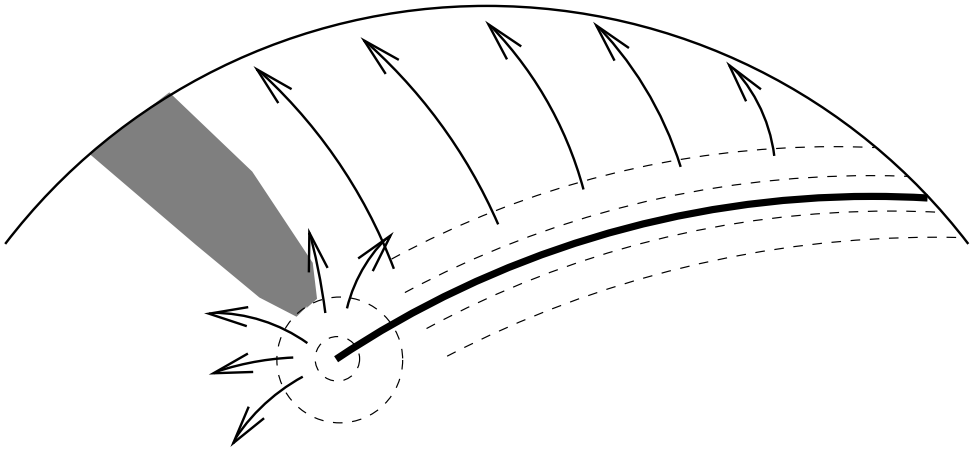


Figure 9.8: Surface fresnel region due to a semi-infinite source in a convex surface.

fields it will be sufficient to solve (9.38) and (9.42) along with (9.44) and (9.47). The solution to (9.38) and (9.42) is the usual

$$\begin{aligned} H_2^0 &= \sum_{m=0}^{\infty} \alpha_m(s_1,\tilde{s}_2)\mathrm{Ai}\left(-\sqrt[3]{2}e^{2\pi i/3}|L|^{1/3}\rho + a_m'\right) \\ &\quad \times\exp\left(iks_1 + ik^{1/3}\frac{a_m' e^{-2\pi i/3}}{\sqrt[3]{2}}\int_0^{s_1}|L|^{2/3}\,\mathrm{d}t\right), \end{aligned} \tag{9.48}$$

where the α_m are to be determined. Multiplying (9.44) by H_2^0, using (9.36) and integrating with respect to ρ from zero to infinity, eventually yields the solvability condition

$$\frac{\partial^2}{\partial\tilde{s}_2^2}\left(\alpha_m(s_1,\tilde{s}_2)\frac{G(s_1,0)^{1/4}}{|L(s_1,0)|^{1/6}}\right) + 2iG(s_1,0)\frac{\partial}{\partial s_1}\left(\alpha_m(s_1,\tilde{s}_2)\frac{G(s_1,0)^{1/4}}{|L(s_1,0)|^{1/6}}\right) = 0. \tag{9.49}$$

The general solution to (9.49) is

$$\alpha_m(s_1,\tilde{s}_2) = \frac{|L(s_1,0)|^{1/6}}{G(s_1,0)^{1/4}}\left(A_m\mathrm{erfc}\left(-e^{-i\pi/4}\frac{\tilde{s}_2}{\sqrt{2\int_0^{s_1}\frac{1}{G(\lambda,0)}\,\mathrm{d}\lambda}}\right) + B_m\right), \tag{9.50}$$

where we must still find the coefficients A_m, B_m for each mode.

9.2.3 Matching the Surface Fresnel Solution to the Airy Layer Solutions

We need to chose the constants A_m, B_m in such a way as to provide a smooth match between the surface fresnel region and the Airy layer solutions on either side of it.

We consider the special case where $G(s_1, 0) = 1$.[1]

Applying Van Dyke's matching rule, we take the 2 term outer of the 1 term inner, (9.50). This is

$$H_2 \to \begin{cases} e^{iks_1}|L(s_1,0)|^{1/6}\left(B_m - A_m e^{i\pi/4}\sqrt{\dfrac{2s_1}{\pi}}\dfrac{\exp\left(i\tilde{s}_2^2/2s_1\right)}{\tilde{s}_2}\right), & \tilde{s}_2 \to \infty, \\ e^{iks_1}|L(s_1,0)|^{1/6}\left(2A_m + B_m - A_m e^{i\pi/4}\sqrt{\dfrac{2s_1}{\pi}}\dfrac{\exp\left(i\tilde{s}_2^2/2s_1\right)}{\tilde{s}_2}\right), & \tilde{s}_2 \to -\infty. \end{cases}$$

We now look at the 2 term 'outer' Airy layer solution which is given by adding together (9.31) and (9.34). Consideration of the metric $(\mathrm{d}\mathbf{r})^2$ indicates that as $s_2^* \to 0$, we have $G \to G_0 s_1^{*2}$, where G_0 is a constant. In addition—Figure 9.6—for $s_1, s_1^*, \tilde{s}_2, \tilde{s}_2^* = \mathcal{O}(1)$, we have the following relationships

$$s_1 \sim s_1^* - k^{-1}\frac{\tilde{s}_2^{*2}}{2s_1^*}, \tag{9.51}$$

$$\tilde{s}_2 \sim -s_1\tilde{s}_2^* \sim -s_1^*\tilde{s}_2^*. \tag{9.52}$$

Taking the 1 term inner of the 2 term outer, it can be seen that a successful match exists provided that we chose the constants

$$A_m = \frac{e^{2i\pi/3}|L(0,0)|^{1/6}k^{2/3}}{2^{5/3}\mathrm{Ai}''(a_m')}, \tag{9.53}$$

$$B_m = \frac{e^{2i\pi/3}|L(0,0)|^{1/6}k^{2/3}}{2^{2/3}\mathrm{Ai}''(a_m')}. \tag{9.54}$$

Thus the surface fresnel region solution exhibits very nice behaviour—it retains both the exponential decay associated with surface fields and the error function profile characteristic of shadow boundaries.

The structure of the solution is illustrated in Figure 9.8. The dashed lines close to the source indicate the inner-F-L and F-L regions. One set of inner-F-L and F-L regions are parallel to the source. These establish surface fields propagating along the geodesics normal to the source as discussed in section 9.1. The inner-F-L and F-L regions that exist around the tip set up the surface diffracted field along the geodesics passing through the tip. The non-uniformity of the surface diffracted field then necessitates the introduction of the surface fresnel region.

[1] For a general surface it is possible to chose A_m, B_m so that the surface Fresnel solution matches into the leading order fields either side but we have not been able to verify that this choice of A_m, B_m provides a successful match to the higher order diffracted field from the tip. We hope to address this difficulty in a future paper.

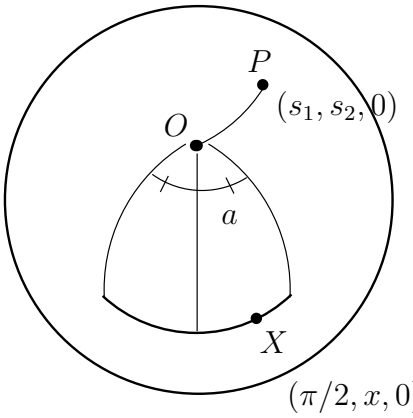


Figure 9.9: Line source along the equator of a sphere.

The next step is to consider finite line sources on surfaces. Solving the inner-F-L region problem in the neighbourhood of each tip reveals a surface fresnel field originating at either end of the source. The shadow boundaries emerging from each end of a finite source in free space will merge to form a Fraunhofer region *if* the excitation of the source is suitable—*i.e.* if the rays from each end of the source are parallel. When we place the same finite source on a convex surface in addition to the excitation of the source, we must also worry about the behaviour of the geodesics from each end of the source along which the leading order surface field propagates. We will now consider a canonical problem to gain insight.

9.3 Focussing Effects

We will consider a line source placed along the equator of a sphere of radius R. The source has a length $2a$ where $2a/\pi < R$, and is excited in phase with a unit dipole moment. We know that the source will excite magnetically polarised surface fields which propagate along the geodesics normal to the line source. This leads to the first difficulty—all these geodesics will pass through the north (and south) pole (NP) of the sphere. The other complication is that surface fresnel regions will be set up from each end of the source along the normal geodesics. These surface fresnel regions will also converge at the NP.

The focussing of creeping rays arising due to an incident plane wave on a body of revolution is considered by [7]. There, the incident field is parallel to the axis and the creeping ray field has a singularity due to the convergence of the geodesics at a focal point. A uniform expansion for the surface field is obtained which is valid both in the neighbourhood of, and away from, the focal point. Saward, [33] considers an

incident plane field on a body of revolution that has a tip. If the horizon is remote from the tip and the incident radiation is not parallel to the axis of the body, the ray solution (after extensive analysis) turns out to be finite in the neighbourhood of the tip, but breaks down along penumbral caustics after the tip has been reached. Our problem is not covered by either of these authors as the finiteness of our source introduces new higher order effects.

We will use the geodesic polar coordinate systems s_1, s_2, s_3 based at the NP (we note that this is also a geodesic normal coordinate system parameterised by the line source) and $s_1(x), s_2(x), s_3$ based at the point x on the line-source. The line $s_2 = 0$ is the shorter of the two geodesics connecting the NP to the centre of the line source—Figure 9.9. Although we have spent the first part of this chapter developing an asymptotic ray picture for the surface fields radiated by finite sources, in order to study the behaviour of the surface fields—and in particular the surface fresnel regions—at the focal point, it is necessary to resort to an integral representation of the solution. Using the results of §6 we can write down the surface field at any point due to a point source. Given an observation point, P, in the Airy layer on the sphere, the surface field will be an integral over the line-source of the expression for the field due to a point source. To avoid confusing various coordinate systems we consider just the electric field for the moment. Equation (6.57) implies $\mathbf{E} \sim E_3 \mathbf{e}_3$ where

$$\begin{aligned} E_3 \;\sim\; & \frac{k^{7/6} e^{-\pi i/12}}{2^{7/6}\sqrt{\pi}} \int_{-a}^{a} \frac{G(0, s_2(x))^{1/4}}{G(s_1(x), s_2(x))^{1/4}} |L(0, s_2(x))|^{1/6} |L(s_1(x), s_2(x))|^{1/6} \\ & \times \frac{\mathrm{Ai}\left(-\sqrt[3]{2}|L(s_1(x), s_2(x))|^{1/3} \rho e^{2\pi i/3} + a'_m\right)}{\mathrm{Ai}''(a'_m)} \\ & \times \exp\left(iks_1(x) + ik^{1/3} \frac{a'_m e^{-2\pi i/3}}{\sqrt[3]{2}} \int_0^{s_1(x)} |L(t, s_2(x)|^{2/3} \,\mathrm{d}t \right) \mathrm{d}x, \end{aligned} \tag{9.55}$$

where $\rho = k^{2/3} s_3$. For a sphere of radius R we have

$$G \;=\; R^2 \sin^2\left(\frac{s_1}{R}\right), \qquad L \;=\; -\frac{1}{R}, \tag{9.56}$$

with $G(0, s_2(x)) = 1$. We will restrict our attention for the moment to the case $R = 1$. We thus just need to be able to write $s_1(x)$ in terms of x and s_1, s_2. In Figure 9.9, the point X and the observation point P are at $(\pi/2, x, 0)$ and $(s_1, s_2, 0)$ in geodesic polar coordinates. In a suitably defined orthogonal coordinate system with the origin at the centre of the sphere these correspond to $(\cos x, \sin x, 0)$ and

$(\cos s_2 \sin s_1, \sin s_2 \sin s_1, \cos s_2)$ respectively. Elementary geometry then gives the distance along the geodesic (great circle) from X to P as

$$s_1(x) = 2\sin^{-1}\left(\frac{1}{\sqrt{2}}\left(1 - \sin s_1 \cos(s_2 - x)\right)^{1/2}\right). \tag{9.57}$$

Thus (9.55) reduces to

$$\begin{aligned} E_3 \;\sim\; & \frac{k^{7/6}e^{-\pi i/12}}{2^{7/6}\sqrt{\pi}} \int_{-a}^{a} \frac{1}{\sin s_1(x)} \frac{\mathrm{Ai}\left(-\sqrt[3]{2}\rho e^{2\pi i/3} + a_m'\right)}{\mathrm{Ai}''(a_m')} \\ & \times \exp\left(ik s_1(x) + ik^{1/3}\frac{a_m' e^{-2\pi i/3}}{\sqrt[3]{2}} s_1(x)\,\mathrm{d}t\right)\,\mathrm{d}x. \end{aligned} \tag{9.58}$$

This integral may be evaluated via stationary phase, yielding a leading order stationary phase contribution from $x = x_0$ satisfying

$$x_0 \;=\; \begin{cases} s_2, & s_2 \in (-a, a)\,, \\ s_2 + \pi, & s_2 \in (-a + \pi, a + \pi)\,, \end{cases} \tag{9.59}$$

along with two endpoint contributions. The stationary phase contribution, only present if $-a < s_2 < a$ or if $-a + \pi < s_2 < a + \pi$, is given by

$$\begin{aligned} E_3 \;\sim\; & \frac{k^{2/3}e^{-\pi i/12 \pm i\pi/4}}{2^{2/3}\sin s_1(x_0)} \frac{\mathrm{Ai}\left(-\sqrt[3]{2}e^{2\pi i/3}\rho + a_m'\right)}{\mathrm{Ai}''\left(a_m'\right)} \frac{1}{\sqrt{\tan s_1}} \\ & \times \exp\left(\left(ik + ik^{1/3}\frac{a_m' e^{-2\pi i/3}}{\sqrt[3]{2}}\right)\left(2\sin^{-1}\left(\frac{1}{\sqrt{2}}(1 \mp \sin s_1)^{1/2}\right)\right)\right), \end{aligned} \tag{9.60}$$

where we take the upper signs if $-a < s_2 < a$ and the lower if $-a + \pi < s_2 < a + \pi$. The endpoint contributions are defined as

$$\begin{aligned} E_3 \;\sim\; & \mp\frac{k^{1/6}e^{5i\pi/12}}{2^{7/6}\sqrt{\pi}\sin s_1(\pm a)} \frac{\mathrm{Ai}\left(-\sqrt[3]{2}e^{2\pi i/3}\rho + a_m'\right)}{\mathrm{Ai}''\left(a_m'\right)} \\ & \times \frac{1 - \sin^2 s_1 \cos^2(s_2 \mp a)}{\sin s_1 \sin(s_1 \mp a)} \exp\left(\left(ik + ik^{1/3}\frac{a_m' e^{-2\pi i/3}}{\sqrt[3]{2}}\right) s_1(\pm a)\right). \end{aligned} \tag{9.61}$$

The upper signs correspond to the contribution from $x = a$ and the lower signs to the contribution from $x = -a$. The magnetic field due to the stationary phase and endpoint contributions can be calculated via Maxwell's equations. We remark that (9.60) and (9.61) could have been written down directly from (9.31) and (9.34), but *only* if the rays have not travelled through the caustic at the north pole. Use of (9.55) has given us additional information about the surface field—namely that there is a phase jump of $\pi/2$ in the leading order field as we pass through the focal point. It is pleasing to note that this is consistent with the phase jump that was observed in

§4.7. Provided that we are away from the line source—*i.e.* $s_1 - \pi/2 = \mathcal{O}(1)$—the expansion for the field breaks down when

$$\sin(\pm a - s_2)\sqrt{\sin s_1} \quad \sim \quad k^{-1/2}. \tag{9.62}$$

For $s_1 = \mathcal{O}(1)$ this happens precisely when $s_2 \pm a = \mathcal{O}(k^{-1/2})$ and corresponds to the ray picture breaking down and surface fresnel regions being set up. In §4.7 we set up a flat plate to produce rays which converged at an $\mathcal{O}(1)$ distance from the plate which is analagous to our line source on a sphere of unit radius. In both cases the angle between the shadow boundary regions/surface fresnel regions (at the focal point/NP for the source in free space/on the sphere) is $\mathcal{O}(1)$. We might expect similar behaviour for both. In light of §4.7 we now position our observation point close to the NP to see what happens. That is we set $s_1 = k^{-\alpha}S_1, 0 < \alpha < 1$. We find that we are still able to carry out stationary phase analysis except when

$$s_2 \pm a \quad = \quad \mathcal{O}(k^{-1/2-\alpha/2}). \tag{9.63}$$

That is to say that the surface fresnel regions shrink as we approach the NP in exactly the same way that they did in §4.7. If $\alpha = 1$ then the ray region (where the expansion is valid) and the surface fresnel regions have the same size and we can do no better than write the solution as the original integral representation (9.58). If we ignore any exponential decay, the behaviour of the surface fresnel regions as we approach the NP is exactly the same as the behaviour of the shadow boundary regions of §4.7 as we approach the focal point there. Thus, it might seem reasonable to expect the surface fresnel regions emerging to the right of the NP to grow like $((s_1 + \pi/2)/k)^{1/2}$ as was the case in §4.7. A closer analysis of the solution reveals that this is *not* what happens. Looking at the surface fresnel region that originated from the right-hand end of the source *after* it has passed through the NP we set

$$x \quad \sim \quad a + k^{-1/2}X, \tag{9.64}$$

$$s_2 \quad \sim \quad a + \pi + k^{-1/2}S_2, \tag{9.65}$$

where $X, S_2 = \mathcal{O}(1)$. After some manipulation, the solution in this surface fresnel region can be obtained as

$$H_2 \quad \sim \quad g(s_1, S_2, \rho)\mathrm{erf}\left(\frac{e^{i\pi/4}}{2}\sqrt{\tan s_1}S_2\right). \tag{9.66}$$

This is valid so long as the argument of the error function is $\mathcal{O}(1)$. Thus it would seem as though the surface fresnel regions emerging from the NP do not remember

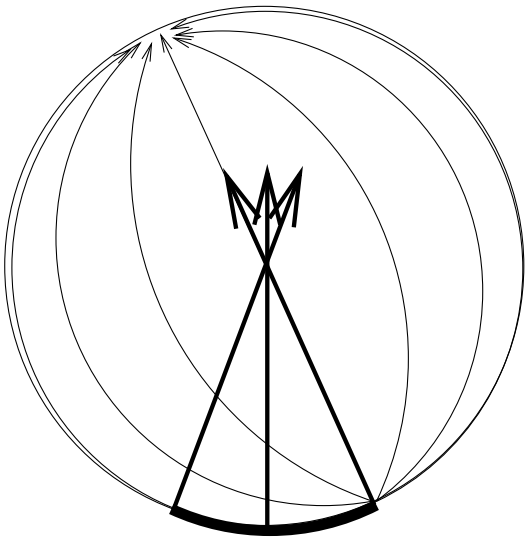


Figure 9.10: Bold rays are leading order rays from the source which form a caustic at the NP. Light rays are the diffracted field from the right-hand tip which form a caustic at the antipodes. The diffracted rays from the left-hand tip are not marked.

that they originally came from the line source. It is also apparent that something interesting occurs when $s_1 = \pi/2$. A look at the ray picture on the sphere—Figure 9.10—reveals that this is precisely where the diffracted rays from the right-hand tip of the source form a point caustic.

This problem needs further investigation as it is not clear whether the rather specific geometry of a sphere has masked any diffraction effects. Suppose that we were to perturb our sphere, so that symmetry was lost. Suppose also that via some clever excitation of the source we ensured that the geodesics along which the leading order field propagates still converged at the NP. In this case there would be a set of geodesics which travel the least distance to get to the NP. If there is a variation in length of the geodesics that is greater than $k^{-1/3}$, the field contributions along the shortest geodesics would dominate exponentially at the NP rendering the caustic analysis that we have just carried out for the sphere unnecessary.

We now consider a source of $\mathcal{O}(1)$ length on the equator of a sphere of radius k^β, for some $\beta > 0$. Although we can write down expressions for the components of the fundamental forms, it will only be necessary to investigate the phase of the integrand, that is the behaviour of $s_1(x)$, near the NP. We make the following scalings

$$S_1 = k^{-\beta} s_1, \tag{9.67}$$

$$X = k^\beta x, \tag{9.68}$$

$$S_2 = k^\beta s_2. \tag{9.69}$$

This means we are looking at the surface of a sphere in a sector where we anticipate the dominant surface fields will be located. We can say

$$s_1(x) = k^\beta 2 \sin^{-1}\left(\frac{1}{\sqrt{2}}\left(1-\sin S_1 \cos\left(\frac{S_2-X}{k^\beta}\right)\right)^{1/2}\right), \tag{9.70}$$

$$\sim 2k^\beta \sin^{-1}\left(\frac{1}{\sqrt{2}}\left(1-\sin S_1\right)^{1/2}\right) + \frac{1}{2k^\beta}\tan S_1 \left(S_2-X\right)^2. \tag{9.71}$$

It should be apparent that for $0 < \beta < 1$ we will be able to perform some kind of stationary phase analysis resulting in a ray picture. For $\beta = 1$ the integral will be reducible to the sum of two error functions. This tells us that we are in the *surface Fraunhofer region*. Thus the growth of the surface fresnel regions dominates the geodesic convergence for sufficiently large radii of curvature. In Figure 9.11 we show the behaviour of the surface fresnel regions for the cases where the radius of the sphere is $\mathcal{O}(1)$ and $\mathcal{O}(k)$ as the geodesics from either end of the source make mulitiple passages of the NP and SP. We also include an intermediate case where the radius is $\mathcal{O}(k^\beta)$ for $0 < \beta < 1$.

9.4 Application: A Spiral Antenna

The example of a spiral antenna on a perfectly conducting surface is of interest to BAe. Many of the antennas mounted on aeroplanes are spiral in nature. We describe below the qualitative behaviour of the surface and GO fields due to spirals of varying length scales. The quantitative results may be found earlier in this chapter. We initially assume that the antenna is excited in phase with constant amplitude.

Length Scale $\ll k^{-1}$.

- The GO field is equivalent to that from a dipole at the origin with a dipole moment equal to the integral of the actual dipole moment of the antenna over the spiral.
- The surface field is equivalent to that due to a dipole at the origin with a dipole moment equal to the integral of the actual dipole moment of the antenna over the spiral.

Figure 9.12 is a schematic of this. All the fields are equivalent to those from a dipole. Therefore the projection of the GO field (thick rays) onto the tangent plane and the surface field (thin rays) are independent of direction. The GO field will however vary as the angle of the observer to the normal direction at the origin changes.

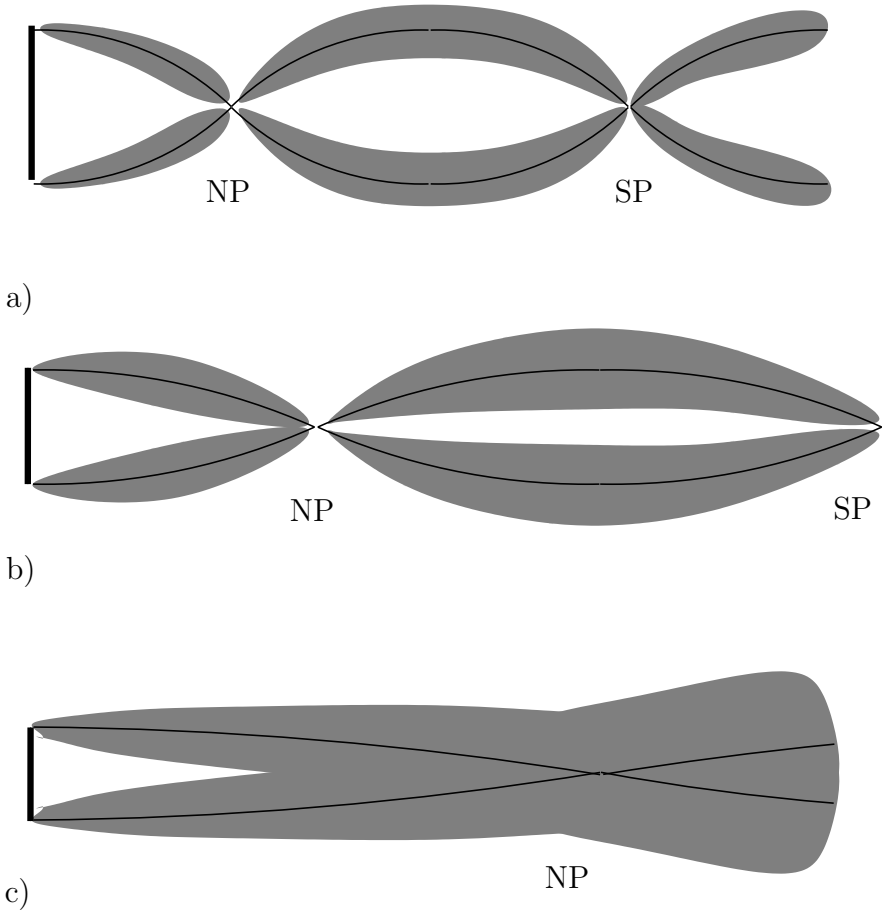


Figure 9.11: Behaviour of surface fresnel regions due to a line source along the equator of a sphere. We have unravelled the geodesics from each end of the source. Shaded areas show surface fresnel regions for a sphere of radius a) $\mathcal{O}(1)$, b) $\mathcal{O}(k^\beta)$ for $0 < \beta < 1$, c) $\mathcal{O}(k)$.

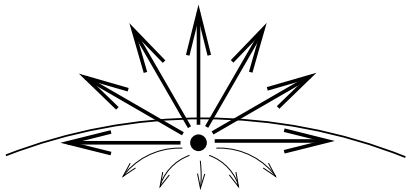


Figure 9.12: Spiral with length scale $\ll k^{-1}$.

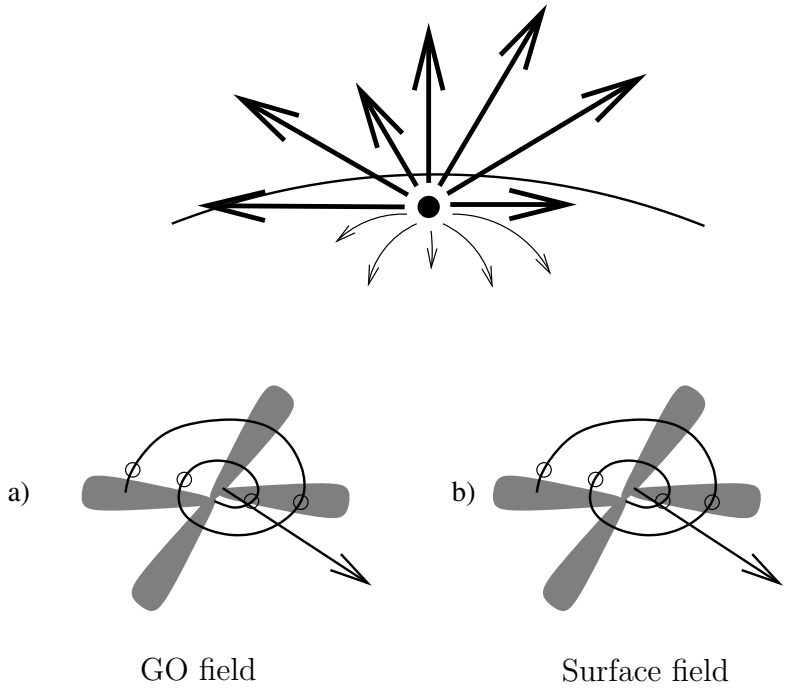


Figure 9.13: Spiral with length scale $\sim k^{-2/3}$.

Length Scale $\sim k^{-2/3}$.

- The GO field is equivalent to that due to an 'anisotropic' dipole at the origin. The field in each direction is obtained by summing the contributions from each point of the source that has a normal plane containing the observation point. We must be careful though, as there will be an $\mathcal{O}(k^{1/3})$ phase shift in the contribution from each point arising because the contributing portions of the source are not actually at the origin. This is illustrated in Figure 9.13a). The projection of the observer's direction onto the tangent plane is given by the ray. The clear circles denote those points of the source whose normal planes contain the observer. The shaded regions are the shadow boundary regions due to the discontinuities at the end of the source. These will appear to originate at the origin as indicated.

- The surface field is equivalent to that from an anisotropic dipole at the origin. For any given observation point, we calculate the geodesic going through the origin and the observation point. There will be contributions to the surface field from all points of the source whose normal directions are in the same direction as this geodesic—denoted by circles in Figure 9.13b). Surface fresnel regions are set up at the end points but will appear to come from the origin. These are

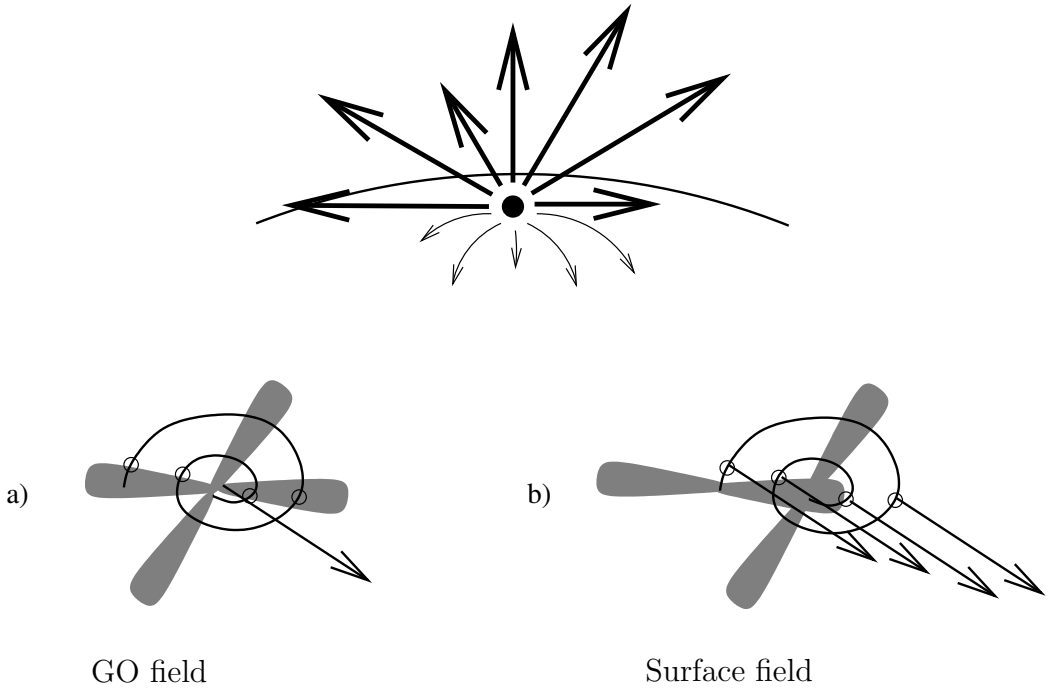


Figure 9.14: Spiral with length scale $\sim k^{-1/3}$.

the shaded regions in Figure 9.13b).

Length Scale $\sim k^{-1/3}$.

- The GO field is as described for the previous case, although this time the phase shift associated with each contribution will be $\mathcal{O}(k^{2/3})$.
- The surface field no longer appears to come from the origin. Contributions still arise from those points whose normal geodesics pass through the observation point. Surface fresnel regions are still set up from either end of the source, but no longer appear to be centred at the origin—in Figure 9.14b) if the observer is in the direction given by the rays, they will see distinct contributions to the field from each point marked by a clear circle.

Length Scale ~ 1.

- The GO field is no longer equivalent to that from a point source at the origin. The observer whose projection onto the tangent plane is in the direction of the rays in Figure 9.15a) will see distinct contributions form each part of the spiral indicated by a clear circle. The shadow boundary regions will also no longer appear to come from the origin.

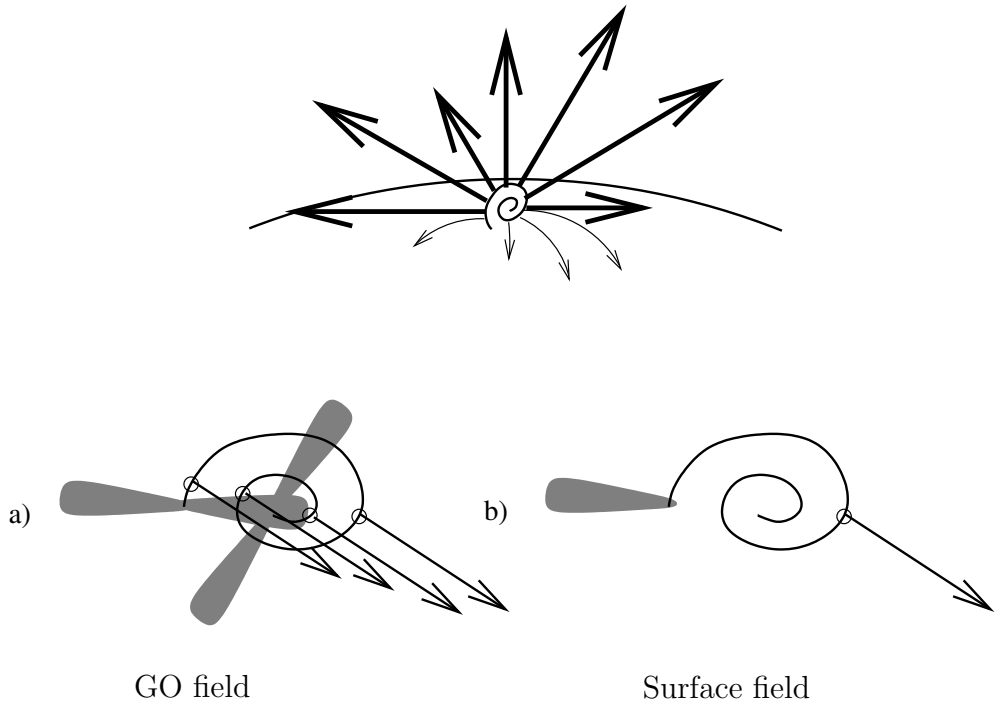


Figure 9.15: Spiral with length scale ~ 1.

- The surface field is dominated by the point on the source closest to the observer as illustrated in Figure 9.15b). Thus, in general it will only be necessary to consider one surface ray passing through each observation point. In addition we will in general only have to worry about one (rather than four) surface fresnel regions.

9.4.1 Out of Phase excitation

This has already been discussed. With a phase dependence of $kt\cos\alpha$, contributions to the GO/surface fields now propagate along rays/geodesics launched at an angle of $\pi/2-\alpha$ to the direction of increasing t.

9.4.2 Discontinuous Sources

At a discontinuity of either the phase or the amplitude we simply split the antenna and consider the two separate continuous problems, relying on the linearity of the system. For the GO field, we simply add the GO field from each of the smaller antennas together. However, to obtain the leading order surface field, more care is needed. We take an $\mathcal{O}(1)$ spiral with a general discontinuity (phase and amplitude). In Figure 9.16 there is a discontinuity in the excitation of the antenna at the arrow

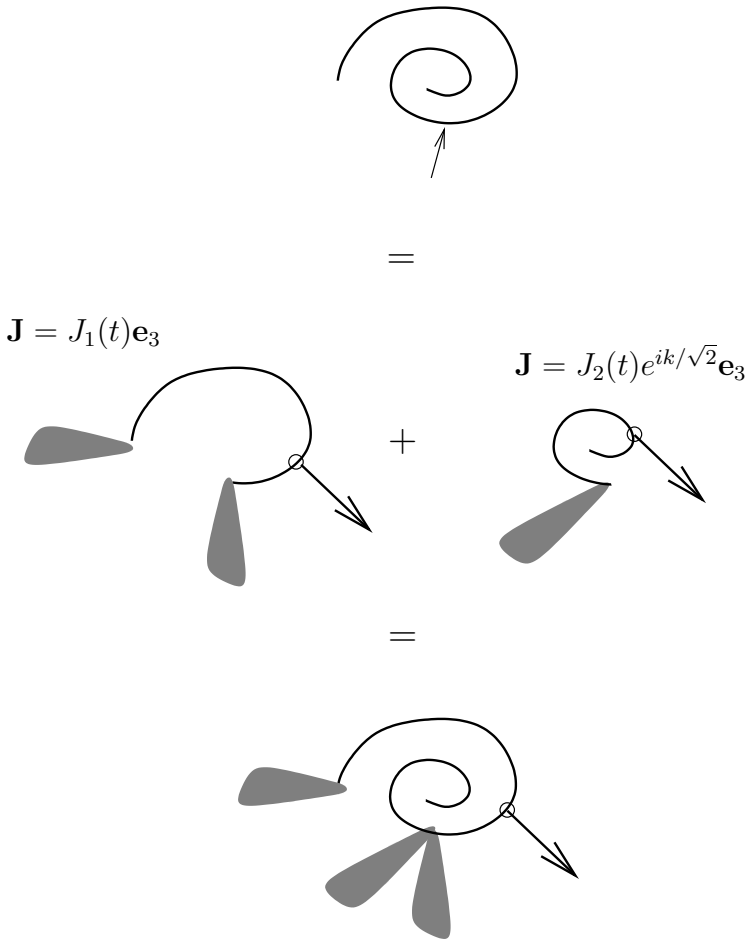


Figure 9.16: General discontinuity on the outer loop of an $\mathcal{O}(1)$ spiral.

marked in the top picture. If the discontinuity were to occur on an inner loop of the spiral it would not be detected in the dominant surface field—see Figure 9.15. We split the antenna at the discontinuity. The behaviour of the dominant surface field for each of the two smaller (but still $\mathcal{O}(1)$) spirals is illustrated on the next line. Again, the projection of the observer's direction on the tangent plane is given by the rays. The observer will receive a dominant contribution from the parts of the antennas indicated by a clear circle. The shaded regions are the surface fresnel regions and the arrows indicate typical surface rays. These two surface fields are added together and the dominant surface field given in the final picture. For the case illustrated in Figure 9.16 there will be three contributions to the higher order diffracted field—one from each endpoint and one from the discontinuity.

Chapter 10

Conclusions and Further Work

This thesis has been motivated by the desire to increase the efficiency and accuracy of numerical algorithms used to calcuate the E-M fields that arise due to sources in the presence of scatterers. Part 1 is background material, with results of industrial importance being found in parts 2 and 3.

10.1 Summary of Results

In part 1 we described the model and introduced the ray theory technique. A WKB ansatz was taken for the field and the initial data integrated along characteristics (or rays) to obtain the solution. We considered the specific example of a plane wave impinging on a convex cylinder. This yielded a lit region where incident and reflected rays are present, and a shadow region behind the cylinder where the leading order field is zero. The ray solution broke down at the tangency point (where the incident field is tangent to the cylinder). Scattering by a convex cylinder is just one of the diffraction problems considered in Keller's GTD. This describes the ray pictures obtained for a variety of canonical problems. We summarised the results for diffraction by edges, tips, curved structures, changes in the material property and at a caustic.

Part 2 is concerned with sources away from structures. We began §4 by reviewing the Sommerfeld problem. Here a plane wave field is incident on a semi-infinite flat plate in two dimensions. In the high frequency limit, the expansion of the exact solution revealed that the scattered field is composed of a reflected field from the plate (with the angle of reflection equal to the angle of incidence) and a higher order radially diffracted field from the tip. The expansion becomes non-uniform close to two lines—the incident and reflected shadow boundaries—which are respectively where the incident and diffracted and the reflected and diffracted rays coincide. We introduced shadow

boundary regions of width $\mathcal{O}(k^{-1/2})$ about these lines. The solution was found to be an error function which smoothly matches between the fields on either side. A finite flat plate produces shadow boundary regions from both ends which merge at an $\mathcal{O}(k)$ distance from the source to form a Fraunhofer region. The corresponding regions for a finite line source in three dimensions were also investigated in §4. The same asymptotic picture was obtained as for the finite plate in two dimensions. Various extensions to the Sommerfeld problem were then considered—illumination of a semi-infinite plate by a point source produces an inner region problem at the tip identical to that due to plane wave illumination. Thus the leading order ray picture consisting of reflected and diffracted fields could be constructed immediately. However, the shadow boundary regions were found to have different solutions from those for plane wave incidence. We concluded the chapter with an investigation into sources which focus their energy at a point. If the focal point is an $\mathcal{O}(1)$ distance from the source we found that the shadow boundary regions from either end of the source shrink in width as they approach the focal point and reform on the other side of an $\mathcal{O}(k^{-1})$ region at the caustic. Moreover, they appear to remember that they were originally set up at the source and not at the caustic. There is also a $\pi/2$ jump in the phase as we pass through the caustic. For a focal point at an $\mathcal{O}(k)$ distance from the source we showed that the growth of the shadow boundary regions dominates the convergence of the leading order rays and that the focal point lies in the Fraunhofer region.

Chapter 5 is of fundamental importance as many of the diffraction effects especially relevant to the aerospace industry are examined for the first time here. The main results concerned scattering of an arbitrary plane wave by an arbitrary three-dimensional convex body. We considerably extended the set of problems for which we can write down an asymptotic representation of the solution. We began by looking at the specific case where the incident rays fall normally to the horizon. Consideration of a Fock-Leontovič (F-L) region at the tangency point revealed that a non-zero surface field is set up that propagates along the surface geodesics and that decays exponentially as it travels into the shadow. This is referred to as the Airy layer. From the Airy layer, creeping rays are launched tangentially to the surface. We then introduced a shadow boundary structure to match between the $\mathcal{O}(1)$ incident and reflected rays in the lit region and the exponentially small creeping ray fields in the shadow. We found that there is a shadow boundary region of $\mathcal{O}(k^{-1/2})$ width which smoothly switches the incident rays on and off, and a transition region of width $\mathcal{O}(k^{-1/3})$ which allows a smooth match between the reflected and creeping ray fields. The case where the incident field no longer falls normally on the horizon was shown to have the same

asymptotic structure and solution. Of key importance in solving this E-M problem was the fact that, in the high frequency limit, the incident and surface fields could be de-coupled into two perpendicular modes. The magnetically/electrically polarised modes were defined as having the magnetic/electric field entirely parallel to the scatterer along the horizon. The problem for each of these polarisations reduces to the scalar equations of acoustics with either a Dirichlet or a Neumann boundary condition. The exponential decay associated with electrically polarised surface modes is greater than that for magnetically polarised surface modes—the latter are thus more important in practice. In §5.5 we considered the fields due to a point source at an $\mathcal{O}(1)$ distance from a convex scatterer. Although we were unable to completely solve this problem, we obtained a complete asymptotic description of the scattered fields that arise when a convex cylinder is illuminated by a line source that is parallel to, and at an $\mathcal{O}(1)$ distance from, the axis of the cylinder in §5.6. Just as in the extension to the Sommerfeld problem we found that all the fields are the same as those due to plane wave illumination with the exception of the $\mathcal{O}(k^{-1/2})$ shadow boundary region where the field now has a different form. The chapter concluded with a brief discussion of whispering gallery (WG) modes. These are solution modes close to the surface of a concave scatterer which allow energy to propagate around the boundary without exhibiting any decay—the surface field does not shed energy as occurs on convex boundaries. The classic open problem of the transition from creeping rays to WG modes at a saddle point was also outlined.

Part 3 is concerned with sources close to scatterers. In §6 we considered the problem of a source on a perfectly conducting convex scatterer. The resulting ray picture comes as no surprise—geometrical optics rays launched into the lit region and creeping rays into the shadow. However, to calculate the amplitudes of the creeping ray fields it is necessary to consider an additional inner-F-L region in the neighbourhood of the source. We also showed that there is no longer any need for the $\mathcal{O}(k^{-1/2})$ shadow boundary region between lit and shadow regions. The transition region is able to match between the lit and shadow regions. We showed that no electrically polarised fields may be set up by this source configuration. Thus we only needed to solve one set of scalar equations which reduced our work considerably. The results we derived are only valid provided that the principal radii of curvature of the surface are both $\mathcal{O}(1)$—that is, large compared to a wavelength. As one or more principal curvatures tends towards zero, the field expansions in the F-L and Airy layer regions become non-uniform. We investigated the surface fields due to a source on a cylinder to gain insight. We introduced two additional asymptotic regions close to the generator of

the cylinder on which the source lies. This guaranteed a smoothly varying surface field everywhere on the cylinder. The chapter concluded with a discussion of the asymptotic structure of the surface fields generated by a source lying on an inflexion line of a cylindrical perfect conductor. An asymptotic region in the neighbourhood of the line of inflexion is required to ensure a smoothly varying field. The problem reduces to the unsolved equation first obtained when considering the transition from creeping rays to WG modes in §5.7.2.

In §7 we investigated the fields that arise when a source is placed at an $\mathcal{O}(k^{-2/3})$ distance from the surface. This corresponds to a source lying in the F-L region. We found an identical asymptotic structure to §6 with slightly different solutions in each region. In addition we found that the source could now excite both electrically and magnetically polarised fields. We then investigated the limits as the source approaches the surface and goes off to infinity and showed that the asymptotic solutions tend towards those for a source on the surface and for a source at an $\mathcal{O}(1)$ distance from the surface respectively.

In §8 we provided a description of the fields generated by arrays of sources on a surface. We showed that employment of the Euler-Maclaurin summation formula yields good approximations for simple one- and two-dimensional arrays of effective point sources. More general arrays of line elements were shown to be equivalent to several arrays of point sources. We also compared the fields generated by arrays with those due to continuously distributed sources. There is a correspondence between the fields produced by both configurations.

In §9 we tied together many of the results and ideas obtained earlier in the thesis. We considered more general line sources lying in the surface. The behaviour of the GO and surface fields is discussed for sources with lengthscales $o(k^{-1}), \mathcal{O}(k^{-2/3}), \mathcal{O}(k^{-1/3})$ and $\mathcal{O}(1)$. The first of these corresponds to a source smaller than a wavelength of the radiation and we showed that it resembles an isotropic point source; the second corresponds to a source entirely contained within an inner-F-L region; the third length scale has the property that contributions to the surface field from different parts of the source will have the same order of magnitude; the largest sources were shown to be reducible to a two-dimensional problem with inner-F-L and F-L regions being introduced along the length of the source. For open sources that are longer than $k^{-1/2}$ in length, we also had to take into account the discontinuities at the end points. These set up a higher order diffracted field propagating along the geodesics passing through each end of the source. Where these geodesics coincide with the

leading order contributions from the rest of the source, the expansion of the surface field becomes non-uniform and we introduced a surface fresnel region to take care of this. It transpired that the field in the surface fresnel region exhibits the exponential decay along the geodesics associated with the surface fields and the error function profile associated with shadow boundaries. We concluded the chapter with a discussion of how these results would be applied in practice to a spiral antenna of different lengthscales.

10.2 Further Work

Although we have made progress on a variety of problems, much remains to be done in this area. We list some of the problems still requiring attention.

- Everything in this thesis has been concerned with perfectly conducting scatterers. The impedance (mixed boundary condition) case also needs to be considered within the asymptotic framework we have outlined. Some preliminary results concerning scattering by convex bodies can be found for example in [35]. The nature of the reflected and surface waves changes here. In particular, this will have implications for the shadow boundary structure existing between the lit and shadow regions.

- In §5.7.2 we outlined the open problem of the transition from creeping ray to whispering gallery modes at an inflexion point of a surface. The same unsolved equation was also obtained in §6.10. A solution to this unresolved problem will significantly increase the applicability of ray theory techniques for high frequency scattering.

- In §9.2.3 we were only able to demonstrate a successful match between the Airy layer and surface fresnel fields for the case $G(s_1, 0) = 1$. We need to extend this matching to cater for general surfaces.

- Discontinuities in either the impedance or curvatures of a scatterer produce higher order diffracted fields. The ray picture is described in [20] and [31] for various configurations. However, it would be interesting to consider these problems within the asymptotic framework that we have described in this thesis. The diffraction of surface fields by a jump in curvature or impedance is another variation of this problem.

- At a more practical level, before ray theory techniques may be accurately used to calculate asymptotic representations of the far field, the *actual* source strength needs to be known. A reliable way of obtaining this information from near-field measurements of the source is desirable. Although this is an ill-posed problem, additional information about the source may allow us to make some progress here.

Appendix A

Fourier Transform of the Heaviside Function

The Heaviside function $H(x)$ is defined as

$$H(x) \;=\; \begin{cases} 0, & x < 0, \\ 1, & x > 0. \end{cases} \tag{A.1}$$

We can write this as

$$H(x) \;=\; \frac{1}{2}\left(1 + \mathrm{sgn}(x)\right), \tag{A.2}$$

where

$$\mathrm{sgn}(x) \;=\; \begin{cases} -1, & x < 0, \\ 0, & x = 0, \\ 1, & x > 0. \end{cases} \tag{A.3}$$

We introduce the inner product

$$< f, g > \;=\; \int_{-\infty}^{\infty} f(x)g(x)\,\mathrm{d}x. \tag{A.4}$$

Then, upon differentiating (A.4), for any test function ϕ that vanishes at infinity we have

$$< \phi, \mathrm{sgn}' > \;=\; - < \phi', \mathrm{sgn} > \;=\; 2\phi(0). \tag{A.5}$$

This tells us that

$$\mathrm{sgn}' \;=\; 2\delta, \tag{A.6}$$

in the distribution sense—*i.e.* for all functions ϕ

$$< \phi, \mathrm{sgn}' > \;=\; < \phi, 2\delta > . \tag{A.7}$$

Taking the Fourier transform of (A.6) reveals

$$\overline{\text{sgn}} \;=\; \frac{2i}{s}\bar{\delta}. \tag{A.8}$$

By using the definitions of the inner product and the Fourier transform we can show

$$<\bar{\delta},\phi> \;=\; <\delta,\bar{\phi}> \;=\; \int_{-\infty}^{\infty}\phi(x)e^{isx}\,\mathrm{d}x\Big|_{s=0} \;=\; <1,\phi>\,. \tag{A.9}$$

Therefore

$$\bar{\delta} \;=\; 1. \tag{A.10}$$

To calculate the Fourier transform of 1, we use (A.10) and the similarity of the Fourier transform and its inverse to say

$$\bar{1} \;=\; 2\pi\delta. \tag{A.11}$$

Combining (A.8), (A.10) and (A.11) yields the final result

$$\overline{H(s)} \;=\; \frac{i}{s}+\pi\delta(s). \tag{A.12}$$

Appendix B

Canonical Problem for Small α

Consider the problem

$$\nabla^2\phi + k^2\phi = 0, \quad y > 0, \tag{B.1}$$

$$\frac{\partial\phi}{\partial y} = H(x)e^{ik\cos\alpha x}, \quad y = 0, \tag{B.2}$$

where $H(x)$ is the Heaviside function. We will consider the two cases $\alpha = \mathcal{O}(1)$ and $\alpha \ll \mathcal{O}(1)$. In both cases we begin by taking a Fourier transform of the problem with respect to x to obtain the exact solution

$$\phi = \frac{1}{2\pi k^{1/2}} \int_{-\infty}^{\infty} \left(\frac{i}{s+\cos\alpha} + \pi\delta\left(s+\cos\alpha\right) \right) \frac{e^{ik\left(\left(1-s^2\right)^{1/2}y - isx\right)}}{\left(1-s^2\right)^{1/2}} \,\mathrm{d}s. \tag{B.3}$$

We may evaluate the delta function contribution immediately, ϕ' say, leaving

$$\phi = \phi' + \frac{1}{2\pi k^{1/2}} \int_{-\infty}^{\infty} \frac{i}{s+\cos\alpha} \frac{e^{ik\left(\left(1-s^2\right)^{1/2}y - isx\right)}}{\left(1-s^2\right)^{1/2}} \,\mathrm{d}s. \tag{B.4}$$

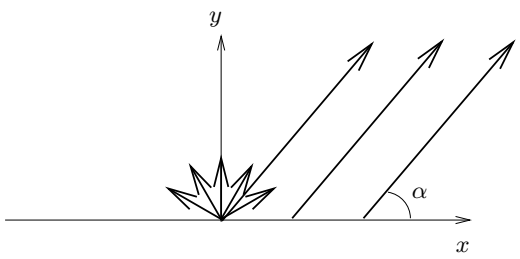
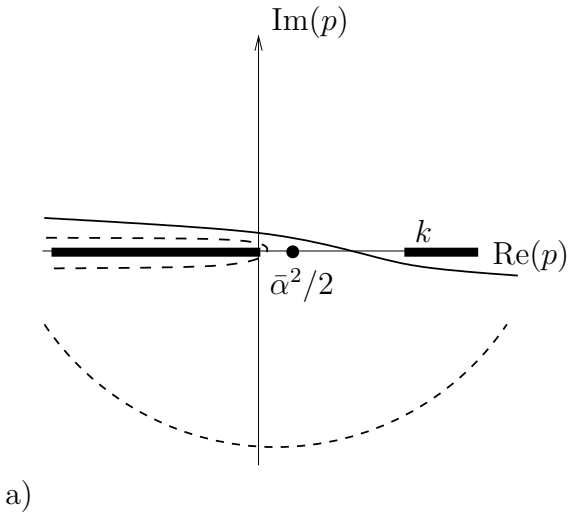
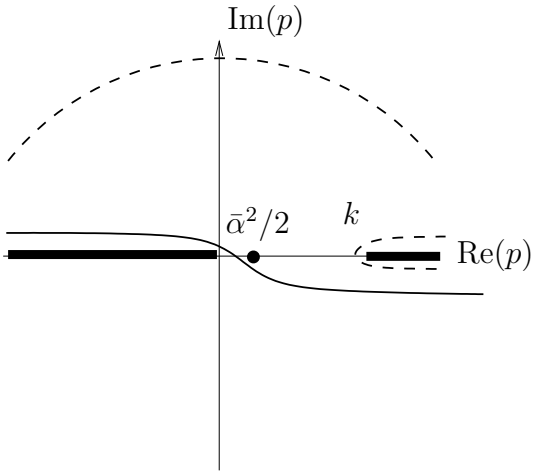


Figure B.1: Ray picture for $\alpha = \mathcal{O}(1)$.



a)



b)

Figure B.2: Integration contours for $\alpha = \mathcal{O}(k^{-1/2})$ when a) $x > 0$, b) $x < 0$. Heavy solid lines are branch cuts.

$\alpha = \mathcal{O}(1)$

We deform the contour into a steepest descents contour through the saddle point (exactly as in Figure 4.5). Depending on the sense in which the steepest descents contour encloses the pole, the pole contribution and ϕ' either cancel each other out or add together to produce the leading order radiated field. The saddle point contribution is always present and corresponds to the diffracted field from the origin. In short, the solution may be written

$$\phi \sim \frac{e^{ik\sin\alpha y + ik\cos\alpha x}}{k\sin\alpha} + \frac{1}{\sqrt{2\pi r}k^{3/2}}\frac{(\cos\theta)^{3/2}}{(\sin\theta)^{1/2}}\frac{e^{ikr+i\pi/4}}{(\cos\alpha-\cos\theta)}, \tag{B.5}$$

with the first term only present in $\theta < \alpha$ as illustrated in Figure B.1.

$\alpha \ll 1$

For small α we scale $\bar{\alpha} = k^{\beta}\alpha$. Expanding $\cos\alpha$ for small α implies that that the dominant contribution to (B.4) comes from near $s = -1$. Thus we set

$$s = -1 + k^{-2\beta}p. \tag{B.6}$$

Upon scaling $\bar{y} = k^{\beta}y$ and taking $\beta = 1/2$ (B.4) becomes

$$\phi \sim \phi' + \frac{e^{ikx}}{2^{3/2}\pi k^{1/2}}\int_{-\infty}^{\infty}\frac{i}{p-\frac{\bar{\alpha}^2}{2}}\frac{e^{i\sqrt{2p}\bar{y}-ipx}}{\sqrt{p}}\,\mathrm{d}p. \tag{B.7}$$

As $\alpha \to 0$ the steepest descents contours wrap themselves around the branch cuts as illustrated in Figure B.2. We must now close the contour in either the upper or lower half plane depending on $x \gtrless 0$. In $x > 0$ the contour is as illustrated in Figure B.2a). The pole contribution and ϕ' will add together to give us a leading order field. In addition there is a branch cut contribution (which we have not been able to evaluate) which will be the same size as the leading order field arising from the pole—namely $\mathcal{O}(k^{-1/2})$. For $x < 0$ the pole contribution and ϕ' cancel leaving us with just a branch cut contribution of size $\mathcal{O}(k^{-1})$. Again we have not been able to evaluate this contribution. The contour is illustrated in Figure B.2b). The pole contribution and ϕ' may be associated with the leading order field in (B.5) and the branch cut contributions with the diffracted field. To explain the difference in size of the diffracted field for $x \gtrless 0$ we remind the reader that in §4.1.2 we introduced shadow boundary regions where the expansion of the field became non-uniform. This was precisely where the

diffracted field was parallel to the leading order radiated field. In terms of the x, y coordinates, the dominant radiated and diffracted fields are indeed parallel to lowest order when we are close to $y = 0$. Thus we would expect these two fields to have the same size. The above analysis indicates that there is a boundary layer of width $\mathcal{O}(k^{-1/2})$ close to $y = 0$ for positive x where the field is $\mathcal{O}(k^{-1/2})$ in size, with the field being $\mathcal{O}(k^{-1})$ everywhere else. We also comment that the case $\alpha = 0$ is encompassed within the canonical scaling $\alpha = \mathcal{O}(k^{-1/2})$.

Appendix C

Maxwell's Equations in Geodesic Coordinates

We derive Maxwell's equations in terms of the geodesic normal coordinate system described in section 5.1.

We first calculate ∇s_j[1] in terms of unit vectors $\mathbf{e}_i$, which are defined by

$$\mathbf{e}_i = \frac{1}{h_i}\frac{\partial \mathbf{r}}{\partial s_i}, \tag{C.1}$$

where

$$h_i^2 = \frac{\partial \mathbf{r}}{\partial s_i} \cdot \frac{\partial \mathbf{r}}{\partial s_i}. \tag{C.2}$$

Using this definition and (5.1) we see that $\mathbf{e}_1$, $\mathbf{e}_2$ lie in the surface and that $\mathbf{e}_3 = \mathbf{n}$ is normal to the surface. ∇s_j will be in a direction perpendicular to level sets of s_j. It is also immediately apparent that $h_3 = 1$. Taking $\mathbf{e}_1 \cdot \mathbf{e}_2 = \cos\gamma$ we have—see e.g. Figure C.1

$$\nabla s_1 = |\nabla s_1| \left(\frac{1}{\sin\gamma}\mathbf{e}_1 - \frac{1}{\tan\gamma}\mathbf{e}_2 \right), \tag{C.3}$$

$$\nabla s_2 = |\nabla s_2| \left(-\frac{1}{\tan\gamma}\mathbf{e}_1 + \frac{1}{\sin\gamma}\mathbf{e}_2 \right), \tag{C.4}$$

$$\nabla s_3 = |\nabla s_3|\mathbf{e}_3. \tag{C.5}$$

In addition we can say

$$|\nabla s_1| = \frac{1}{h_1 \sin\gamma}, \tag{C.6}$$

$$|\nabla s_2| = \frac{1}{h_2 \sin\gamma}, \tag{C.7}$$

$$|\nabla s_3| = 1. \tag{C.8}$$

[1] We note that similar calculations in [33] go astray. We do not anticipate that this will change any of the results derived therein.

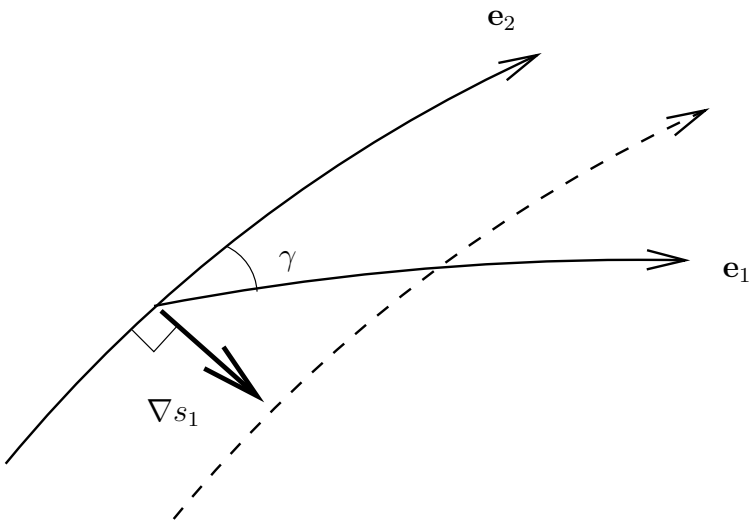


Figure C.1: Calculation of ∇s_1.

Solving (C.3) - (C.4) for $\mathbf{e}_1, \mathbf{e}_2$ yields

$$\mathbf{e}_1 = h_1 \nabla s_1 + \cos\gamma h_2 \nabla s_2, \tag{C.9}$$

$$\mathbf{e}_2 = \cos\gamma h_1 \nabla s_1 + h_2 \nabla s_2. \tag{C.10}$$

The following identities will also be useful

$$\mathbf{e}_1 \wedge \mathbf{e}_2 = \sin\gamma \mathbf{e}_3, \tag{C.11}$$

$$\mathbf{e}_1 \wedge \mathbf{e}_3 = -\frac{1}{\sin\gamma}\mathbf{e}_2 + \frac{1}{\tan\gamma}\mathbf{e}_1, \tag{C.12}$$

$$\mathbf{e}_2 \wedge \mathbf{e}_3 = \frac{1}{\sin\gamma}\mathbf{e}_1 - \frac{1}{\tan\gamma}\mathbf{e}_2. \tag{C.13}$$

Using the vector identities

$$\nabla \wedge f\mathbf{u} = \nabla f \wedge \mathbf{u} + f \nabla \wedge \mathbf{u}, \tag{C.14}$$

$$\nabla f = \sum \frac{\partial f}{\partial s_j} \nabla s_j, \tag{C.15}$$

along with (C.9) - (C.10), we can write

$$\begin{aligned} \nabla \wedge \mathbf{F} &= \sum_i \nabla \wedge (F_i \mathbf{e}_i), \\ &= \sum_i \nabla F_i \wedge \mathbf{e}_i + F_i \nabla \wedge \mathbf{e}_i, \\ &= \sum_{i,j} \frac{\partial F_i}{\partial s_j} \nabla s_j \wedge \mathbf{e}_i \\ &+ F_1 \nabla \wedge (h_1 \nabla s_1 + \cos\gamma h_2 \nabla s_2) + F_2 \nabla \wedge (h_1 \cos\gamma \nabla s_1 + h_2 \nabla s_2). \end{aligned} \tag{C.16}$$

A further application of (C.14) on the second and third terms, followed by manipulation using (C.3) - (C.8) and (C.11) - (C.13) eventually gives us the time-harmonic Maxwell's equations in the high frequency limit as

$$\frac{1}{h_2\sin\gamma}\frac{\partial E_3}{\partial s_2}-\frac{1}{\sin\gamma}\frac{\partial E_2}{\partial s_3}-\frac{1}{\tan\gamma}\frac{\partial E_1}{\partial s_3}-\frac{E_1}{h_2\sin\gamma}\frac{\partial}{\partial s_3}(h_2\cos\gamma)-\frac{E_2}{h_2\sin\gamma}\frac{\partial h_2}{\partial s_3}-ikH_1 = 0, \tag{C.17}$$

$$\frac{1}{\sin\gamma}\frac{\partial E_1}{\partial s_3}+\frac{1}{\tan\gamma}\frac{\partial E_2}{\partial s_3}-\frac{1}{h_1\sin\gamma}\frac{\partial E_3}{\partial s_1}+\frac{E_1}{h_1\sin\gamma}\frac{\partial h_1}{\partial s_3}+\frac{E_2}{h_1\sin\gamma}\frac{\partial}{\partial s_3}(h_1\cos\gamma)-ikH_2 = 0, \tag{C.18}$$

$$\begin{aligned}&\frac{1}{h_1\tan\gamma}\frac{\partial E_1}{\partial s_1}-\frac{1}{h_2\sin\gamma}\frac{\partial E_1}{\partial s_2}+\frac{1}{h_1\sin\gamma}\frac{\partial E_2}{\partial s_1}-\frac{1}{h_2\tan\gamma}\frac{\partial E_2}{\partial s_2}-\frac{E_1}{h_1h_2\sin\gamma}\frac{\partial h_1}{\partial s_2}\\&+\frac{E_1}{h_1h_2\sin\gamma}\frac{\partial}{\partial s_1}(h_2\cos\gamma)+\frac{E_2}{h_1h_2\sin\gamma}\frac{\partial h_2}{\partial s_1}-\frac{E_2}{h_1h_2\sin\gamma}\frac{\partial}{\partial s_2}(h_1\cos\gamma)-ikH_3 = 0,\end{aligned} \tag{C.19}$$

$$\frac{1}{h_2\sin\gamma}\frac{\partial H_3}{\partial s_2}-\frac{1}{\sin\gamma}\frac{\partial H_2}{\partial s_3}-\frac{1}{\tan\gamma}\frac{\partial H_1}{\partial s_3}-\frac{H_1}{h_2\sin\gamma}\frac{\partial}{\partial s_3}(h_2\cos\gamma)-\frac{H_2}{h_2\sin\gamma}\frac{\partial h_2}{\partial s_3}+ikE_1 = 0, \tag{C.20}$$

$$\frac{1}{\sin\gamma}\frac{\partial H_1}{\partial s_3}+\frac{1}{\tan\gamma}\frac{\partial H_2}{\partial s_3}-\frac{1}{h_1\sin\gamma}\frac{\partial H_3}{\partial s_1}+\frac{H_1}{h_1\sin\gamma}\frac{\partial h_1}{\partial s_3}+\frac{H_2}{h_1\sin\gamma}\frac{\partial}{\partial s_3}(h_1\cos\gamma)+ikE_2 = 0, \tag{C.21}$$

$$\begin{aligned}&\frac{1}{h_1\tan\gamma}\frac{\partial H_1}{\partial s_1}-\frac{1}{h_2\sin\gamma}\frac{\partial H_1}{\partial s_2}+\frac{1}{h_1\sin\gamma}\frac{\partial H_2}{\partial s_1}-\frac{1}{h_2\tan\gamma}\frac{\partial H_2}{\partial s_2}-\frac{H_1}{h_1h_2\sin\gamma}\frac{\partial h_1}{\partial s_2}\\&+\frac{H_1}{h_1h_2\sin\gamma}\frac{\partial}{\partial s_1}(h_2\cos\gamma)+\frac{H_2}{h_1h_2\sin\gamma}\frac{\partial h_2}{\partial s_1}-\frac{H_2}{h_1h_2\sin\gamma}\frac{\partial}{\partial s_2}(h_1\cos\gamma)+ikE_3 = 0.\end{aligned} \tag{C.22}$$

All that remains now is to obtain expressions for h_i and γ in terms of the first and second fundamental forms (5.1) - (5.2).

From (5.1) we have

$$\frac{\partial\mathbf{r}}{\partial s_1} = \frac{\partial\mathbf{R}}{\partial s_1}+s_3\frac{\partial\mathbf{n}}{\partial s_1}, \tag{C.23}$$

$$\frac{\partial\mathbf{r}}{\partial s_2} = \frac{\partial\mathbf{R}}{\partial s_2}+s_3\frac{\partial\mathbf{n}}{\partial s_2}, \tag{C.24}$$

$$\frac{\partial\mathbf{r}}{\partial s_3} = \mathbf{n}. \tag{C.25}$$

Now $\mathbf{n}$ is a unit vector. It follows that

$$\frac{\partial\mathbf{n}}{\partial s_1}\cdot\mathbf{n} = \frac{\partial\mathbf{n}}{\partial s_2}\cdot\mathbf{n} = 0. \tag{C.26}$$

As $\frac{\partial \mathbf{R}}{\partial s_i}$ lies in the surface, $\frac{\partial \mathbf{R}}{\partial s_i} \cdot \mathbf{n} = 0$, and hence

$$\frac{\partial \mathbf{r}}{\partial s_1} \cdot \frac{\partial \mathbf{r}}{\partial s_3} = 0, \tag{C.27}$$

$$\frac{\partial \mathbf{r}}{\partial s_2} \cdot \frac{\partial \mathbf{r}}{\partial s_3} = 0. \tag{C.28}$$

We also have

$$\frac{\partial \mathbf{R}}{\partial s_i \partial s_j} \cdot \mathbf{n} + \frac{\partial \mathbf{R}}{\partial s_i} \cdot \frac{\partial \mathbf{n}}{\partial s_j} = 0. \tag{C.29}$$

Since $F = 0$, we can deduce that

$$\frac{\partial \mathbf{r}}{\partial s_1} \cdot \frac{\partial \mathbf{r}}{\partial s_2} = -2s_3 M + s_3^2 \frac{\partial \mathbf{n}}{\partial s_1} \cdot \frac{\partial \mathbf{n}}{\partial s_2}, \tag{C.30}$$

and that the vectors $\frac{\partial \mathbf{R}}{\partial s_1}$, $\frac{\partial \mathbf{R}}{\partial s_2}$, $\mathbf{n}$ are orthogonal. Thus we can write

$$\frac{\partial \mathbf{n}}{\partial s_1} = a\frac{\partial \mathbf{R}}{\partial s_1} + b\frac{\partial \mathbf{R}}{\partial s_2} + c\mathbf{n}, \tag{C.31}$$

where

$$\begin{aligned} a &= \left(\frac{\partial \mathbf{n}}{\partial s_1} \cdot \frac{\partial \mathbf{R}}{\partial s_1}\right) / \left(\frac{\partial \mathbf{R}}{\partial s_1} \cdot \frac{\partial \mathbf{R}}{\partial s_1}\right) = -\frac{L}{E}, \\ b &= \left(\frac{\partial \mathbf{n}}{\partial s_1} \cdot \frac{\partial \mathbf{R}}{\partial s_2}\right) / \left(\frac{\partial \mathbf{R}}{\partial s_2} \cdot \frac{\partial \mathbf{R}}{\partial s_2}\right) = -\frac{M}{G}, \\ c &= \frac{\partial \mathbf{n}}{\partial s_1} \cdot \mathbf{n} = 0. \end{aligned} \tag{C.32}$$

Doing the same for $\frac{\partial \mathbf{n}}{\partial s_2}$ we have

$$\frac{\partial \mathbf{n}}{\partial s_1} = -\frac{L}{E}\frac{\partial \mathbf{R}}{\partial s_1} - \frac{M}{G}\frac{\partial \mathbf{R}}{\partial s_2}, \tag{C.33}$$

$$\frac{\partial \mathbf{n}}{\partial s_2} = -\frac{M}{E}\frac{\partial \mathbf{R}}{\partial s_1} - \frac{N}{G}\frac{\partial \mathbf{R}}{\partial s_2}. \tag{C.34}$$

We can therefore write the scaling factors as

$$h_1^2 = E - 2s_3 L + s_3^2 \left(\frac{L^2}{E} + \frac{M^2}{G}\right), \tag{C.35}$$

$$h_2^2 = G - 2s_3 N + s_3^2 \left(\frac{M^2}{E} + \frac{N^2}{G}\right), \tag{C.36}$$

$$h_3^2 = 1. \tag{C.37}$$

Also,

$$\begin{aligned} \cos\gamma &= \frac{\mathbf{r}_1 \cdot \mathbf{r}_2}{h_1 h_2} \\ &= \frac{s_3 M \left(s_3 \left(\frac{L}{E} + \frac{N}{G}\right) - 2\right)}{\left(E - 2s_3 L + s_3^2 \left(\frac{L^2}{E} + \frac{M^2}{G}\right)\right)^{1/2} \left(G - 2s_3 N + s_3^2 \left(\frac{M^2}{E} + \frac{N^2}{G}\right)\right)^{1/2}}. \end{aligned} \tag{C.38}$$

Appendix D

Reciprocity

Reciprocity is a useful tool which lets us construct solutions to problems based on our knowledge of other solutions. In words, reciprocity states: the field at A due to a unit source at B is equal to the field at B due to a unit source at A. In free space this is a natural consequence of the two and three dimensional Green's functions being symmetric in the source and observation points $\mathbf{r}'$, $\mathbf{r}$, but is not immediately obvious in the presence of boundaries. We consider the two problems

$$\begin{aligned} \nabla \wedge \mathbf{E}_1 - ik\mathbf{H}_1 &= \mathbf{0}, & \text{(D.1)} \\ \nabla \wedge \mathbf{H}_1 + ik\mathbf{E}_1 &= \mathbf{J}_1\delta(\mathbf{r}-\mathbf{r}_1), & \text{(D.2)} \end{aligned}$$

and

$$\begin{aligned} \nabla \wedge \mathbf{E}_2 - ik\mathbf{H}_2 &= \mathbf{0}, & \text{(D.3)} \\ \nabla \wedge \mathbf{H}_2 + ik\mathbf{E}_2 &= \mathbf{J}_2\delta(\mathbf{r}-\mathbf{r}_1), & \text{(D.4)} \end{aligned}$$

in the domain V which encloses perfectly conducting surfaces S and is bounded by ∂V. Taking the dot product of (D.2) with $\mathbf{E}_2$ and (D.4) with $\mathbf{E}_1$ and integrating the difference over V gives

$$\int_V \mathbf{E}_2 \,.\, \nabla \wedge \mathbf{H}_1 - \mathbf{E}_1 \,.\, \nabla \wedge \mathbf{H}_2 \,\mathrm{d}V = \mathbf{E}_2(\mathbf{r}_1) \,.\, \mathbf{J}_1 - \mathbf{E}_1(\mathbf{r}_2) \,.\, \mathbf{J}_2. \qquad \text{(D.5)}$$

The identity

$$\nabla \,.\, (\mathbf{a} \wedge \mathbf{b}) = \mathbf{a} \,.\, \nabla \wedge \mathbf{b} - \mathbf{b} \,.\, \nabla \wedge \mathbf{a},$$

and the divergence theorem reduces (D.5) to

$$\begin{aligned} \int_{\partial V} (\mathbf{E}_2 \wedge \mathbf{H}_1 - \mathbf{E}_1 \wedge \mathbf{H}_2) \,.\, \mathrm{d}\mathbf{S} + \int_S (\mathbf{E}_2 \wedge \mathbf{H}_1 - \mathbf{E}_1 \wedge \mathbf{H}_2) \,.\, \mathrm{d}\mathbf{S} \\ = \mathbf{E}_2(\mathbf{r}_1) \,.\, \mathbf{J}_1 - \mathbf{E}_1(\mathbf{r}_2) \,.\, \mathbf{J}_2. \qquad \text{(D.6)} \end{aligned}$$

At a large distance from sources and surfaces, the fields looks like those due to a point source, with a $1/kr$ amplitude. This means the integral over ∂V is $\mathcal{O}(k^{-2})$. The integral over S is also zero as the perfectly conducting boundary condition $\mathbf{E} \cdot \mathbf{t} = 0$ tells us that the integrand has no component in the $\mathbf{n}$ direction. We have thus proved reciprocity.

Appendix E

Maxwell's Equations for Surface Fresnel Regions

We take the ansatz

$$\mathbf{F} = e^{iks_1+ik^{1/3}v(s_1)}\left(\mathbf{F}^0+\frac{\mathbf{F}^1}{k^{1/3}}+\frac{\mathbf{F}^2}{k^{1/2}}+\frac{\mathbf{F}^3}{k^{2/3}}+\frac{\mathbf{F}^4}{k^{5/6}}+\frac{\mathbf{F}^5}{k}+\ldots\right), \quad \text{(E.1)}$$

for the fields, where $\tilde{s}_2 = k^{1/2}s_2$ and $\rho = k^{2/3}s_3$. Substituting the ansatz and scalings into Maxwell's equations gives us terms of $\mathcal{O}(k)$:

$$\begin{aligned} H_1^0 &= 0, && \text{(E.2)}\\ E_3^0 + H_2^0 &= 0, && \text{(E.3)}\\ H_3^0 - E_2^0 &= 0, && \text{(E.4)}\\ E_1^0 &= 0, && \text{(E.5)}\\ H_3^0 - E_2^0 &= 0, && \text{(E.6)}\\ E_3^0 + H_2^0 &= 0, && \text{(E.7)} \end{aligned}$$

terms of $\mathcal{O}(k^{2/3})$:

$$\begin{aligned} -\frac{\partial E_2^0}{\partial \rho} - iH_1^1 &= 0, && \text{(E.8)}\\ -iE_3^1 - iH_2^1 &= 0, && \text{(E.9)}\\ iE_2^1 - iH_3^1 &= 0, && \text{(E.10)}\\ -\frac{\partial H_2^0}{\partial \rho} + iE_1^1 &= 0, && \text{(E.11)}\\ -iH_3^1 + iE_2^1 &= 0, && \text{(E.12)}\\ iH_2^1 + iE_3^1 &= 0, && \text{(E.13)} \end{aligned}$$

terms of $\mathcal{O}(k^{1/2})$:

$$\frac{1}{\sqrt{G}}\frac{\partial E_3^0}{\partial \tilde{s}_2} - iH_1^2 = 0, \tag{E.14}$$

$$E_3^2 + H_2^2 = 0, \tag{E.15}$$

$$H_3^2 - E_2^2 = 0, \tag{E.16}$$

$$\frac{1}{\sqrt{G}}\frac{\partial H_3^0}{\partial \tilde{s}_2} + iE_1^2 = 0, \tag{E.17}$$

$$H_3^2 - E_2^2 = 0, \tag{E.18}$$

$$E_3^2 + H_2^2 = 0, \tag{E.19}$$

terms of $\mathcal{O}(k^{1/3})$:

$$H_1^3 = i\frac{\partial E_2^1}{\partial \rho}, \tag{E.20}$$

$$E_3^3 + H_2^3 = -\frac{\partial^2 H_2^0}{\partial \rho^2} + \frac{\partial v}{\partial s_1}H_2^0 - \rho|L|H_2^0, \tag{E.21}$$

$$H_3^3 - E_2^3 = \frac{\partial v}{\partial s_1}E_2^0 - \rho|L|E_2^0, \tag{E.22}$$

$$E_1^3 = -i\frac{\partial H_2^1}{\partial \rho}, \tag{E.23}$$

$$H_3^3 - E_2^3 = \frac{\partial^2 E_2^0}{\partial \rho^2} - \frac{\partial v}{\partial s_1}E_2^0 + \rho|L|E_2^0, \tag{E.24}$$

$$E_3^3 + H_2^3 = -\frac{\partial v}{\partial s_1}H_2^0 + \rho|L|H_2^0, \tag{E.25}$$

terms of $\mathcal{O}(k^{1/6})$:

$$\frac{1}{\sqrt{G}}\frac{\partial E_3^1}{\partial \tilde{s}_2} - \frac{\partial E_2^2}{\partial \rho} - iH_1^4 = 0, \tag{E.26}$$

$$\frac{\partial E_1^2}{\partial \rho} - iE_3^4 - iH_2^4 = 0, \tag{E.27}$$

$$-\frac{1}{\sqrt{G}}\frac{\partial E_1^1}{\partial \tilde{s}_2} + iE_2^4 - iH_3^4 = 0, \tag{E.28}$$

$$\frac{1}{\sqrt{G}}\frac{\partial H_3^1}{\partial \tilde{s}_2} - \frac{\partial H_2^2}{\partial \rho} + iE_1^4 = 0, \tag{E.29}$$

$$\frac{\partial H_1^2}{\partial \rho} - iH_3^4 + iE_2^4 = 0, \tag{E.30}$$

$$-\frac{1}{\sqrt{G}}\frac{\partial H_1^1}{\partial \tilde{s}_2} + iH_2^4 + iE_3^4 = 0, \tag{E.31}$$

and terms of $\mathcal{O}(1)$:

$$H_1^5 = \frac{i\tilde{s}_2}{2G^{3/2}}\frac{\partial G(s_1,0)}{\partial s_2}\frac{\partial E_3^0}{\partial \tilde{s}_2} - iE_2^0\frac{N}{G} + i\frac{\partial E_2^3}{\partial \rho} - \frac{i}{\sqrt{G}}\frac{\partial E_3^2}{\partial \tilde{s}_2}, \quad \text{(E.32)}$$

$$E_3^5 + H_2^5 = -\frac{\partial^2 H_2^1}{\partial \rho^2} + \frac{\partial v}{\partial s_1}H_2^1 - \rho|L|H_2^1 + \frac{2i\rho M}{\sqrt{G}}\frac{\partial E_2^0}{\partial \rho} + i\frac{\partial E_3^0}{\partial s_1} + i\frac{2M}{\sqrt{G}}E_2^0, \quad \text{(E.33)}$$

$$H_3^5 - E_2^5 = \frac{\partial v}{\partial s_1}E_2^1 - \rho|L|E_2^1 - i\frac{\partial E_2^0}{\partial s_1} - i\frac{E_2^0}{\sqrt{G}}\frac{\partial \sqrt{G}}{\partial s_1} - \frac{2\rho M}{\sqrt{G}}E_1^1 + \frac{i}{\sqrt{G}}\frac{\partial E_1^2}{\partial \tilde{s}_2}, \quad \text{(E.34)}$$

$$E_1^5 = -\frac{i\tilde{s}_2}{2G^{3/2}}\frac{\partial G(s_1,0)}{\partial s_2}\frac{\partial H_3^0}{\partial \tilde{s}_2} + iH_2^0\frac{N}{G} - i\frac{\partial H_2^3}{\partial \rho} + \frac{i}{\sqrt{G}}\frac{\partial H_3^2}{\partial \tilde{s}_2}, \quad \text{(E.35)}$$

$$H_3^5 - E_2^5 = \frac{\partial^2 E_2^1}{\partial \rho^2} - \frac{\partial v}{\partial s_1}E_2^1 + \rho|L|E_2^1 + \frac{2i\rho M}{\sqrt{G}}\frac{\partial H_2^0}{\partial \rho} + i\frac{\partial H_3^0}{\partial s_1} + i\frac{2M}{\sqrt{G}}H_2^0, \quad \text{(E.36)}$$

$$E_3^5 + H_2^5 = -\frac{\partial v}{\partial s_1}H_2^1 + \rho|L|H_2^1 + i\frac{\partial H_2^0}{\partial s_1} + i\frac{H_2^0}{\sqrt{G}}\frac{\partial \sqrt{G}}{\partial s_1} + \frac{2\rho M}{\sqrt{G}}H_1^1 - \frac{i}{\sqrt{G}}\frac{\partial H_1^2}{\partial \tilde{s}_2}. \quad \text{(E.37)}$$

Bibliography

[1] Abramowitz and Stegun. *Handbook of Mathematical Functions*. Dover, 1965.

[2] Babič, V.M. and Buldyrev, V.S. *Short-Wavelength Diffraction Theory*. Springer-Verlag, 1972.

[3] Bender, C.M. and Orszag, S.A. *Advanced Mathematical Methods for Scientists and Engineers*. McGraw-Hill, 1978.

[4] Billingham, J. and King, A.C. *Wave Motion*. CUP, 2000.

[5] Bleaney, B.I. and Bleaney, B. *Electricity and Magnetism*. Oxford Science Publications, 1976.

[6] N. Bleistein. *Mathematical Methods for Wave Phenomena*. Academic Press, Inc, 1984.

[7] Bouche, D. and Auzanneau, F. Champ à la surface d'un objet axisymétrique conducteur au voisinage d'un point focal de rayons rampants. *Ann. Télécommun.*, 1992.

[8] Buchal, R.N. and Keller, J.B. Boundary layer problems in diffraction theory. *Comm. Pure Appl Math.*, 13:85–114, 1960.

[9] Chapman, S.J., Lawry, J., Ockendon, J.R., and Tew, R.H. On the theory of complex rays. *SIAM Review*, 41:417–509, 1999.

[10] Engineer, J.C., Tew, R.H., and King, J.R. Diffraction by slender bodies. *European Journal of Applied Mathematics*, 9(2):129–158, 1998.

[11] Felsen and Marcuwitz. *Radiation and Scattering of Waves*. IEEE Press, 1994.

[12] Felsen, L.B. and Idemen, M. Diffraction of a whispering gallery mode by the edge of a thin concave cylindrically curved surface. *Trans on Antennas and Propagation*, AP-29(4), 1979.

[13] Felsen, L.B. and Ishihara, T. High frequency fields excited by a line source located on a concave cylindrical impedance surface. *Trans on Antennas and Propagation*, AP-27(2), Mar 1979.

[14] Felsen, L.B. and Ishihara, T. High surface fields excited by a point source on a concave perfectly conducting cylindrical boundary. *Radio Science*, 14(2):205–216, April 1979.

[15] Felsen, L.B., Ishihara, T., and Green, A. High frequency fields excited by a line source located on a perfectly conducting concave cylindrical surface. *Trans on Antennas and Propagation*, AP-26(6), Nov 1978.

[16] V.A. Fock. *Electromagnetic Diffraction and Propagation Problems*. Pergamon Press, 1965.

[17] Fock, V. and Leontovich, M. Solution of the problem of propagation of electromagnetic waves along the earth's surface by the method of parabolic equation. *Journal of Physics*, 10(1):13–24, 1946.

[18] E.J. Hinch. *Perturbation Methods*. CUP, 1994.

[19] D.S. Jones. *The Theory of Electromagnetism*. Pergamon Press, Ltd, 1964.

[20] Kaminetzky, L. and Keller, J.B. Diffraction coefficients for higher order edges and vertices. *SIAM, Journal of Applied Mathematics*, pages 109–134, 1972.

[21] J.B. Keller. A geometrical theory of diffraction. *Proc Symp Appl Math*, 8:27–52, 1958.

[22] J.B. Keller. Geometrical theory of diffraction. *Journal of the Optical Society of America*, 52(2):116–130, 1962.

[23] Keller, J.B. and Lewis, R.M. Asymptotic methods for partial differential equations and maxwell's equations. *Surveys in Applied Mathematics*, 1, 1995.

[24] J.M.H. Lawry. *Complex Ray Theory*. PhD thesis, University of Oxford, 1996.

[25] D. Ludwig. Uniform asymptotic expansions at a caustic. *Comm. Pure Appl Math.*, 19(215-250), 1966.

[26] Nagesh, S.R. and Vedavathy, T.S. A procedure for synthesizing a specified sidelobe topography using an arbitrary array. *IEEE Transactions on Antennas and Propagation*, 43(7):742–745, 1995.

[27] B.G. Nikolaev. Wave processes in diffraction by a perfectly reflecting cone in the axisymmetric case. *Journal of Soviet Mathematics*, 3(1):125–141, 1975.

[28] Ockendon, J.R., Howison, S.D., Lacey, A., and Movchan, A. *Applied Partial Differential Equations*. OUP, 1999.

[29] Ockendon, J.R. and Tew, R.H. Multiple scales expansions near critical rays. *SIAM Journal on Applied Mathematics*, 52:327–336, 1992.

[30] J. Roe. *Elementary Geometry*. OUP, 1993.

[31] Rogoff, Z.M. and Kiselev, A.P. Diffraction at jump of curvature on an impedance boundary. *Wave Motion*, pages 183–208, 2001.

[32] V. Saward. Master's thesis, University of Oxford, 1995.

[33] V. Saward. *Some Problems in Diffraction Theory*. PhD thesis, University of Oxford, 1997.

[34] D.J. Shpak. A method for the optimal pattern synthesis of linear arrays with prescribed nulls. *IEEE Transactions on Antennas and Propagation*, 44(3):286–294, 1996.

[35] B. Smith. PhD thesis, University of Nottingham.

[36] V.P. Smyshlyaev. Private Communication.

[37] V.P. Smyshlyaev. The high-frequency diffraction of electromagnetic waves by cones of arbitrary cross sections. *SIAM Journal of Applied Mathematics*, 53(3):670–688, 1993.

[38] V.P. Smyshlyaev. On evaluation of the diffraction coefficients for arbitrary non-singular directions of a smooth convex cone. *SIAM Journal of Applied Mathematics*, 60(2):536–573, 2000.

[39] R.H. Tew. *Imaging Theory of Surface-Breaking Discontinuities*. PhD thesis, University of Oxford, 1987.

[40] Tew, R.H., Chapman, S.J., King, J.R., Ockendon, J.R., Smith, B.J., and Zafarullah, I. Scalar wave diffraction by tangent rays. *Wave Motion*, 32:363–380, 2000.

[41] Weatherburn. *Differential Geometry*. CUP, 1931.